POLITECNICO DI TORINO

DEPARTMENT OF APPLIED SCIENCE AND TECHNOLOGY

Master of Science in Physics of Complex Systems

Final dissertation

Phase transition in vehicular traffic: a Boltzmann-type kinetic approach

Supervisor: Prof. Andrea Tosin
Co-supervisor: Dr. Mattia Zanella

Candidate: Adele Ravagnani

ACADEMIC YEAR 2019/2020

Abstract

This thesis aims at studying phase transition in vehicular traffic with a Boltzmann-type kinetic approach. Phase transition naturally emerges from the derivation of macroscopic quantities as a consequence of binary microscopic interactions. No ansatz is needed, contrary to macroscopic models.
First, the kinetic traffic model is presented referring to the literature. It is based on a *follow-the-leader approach* and analytical results are obtained in the *quasi-invariant interaction regime*. Both the case with and without autonomous vehicles are considered. In particular, the introduction of autonomous vehicles is investigated as a tool to mitigate road risk and relies on a *Model Predictive Control* approach. Two control strategies, which lead to different conclusions, are adopted: the binary variance and the desired speed control. The innovation of this thesis consists in modeling nonlinear interaction rules, which cause the emergence of a bifurcation and therefore, of phase transition. This feature is derived and characterized by referring to linear and nonlinear stability analysis.
Then, phase transition under uncertain vehicle interactions is investigated. As in previous works, an uncertain parameter, which distinguishes several classes of vehicles, is introduced in the interaction rules. The original findings of this dissertation are due to the coexistence of the nonlinearity and the uncertainty in the microscopic interaction rules. Several discrete and continuous uncertain parameters are considered and general results which identify the stable fixed point of the system and the critical density of the phase transition, are stated and proved.
Theoretical findings are validated by means of simulations, based on Monte Carlo methods. The numerical solution of the Boltzmann-type equation is obtained by means of the Nanbu-Babovsky's scheme and it is compared to the asymptotic Fokker-Planck solution, which is obtained analytically in the *quasi-invariant interaction regime*.

Acknowledgements

I would like to thank Professor Tosin and Doctor Zanella for their support in my Master's thesis work. It has been a fundamental opportunity to carry out research in the field of kinetic modeling and its diverse applications. I enjoyed exploring this world with your research ideas and suggestions.

Heartfelt thanks to Niccolò. You have been my fundamental supporter since day one. You gave me strength in every moment of these five years of Physics. I am grateful I have shared this journey with you. I could not ask for a better companion.

Thanks to my sister Cecilia: we are strong together. Thanks also to my parents, Fiorinda and Valter. Despite all, you helped me during these years, in your own way.

Thanks to Ilaria, Giuseppe and Giulia. Talking and going out with you recharged me after intense days of studying. Thanks to Carla, Vanessa and all the fantastic people I met and made my stay in Paris. Thanks for laughing together, for infusions after parties, for big talks.

Finally, I would like to thank the Collegio Carlo Alberto for the academic and economic support it gave me in these five years. Being an honors student at Collegio has been a priceless opportunity to complement and strengthen my preparation in a top-level research institution and to fund my studies. It has been challenging and fundamental both for my scientific and personal growth.

Contents

Chapter 1

Introduction

The goal of this master thesis is to study phase transition in vehicular traffic with a Boltzmann-type kinetic approach. Phase transition naturally emerges from the derivation of macroscopic quantities as a consequence of microscopic interaction rules. No ansatz is needed, contrary to macroscopic models.

In the first two sections of this introductory chapter, the background and the state of the art on the topics relevant for the thesis are respectively outlined. Then, the original contributions of the dissertation are summarized. Finally, the thesis structure is presented.

1.1 Background

Kinetic modeling of interacting multi-agent systems has its roots in statistical physics and it is based on the Boltzmann equation, which was firstly introduced to study rarefied gas [5; 9; 10; 11]. It allows to describe macroscopic properties of a gas starting from the simple mechanics of colliding molecules. The legacy of this theory is massive: the emergence of a variety of collective phenomena - for instance in traffic, wealth distribution, financial markets, opinion formation and swarming - can be explained starting from the modeling of simple interactions.

All these systems consider a huge number of indistinguishable agents. They are equipped with an attribute, which can be their speed in the case of vehicular traffic or their wealth for economic systems describing wealth distribution. Once each agent binary interacts with other agents or with an external background, its attribute changes according to an interaction

rule. Interaction rules represent the core of kinetic models and contain the physics of the system. They are embedded in the Boltzmann-type equation [30], which determines the dynamics of the system and therefore, macroscopic quantities and their evolution are derived.
The Boltzmann-type equation is usually extremely complex and solving it analytically turns out to be difficult. Therefore, referring to the *grazing collisions regime* [49], the *quasi-invariant interaction regime* is considered. Analogously to statistical mechanics where in this limit collisions between gas molecules are mainly tangential and so, the momentum transfer is small [49], microscopic states of agents result to be weakly modified by interactions. The Boltzmann-type integro-differential equation is approximated by a Fokker-Planck partial differential equation (PDE), which can be solved analytically. For complex systems modeling, this regime was first investigated in the context of a market economy [12] and then it has been adopted for problems such as opinion [42] and traffic [46; 47] modeling.

On the one hand, the complexity of the system should be contained in the interaction rules, in order to preserve the physics and to realistically describe the dynamics. On the other hand, it should be possible to devise efficient numerical methods, which allow to confirm theoretical findings. In order to solve numerically the Boltzmann equation, a splitting approach and Monte Carlo (MC) procedures are usually adopted [29; 30]. Direct Simulation Monte Carlo (DSMC) methods, such as Nanbu-Babovsky's and Bird's schemes, are more computationally convenient than deterministic approaches but the accurateness of their results is worse and their convergence is slower [29].
If the variation of the Knudsen number is large, DSMC methods are not suited to deal with the problem so, time relaxed MC methods are used.
Finally, in order to study the impact of uncertainty in complex systems, Uncertainty Quantification (UQ) methods are employed [13; 44; 47; 51].

1.2 State of the art

Among the several applications of the kinetic approach, traffic modeling is gaining importance in order to complement phenomenological procedures with an exhaustive description of the unsteady dynamics of traffic. The mesoscopic approach has been adopted since the sixties and it has revealed its potentialities compared to the traditional macroscopic and microscopic strategies [32].

This thesis is based on three recently published papers [45; 46; 47], which investigate the introduction of autonomous vehicles as a tool to mitigate road risk.
The goal of [46] is to develop a hierarchical description of traffic: after the homogeneous case is extensively studied, hydrodynamic models are derived from the inhomogeneous Boltzmann-type kinetic equation. First, traffic modeling in absence of autonomous vehicles is investigated. Binary interactions are based on the *follow-the-leader approach* [18]: they are anisotropic, so the leading vehicle does not change its speed while the rear vehicle does. For small densities, the rear vehicle tends to the maximum allowed speed. When the density increases, it tends to a fraction of the speed of the leading vehicle and this fraction is given by a decreasing function of the traffic density. These interaction rules, which also contain a stochastic part that models the diffusive behavior, are embedded in the homogeneous Boltzmann-type kinetic equation. Therefore, it is possible to derive the asymptotic speed distribution, which is conceptually analogous to the Maxwellian for rarefied gases. It turns out to be a beta probability density function consistently with experimental data [27]. The mean speed at equilibrium is also obtained and thus *speed* and *fundamental diagrams*. In order to derive these macroscopic quantities, the *quasi-invariant interaction regime* is adopted.

The introduction of a fraction of autonomous vehicles reveals its potential to decrease the variance of the asymptotic speed distribution [45; 46] and consequently road risk. Thanks to their automatic technologies, these driver-assist cars can make the speed variability within the stream of vehicles decrease. Since speed variability is one of the major causes of car accidents [50], autonomous vehicles can be employed as a tool to mitigate road risk.

In order to deal with this issue, an approach based on *Model Predictive Control* (MPC) [8] is used. It has been firstly introduced in the context of traffic [45] being inspired by an analogous approach, which was devised to deal with opinion consensus [1]. The interpenetration of different application fields is evident. A receding horizon strategy is adopted in order to minimize a binary cost functional, aiming at reducing road risk. The problem is solved by Pontryagin's maximum principle [34] and feedback controlled microscopic rules are obtained. Finally, these rules are embedded in the homogeneous Boltzmann-type equation. The innovation of this strategy relies on the fact that the control dynamics have not to be ordered a priori or a posteriori, but naturally emerge from the prescribed microscopic interactions. Even though the control obtained with MPC is suboptimal compared to the theoretical optimal one, the consistency of this approximation is guaranteed for multi-agent kinetic systems [22] and it is a competitive technique due to its lower computational cost.

These traffic models are further extended in [47], where Uncertainty Quantification (UQ) is performed. An uncertain parameter z, which models different classes of vehicles, is introduced in the interaction rules; consequently, the Boltzmann-type equation becomes stochastic. Different probability distributions for z are considered and the mean (with respect to z) asymptotic speed distribution is obtained. This analysis allows to explain two macroscopic features that are experimentally observed: the macroscopic scattering of the *fundamental diagram* and the multi-modal behavior of the asymptotic speed distribution. Moreover, this procedure is innovative and simpler than the traditional approach, which would require an evolution equation for each class of vehicles.

In the second part of the paper, the controlled case is investigated. The strategy is analogous to the one used in [46]. However, with a deterministic control, a Boltzmann-type equation for non-Maxwellian-like particles is obtained and more demanding procedures are required. Both the control strategies considered, stochastic and deterministic, manage to reduce the scattering of the *fundamental diagram* and therefore, road risk.

Theoretical findings are numerically tested by using Stochastic Collocation and Stochastic Galerkin-generalized Polynomial Chaos methods [13; 51]. On the one hand, these UQ studies pave the way for the development of these techniques in traffic modeling. On the other hand, they give an insight into the research topic of numerical methods for UQ, which is having a great boost in recent times.

1.3 Innovative findings

The original contributions of this dissertation are manifold. In this section, they are briefly summarized.

Phase transition in the uncontrolled traffic model

The novelty of this dissertation, compared to the kinetic traffic model of [46], amounts to introduce a nonlinearity in the interaction rules. The consequence is that the evolution of the mean speed is ruled by a nonlinear differential equation, which is studied by linear and nonlinear stability analysis. A bifurcation diagram is derived: there are two fixed points, one stable and one unstable, for all values of density except for a critical value ρ_c at which the two fixed points merge. This critical density ρ_c of the system marks the sharp transition from the free to the congested flow regime. The presence of the phase transition is also evident by deriving the asymptotic speed distribution, which is fundamental to highlight traffic features related to road risk. For densities greater than the critical density ρ_c, the system is in the congested phase and the asymptotic speed distribution is a beta probability density function. When the density is smaller than or equal to the threshold i.e. ρ_c, the asymptotic speed distribution suddenly shrinks to a Dirac delta centered at the maximum allowed speed.

By using the Nanbu-Babovsky's scheme for Maxwellian-like particles, theoretical results are numerically tested. The agreement is strong: as theoretically expected, the numerical equilibrium solution of the Boltzmann-type equation converges toward the solution of the Fokker-Planck PDE, which is obtained analytically in the *quasi-invariant interaction regime*. These simulations give also an insight on the convergence to equilibrium, which is theoretically studied: it is exponential in time for all densities except the critical, for which it is polynomial.

Phase transition in the controlled traffic model

A fraction of autonomous vehicles is taken into account in the model by introducing a control parameter in the nonlinear interaction rules. Two control strategies, which lead to different results, are considered: the binary variance control and the desired speed control [46]. Concerning the former, if the analysis was just limited to *speed* and *fundamental diagrams*, no difference would be revealed compared to the uncontrolled case. Indeed, the mean speed at equilibrium is not affected by the introduction of the binary variance control. Instead, the study of the asymptotic speed distribution shows that, even though the phase transition from a beta distribution to a Dirac delta is preserved, the parameters which characterize the beta distribution are different from the uncontrolled case. In the controlled case, the parameters also depend on the fraction of autonomous vehicles in the system. Moreover, it is proved that in the congested flow regime, the variance of the asymptotic speed distribution decreases once the binary variance control is introduced. Coherently with the literature [46], this strategy can effectively reduce road risk; however, the novelty is that a range of densities for which the variance is identically equal to 0 is identified and it corresponds to the free flow regime.

On the other hand, the phase transition is not preserved by the desired speed control and there exist some density values for which the variance of the asymptotic speed distribution does not decrease compared to the uncontrolled case. Anyway, as in previous works [46], a specific regime for which the variance decreases by introducing the desired speed control, is identified: the so-called *infinite effective penetration rate limit*. The fact that the phase transition is not preserved by the desired speed control strategy can be a practical benefit: the discontinuity in the traffic could be canceled by introducing autonomous vehicles equipped with this control strategy.

Numerical tests are performed with the Nanbu-Babovsky's scheme and as in the uncontrolled case, simulation results fit theoretical findings.

Phase transition under uncertain vehicle interactions

An uncertain parameter z, which models different classes of vehicles, is introduced in the nonlinear interaction rules by referring to [44; 47]. Several probability distributions for z are considered and mean (with respect to z) macroscopic quantities are obtained. Concerning the analysis of the stability of the fixed points for the evolution equation of the mean speed, two general results, one for discrete and another for continuous uncertain parameters, are stated and proved. The unique stable fixed point of the system at equilibrium turns out to be equivalent to the mean with respect to z of the stable fixed points which are derived in the deterministic case i.e. for fixed uncertain parameter.

If the uncertain parameter is discrete, the phase transition is preserved by the introduction of the uncertainty and a general result for the expression of the critical density is derived. The critical point of the system coincides with the one corresponding to the type of vehicles with the biggest z. An analogous result is derived for an uncertain parameter which is uniformly distributed in a bounded interval. On the other hand, the phase transition is not preserved if the uncertain parameter follows a Gamma distribution.

As in deterministic cases, the *quasi-invariant interaction regime* is considered in order to derive mean equilibrium speed distributions. If possible, they are computed analytically, otherwise quadrature formulae are used. The piecewise trait of the mean speed at equilibrium is reflected in the shape of the mean equilibrium speed distribution. For instance, in the case of a discrete uncertain parameter which can assume two values with given probabilities, two regions are distinguished in the congested flow regime. In one of these density intervals, the mean equilibrium speed distribution is a linear combination of two beta distributions, while in the other interval it is a linear combination of a beta and a Dirac delta distribution. In the free flow regime, it is a Dirac delta.
Coherently with literature [47] and with experimental data [27], multi-modal mean equilibrium speed distributions are obtained, due to the introduction of the uncertain parameter. However, because of the nonlinearity in the interaction rules, density intervals in which the behavior of the mean equilibrium speed distribution is different are distinguished.

In order to perform numerical tests, a Monte Carlo method is employed for UQ. The numerical solution of the Boltzmann-type equation averaged with respect to z is compared to the mean Fokker-Planck solution obtained in the *quasi-invariant interaction regime*. Due to the Monte Carlo trait of the algorithm employed, the expected convergence is $\mathrm{O}(M^{-\frac{1}{2}})$, where M is the sample size and fluctuations are present in the solution statistics. L^2-error is computed as a function of the uncertain parameter's sample size M: it represents the numerical error made with respect to the mean Fokker-Planck theoretical solution and as expected, it is $\mathrm{O}(M^{-\frac{1}{2}})$. The other two contributions to the numerical error, one related to the Nanbu-Babovsky's scheme and the other to the *quasi-invariant interaction regime*, are also analyzed.

1.4 Thesis structure

The thesis is organized as follows. After this introductory chapter, chapter 2, *Toolbox*, covers the theoretical (section 2.1) and numerical (section 2.2) topics which are fundamental for the dissertation. In the final section 2.3, a classical example of application is illustrated.

Chapter 3, *Kinetic traffic modeling*, examines in depth the traffic model which is used in the literature and which constitutes the basis for subsequent studies. All the features and the tools which are employed in [45; 46], are deepened and explained.

Chapters 4 and 5, *Phase transition in kinetic traffic modeling* and *Phase transition under uncertain vehicle interactions*, represent the core of the thesis. In the former, nonlinear interaction rules are introduced in the traffic model and the emergence of the phase transition is studied; both the case with and without autonomous vehicles are considered. Chapter 5 investigates phase transition in an uncontrolled model with an uncertain parameter.

Each of chapters 3, 4 and 5 has a section *Numerical tests* where theoretical findings previously obtained are validated by means of simulations, based on Monte Carlo sampling.

Chapter 2

Toolbox

Kinetic modeling of interacting multi-agent systems has its roots in statistical physics and is based on the Boltzmann equation, which was firstly introduced to study rarefied gas [5; 9; 10; 11].

In this chapter, this fundamental equation is presented together with its main properties. Then, the corresponding Boltzmann-type equation for binary interaction models is derived. The second section is devoted to numerical methods for kinetic equations; in particular, the Nanbu-Babovsky's scheme, which is Monte Carlo based, is examined in depth. In the last section, a classical example of application, the Kac model, is studied both theoretically and numerically.

2.1 Kinetic equations

2.1.1 The Boltzmann equation

In 1872, Ludwig Boltzmann wrote a paper where he stated and proved the so-called Boltzmann equation. This equation aims at describing non-equilibrium systems. It represents the basis for the kinetic theory of gases and it can also be employed in other fields such as neutron transport, gas mixtures, polyatomic gases [9].

The Boltzmann equation allows to describe macroscopic properties of a gas starting from the simple mechanics of colliding molecules. As it will be evident from this dissertation, the legacy of this equation is massive: since the early 2000s, it represents the basis for applied studies which investigate multi-agent systems. The emergence of a variety of collective phenomena - for instance in traffic, wealth distribution, financial markets, opinion formation and swarming - can be explained starting from the modeling of simple interactions [30].

In the following, a derivation of the Boltzmann equation for a monoatomic rarefied gas will be sketched and its properties outlined. We recall that rarefied gases are characterized by very low density and so, by large mean free path. Since the Knudsen number ϵ is defined as

$$\epsilon = \frac{\lambda}{D} = \frac{\text{mean free path of a molecule}}{\text{characteristic dimension of the flow}} \ , \tag{2.1}$$

$\epsilon \sim 1$ or higher for rarefied gases.

Let us consider a gas which is constituted by N indistinguishable molecules that elastically interact in the three dimensional phase space. The molecules are considered as hard spheres with diameter equal to σ and mass m [11]. The simplicity of the hard sphere model is justified since we are interested in the limit $N \to +\infty$ and in this limit, there is not dependence on the kind of interaction between molecules [11]. It is also assumed that interactions are binary; higher order interactions are neglected [11]. If $\vec{v}_1$ and $\vec{v}_2$ are the velocities of two interacting particles, the following conservation rules hold [11]:

$$\begin{aligned} &\vec{v}_1 + \vec{v}_2 = \vec{v'}_1 + \vec{v'}_2 \\ &|\vec{v}_1|^2 + |\vec{v}_2|^2 = |\vec{v'}_1|^2 + |\vec{v'}_2|^2 \ , \end{aligned} \tag{2.2}$$

where $'$ denotes the velocities after the collision. Therefore,

$$\begin{aligned} &\vec{v'}_1 = \vec{v}_1 - [(\vec{v}_1 - \vec{v}_2) \cdot \vec{n}]\vec{n} \\ &\vec{v'}_2 = \vec{v}_2 + [(\vec{v}_1 - \vec{v}_2) \cdot \vec{n}]\vec{n} \ , \end{aligned} \tag{2.3}$$

where $\vec{n}$ is the unit vector $\vec{n} = (\vec{x}_1 - \vec{x}_2)/|\vec{x}_1 - \vec{x}_2|$ [11]. We observe that [5]

$$\begin{aligned} &\vec{v'}_1 \cdot \vec{n} = \vec{v}_2 \cdot \vec{n} \\ &\vec{v'}_2 \cdot \vec{n} = \vec{v}_1 \cdot \vec{n} \ . \end{aligned}$$

This means that if the binary interaction occurs between two particles at a collision angle $\vec{n}$, then their velocity components which are parallel to $\vec{n}$ are exchanged while their velocity components which are orthogonal to $\vec{n}$ are unchanged by the collision [5].

The so-called *Boltzmann-Grad limit* [11] is considered i.e. $N \to +\infty$, $\sigma \to 0$ such that $N\sigma^2$ is finite. If a 1 cm^3 box is considered in standard conditions, then $N \simeq 10^{20}$, $\sigma \simeq 10^{-8}$ cm and $N\sigma^2 \simeq 10^4$ cm^2 [11].

The starting point of the derivation of the Boltzmann equation is the Liouville equation [11]. It is defined in terms of $P_N(t, \vec{z})$ with $\vec{z} \in \Omega^N \times \mathbb{R}^{3N}$, which represents the probability density in the $6N$-dimensional phase space. In particular, Ω^N represents the N-dimensional configuration space and $\mathbb{R}^{3N}$ is the $3N$-dimensional velocity space. The Liouville equation is the following partial differential equation [11]:

$$\frac{\partial P_N}{\partial t} + \sum_{i=1}^{N} \vec{v}_i \cdot \frac{\partial P_N}{\partial \vec{x}_i} = 0 \tag{2.4}$$

with suited boundary conditions. Due to the fact that we are dealing with hard spheres, $P_N = 0$ if $|\vec{x}_i - \vec{x}_j| < \sigma$, $i \neq j$ [11]. Therefore, equation (2.4) is defined on a subset Λ of $\Omega^N \times \mathbb{R}^{3N}$: Λ is obtained by removing from the phase space the points for which $P_N = 0$ [11]. We recommend [9; 11] for detailed calculations and discussions.

The Liouville equation (2.4) is defined in terms of P_N, which depends on a number of variables which is $O(N)$ so, it is intractable form a practical point of view [11]. Starting from this observation, Maxwell and Boltzmann focused on the *one-particle distribution function* $P_N^{(1)}$ [11], which just depends on seven variables. $P_N^{(1)}(t, \vec{x}_1, \vec{v}_1)$ represents the probability density of finding a gas molecule at time t, in position $\vec{x}_1$, with velocity $\vec{v}_1$ [11]:

$$P_N^{(1)}(t, \vec{x}_1, \vec{v}_1) = \int_{\Omega^{N-1} \times \mathbb{R}^{3N-3}} P_N(t, \vec{x}_1, \vec{v}_1, \ldots, \vec{x}_N, \vec{v}_N) d\vec{x}_2 d\vec{v}_2 \ldots d\vec{x}_N d\vec{v}_N \ , \tag{2.5}$$

where Ω^{N-1} represents the $N-1$-dimensional configuration space and $\mathbb{R}^{3N-3}$ is the $3N-3$-dimensional velocity space.

Boltzmann wrote the equation which inherited his name by means of a heuristic argument [11]. He stated that

$$\frac{\partial P_N^{(1)}}{\partial t} + \vec{v}_1 \cdot \frac{\partial P_N^{(1)}}{\partial \vec{x}_1} = G - L \tag{2.6}$$

where G and L are the gain and loss term respectively [11]. $G d\vec{x}_1 d\vec{v}_1 dt$ represents the expected number of molecules which acquire a position in $[\vec{x}_1, \vec{x}_1 + d\vec{x}_1]$ and a velocity in $[\vec{v}_1, \vec{v}_1 + d\vec{v}_1]$ due to a collision in the time range $[t, t + dt]$ [11]. Analogously, $L d\vec{x}_1 d\vec{v}_1 dt$ is the number of molecules which have a position in $[\vec{x}_1, \vec{x}_1 + d\vec{x}_1]$ and a velocity in $[\vec{v}_1, \vec{v}_1 + d\vec{v}_1]$ and due to a collision in $[t, t+dt]$, gain position and velocity attributes outside of the previous ranges [11]. We refer to [9; 11] for detailed calculations of G and L, which allow to obtain the Boltzmann equation. It is fundamental to stress that the *molecular chaos assumption* or *Boltzmann ansatz* [11] plays a crucial role. It consists in assuming that molecules are not correlated and therefore [11],

$$P_N^{(2)}(t, \vec{x}_1, \vec{v}_1, \vec{x}_2, \vec{v}_2) = P_N^{(1)}(t, \vec{x}_1, \vec{v}_1) P_N^{(1)}(t, \vec{x}_2, \vec{v}_2) \tag{2.7}$$

or

$$\begin{aligned} P_N^{(2)}(t, \vec{x}_1, \vec{v}_1, \vec{x}_1 + \sigma\vec{n}, \vec{v}_2) = P_N^{(1)}(t, \vec{x}_1, \vec{v}_1) P_N^{(1)}(t, \vec{x}_1 + \sigma\vec{n}, \vec{v}_2) \\ \text{for } (\vec{v}_2 - \vec{v}_1) \cdot \vec{n} < 0 \end{aligned} \tag{2.8}$$

where $P_N^{(2)}$ is the *two-particle distribution function.* $P_N^{(2)}(t, \vec{x}_1, \vec{v}_1, \vec{x}_2, \vec{v}_2)$ represents the probability density of finding two gas molecules at time t, one in position $\vec{x}_1$ with velocity $\vec{v}_1$ and another in position $\vec{x}_2$ with velocity $\vec{v}_2$ [9; 11]. The second form of the molecular chaos assumption i.e. (2.8) expresses well its meaning: only molecules which are about to collide are statistical independent.
If a 1 cm^3 box is considered in standard conditions, the *Boltzmann-Grad limit* holds. Then, $N\sigma^3 \simeq 10^{-4}$ cm^3 and this quantity represents a rough estimate of the volume occupied by N interacting particles [11]. Since the ratio between $N\sigma^3$ and the total volume of the box is about 10^{-4}, it is unlikely that a collision occurs. Therefore, it is justified to consider two interacting particles as two randomly chosen molecules and to assume their statistical independence and that their probability density is the product of the probability densities related to each particle.

As well as the heuristic argument, the Boltzmann equation can be directly derived from the Liouville equation. We recommend [9; 11] for details. If equation (2.4) is integrated with respect to the molecules labeled by $2, \ldots N$, an equation which rules the evolution of $P_N^{(2)}$ is obtained [11]. Then, by reworking on it, the following equation can be written [9]:

$$\frac{\partial P_N^{(1)}}{\partial t} + \vec{v}_1 \cdot \frac{\partial P_N^{(1)}}{\partial \vec{x}_1} = (N-1)\sigma^2 \int [P_N^{(2)\prime} - P_N^{(2)}] |\vec{V}_1 \cdot \vec{n}| d\vec{n} d\vec{v}_2 \tag{2.9}$$

where $\vec{V}_1 = \vec{v}_1 - \vec{v}_2$.
Thanks to assumption (2.7), the Boltzmann equation is derived [11]:

$$\frac{\partial P}{\partial t} + \vec{v} \cdot \frac{\partial P}{\partial \vec{x}} = N\sigma^2 \int [PP'_* - PP_*] |\vec{V} \cdot \vec{n}| d\vec{n} d\vec{v}_* \tag{2.10}$$

where $\vec{x}_1 \to \vec{x}$, $\vec{v}_1 \to \vec{v}$, $\vec{x}_2 \to \vec{x}_*$, $\vec{v}_2 \to \vec{v}_*$, P denotes the *one-particle distribution function* $P_N^{(1)}$ and $P_* = P_N^{(1)}(t, \vec{x}_*, \vec{v}_*)$.

Let us rewrite equation (2.10) with a notation that will be adopted in the following. The *one-particle distribution function* is denoted by $f = f(t, \vec{x}, \vec{v})$ and the integral of the right-hand side of equation (2.10) by $Q(f, f)(t, \vec{x}, \vec{v})$. Therefore, the Boltzmann equation turns out to be the following partial integro-differential equation [5; 30]:

$$\partial_t f(t, \vec{x}, \vec{v}) + \vec{v} \cdot \nabla_x f(t, \vec{x}, \vec{v}) = Q(f, f)(t, \vec{x}, \vec{v}) \tag{2.11}$$

where

$$Q(f, f)(t, \vec{x}, \vec{v}) = \alpha \int_{\mathbb{R}^3 \times S_+} (f' f'_* - f f_*) |\vec{n} \cdot (\vec{v} - \vec{v_*})| d\vec{v}_* d\vec{n} \ . \tag{2.12}$$

$Q(f, f)(t, \vec{x}, \vec{v})$ is the so-called *collision operator* [5] and $B(\vec{n} \cdot (\vec{v} - \vec{v_*})) = |\vec{n} \cdot (\vec{v} - \vec{v_*})|$ is the collision frequency [5]; α is a constant.
The Boltzmann equation describes the evolution of the probability density of molecules $f(t, \vec{x}, \vec{v})$ for a rarefied gas. This quantity changes in two different ways, by transport or by collision. The first phenomenon is expressed by the second term in the left-hand side of (2.11): if a given particle does not collide, its velocity is unchanged while its position changes and we have $(t_0, \vec{x}, \vec{v}) \to (t + t_0, \vec{x} + (t - t_0)\vec{v}, \vec{v})$ [5]. Instead, the collision phenomenon is described by the *collision kernel* $Q(f, f)$: velocities change according to microscopic interactions between molecules.

2.1.2 Collision invariants

Let us drop the notation for vectors and let us focus on the homogeneous Boltzmann equation

$$\partial_t f(t, v) = Q(f, f)(t, v) \ . \tag{2.13}$$

In order to consider some properties of the *collision kernel* $Q(f, f)$, we focus on functionals defined as [5]

$$\Phi(f) \equiv \int_{\mathbb{R}^3} \phi(v) f(v) dv \tag{2.14}$$

and such that

$$\int_{\mathbb{R}^3} \phi(v) Q(f, f) dv = 0 \ . \tag{2.15}$$

It can be proved [5] that (2.15) holds if

$$\phi(v) + \phi(v^*) = \phi(v') + \phi(v^{*\prime}) \tag{2.16}$$

and the function $\phi(\cdot)$ which satisfies (2.16) is called *collision invariant* [5]. In this case, the functional $\Phi(\cdot)$ in (2.14) is constant in time for every function f which solves the Boltzmann equation.

It can also be proved [5] that if $\phi \in C^2$ and (2.16) holds, then we have

$$\phi(v) = a + b \cdot v + c|v|^2 \text{ with } a, c \in \mathbb{R} \text{ and } b \in \mathbb{R}^3 \ . \tag{2.17}$$

Significant examples of collision invariants are $\phi(v) = 1$, $\phi(v) = e_i \cdot v$ with $i = 1{,}2{,}3$ and e_i unit vectors, $\phi(v) = |v|^2/2$. Thanks to them, we obtain the conservation of mass, of momentum and of energy respectively [5].

2.1.3 Maxwellian distribution

Let us consider the left-hand side of (2.15) with $\phi(v) = \log f(v)$. It can be proved [5] that

$$\int_{\mathbb{R}^3} \log f Q(f, f) dv \leq 0 \tag{2.18}$$

and (2.18) is called *Boltzmann inequality* [5]. The equality corresponds to the case in which $\phi(v) = \log f(v)$ is a collision invariant. Therefore, due to (2.17), we have that the equality holds if and only if [5]

$$f(v) = \exp(a + b \cdot v + c|v|^2) = A \exp(-\beta|v - v_0|^2) \text{ with } A, \beta > 0 \text{ and } v_0 \in \mathbb{R}^3. \tag{2.19}$$

Equation (2.19) defines the so-called *Maxwellian distributions* i.e. the solutions f of the Boltzmann equation which lead to $Q(f, f) = 0$ [5].

It is worth noticing that starting from the Boltzmann equation, it is possible to derive the *H-theorem*, which represents the first analytical proof of the second principle of thermodynamics and the macroscopic balance equations, which constitute the basis for hydrodynamic models. We recommend [5; 9; 10; 11] for examining in depth these topics.

2.1.4 Binary interaction models

In previous subsections, the Boltzmann equation and its main properties are outlined. However, the aim of this dissertation is to focus on vehicular traffic, which is a multi-agent system. In this subsection, a model, which constitutes the basis for the kinetic traffic model that will be employed in the following, is examined in depth. The starting point is modeling interaction rules and then, the binary interaction model is constructed step-by-step. The derivation of the model is grounded on probability theory and it highlights the statistical trait of the kinetic description.

Let us focus on a one dimensional system therefore agents are equipped with scalar attributes, which could be speed, opinion or wealth depending on the system studied. Due to the fact that only binary interactions are considered, the following interaction rules can be written [30]:

$$\begin{aligned} v' &= p_1 v + q_1 w \\ w' &= p_2 v + q_2 w \ , \end{aligned} \tag{2.20}$$

where (v, w) and (v', w') are the agents' attributes before and after the interaction respectively. The parameters $p_1, p_2, q_1, q_2 > 0$ can be either constants or random variables; in the following, we will consider them as random variables. We assume $v, v', w, w' \in V \subseteq \mathbb{R}$, which is the so-called *physical admissibility condition*. Parameters in the interaction rules (2.20) have to be chosen such that the *physical admissibility condition* is guaranteed for post-interaction attributes i.e. v', w'. This requirement represents a difference compared to the context of rarefied gases, where molecules' speeds are unconstrained i.e. $v \in \mathbb{R}$ and it will become clearer in chapter 3, where traffic modeling is investigated.

We would like to rephrase interaction rules (2.20) in terms of random processes in order to derive the associated Boltzmann-type equation. Therefore, let us introduce the random variable $X(t)$ with probability density $f = f(t, v)$: it allows to describe the number of agents with attribute v at time t [30]. If $X(t) \in V$,

$$\mathbb{P}(X \in A) = \int_A f(t, v) dv \quad \forall A \subseteq V \, . \tag{2.21}$$

where A is a measurable set.
Analogously, another random variable $Y(t)$ with the same density $f(t, v)$ is introduced. Interaction rules (2.20) can be rewritten as [30]

$$\begin{aligned} X'(t) &= p_1 X(t) + q_1 Y(t) \\ Y'(t) &= p_2 X(t) + q_2 Y(t) \ . \end{aligned} \tag{2.22}$$

The variation of $X(t)$ and $Y(t)$ is due to binary interactions between agents. In a time interval $\Delta t << 1$, two agents may interact: if so, their microscopic states change according to the interaction rules. Therefore, we can write

$$X(t+\Delta t) = \begin{cases} X'(t) & \text{if interaction occurs} \\ X(t) & \text{else} \ . \end{cases}$$

Let us assume that the interaction probability is proportional to the time interval Δt and that the proportionality constant is equal to μ, the so-called *interaction kernel* [30]. In general, $\mu = \mu(v, w)$ i.e. it is a function of the attributes of interacting agents and it is analogous to the *collision kernel* in the framework of rarefied gases. Then, a random variable T, which models the probability with which interactions occur, is defined as [30]

$$T \sim \text{Bernoulli}(\mu\Delta t)$$

so,

$$\begin{aligned} &\mathbb{P}(T=1) = \mu\Delta t \\ &\mathbb{P}(T=0) = 1 - \mu\Delta t \ . \end{aligned}$$

The condition $\mu\Delta t \leq 1$ holds since we will be interested in the limit
$\Delta t \to 0^+$.
Then, $X(t+\Delta t)$ can be rewritten as

$$X(t+\Delta t) = TX'(t) + (1-T)X(t) \ . \tag{2.23}$$

Analogously, we have:

$$Y(t+\Delta t) = TY'(t) + (1-T)Y(t) \ . \tag{2.24}$$

If $\phi = \phi(v)$ is a generic *observable quantity*, equations (2.23) and (2.24) can be generalized as

$$\phi\big(X(t+\Delta t)\big) = \phi\big(TX'(t) + (1-T)X(t)\big) \tag{2.25}$$

and

$$\phi\big(Y(t+\Delta t)\big) = \phi\big(TY'(t) + (1-T)Y(t)\big) \ . \tag{2.26}$$

Moreover, the average variation of $\phi(v)$ due to interactions (2.22) can be obtained. In particular we are interested in

$$\langle \phi(X(t+\Delta t)) + \phi(Y(t+\Delta t))\rangle - \langle \phi(X(t)) + \phi(Y(t))\rangle \ ,$$

where the average $\langle\cdot\rangle$ is performed with respect to all random variables i.e. $X, Y, T, p_1, p_2, q_1, q_2$.
By referring to (2.23) - (2.24), we have that

$$\begin{aligned}\langle\phi(X(t+\Delta t))\rangle &= \langle\mu\Delta t\phi(X'(t))\rangle + \langle(1-\mu\Delta t)\phi(X(t))\rangle \\ \langle\phi(Y(t+\Delta t))\rangle &= \langle\mu\Delta t\phi(Y'(t))\rangle + \langle(1-\mu\Delta t)\phi(Y(t))\rangle\end{aligned} \tag{2.27}$$

where the average with respect to T has been calculated. Therefore, we obtain

$$\begin{aligned}&\langle\phi(X(t+\Delta t)) + \phi(Y(t+\Delta t))\rangle = \langle\mu\Delta t\phi(X'(t))\rangle + \langle(1-\mu\Delta t)\phi(X(t))\rangle + \\ &+ \langle\mu\Delta t\phi(Y'(t))\rangle + \langle(1-\mu\Delta t)\phi(Y(t))\rangle \iff \\ &\iff \langle\phi(X(t+\Delta t)) - \phi(X(t))\rangle + \langle\phi(Y(t+\Delta t)) - \phi(Y(t))\rangle = \\ &= \Delta t\Big[\langle\mu\phi(X'(t))\rangle - \langle\mu\phi(X(t))\rangle + \langle\mu\phi(Y'(t))\rangle - \langle\mu\phi(Y(t))\rangle\Big] .\end{aligned} \tag{2.28}$$

Equation (2.28) can be divided by Δt and the limit $\Delta t \to 0^+$ can be considered:

$$\begin{aligned}\lim_{\Delta t\to 0^+} &\frac{\langle\phi(X(t+\Delta t)) - \phi(X(t))\rangle + \langle\phi(Y(t+\Delta t)) - \phi(Y(t))\rangle}{\Delta t} = \\ &= \langle\mu\phi(X'(t))\rangle - \langle\mu\phi(X(t))\rangle + \langle\mu\phi(Y'(t))\rangle - \langle\mu\phi(Y(t))\rangle\end{aligned} \tag{2.29}$$

and this is equivalent to

$$\begin{aligned}\frac{d}{dt}\langle\phi(X(t)) + \phi(Y(t))\rangle = \langle\mu\phi(X'(t))\rangle - \langle\mu\phi(X(t))\rangle + \\ + \langle\mu\phi(Y'(t))\rangle - \langle\mu\phi(Y(t))\rangle .\end{aligned} \tag{2.30}$$

By assumption, the two random processes $X(t)$ and $Y(t)$ are independent therefore their joint probability distribution is

$$\pi(t, v, w) = f(t, v)f(t, w) .$$

This assumption is equivalent to the *Boltzmann ansatz*, previously introduced in the context of the kinetic theory of rarefied gases and its not completely grounded on the physics of the problem when dealing with multi-agent systems. However, it allows to obtain an equation in closed form and therefore, it represents a compromise between the desire of most realistically describe the dynamics and that of have insight into the process thanks to an approximate mathematical model [30].

Consequently, since $X'(t)$ and $Y'(t)$ are linear combinations of $X(t)$ and $Y(t)$ - see relations (2.22), they are independent random variables as well and so, we have

$$\begin{aligned}\langle\phi(X'(t))\rangle_{X'} =&\langle\int_V\int_V\phi(v')\pi(t,v,w)dvdw\rangle_{p_1,q_1} =\\=&\langle\int_V\int_V\phi(v')f(t,v)f(t,w)dvdw\rangle_{p_1,q_1}\\\langle\phi(Y'(t))\rangle_{Y'} =&\langle\int_V\int_V\phi(w')\pi(t,v,w)dvdw\rangle_{p_2,q_2} =\\=&\langle\int_V\int_V\phi(w')f(t,v)f(t,w)dvdw\rangle_{p_2,q_2}\ .\end{aligned} \tag{2.31}$$

Therefore, equation (2.29) becomes

$$\begin{aligned}&\frac{d}{dt}\Big[2\int_V\phi(v)f(t,v)dv\Big] =\\&=\langle\int_V\int_V\mu\big[\phi(v')+\phi(w')-\phi(v)-\phi(w)\big]f(t,v)f(t,w)dvdw\rangle\end{aligned} \tag{2.32}$$

and finally

$$\begin{aligned}&\frac{d}{dt}\int_V\phi(v)f(t,v)dv =\\&=\frac{1}{2}\langle\int_V\int_V\mu\big[\phi(v')+\phi(w')-\phi(v)-\phi(w)\big]f(t,v)f(t,w)dvdw\rangle\end{aligned} \tag{2.33}$$

where the average $\langle\cdot\rangle$ in equation (2.33) is the one with respect to the random parameters p_1, p_2, q_1, q_2.
Equation (2.33) is the *weak form* of the Boltzmann-type kinetic equation for binary interaction models [30]. It holds for all possible choices of the *observable quantity* $\phi(v)$.

The similarity with the Boltzmann equation is more evident if the *strong form* of (2.33) is derived [30]. Let us consider: $\phi(\cdot) = \delta(v-\cdot)$ i.e. a Dirac delta observable, $v \to v_1$, $w \to v_2$ and by simplicity, a constant *interaction kernel* i.e. $\mu = 1$. Then, equation (2.33) becomes

$$\partial_t f(t,v) = \frac{1}{2}\langle\int_V\int_V\big[\delta(v-v_1')+\delta(v-v_2')\big]f(t,v_1)f(t,v_2)dv_1dv_2\rangle - f(t,v)\ , \tag{2.34}$$

where the interaction rules are

$$\begin{aligned}v_1' &= p_1v_1 + q_1v_2\\v_2' &= p_2v_1 + q_2v_2\ .\end{aligned}$$

This equation can be also rewritten as [30]

$$\partial_t f(t,v) = Q_+(f,f)(t,v) - f(t,v) \ , \tag{2.35}$$

where $Q_+(f,f)(t,v)$ is the so-called *gain operator* and it is defined as

$$Q_+(f,f)(t,v) := \frac{1}{2}\langle \int_V \int_V \Big[\delta(v-v_1') + \delta(v-v_2')\Big] f(t,v_1)f(t,v_2)dv_1dv_2\rangle \ . \tag{2.36}$$

Therefore, the evolution in time of the density $f(t,v)$ is due to the balance between a gain and a loss operator.

Insight on the physical meaning of this equation can also be gained by focusing on equation (2.33). In the left-hand side, the term $\int_V \phi(v)f(t,v)dv$ represents the mean of a given *observable quantity* $\phi(v)$. Instead, in the right-hand side the term $\frac{1}{2}\Big[\phi(v')+\phi(w')-\phi(v)-\phi(w)\Big]$ is the mean variation of $\phi(v)$, which occurs in a binary interaction (2.20). Consequently, equation (2.33) claims that the variation in time of the mean of a given *observable quantity* $\phi(v)$ is equal to the average of the mean variation of $\phi(v)$ due to a binary interaction (2.20).

Remark 2.1.1. In analogy to the kinetic theory of rarefied gases, only binary interactions have been regarded in the derivation of equation (2.33). However, by referring to its physical meaning, it is possible to derive a Boltzmann-type kinetic equation, which also considers interactions between three or more agents [43]. Interaction rules can be written as

$$v_i' = v_i + I(v_1, v_2, \ldots, v_N; p_1, \ldots, p_N) \quad i = 1, \ldots, N \ ,$$

where $I(v_1, v_2, ..., v_N; p_1, ..., p_N)$ is the interaction function, which depends on the attributes of all N agents and on N random variables.
The term $\frac{1}{2}\Big[\phi(v') + \phi(w') - \phi(v) - \phi(w)\Big]$ can be written as

$$\frac{1}{N}\sum_{i=1}^{N}\Big[\phi(v_i') - \phi(v_i)\Big] \tag{2.37}$$

and the *Boltzmann ansatz* becomes $f(t,v_1,...,v_N) = f(t,v_1)...f(t,v_N)$. Therefore, we obtain [43]

$$\frac{d}{dt}\int_V \phi(v)f(t,v)dv = \frac{1}{N}\langle \int_{V^N} \mu \sum_{i=1}^{N}\Big[\phi(v_i') - \phi(v_i)\Big] f(t,v_1)...f(t,v_N)dv_1...dv_N\rangle \tag{2.38}$$

where the average $\langle\cdot\rangle$ is considered with respect to the random variables $p_1, ..., p_N$. □

Remark 2.1.2. The Boltzmann-type kinetic equation (2.33) has been derived in the homogeneous case. In order to obtain the corresponding heterogeneous equation, the following probability density has to be introduced: $f = f(t, x, v)$ where $x \in S$ represents the space position of the agents. The normalization condition becomes

$$\int_S \int_V f(t, x, v) dv dx = 1 \quad \forall t \geq 0 \ .$$

The inhomogeneous Boltzmann-type kinetic equation is [46]

$$\begin{aligned} \partial_t \int_V \phi(v) f(t, x, v) dv + \partial_x \int_V v\phi(v) f(t, x, v) dv = \\ = \frac{1}{2} \langle \int_V \int_V \mu \big[\phi(v') + \phi(w') - \phi(v) - \phi(w)\big] f(t, x, v) f(t, x, w) dv dw \rangle \ . \end{aligned}$$

This equation states that the time variation of the density function is both due to the transport, resulting from the inhomogeneity in space and to binary interactions between agents.
Contrary to the homogeneous case,

$$\rho(t, x) \equiv \int_V f(t, x, v) dv \ ,$$

which represents the density of agents at time t in position x, is not constant in time because of the transport in space. □

Symmetric interactions

Let us consider interaction rules (2.20) in a symmetric situation i.e. $p_1 = q_2 = p$ and $p_2 = q_1 = q$ [30]. Let us also assume that p, q are fixed parameters with $p > q > 0$ and $\mu = 1$. Therefore, the Boltzmann-type kinetic equation becomes

$$\frac{d}{dt} \int_V \phi(v) f(t, v) dv = \int_V \int_V \big[\phi(v') - \phi(v)\big] f(t, v) f(t, w) dv dw \ . \tag{2.39}$$

The following initial conditions can be imposed without loss of generality [30]:

$$\begin{aligned} \int_V f_0(v) dv = 1 \\ \int_V v f_0(v) dv = 0 \\ \int_V v^2 f_0(v) dv = 1 \end{aligned} \tag{2.40}$$

where $f_0(v) = f(t=0,v)$ is the initial density.

If $\phi(v) = v$, an evolution equation for the first moment $m(t)$ is obtained:

$$\frac{d}{dt}\underbrace{\int_V v f(t,v)dv}_{=m(t)} = \int_V\int_V \Big[(p-1)v + qw\Big] f(t,v)f(t,w)dvdw \iff$$
$$\iff \dot{m}(t) = (p+q-1)m(t) \implies m(t) = m(0)\exp\{(p+q-1)t\}\ . \tag{2.41}$$

Due to the fact that $m(0) = 0$ - see equation (2.40), $m(t) = 0\ \forall t$ and so, the first moment is conserved. This is not the case of the second moment $E(t)$. Indeed, if we set $\phi(v) = v^2$, we obtain

$$\frac{d}{dt}\underbrace{\int_V v^2 f(t,v)dv}_{=E(t)} = \int_V\int_V \Big[(p^2-1)v^2 + q^2w^2 + 2pqvw\Big] f(t,v)f(t,w)dvdw \iff$$
$$\iff \dot{E}(t) = (p^2+q^2-1)E(t) + 2pqm^2(t)$$
$$\implies E(t) = \underbrace{E(0)}_{=1}\exp\{(p^2+q^2-1)t\} = \exp\{(p^2+q^2-1)t\}\ . \tag{2.42}$$

Therefore, $E(t)$ is conserved if and only if $p^2+q^2-1=0$ otherwise it can grow or decrease exponentially, thus highlighting the variety of behaviors depending on the choice of the fixed parameters p,q.

Anyway, the main goal is to obtain the evolution of the distribution $f(t,v)$. In particular, its behavior at equilibrium allows us to make comparison with experimental data and state whether the model is suited to describe the system. Two main strategies are usually employed to tackle this problem. The first relies on *self-similarity* [30]: the solution of (2.39) relaxes at equilibrium towards the so-called *self-similar* profile, which is associated to different initial conditions. Practically, the following solution is introduced [30]:

$$g(t,v) := \sqrt{E(t)}\, f\Big(t, v\sqrt{E(t)}\Big),$$

which is still a probability density and has a conserved second moment.
The other approach is based on the so-called *grazing collisions regime*, which was deeply investigated by Cedric Villani in the classical kinetic theory of rarefied gases [49]. In this context, it consists in considering $p \simeq 1$ and $q \simeq 0$

that means a regime in which the agents' attributes are weakly modified by the interactions [30]. This limit will be examined in depth in section 3.6, where it will allow to obtain the asymptotic solution of the Boltzmann-type kinetic equation.

2.2 Monte Carlo methods for kinetic equations

In the previous section, the Boltzmann-type equation for multi-agent systems has been derived. It will be the basis for our subsequent studies, which will focus on traffic modeling. The theoretical analysis will be supported by numerical tests, which allow to confirm theoretical findings.

Equation (2.35) is an integro-differential equation, which is difficult to solve numerically because of the *curse of dimensionality* and its nonlinear trait. A first idea could be to tackle this equation by relying on quadrature formulae [3; 39; 48]. If the density function $f(t, v)$ depends on N parameters such as grid points, a quadrature formula based on this set of points is employed. Consequently, the computational cost is $O(N^{\alpha})$ with $\alpha \geq 2$ for each time step [29]. A Monte Carlo approach permits to consistently improve this high cost, which becomes of the order of the number of particles [29]. Moreover, it also allows to preserve most of the physical properties of the system and it does not impose artificial constraints in the velocity space [29]. However, due to their statistical character, Monte Carlo procedures lead to results with statistical fluctuations and they have lower accuracy than deterministic approaches [29; 30].

The first Monte Carlo based methods are the Direct Simulation Monte Carlo (DSMC), in particular the Bird's and the Nanbu-Babovsky's scheme [29; 30]. They consider a finite number of particles with given initial velocities. As time evolves, in each time step each of them may collide with another molecule, which is randomly selected, thus changing its velocity. Therefore, a probabilistic approach is employed and it is perfectly suited to the kinetic framework, which is based on a statistical description of the system.

In the next subsection, the Nanbu-Babovsky's scheme is examined in depth since it will be employed in chapters 3 and 4. This approach is more suited to deal with homogeneous problems while the Bird's scheme is

generally employed in inhomogeneous situations. If the Boltzamnn equation has the transport term, a splitting approach is adopted [29; 30]. First, the corresponding homogeneous equation is solved by using DSMC methods (interaction step) then, the output of this first step is used as an input of the transport step, where the equation to be solved does not include the collision term. This allows to capture both the transport and the collision dynamics since each of them is solved in its associated temporal scale.
If the variation of the Knudsen number is large, DSMC methods are not effective to deal with the problem so, Time Relaxed Monte Carlo (TRMC) methods are used. We recommend [29; 30] for the Bird's, inhomogeneous and TRMC methods.

2.2.1 The Nanbu-Babovsky's scheme

In following chapters, the Nanbu-Babovsky's scheme will be used in order to solve numerically the Boltzmann-type kinetic equation for Maxwellian-like particles i.e. with constant *collision kernel*. Let us explain this simulation method in the more general context of the Boltzmann equation for constant *collision kernels*.

The equation we would like to solve is the following:

$$\partial_t f(t,v) = \frac{1}{\epsilon}\Big[P(f,f) - Kf(t,v)\Big] \ , \tag{2.43}$$

with the initial condition $f(t=0,v) = f_0(v)$. $P(f,f) := Q_+(f,f)(t,v)$ is the *gain operator*, $K \neq 0$ is a normalization constant i.e. $K = \int f(t,v)dv$ and the parameter $\epsilon > 0$ is the Knudsen number, which is defined in (2.1).
Let us consider the following time discretisation. The final time is T and Δt represents the time step therefore, $t^n = n\Delta t$ with $n = 0,1,...,N_T$. If f^n is an approximation of $f(t^n, v)$ and the forward Euler scheme is employed, equation (2.43) implies [29]

$$f^{n+1} = \left(1 - \frac{K\Delta t}{\epsilon}\right) f^n + \frac{K\Delta t}{\epsilon}\frac{P(f^n,f^n)}{K} \ . \tag{2.44}$$

Given the condition $\frac{K\Delta t}{\epsilon} \leq 1$, f^{n+1} is a convex combination of f^n and $\frac{P(f^n,f^n)}{K}$. At every time step, a particle collides with probability $\frac{K\Delta t}{\epsilon}$ and it does not with probability $1 - \frac{K\Delta t}{\epsilon}$.
By referring to (2.44), the Nanbu's scheme is stated in algorithm 1.

Algorithm 1: The Nanbu's scheme

Initialize
- Sample particles' initial speeds from the initial distribution $f_0(v)$: $\{v_1^0, v_2^0, ..., v_N^0\}$

For $n = 1, ..., N_T$
- **for** $i = 1, ..., N$
  - **with probability** $1 - K\Delta t/\epsilon$**:**
    - $v_i^{n+1} \leftarrow v_i^n$
  - **with probability** $K\Delta t/\epsilon$**:**
    - select a random particle j
    - compute v_i' with the interaction rules of the model considering i and j as interacting particles
    - $v_i^{n+1} \leftarrow v_i'$

Return the numerical distribution $f_N(t, v) = \frac{1}{N}\sum_{i=1}^{N} \delta(v - v_i(t))$ by using a suited histogram

We observe that in algorithm 1, energy is not conserved in each interaction. Indeed, if E_{FIN} is the post-collision energy of the interacting pair (i, j) and E_0 is its pre-collision energy, we have

$$E_{FIN} = \frac{m}{2}(v_i'^2 + v_j^2) \neq E_0 = \frac{m}{2}(v_i^2 + v_j^2) \ .$$

This issue was tackled by Babovsky, who proposed the conservative scheme of algorithm 2 (p. 31). It is based on the following observation. Let us introduce the random variable X, which describes the number of colliding particles in the time step Δt. Due to the probabilistic interpretation of equation (2.44), we have $\mathbb{E}[X] = NK\Delta t/\epsilon$. Consequently, the expected number of interacting pairs is $N_c = NK\Delta t/(2\epsilon)$.
In algorithm 2, the function $\mathrm{Sround}(x)$ is employed. It is a stochastic integer rounding function and it defined as

$$\mathrm{Sround}(x) = \begin{cases} \lfloor x \rfloor + 1 & \text{with probability } x - \lfloor x \rfloor \\ \lfloor x \rfloor & \text{with probability } \lfloor x \rfloor + 1 - x \ . \end{cases}$$

In [4], it is proved that numerical results which are obtained with the Nanbu's and the Nanbu-Babovsky's schemes, converge to solutions of the Boltzmann equation. This holds if some criteria - the uniqueness and regularity of the solution on the time interval considered, a condition on the starting measure, another on the *collision kernel*, a large enough number

Algorithm 2: The Nanbu-Babovsky's scheme

Initialize
    Sample particles' initial speeds from the initial distribution $f_0(v)$: $\{v_1^0, v_2^0, ..., v_N^0\}$

For $n = 1, ..., N_T$
    introduce $N_C = \text{Sround}(KN\Delta t/(2\epsilon))$
    select N_C pairs of interacting particles uniformly among all $\binom{N}{2}$ pairs
    for each interacting pair (i, j)
        $v_i^{n+1} \leftarrow v_i'$
        $v_j^{n+1} \leftarrow v_j'$
    for all particles which are not part of the N_C **interacting pairs**
        $v_i^{n+1} \leftarrow v_i^n$

Return the numerical distribution $f_N(t, v) = \frac{1}{N}\sum_{i=1}^{N} \delta(v - v_i(t))$ by using a suited histogram

of particles, a sufficient small time step - are satisfied. This issue can be examined in depth by referring to [4].

Algorithms 1 and 2 hold for Maxwellian molecules and they can be generalized to non-constant *collision kernels*. We recommend [29; 30] for their discussions.

2.2.2 Accuracy of Monte Carlo methods

In the previous subsection, Monte Carlo methods which allow to solve the Boltzmann integro-differential equation are presented. They are easy to implement and they are less refined from a mathematical point of view than other numerical methods. They are also extremely powerful in terms of computational cost but as we have already mentioned, they have lower accuracy than deterministic approaches. In this subsection, their accuracy will be investigated in the general framework of Monte Carlo integration [7; 30].

Let us consider the following integral:

$$I[f] = \int_0^1 f(x)dx \ , \tag{2.45}$$

where $f = f(x)$ is a Lebesgue integrable function. If $X \sim \mathcal{U}([0,1])$ i.e. X is a random variable uniformly distributed in the interval [0,1], then

$I[f] = \mathbb{E}[f(X)]$.
Analogously, in d dimensions, we have that $\vec{X}$ is a random vector which is uniformly distributed in the unit cube $[0,1]^d$ and

$$I[f] = \mathbb{E}[f(\vec{X})] = \int_{[0,1]^d} f(\vec{x}) d\vec{x} \ . \tag{2.46}$$

Let us consider $\{X_1, ..., X_N\}$ where each random variable is such that $X_n \sim \mathcal{U}([0,1])$ with $n = 1, ..., N$. Then, the integral (2.45) can be approximated by the average of the function f evaluated in these N points [7; 30]:

$$I_N[f] = \frac{1}{N} \sum_{n=1}^{N} f(X_n) \ . \tag{2.47}$$

We observe that $\{X_1, ..., X_N\}$ are independent and identically distributed (i.i.d) and

$$\mathbb{E}\big[I_N[f]\big] = I[f] \ . \tag{2.48}$$

Therefore, by the Strong Law of Large Numbers [15], we have

$$\mathbb{P}\Big(\lim_{N\to+\infty} I_N[f] = I[f]\Big) = 1 \ , \tag{2.49}$$

which states that the empirical approximation $I_N[f]$ converges almost surely to $I[f]$.
Moreover, according to the Central Limit Theorem [15], we obtain that

$$\frac{I_N[f] - I[f]}{\sigma_f/\sqrt{N}} \xrightarrow{d} N(0,1) \ , \tag{2.50}$$

where $N(0,1)$ is the standard normal distribution and σ_f is defined as

$$\sigma_f = \sqrt{\int_0^1 \big(f(x) - I[f]\big)^2 dx} \ . \tag{2.51}$$

Result (2.50) is equivalently claimed by the following theorem [7; 30].

Theorem 2.2.1. *Let us introduce the Monte Carlo integration error*

$$\epsilon_N[f] := I[f] - I_N[f].$$

If N is large,

$$\epsilon_N[f] \approx \sigma_f N^{-\frac{1}{2}} \nu$$

where ν is a normal random variable i.e. $\nu \sim N(0,1)$ and more precisely,

$$\lim_{N\to+\infty} \mathbb{P}\bigg(a < \frac{\sqrt{N}}{\sigma_f}\epsilon_N < b\bigg) = \mathbb{P}(a < \nu < b) = \frac{1}{\sqrt{2\pi}} \int_a^b e^{-\frac{x^2}{2}} dx \ .$$

This theorem states that the Monte Carlo integration error is $O(N^{-\frac{1}{2}})$ with a proportionality constant that is the variance of f. Moreover, this error is normally distributed. In the following, we prove $\epsilon_N[f] = O(N^{-\frac{1}{2}})$ [7; 30]. We recommend [15] from a complete proof of theorem 2.2.1.

Proof. Let us introduce the following random variables: $Z_n = \frac{f(X_n)-I[f]}{\sigma_f}$ where X_n are i.i.d., $X_n \sim \mathcal{U}([0,1])$ and $n = 1, ..., N$. Then, we have

$$\begin{aligned}
&\mathbb{E}[Z_n] = 0 \\
&\mathbb{E}[Z_n^2] = 1 \\
&\mathbb{E}[Z_n Z_m] = 0 \quad \text{if } n \neq m \ .
\end{aligned}$$

Moreover,

$$S_N = \frac{1}{N}\sum_{n=1}^{N} Z_n = \frac{1}{N}\sum_{n=1}^{N} \frac{f(X_n)-I[f]}{\sigma_f} = \frac{\epsilon_N[f]}{\sigma_f} \iff \epsilon_N[f] = \sigma_f S_N \tag{2.52}$$

and

$$\mathbb{E}[S_N^2] = \mathbb{E}\left[\frac{1}{N^2}\Big(\sum_{n=1}^{N} Z_n\Big)^2\right] = \frac{1}{N^2}\left\{\underbrace{\mathbb{E}\Big[\sum_{n=1}^{N} Z_n^2\Big]}_{=N\cdot 1} + \underbrace{\mathbb{E}\Big[\sum_{n=1}^{N}\sum_{m\neq n} Z_n Z_m\Big]}_{=0}\right\} = N^{-1} \ . \tag{2.53}$$

If the root mean square error ($RMSE$) is defined as $RMSE \coloneqq \sqrt{\mathbb{E}[\epsilon_N^2[f]]}$, we obtain

$$RMSE = \sqrt{\mathbb{E}[\epsilon_N^2[f]]} = \sqrt{\mathbb{E}[\sigma_f^2 S_N^2]} = \frac{\sigma_f}{\sqrt{N}} \ ,$$

where in the second and in the last equality, equation (2.52) and equation (2.53) have been used respectively. □

Remark 2.2.2. Theorem 2.2.1 is related to a one dimensional problem. If a problem in d dimensions is considered - see equation (2.46), an analogous result is obtained. The convergence rate is still $O(N^{-\frac{1}{2}})$ and the proportionality constant σ_f [7; 30]. □

Remark 2.2.3. Identical conclusions about the accuracy are drawn if the following integral is considered:

$$I[f] = \int_\Omega f(x)g(x)dx \ , \Omega \subseteq \mathbb{R}$$

where $g = g(x)$ is a probability density function. In this case, we consider $X \sim g(x)$ and therefore, $I[f] = \mathbb{E}[f(X)]$.
$\square$

Theorem 2.2.1 is a probabilistic result: the committed error can be assessed within some confidence interval. If we want to obtain a maximum error ϵ with confidence level c, the sample size has to be

$$N = \epsilon^{-2}\sigma_f^2 s(c) \tag{2.54}$$

where

$$c = \int_{-s(c)}^{s(c)} \frac{1}{\sqrt{2\pi}} e^{-\frac{x^2}{2}} dx = \operatorname{erf}\left(\frac{s(c)}{\sqrt{2}}\right) .$$

Usually, σ_f is unknown but it can be obtained empirically. The sample points $\{X_1^1, ..., X_N^1, X_1^2, ..., X_N^2, ..., X_1^M, ...X_N^M\}$ are considered and

$$\begin{aligned}
I_N^{(j)} &= \frac{1}{N}\sum_{i=1}^{N} f(X_i^{(j)}) \quad \text{where } j = 1, ..., M \\
\bar{I}_N &= \frac{1}{M}\sum_{j=1}^{M} I_N^{(j)} \\
\bar{\epsilon}_N &= \sqrt{\frac{1}{M}\sum_{j=1}^{M}\left(I_N^{(j)} - \bar{I}_N\right)^2} \\
\bar{\sigma}_f &= \sqrt{N}\bar{\epsilon}_N \ .
\end{aligned}$$

Now, let us compare the convergence rate of Monte Carlo methods with that of deterministic methods. It is consistently improved by the former indeed, it is $O(N^{-\frac{1}{2}})$ while grid-based methods lead to convergence rates which are $O(N^{-\frac{k}{d}})$, where k is the order of the method and d is the dimension [7]. By directly comparing these two accuracy rates, we have that in high-dimension and if $k/d < 1/2$, Monte Carlo wins over grid-based. This comparison is not significant if the function to be integrated is periodic, indeed in this case $k \to +\infty$. However, in high dimensions Monte Carlo methods are more suited to deal with these estimation problems than grid-based methods since it is extremely unpractical to conceive a grid and the convergence rate of MC methods does not depend on d [7].
It is worth pointing out that MC methods are global, since each point in the sample set $\{X_1, ..., X_N\}$ is selected over the whole domain. Instead, grid-based methods are local [7].

Monte Carlo methods are robust since their convergence rate just depends on N. On the other hand, they are extremely slow since their rate is $O(N^{-\frac{1}{2}})$. Two different kinds of strategies can be adopted to accelerate their convergence. The first are the so-called *variance reduction strategies* [7; 30]: they consist in reducing the proportionality constant σ_f in the convergence rate. Indeed, we observe that by theorem 2.2.1, $N = O(\sigma_f^2/\epsilon_N^2)$ and if σ_f decreases, so does N, which measures the computational time. The second class of strategies is the so-called *quasi-Monte Carlo* methods [7; 30]. In this case, the sequence of points $\{X_1, ..., X_N\}$, which allows to compute the approximation $I_N[f]$ of the integral, is quasi-random that means points are correlated. The convergence rate turns out to be $O(N^{-1}(\log N)^k)$ for a given k. We suggest [7; 30] for the discussion of *variance reduction strategies*.

2.3 Hands-on application: the Kac model

One classical example of application is the Kac model [25; 30]. The importance of this model relies on the fact that it is analytically solvable and it paves the way for further development of mathematical tools. Moreover, this model gives insight on the physical phenomena of chaos propagation.

Let us consider the binary interaction model studied in section 2.1.4 with the following interaction rules [30]:

$$\begin{aligned} v' &= \cos\theta v - \sin\theta w \\ w' &= \sin\theta v + \cos\theta w \ , \end{aligned} \tag{2.55}$$

where $\theta \sim \mathcal{U}\big([-2\pi,2\pi]\big)$ i.e. θ is a random variable which is uniformly distributed in the interval $[-2\pi,2\pi]$.
It is evident that the post interaction speeds (v', w') are the result of a rotation of the vector $\vec{x} = (v, w)$ by an angle θ. Therefore, the modulus of the velocity vector $\vec{x} = (v, w)$ is unchanged by the interaction:

$$(v')^2 + v^2 = (w')^2 + w^2 \tag{2.56}$$

and so, the conservation of energy follows [30].

Let us consider the following initial speed distribution [31]:

$$f_0(v) \equiv f(0, v) = \frac{2}{\sqrt{\pi}} v^2 e^{-v^2} \ . \tag{2.57}$$

We look for a solution of the Boltzmann equation

$$\partial_t f(t,v) = \int_{\mathbb{R}} \int_0^{2\pi} \frac{1}{2\pi} f(t, v\cos\theta - w\sin\theta) f(t, v\sin\theta + w\cos\theta) dw d\theta - f(t,v) \tag{2.58}$$

of the kind

$$f(t,v) = (A + Bv^2)e^{-C(t)v^2} \quad \text{with } A, B \in \mathbb{R} \ . \tag{2.59}$$

Then, if the conservation of mass and energy are imposed, an analytical solution $f(t,v)$ of the Boltzmann equation (2.58) can be obtained [31]:

$$f(t,v) = \frac{1}{2}\left[\frac{3}{2}\Big(1 - C(t)\Big)\sqrt{C(t)} + \Big(3C(t) - 1\Big)\Big(C(t)\Big)^{\frac{3}{2}} v^2\right] e^{-C(t)v^2} \tag{2.60}$$

where

$$C(t) = \left[3 - 2e^{-\sqrt{\pi}t/16}\right]^{-1} \ . \tag{2.61}$$

We recommend the Appendix A.1 of [31] for a complete derivation of $f(t,v)$.

In order to test this finding, numerical simulations are carried out. As explained in section 2.2, the Nanbu-Babovsky's scheme [29; 30] can be adopted. All simulations are carried out with MATLAB®.
The following parameters are chosen:

- $\epsilon = 1$, $\Delta t = 0.01$;
- number of particles $N = 10^5$;
- speed domain $[-6{,}6]$ is discretized in $N_v = 101$ points.

In figure 2.1 (p. 37), the initial distribution (2.57) and the one sampled from it are plotted. In figures 2.2 - 2.4 (pp. 37-38), the theoretical speed distribution $f(t,v)$ defined in (2.60) is compared with the numerical solution of the Boltzmann equation (2.58) for different final times: $t = 2,\ 5,\ 10$. Distributions are plotted by using a suited histogram. By qualitatively inspecting the plots, we can claim that if $t = 10$, the system has reached equilibrium indeed there is stability and the simulation speed distribution perfectly matches the theoretical one. In section 3.12, we will introduce a quantitative criterion in order to outline whether the system is in its stationary state.

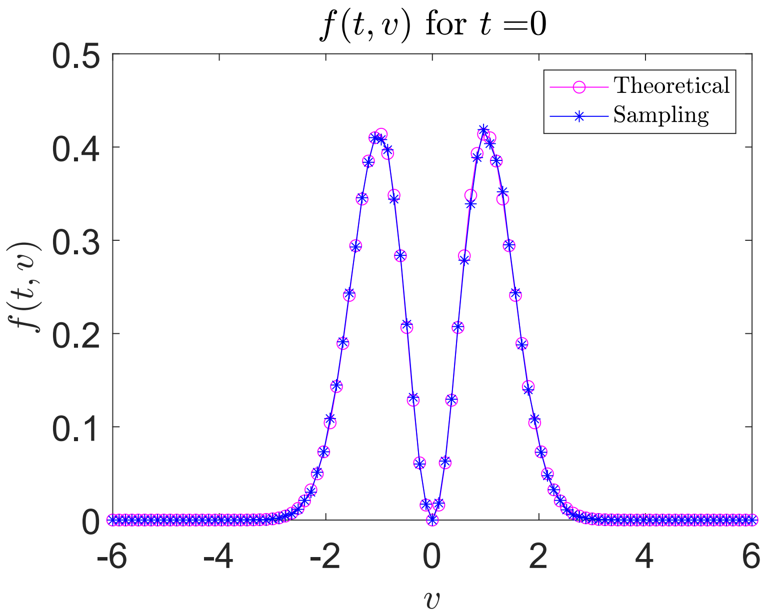

Figure 2.1: Comparison between the initial speed distribution (2.57) (theoretical) and the one sampled from it (sampling)

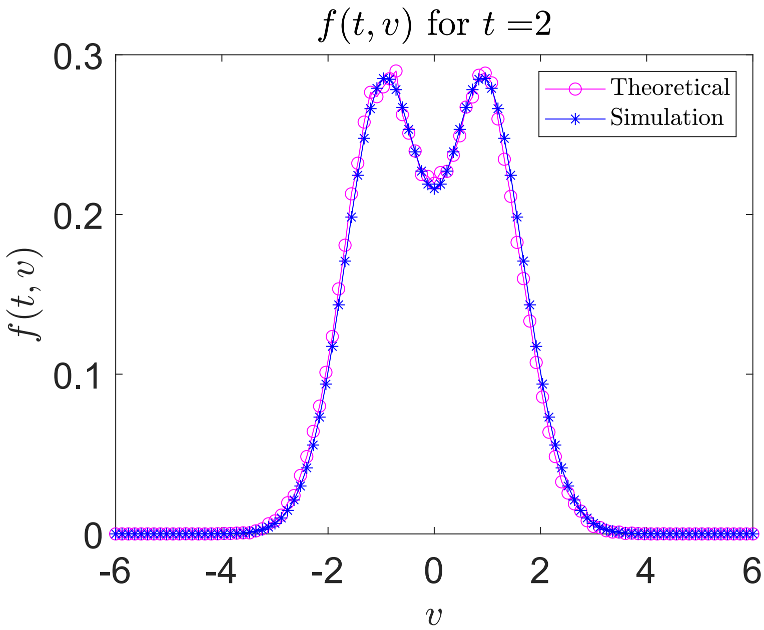

Figure 2.2: Comparison between the speed distribution (2.60) (theoretical) and the numerical solution of the Boltzmann equation (2.58) (simulation) for $t = 2$

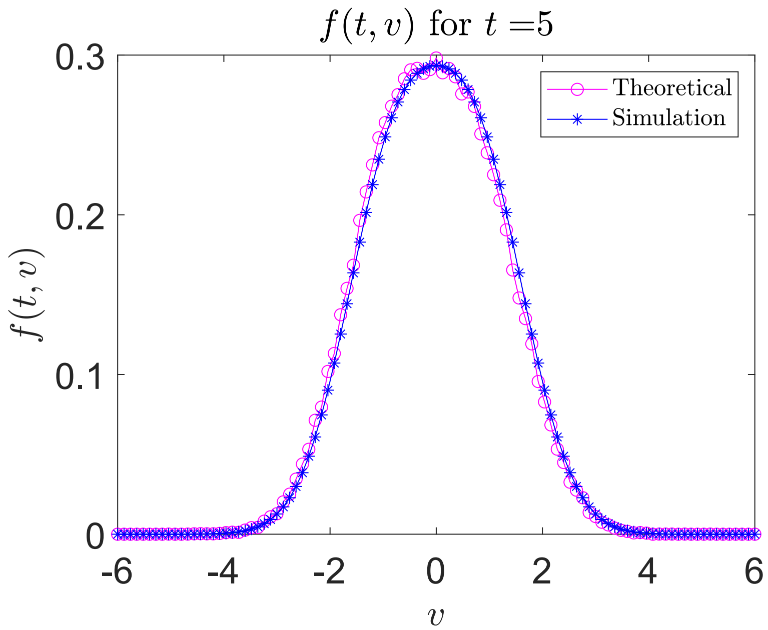

Figure 2.3: Comparison between the speed distribution (2.60) (theoretical) and the numerical solution of the Boltzmann equation (2.58) (simulation) for $t = 5$

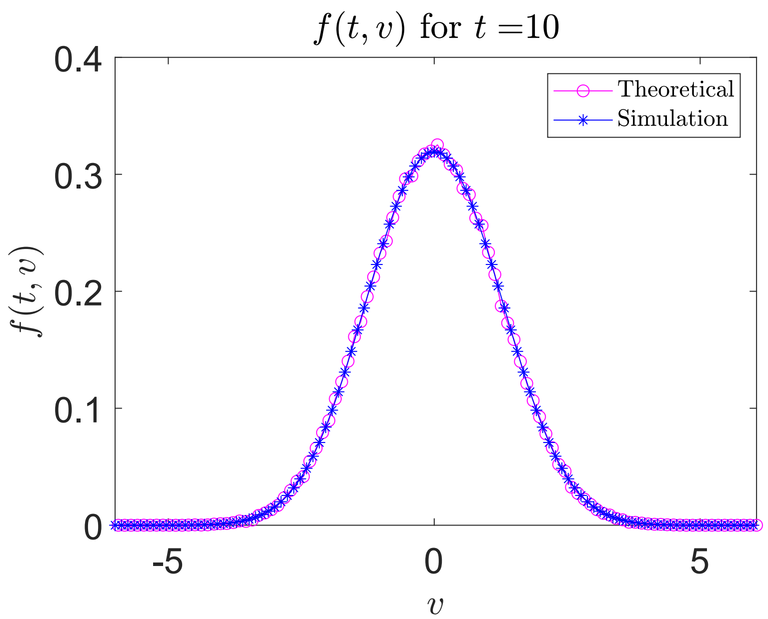

Figure 2.4: Comparison between the speed distribution (2.60) (theoretical) and the numerical solution of the Boltzmann equation (2.58) (simulation) for $t = 10$

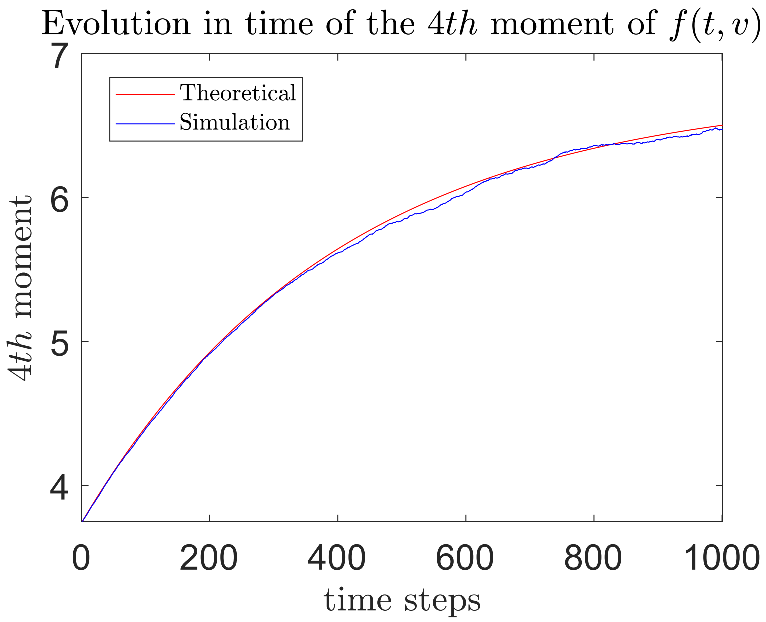

Figure 2.5: Comparison between the forth moment $m4^{TH}$ of $f(t,v)$ (theoretical) and $m4^{SIM}$ (simulation) as a function of time. They are both defined in (2.62)

In figure 2.5, the forth moment of $f(t,v)$ is plotted as a function of time. It is defined as follows:

$$
\begin{aligned}
m4^{TH}(t) &\equiv \sum_{k=1}^{N_v} V_k^4 f(t,V_k)dv \\
m4^{SIM}(t) &\equiv \frac{1}{N}\sum_{i=1}^{N} v_i^4(t)\ ,
\end{aligned}
\tag{2.62}
$$

where TH stands for theoretical, SIM stands for simulation, V_k with $k=1,...N_v$ are the points of the discretized speed domain, dv is the speed step of the discretized speed domain and $v_i(t)$ with $i=1,...N$ are the particles' speed which are obtained numerically at each time step. We observe that the numerical forth moment fluctuates around theoretical values with an error that depends on the number of agents N and the time step Δt. Due to the Monte Carlo trait of the Nanbu-Babovsky's scheme, we expect that the error is $O(N^{-\frac{1}{2}})$.

Contrary to moments of order $k \leq 3$, the forth moment is not conserved in the Kac model and it increases with time.

Chapter 3

Kinetic traffic modeling

Since the sixties, the mesoscopic approach has been adopted to study traffic modeling and it has revealed its potentialities compared to the traditional macroscopic and microscopic strategies.

In this chapter, the traffic model, which represents the basis for this dissertation, is explained referring to [45; 46; 47]. The main research methodologies which will be employed for successive studies, are examined in depth. In more detail, after providing an overview about traffic modeling, the subsequent five sections are devoted to study an uncontrolled system i.e. a system without autonomous vehicles. Then, the controlled case is investigated in other five sections. In the penultimate section, all theoretical findings are numerically validated. Finally, conclusions are drawn.

3.1 Vehicular traffic modeling and the kinetic approach

Among the several applications of the kinetic approach, traffic modeling is gaining importance. Understanding vehicular traffic has social and economic consequences: it can lead to replan urban mobility in order to consider environmental and management issues. Due to its complexity, a phenomenological approach is not sufficient to tackle this problem. Even though data and experimental observations give insight into the physics of traffic, this approach is not predictive and it does not provide an exhaustive description of the unsteady dynamics of traffic. A theoretical strategy, which relies on mathematical modeling, is required [32].

Several approaches can be adopted in order to study vehicular traffic.

They are characterized by different scales of the representation and different approximations. The microscopic approach consists in considering the detailed dynamics: a set of second-order differential equations is considered and each of them is associated to each agent [32]. Therefore, as the number of agents increases, so does the number of motion equations thus making this approach not competitive from a computational point of view and difficult to handle analytically.

In order to overcome these difficulties, the macroscopic approach can be employed: it does not trace each agent but it considers the evolution of macroscopic quantities of the system such as the traffic density and the traffic flux [32]. This approach relies on the *continuum hypothesis*, which assumes the Knudsen number being much smaller than 1: $\epsilon << 1$ [32]. Due to the fact that this parameter is defined as the ratio between the mean free path of an agent and the characteristic dimension of the flow, it is equivalent to assume that the latter is much bigger than the former. Therefore, macroscopic quantities are defined as continuous space functions. More computational efficiency than the microscopic approach comes along with less modeling accuracy.

When the Knudsen number is of the order of the unity i.e. $\epsilon \sim 1$, kinetic modeling can be used [32]. This approach is based on the Boltzmann equation, which was firstly introduced to study rarefied gas. The scale of representation is the mesoscopic one: the object of interest is the speed distribution function and the collision kernel of the Boltzmann-type equation depends on the microscopic interactions rules. Starting from this equation, macroscopic quantities and their evolution are derived. Collective behaviors naturally emerge and they are the result of the microscopic interactions between agents.

3.1.1 An overview of pioneering kinetic traffic models

Kinetic traffic models are based on common assumptions [32]. An asymptotic number of indistinguishable and point-like vehicles is considered. Each of them is equipped with a speed and once it binary interacts with others, only its speed changes according to interaction rules. Interactions are purely binary, anisotropic and conservative.

The Prigogine model [32] is one of the first works of traffic modeling with

a Boltzmann-type kinetic approach. It is mainly based on a collision kernel made up of two contributions, a relaxation and an interaction term, and on the *vehicular chaos hypothesis*, which assumes uncorrelated vehicles. The relaxation term in the collision operator has been criticized by subsequent models, due to the fact that it is function of a desired speed distribution, which is given a priori. The Paveri Fontana model [32] overcomes this issue by introducing a further variable, which represents the desired speed and thus, considering its dependency on the system's evolution.
However, Prigogine and Paveri Fontana models are not suited to properly describe inhomogeneous traffic flows. Due to the physical constraint which requires velocities to be greater than or equal to 0, the traffic flow only propagates in the positive direction of the spatial axis. This is in strike contrast with experience, where traffic jams travel backwards [24]. This issue is tackled by Klar and coworkers by referring to Enskog-like models of dense gases [32]: the speed distribution associated to the spatial coordinate x also depends on what happens at $x' > x$.

In this chapter, we will dwell upon traffic modeling with a Boltzmann-type kinetic approach by referring to [45; 46; 47]. These papers were recently published and investigated the introduction of autonomous vehicles as a tool to mitigate road risk. The development of autonomous vehicles is extremely promising for their lower environmental impact and their potentiality to mitigate road risk: it will lead to a reshape and innovation of our urban mobility.

3.2 Interaction rules

The basis of this dissertation is the Boltzmann-type kinetic equation for binary interactions, which is explained in subsection 2.1.4.

Let us introduce $f = f(t,v)$, which is the speed distribution function. It is such that $f(t,v)dv$ is the relative number of agents which have a speed in the interval $[v, v + dv]$ at time $t \geq 0$. The speed as other quantities, such as the traffic density ρ, are dimensionless: we assume that $v, \rho \in [0,1]$ [46].

The interaction rules represent the core of kinetic models: they contain the physics of the system and express how the microscopic state of each agent changes. They are defined as [46]

$$\begin{aligned} v' &= v + \gamma I(v, w; \rho) + D(v; \rho)\eta \\ w' &= w \end{aligned} \tag{3.1}$$

where v and w are the speeds of vehicles before the interaction while v' and w' represent their post-interaction speeds. The coefficient $\gamma > 0$ is a proportionality parameter, while η is a centered random variable, with zero mean and variance σ^2 and $D(v;\rho) \geq 0$ is a diffusion coefficient. Thanks to the term $D(v;\rho)\eta$, a stochastic component is included in the model, allowing to consider the intrinsic stochasticity in each agent's behavior.

The function $I(v, w; \rho)$ is the interaction function and it is defined as [46]

$$I(v, w; \rho) = P(\rho)(1 - v) + (1 - P(\rho))(P(\rho)w - v) \ , \tag{3.2}$$

where $P(\rho)$ is the probability of accelerating [46]

$$P(\rho) = (1 - \rho)^{\mu}, \mu > 0 \ . \tag{3.3}$$

In figure 3.1, the probability of accelerating is displayed for different values of the exponent μ. It is a decreasing function of the traffic density ρ and when numerical tests are performed, the exponent μ is chosen equal to 2. This choice will be cleared up in the following.

From (3.1), it is clear that binary interactions are based on the *follow-the-leader approach* [18]: they are anisotropic, so the leading vehicle i.e. the agent with speed w does not change its speed while the rear vehicle i.e. the agent with speed v does. Referring to the terminology of [32], the vehicle with speed v is the candidate vehicle while the one with speed w is the field vehicle. Due to the anisotropic character of traffic interactions,

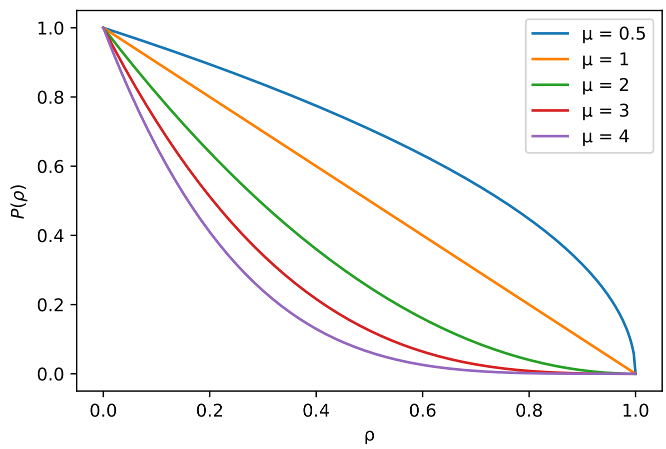

Figure 3.1: Probability of accelerating (3.3) for different parameters μ

binary interactions only occur for candidate vehicles which are ahead of field vehicles.

The interaction function defined in (3.2) expresses that: for small densities i.e. when $P(\rho)$ approaches 1, the rear vehicle tends to the maximum allowed speed i.e. 1, while when the density increases i.e. when $P(\rho)$ tends to 0, it tends to a fraction of the speed of the leading vehicle and this fraction is given by the probability of accelerating $P(\rho)$. These interaction rules also contain a stochastic part that models diffusive behaviors [46].

3.3 Physical admissibility of the interaction rules

Once that the binary interaction rules are defined, their physical admissibility has to be checked. This is equivalent to identify the criteria for which post-interaction speeds satisfy the physical constraint i.e. v', $w' \in [0,1]$. In [46], the following proposition is stated and proved.

Proposition 3.3.1. *Let us consider the interaction rules defined in* (3.1) *and let us assume that* $\gamma \in [0,1]$.
If $\exists c > 0$ *such that*

$$\begin{cases} |\eta| \leq c(1-\gamma) \\ cD(v;\rho) \leq \min\{v,1-v\}, \ \forall v,\rho \in [0,1] \end{cases}$$

then the interaction rules satisfy the physical admissibility requirement i.e. v', $w' \in [0,1]$ $\forall v,w \in [0,1]$ *and* $\forall \rho \in [0,1]$.

Proof. First of all, we observe that $w' = w \in [0,1]$.

Let us start to prove that

$$v' \geq 0 \iff v + \gamma\Big[P(\rho)(1-v) + (1-P(\rho))(P(\rho)w - v)\Big] + D(v;\rho)\eta \geq 0.$$

We observe that $\gamma P(\rho)$, $P(\rho)w \geq 0$ therefore,

$$v - \gamma\Big[P(\rho)v + (1-P(\rho))v\Big] + D(v;\rho)\eta \geq 0 \iff (1-\gamma)v + D(v;\rho)\eta \geq 0$$

$$\implies v' \geq 0.$$

By hypothesis, $\exists c > 0$ such that $\eta \geq -c\underbrace{(1-\gamma)}_{\leq 0}$ and $D(v;\rho) \leq \frac{v}{c}$. This implies that the sufficient condition for $v' \geq 0$ becomes

$$(1 - \gamma)v + D(v;\rho)\eta \geq (1-\gamma)v + \tfrac{v}{c}c(\gamma-1) = 0.$$

Analogously, let us prove that $v' \leq 1$. Due to the fact that $P(\rho)w \leq 1$, a sufficient condition for $v' \leq 1$ is

$$v + \gamma\Big[P(\rho)(1-v) + (1-P(\rho))(1-v)\Big] + D(v;\rho)\eta \leq 1 \iff$$

$$\iff (\gamma-1)(1-v) + D(v;\rho)\eta \leq 0.$$

By using the hypothesis $\exists c > 0$ such that $\eta \leq c(1-\gamma)$ and $D(v;\rho) \leq \frac{1-v}{c}$, we obtain

$$(\gamma-1)(1-v) + D(v;\rho)\eta \leq (\gamma-1)(1-v) + \tfrac{1-v}{c}c(1-\gamma) = 0.$$

$\square$

Proposition 3.3.1 implies that: $\eta \in [-c(1-\gamma), c(1-\gamma)]$ i.e. it is a random variable with compact support [46]. This is coherent with the fact that η has zero mean i.e. $\langle\eta\rangle = 0$. Moreover, proposition 3.3.1 also implies that $D(v=0;\rho) = D(v=1;\rho) = 0 \ \forall\rho \in$ [0,1] [46]. This point will be taken into account when the diffusion coefficient $D(v;\rho)$ will be chosen - see remark 3.6.1.

3.4 Mean speed at equilibrium

The Boltzmann-type kinetic equation for binary interaction models can be written. We refer to [30] and to the derivation of equation (2.33) explained in detail in subsection 2.1.4.

This equation rules the evolution of the distribution function $f = f(t,v)$. If $\phi = \phi(v)$ is a generic observable, the equation in weak form [30; 46] is

$$\frac{d}{dt}\int_0^1 \phi(v)f(t,v)dv = \frac{1}{2}\langle\int_0^1\int_0^1 [\phi(v')+\phi(w')-\phi(v)-\phi(w)]f(t,v)f(t,w)dvdw\rangle \tag{3.4}$$

where $\langle\cdot\rangle$ is the expectation with respect to the distribution of the centered random variable η. A constant *interaction kernel* has been chosen i.e. $\mu = 1$ and this is equivalent to consider *Maxwellian interactions* in the framework of the kinetic theory of rarefies gases [9; 11]. In traffic, this assumption is justified since speeds of interacting vehicles can be realistically considered as uncorrelated. We also observe that $\phi(w') - \phi(w) = 0$, due to (3.1).

First, let us consider $\phi(v) = 1$. In this case,

$$\frac{d}{dt}\int_0^1 \phi(v) f(t,v) dv = 0 \ . \tag{3.5}$$

This means that, given the initial speed distribution $f_0(v) := f(t = 0, v)$ properly normalized, $f(t,v)$ will be normalized and therefore, a distribution probability $\forall t > 0$ [46].

Instead, if $\phi(v) = v$, an equation which rules the evolution of the mean speed will be derived. Let us define the mean speed as [46]

$$V(t) := \int_0^1 v f(t,v) dv \ . \tag{3.6}$$

Then, by plugging $\phi(v) = v$ in (3.4), we end up with the following equation [46]:

$$\frac{d}{dt}V(t) = \frac{\gamma}{2}\Big\{P(\rho)\big[1 + \big(1 - P(\rho)\big)V(t)\big] - V(t)\Big\} \ . \tag{3.7}$$

Equation (3.7) is an ordinary differential equation (ODE), which is equipped with the initial condition

$$V_0 := V(t = 0) = \int_0^1 v f_0(v) dv \ . \tag{3.8}$$

Therefore, the solution of (3.7) is

$$\begin{aligned} V(t) = V_0 \exp\Big\{ -\frac{\gamma}{2}\big[P(\rho) + (1 - P(\rho))^2\big]t\Big\} + \\ + \frac{P(\rho)}{P(\rho) + (1 - P(\rho))^2}\Big(1 - \exp\Big\{ -\frac{\gamma}{2}\big[P(\rho) + (1 - P(\rho))^2\big]t\Big\}\Big) \ . \end{aligned} \tag{3.9}$$

If $t \to +\infty$, the mean speed at equilibrium is obtained [46]:

$$V_\infty(\rho) = \frac{P(\rho)}{P(\rho) + (1 - P(\rho))^2} \ . \tag{3.10}$$

This quantity allows to derive the *speed* and the *fundamental diagrams*.

Remark 3.4.1. From (3.9), it is clear that the first moment of the speed distribution i.e. the mean speed $V(t)$ is not conserved. □

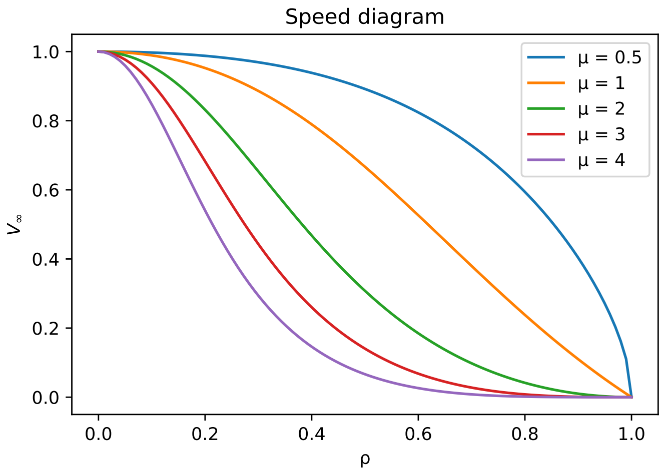

Figure 3.2: Speed diagram for different parameters μ

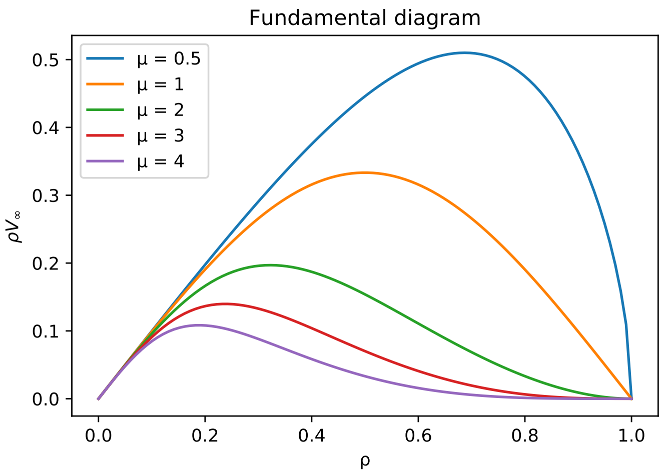

Figure 3.3: Fundamental diagram for different parameters μ

3.5 Speed and fundamental diagrams

The *speed* and the *fundamental diagrams* are macroscopic relations, based on the mean speed at equilibrium $V_\infty(\rho)$. The former is the mapping $\rho \mapsto V_\infty(\rho)$, while the latter is $\rho \mapsto q = \rho V_\infty(\rho)$, where q is the flux of vehicles at a given density [32; 46]. The flux q is central since it is usually the most precise measurable quantity [32].

Several criteria, which make the diagrams compatible with experimental data, can be outlined [32]:

- the flux $q = q(\rho)$ should be monotonically increasing in the density interval $[0, \bar{q}]$, where $\bar{q} \in (0,1)$;
- the flux $q = q(\rho)$ should be decreasing in the density interval $[\bar{q},1]$;
- the maximum $\bar{q}$ of the flux q should be unique;
- the flux $q = q(\rho)$ should be concave for $\rho \in [0,1]$.

The last property is not so strict [32]: sometimes q is allowed to be convex in the density interval $[\bar{q},1]$.

We refer to these criteria when the parameter μ, which enters the definition of the probability of accelerating $P(\rho)$, is set. In figures 3.2 - 3.3 (p. 48), *speed* and *fundamental diagrams* are displayed for different values of μ. Except for the cases $\mu = 0.5$ and $\mu = 1$, other values of the exponent μ lead to convex flux in the decreasing branch. If $\mu = 0.5$, the mean speed at equilibrium is not really meaningful since it takes values greater than 0.8 for more than 60% of the density interval; therefore this case is excluded. On the other hand, $\mu = 1$ roughly models the probability of accelerating. So, $\mu = 2$ is chosen: it is more suited to describe our dynamics compared to the other cases, which lead to similar diagrams, since it captures all aspects without being too extreme.

3.6 The quasi-invariant interaction regime and the asymptotic speed distribution

The object of the homogeneous Boltzmann-type equation (3.4) is the speed distribution function $f(t, v)$. In particular, we are interested in the asymptotic speed distribution $f_\infty = f_\infty(v)$, which represents the distribution at equilibrium and is the solution of

$$\frac{1}{2}\langle \int_0^1 \int_0^1 [\phi(v') - \phi(v)] f_\infty(v) f_\infty(w) dv dw \rangle = 0 \ . \tag{3.11}$$

Due to its complexity and its high-resolution in time, it is extremely difficult to solve equation (3.11) analytically and the *quasi-invariant interaction regime* is usually adopted e.g. [12; 42; 46; 47]. In this limit, attributes' agents result to be weakly modified by interactions and the Boltzmann-type integro-differential equation is approximated by a Fokker-Planck partial differential equation (PDE), which can be solved analytically.

This regime corresponds to an adjustment of the so-called *grazing collisions regime*, which was deeply investigated by Cedric Villani in the classical kinetic theory of rarefied gases [49]. Collisions between molecules are mainly tangential and so, the momentum transfer is small. In [49], the Fokker-Planck equation is derived from the Boltzmann equation in this regime; this is performed for several interacting potentials and with a more general reach of previous works.

In the context of complex systems modeling, the *quasi-invariant interaction regime* was first investigated in the context of a market economy [12] and then, it has been adopted for other problems such as opinion modeling [42] and traffic modeling [46; 47]. Both in [12] and in [42], the authors carried a detailed analysis of the evolution of the first moment - the average wealth and the average opinion respectively - and higher moments. By means of measure theory's results, they showed the difficulty of studying in detail the distribution function of agents' attributes. Therefore, they relied on kinetic theory and in particular, on *grazing interactions*, in order to obtain a more easily solvable asymptotics of the Boltzmann-type equation.

In the *quasi-invariant interaction regime*, we assume [46]

$$\gamma, \sigma^2 \to 0^+ \text{ such that } \frac{\sigma^2}{\gamma} \to \lambda > 0 \; . \tag{3.12}$$

From a physical point of view, this is equivalent to claim that $v' \simeq v$ i.e. after an interaction, the rear vehicle has a speed v' which is close to its initial speed v. The balance condition, which defines λ, is fundamental to ensure that both the deterministic and the stochastic component of interaction rules are relevant. Only in this way, we obtain an asymptotic speed distribution which is the direct consequence of the microscopic binary interactions (3.1).

Let us define the following time scale: $\tau := \frac{\gamma}{2}t$ [46]. If $\gamma \to 0^+$, τ is a time scale much smaller than t and with bigger interaction frequencies: indeed, in the t scale, interactions occur as $1/t = O(1)$ while in the τ scale, they occur with frequency $1/\tau = O(1/\gamma) >> 1$.
Let us introduce the scaled distribution function $\tilde{f}(\tau, v) := f(2\tau/\gamma, v)$ [46]. Due to the fact that $\partial_\tau \tilde{f} = \frac{2}{\gamma}\partial_t f$, equation (3.4) can be rewritten as

$$\frac{d}{d\tau}\int_0^1 \phi(v)\tilde{f}(\tau, v)dv = \frac{1}{\gamma}\langle \int_0^1 \int_0^1 [\phi(v') - \phi(v)]\tilde{f}(\tau, v)\tilde{f}(\tau, w)dvdw\rangle \; . \tag{3.13}$$

Let us assume that the observable $\phi(v)$ is such that $\phi(v) \in C^3([0,1])$. Then, the condition $v' \simeq v$ allows us to perform a Taylor expansion of $\phi(v')$ in the vicinity of v [46]:

$$\phi(v') = \phi(v) + \phi'(v)(v'-v) + \frac{1}{2}\phi''(v)(v'-v)^2 + \frac{1}{3!}\phi'''(\bar{v})(v'-v)^3 \ , \tag{3.14}$$

where $\bar{v} \in (\min\{v',v\}, \max\{v',v\})$ and $v'-v = \gamma I(v,w;\rho) + \eta D(v;\rho)$. Expansion (3.14) can be plugged in (3.13) and therefore, we obtain

$$\begin{aligned}
\frac{d}{d\tau}\int_0^1 \phi(v)\tilde{f}(\tau,v)dv &= \int_0^1\int_0^1 \phi'(v)I(v,w;\rho)\tilde{f}(\tau,v)\tilde{f}(\tau,w)dvdw+ \\
&+ \frac{1}{\gamma}\underbrace{\langle\eta\rangle}_{=0}\int_0^1 \phi'(v)D(v;\rho)\tilde{f}(\tau,v)dv \underbrace{\int_0^1 \tilde{f}(\tau,w)dw}_{=1} + \\
&+ \frac{\gamma}{2}\int_0^1\int_0^1 \phi''(v)I^2(v,w;\rho)\tilde{f}(\tau,v)\tilde{f}(\tau,w)dvdw+ \\
&+ \frac{1}{2\gamma}\underbrace{\langle\eta^2\rangle}_{=\sigma^2}\int_0^1 \phi''(v)D^2(v;\rho)\tilde{f}(\tau,v)dv+ \\
&+ \underbrace{\langle\eta\rangle}_{=0}\int_0^1\int_0^1 \phi''(v)I(v,w;\rho)D(v;\rho)\tilde{f}(\tau,v)\tilde{f}(\tau,w)dvdw+ \\
&+ \frac{1}{6\gamma}\langle\int_0^1\int_0^1 \phi'''(\bar{v})\big[\gamma I(v,w;\rho)+\eta D(v;\rho)\big]^3\tilde{f}(\tau,v)\tilde{f}(\tau,w)dvdw\rangle \ ,
\end{aligned} \tag{3.15}$$

which can be equivalently written as [46]

$$\begin{aligned}
\frac{d}{d\tau}\int_0^1 \phi(v)\tilde{f}(\tau,v)dv &= \int_0^1\int_0^1 \phi'(v)I(v,w;\rho)\tilde{f}(\tau,v)\tilde{f}(\tau,w)dvdw+ \\
&+ \frac{\sigma^2}{2\gamma}\int_0^1 \phi''(v)D^2(v;\rho)\tilde{f}(\tau,v)dv + R_\phi(\tilde{f},\tilde{f}) \ ,
\end{aligned} \tag{3.16}$$

where $R_\phi(\tilde{f},\tilde{f})$ is the remainder and it is defined as [46]

$$\begin{aligned}
R_\phi(\tilde{f},\tilde{f}) \coloneqq &\frac{\gamma}{2}\int_0^1\int_0^1 \phi''(v)I^2(v,w;\rho)\tilde{f}(\tau,v)\tilde{f}(\tau,w)dvdw+ \\
&+ \frac{1}{6\gamma}\langle\int_0^1\int_0^1 \phi'''(\bar{v})\big[\gamma I(v,w;\rho)+\eta D(v;\rho)\big]^3\tilde{f}(\tau,v)\tilde{f}(\tau,w)dvdw\rangle \ .
\end{aligned} \tag{3.17}$$

Both the interaction and the diffusion functions are bounded. By considering the definition (3.2), it is clear that $|I(v,w;\rho)| \le 1 \ \forall v,w,\rho \in [0,1]$. On the other hand, $cD(v;\rho) \le \min\{v, 1-v\}$ because of physical admissibility criteria 3.3.1. We also know that $\phi \in C^3([0,1])$, which implies that

$\phi, \phi', \phi'', \phi'''$ are bounded in the speed interval [0,1]. Finally, let us assume that $\langle|\eta|^3\rangle < +\infty$ and let us write $\eta = \tilde{\eta}\sqrt{\sigma^2}$, where $\tilde{\eta}$ is a random variable with zero mean, unitary variance and finite third moment [46]. So, $\langle|\eta|^3\rangle \sim (\sigma^2)^{\frac{3}{2}}$. Consequently, we obtain

$$\exists K > 0 \text{ such that } |R_\phi(\tilde{f}, \tilde{f})| \leq K\left\{\gamma + \gamma^2 + \sigma^2 + \frac{\sigma^2}{\gamma}\sqrt{\sigma^2}\right\}. \tag{3.18}$$

In the *quasi-invariant interaction regime* (3.12), the remainder $R_\phi(\tilde{f}, \tilde{f})$ tends to 0. Therefore, equation (3.16) becomes

$$\begin{aligned}\frac{d}{d\tau}\int_0^1 \phi(v)\tilde{f}(\tau, v)dv = \int_0^1 \phi'(v)\Big(\int_0^1 I(v, w; \rho)\tilde{f}(\tau, w)dw\Big)\tilde{f}(\tau, v)dv+\\ +\frac{\lambda}{2}\int_0^1 \phi''(v)D^2(v; \rho)\tilde{f}(\tau, v)dv\end{aligned} \tag{3.19}$$

and it can be integrated by parts, in order to obtain a Fokker-Planck PDE [46]. Therefore, we get

$$\begin{aligned}&\int_0^1 \phi(v)\partial_\tau\tilde{f}dv = \phi(v)\Big(\int_0^1 I(v, w; \rho)\tilde{f}(\tau, w)dw\Big)\tilde{f}(\tau, v)\Big|_{v=0}^{v=1}+\\ &-\int_0^1 \phi(v)\partial_v\Big(\big(\int_0^1 I(v, w; \rho)\tilde{f}(\tau, w)dw\big)\tilde{f}(\tau, v)\Big)dv+\\ &+\frac{\lambda}{2}\Big\{\phi'(v)D^2(v, \rho)\tilde{f}(\tau, v)\Big|_{v=0}^{v=1} - \phi(v)\partial_v\Big(D^2(v; \rho)\tilde{f}(\tau, v)\Big)\Big|_{v=0}^{v=1}+\\ &+\int_0^1 \phi(v)\partial_v^2\Big(D^2(v; \rho)\tilde{f}(\tau, v)\Big)dv\Big\},\end{aligned} \tag{3.20}$$

which can be rewritten as [46]

$$\partial_\tau\tilde{f} = \frac{\lambda}{2}\partial_v^2\Big(D^2(v; \rho)\tilde{f}\Big) - \partial_v\Big(\big(\int_0^1 I(v, w; \rho)\tilde{f}(\tau, w)dw\big)\tilde{f}\Big) \tag{3.21}$$

with the following boundary conditions:

$$\begin{cases}\big(\int_0^1 I(v, w; \rho)\tilde{f}(\tau, w)dw\big)\tilde{f}(\tau, v) + \frac{\lambda}{2}\partial_v\Big(D^2(v; \rho)\tilde{f}(\tau, v)\Big) = 0\\ D^2(v; \rho)\tilde{f}(\tau, v) = 0\ ,\end{cases} \tag{3.22}$$

which have to hold for $v = 0{,}1\ \forall\tau > 0$.

Let us plug the interaction function (3.2) in (3.21) and let us introduce $\tilde{V}(\tau) = V(2\tau/\gamma)$ i.e. the scaled mean speed [46]. Then, the final form of the Fokker-Planck PDE is

$$\partial_\tau \tilde{f} = \frac{\lambda}{2}\partial_v^2\Big(D^2(v;\rho)\tilde{f}\Big) - \partial_v\bigg\{\Big[P(\rho)\Big(1 + \big(1 - P(\rho)\big)\tilde{V}\Big) - v\Big]\tilde{f}\bigg\} \ . \tag{3.23}$$

If the asymptotic limit i.e. $\tau \to +\infty$ is considered, then $\tilde{V} \to V_\infty(\rho)$, which is reported in (3.10). Moreover, we have

$$V_\infty(\rho)\Big[P(\rho)+(1-P(\rho))^2\Big] = P(\rho) \iff V_\infty(\rho) = P(\rho)\Big[1+\big(1-P(\rho)\big)V_\infty(\rho)\Big] \ . \tag{3.24}$$

So, if $\tau \to +\infty$, the Fokker-Planck equation (3.23) becomes

$$\frac{\lambda}{2}\partial_v^2\Big(D^2(v;\rho)\tilde{f}_\infty\Big) - \partial_v\Big(\big(V_\infty(\rho) - v\big)\tilde{f}_\infty\Big) = 0 \ . \tag{3.25}$$

For the diffusion coefficient, the following form is chosen [46]:

$$D(v;\rho) := a(\rho)\sqrt{v(1-v)} \ , a(\rho) \geq 0 \ . \tag{3.26}$$

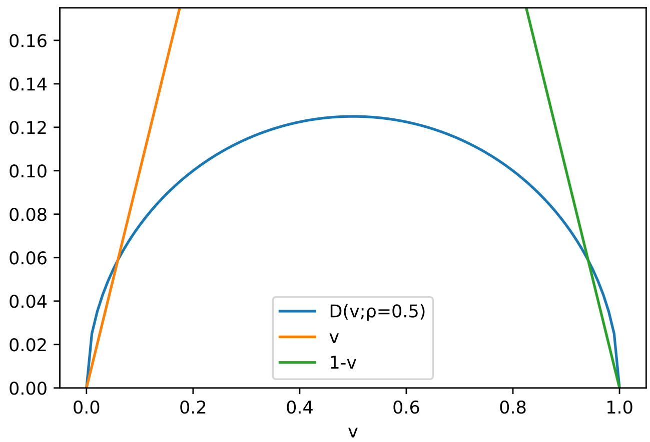

Figure 3.4: The diffusion coefficient (3.26) with $\rho = 0.5$, $a(\rho) = \rho(1-\rho)$ together with the straight lines v and $1 - v$

Remark 3.6.1. The diffusion coefficient must satisfy proposition 3.3.1, in order to ensure physical admissibility of the interaction rules (3.1).
If we consider figure 3.4, it is evident that

$$\nexists c > 0 \text{ such that } cD(v;\rho) \leq \min\{v,1-v\} \ \forall v,\rho \in [0,1] \ .$$

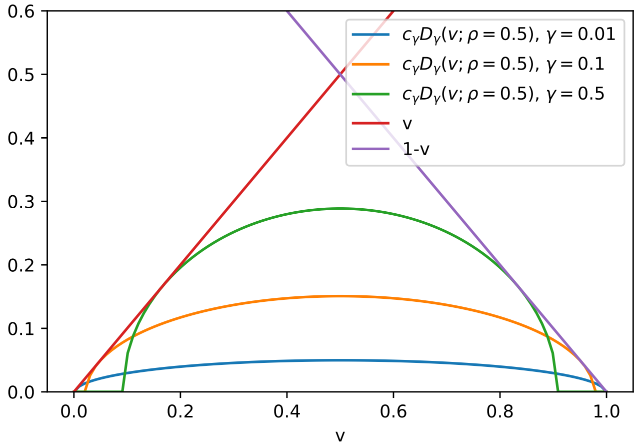

Figure 3.5: The diffusion coefficient (3.27) with $\rho = 0.5$, $a(\rho) = \rho(1-\rho)$ and for different parameters γ, together with the straight lines v and $1-v$

In particular, the physical admissibility property does not hold for speeds in the neighborhood of $v = 0$ and $v = 1$. This is clear from figure 3.4 where the diffusion coefficient (3.26) is plotted by considering $a(\rho) = \rho(1-\rho)$, a choice which will be motivated in the following.
So, let us consider the γ-dependent diffusion coefficient [46]

$$D_\gamma(v;\rho) \coloneqq a(\rho)\sqrt{\max\left\{0, (1+\gamma)v(1-v) - \frac{\gamma}{4}\right\}}\ , \tag{3.27}$$

which satisfies proposition 3.3.1 with $c = c_\gamma \coloneqq \frac{1}{a(\rho)}\sqrt{\frac{\gamma}{1+\gamma}}$. A graphical representation of this fact is given in figure 3.5.
Actually, in the *quasi-invariant interaction regime*, we have

$$D_\gamma(v;\rho) \to D(v;\rho) \quad \text{if } \gamma \to 0^+ \ .$$

Therefore, the choice (3.26) is physical admissible in the *quasi-invariant interaction regime*. □

Eventually, the asymptotic speed distribution turns out to be a beta probability density function [46]

$$\tilde{f}_\infty(v) = \frac{v^{\alpha-1}(1-v)^{\beta-1}}{B(\alpha,\beta)}\ , \tag{3.28}$$

with the following parameters [46]:

$$
\begin{aligned}
\alpha &:= \frac{2V_\infty(\rho)}{\lambda a^2(\rho)} \\
\beta &:= \frac{2(1-V_\infty(\rho))}{\lambda a^2(\rho)}
\end{aligned}
\tag{3.29}
$$

and $B(\alpha,\beta)$ is the beta function i.e. $B(\alpha,\beta) = \int_0^1 x^{\alpha-1}(1-x)^{\beta-1}dx$.

Let us note that (3.25) is accompanied with boundary conditions (3.22). These conditions are satisfied if [46]

$$
a^2(\rho) \le \frac{1}{\lambda}\min\{V_\infty(\rho), 1-V_\infty(\rho)\}\ . \tag{3.30}
$$

Indeed, if (3.30) holds, the asymptotic distribution function $\tilde{f}_\infty$ and its derivative $\partial_v \tilde{f}_\infty$ are null in the extreme values of the speed domain i.e. $v = 0, 1$ [46]. A suited choice of the function $a(\rho)$, which satisfies (3.30), is $a(\rho) = \rho(1-\rho)$ [46].

In figure 3.6, the asymptotic speed distribution (3.28) is plotted for different values of densities.

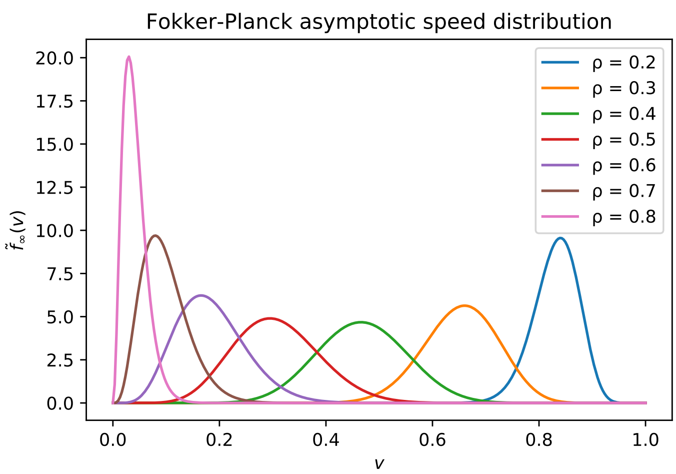

Figure 3.6: The asymptotic speed distribution (3.28) for different values of densities, $\lambda = 1$, $\mu = 2$, $a(\rho) = \rho(1-\rho)$

If X is a random variable such that $X \sim \tilde{f}_\infty$,

$$
\begin{aligned}
\mathbb{E}[X] &= \frac{\alpha}{\alpha+\beta} = V_\infty(\rho) \\
\mathrm{Var}(X) &= \frac{\alpha\beta}{(\alpha+\beta)^2(\alpha+\beta+1)} = \frac{\lambda a^2(\rho)}{2+\lambda a^2(\rho)} V_\infty(\rho)(1-V_\infty(\rho))
\end{aligned}
\tag{3.31}
$$

and as expected, the first moment of the asymptotic speed distribution is the mean speed at equilibrium.

Remark 3.6.2. The asymptotic speed distribution (3.28) is conceptually analogous to the Maxwellian for rarefied gases, which we mentioned in subsection 2.1.3. □

Remark 3.6.3. The asymptotic speed distribution is a beta probability distribution function. This finding is compatible with experimental data: for instance in [27], the beta distribution turns out to be the one which best fits collected data about the traffic flow. □

3.7 Controlled interaction rules and the MPC approach

The increasing development and spreading of autonomous vehicles has shown their potentiality to mitigate road risk. This source of accidents is mainly due to speed variability in the traffic flow [50].

In the following sections, autonomous vehicles are introduced in the model as hidden leaders: their are standard agents and others do not interact with them differently. Their ability to decrease road risk is investigated: the idea is that thanks to their automatic technologies, these driver-assist cars can make the speed variability within the stream of vehicles decrease. The variance of the asymptotic speed distribution quantifies speed variability and consequently, road risk; therefore, this quantity is compared to the one obtained in the uncontrolled case in order to show the impact of autonomous vehicles on risk mitigation [46].

First, binary interaction rules are modified as follows [46]:

$$\begin{aligned} v' &= v + \gamma\Big[I(v,w;\rho) + \theta u\Big] + D(v;\rho)\eta \\ w' &= w \end{aligned} \tag{3.32}$$

where u is the control, θ is a Bernoulli random variable of parameter p i.e. $\theta \sim \text{Bernoulli}(p)$ and p represents the penetration rate that is the percentage of autonomous vehicles in the traffic [46]. The control u is the correction of the deterministic part of the interaction due to the presence of autonomous vehicles. Actually, it is [46]

$$u^* = \arg\min_{u\in\mathcal{U}} J(v';u) \tag{3.33}$$

where $J(v';u)$ is a least-square cost functional and $\mathcal{U}$ is the set of controls which are physical admissible. Autonomous vehicles aim at reducing road risk, which is equivalent to reducing speed variability in the traffic flow [50]. Therefore,

$$J(v';u) = \frac{1}{2}\langle\big(V_d(w';\rho) - v'\big)^2 + \nu u^2\rangle_\eta \ , \ \nu > 0 \tag{3.34}$$

where $V_d(w';\rho) = w' = w$ if the control strategy is the **binary variance control** and $V_d(w';\rho) = v_d(\rho) \in [0,1]$ if the control strategy is the **desired speed control** [46]. The first term of $J(v';u)$ represents the binary variance of $V_d(w';\rho)$ and the post-interaction speed v'. The second term νu^2 penalizes large controls with a coefficient $\nu > 0$.

This minimization problem can be rewritten as [45]

$$\begin{aligned} u^* = \arg\min_{u\in\mathcal{U}} & \left\{\frac{1}{2}\int_0^T \langle\big(V_d(w;\rho) - v\big)^2 + \nu u^2\rangle ds\right\} \\ & \text{subject to} \\ & \dot{v} = \bar{\gamma}\Big[I(v,w;\rho) + \theta u\Big] + D(v;\rho)\bar{\eta} \ , v(0) = v_0 \\ & \dot{w} = 0 \ , w(0) = w_0 \end{aligned} \tag{3.35}$$

where T is a given time horizon, Δt is the time step, $\bar{\gamma} = \gamma/\Delta t$ and $\bar{\eta} = \eta/\Delta t$. Two different approaches can be adopted to solve this problem: dynamic programming methods or variational methods such as Pontryagin's maximum principle. The problem becomes intractable if the number N of agents is large therefore a *Model Predictive Control* (MPC) approach [8] is used. The cost functional is not minimized over the whole time horizon T but a receding horizon strategy is adopted. Then, the Pontryagin's maximum principle is employed and feedback controlled microscopic rules, which are embedded in the Boltzmann-type kinetic equation, are obtained [1; 45; 46].

The receding horizon strategy [1; 45; 46] consists in splitting the time horizon T in N_T intervals: $T = N_T\Delta t$, $t^n = n\Delta t$ with $n = 0, ..., N_T$. We assume the control has the following form [1]:

$$u(t) = \sum_{n=0}^{N_T-1} u^n \mathbb{I}\Big[t \in [t^n, t^{n+1}]\Big] \tag{3.36}$$

where $\mathbb{I}[x \in A] = 1$ if $x \in A$ and $\mathbb{I}[x \in A] = 0$ if $x \notin A$.

The value of each u^n is determined by solving the reduced problem [1]

$$
\begin{aligned}
u^n = \arg\min_{u\in\mathbb{R}} & \left\{ \frac{1}{2}\int_{t^n}^{t^{n+1}} \langle \left(V_d(w;\rho)-v\right)^2 + \nu u^2 \rangle ds \right\} \\
& \text{subject to} \\
& \dot{v} = \bar{\gamma}\left[I(v,w;\rho)+\theta u\right] + D(v;\rho)\bar{\eta}\ , v(t^n) = \bar{v}\ ,
\end{aligned}
\tag{3.37}
$$

where we have dropped the constraint $u \in \mathcal{U}$. In the following, it will be shown that the physical admissibility is guaranteed by some conditions on η and $D(v;\rho)$ - see proposition 3.8.1 below. Therefore, it is not needed to define a set of physical admissible controls a priori and it is much easier to handle an unconstrained optimization problem.
Once the control u^n, which is defined on the time interval $[t^n, t^{n+1}]$, is obtained from (3.37), the post-interaction speeds are given by solving

$$
\begin{cases}
\dot{v} = \bar{\gamma}\left[I(v,w;\rho)+\theta u^n\right] + D(v;\rho)\bar{\eta} \\
\dot{w} = 0
\end{cases}
\tag{3.38}
$$

thus obtaining $\bar{v} = v(t^{n+1})$. This represents the initial condition for solving again equation (3.37) thus getting u^{n+1}. This procedure is repeated until $t^{n+1} = T$.

This receding horizon strategy is an iterative procedure over a sequence of finite time steps. The complexity of (3.37) is reduced compared to (3.35) since it is a minimization problem in the single variable u^n. Moreover, this method allows to obtain the control at each time step as a function of the interaction speeds. The innovation of this strategy relies on the fact that the control dynamics naturally emerge from the prescribed microscopic interactions. Even though the control obtained with MPC is suboptimal compared to the theoretical optimal one i.e. the solution of (3.35) [8], the consistency of this approximation is guaranteed for multi-agent kinetic systems [20; 22] and it is a competitive technique due to its computational cost, which is of the order of agents' number [1].

In order to solve the minimization problem (3.37), the Pontryagin's maximum principle is employed [1; 45; 46]. Its one dimensional version is stated in the following.

3.7.1 The Pontryagin's maximum principle

Let us consider the following problem:

$$\begin{aligned} \max \int_0^T & f_0(x(t),u(t),t)dt \\ & \text{subject to} \\ & \dot{x}(t) = f(x(t),u(t),t)\ ,\ x(0)=x_0 \\ & u(t) \in \mathbb{R} \end{aligned} \tag{3.39}$$

where $f, f_0 \in C^1([0,T])$. Let us define the Hamiltonian H as

$$H(x,u,\lambda,t) := f_0(x,u,t) + \lambda f(x,u,t)\ , \lambda \in \mathbb{R}\ . \tag{3.40}$$

Then, the Pontryagin's maximum principle in $1D$ [34; 40] is the following theorem.

Theorem 3.7.1. *Let us consider $u^*(t)$, which is an optimal control, piecewise-defined in the interval $[0,T]$. Its associated state variable is $x^*(t)$.*
Then, $\exists\lambda(t) : [0,T] \to \mathbb{R}$ with $\lambda \in C^1$ such that the following conditions hold $\forall t \in [0,T]$:
(i) $u^*(t) = \max_{u\in\mathbb{R}} H(x^*(t),u(t),\lambda(t),t)$
(ii) λ is differential $\forall t$ such that $u^*(t)$ is continuous and

$$\dot{\lambda}(t) = -\partial_x H(x^*(t),u^*(t),\lambda(t),t)$$

(iii) $\lambda(T) = 0$.

We observe that this theorem provides an optimality condition which is necessary but not sufficient.
We recommend [34; 40] for its proof and further details.

3.7.2 Feedback controlled microscopic rules

Now, we can solve the reduced minimization problem (3.37); in this case, the time horizon is the interaction interval $[t, t+\Delta t]$. The related Hamiltonian is

$$H = \frac{1}{2}\langle\big(V_d(w;\rho)-v\big)^2 + \nu u^2\rangle + \lambda\Big[\bar{\gamma}I(v,w;\rho) + \bar{\gamma}\theta u + D(v;\rho)\bar{\eta}\Big]\ , \tag{3.41}$$

where $\lambda \in \mathbb{R}$. Let us impose the conditions of theorem 3.7.1:

$$\begin{cases} \partial_u H = 0 \iff \nu u + \lambda\bar{\gamma}\theta = 0 \\ \dot{\lambda} = -\partial_v H \iff \dot{\lambda} = \langle\big(V_d(w;\rho)-v\big)\rangle - \lambda\bar{\gamma}\partial_v I(v,w;\rho) - \lambda\bar{\eta}\partial_v D(v;\rho) \\ \lambda(t+\Delta t) = 0\ . \end{cases} \tag{3.42}$$

By using the backward Euler scheme, the second condition can be discretized in the interaction interval $[t, t+\Delta t]$:

$$\lambda' := \lambda(t+\Delta t) = \lambda + \Delta t\Big[\langle V_d(w';\rho) - v'\rangle - \lambda'\bar{\gamma}\partial_v I(v',w';\rho) - \lambda'\bar{\eta}\partial_v D(v';\rho)\Big]$$

and then, combined with the third equality. This results in

$$\lambda = -\Delta t\langle V_d(w';\rho) - v'\rangle \ . \tag{3.43}$$

On the other hand, the first condition of (3.42) gives

$$u = -\frac{\bar{\gamma}\theta}{\nu}\lambda \ . \tag{3.44}$$

By plugging (3.43) in (3.44) and by referring to (3.32), we obtain the control u as a function of the interacting velocities:

$$u = \frac{\theta\gamma}{\nu+\theta^2\gamma^2}\big(V_d(w;\rho) - v\big) - \frac{\theta\gamma^2}{\nu+\theta^2\gamma^2} I(v,w;\rho) \ . \tag{3.45}$$

It represents the speed correction which is made by autonomous vehicles at each interaction which occurs in the time step Δt. As assumed in (3.36), the control is constant in this time horizon.

Finally, this result is plugged in (3.32) and the feedback controlled microscopic interaction rules are obtained:

$$\begin{aligned} v' &= v + \underbrace{\frac{\gamma^2\theta^2}{\nu+\gamma^2\theta^2}\Big[V_d(w;\rho) - v\Big] + \frac{\gamma\nu}{\nu+\gamma^2\theta^2} I(v,w;\rho)}_{\gamma\mathcal{I}(v,w;\rho)} + D(v;\rho)\eta \\ w' &= w \ , \end{aligned} \tag{3.46}$$

where $\mathcal{I}(v,w;\rho)$ is the new interaction function.

The physical admissibility of these interaction rules has to be checked and once its criteria identified, they can be embedded into the Boltzmann-type kinetic equation, which rules the dynamics of the system.

3.8 Physical admissibility of the feedback controlled interaction rules

Proposition 3.8.1. *Let us consider the interaction rules defined in* (3.46) *and let us assume that* $\gamma \in [0{,}1]$ *and* $\nu > 0$.
If $\exists c > 0$ *such that*

$$\begin{cases} |\eta| \le c\left(1 - \frac{\nu+\gamma}{\nu+\gamma^2}\gamma\right) \\ cD(v;\rho) \le \min\{v, 1-v\}, \ \forall v, \rho \in [0{,}1] \end{cases}$$

then the interaction rules satisfy the physical admissibility requirement i.e. v'*,* $w' \in [0,1]$ $\forall v, w \in [0,1]$ *and* $\forall \rho \in [0,1]$*.*

Proof. First, we observe that $w' = w \in [0,1]$.

Let us start to prove that

$$v' \geq 0 \iff v + \gamma \mathcal{I}(v, w; \rho) + D(v; \rho)\eta \geq 0 \ .$$

We observe that $P(\rho)$, $P(\rho)w$, $V_d(w; \rho) \geq 0$ therefore it is sufficient to show that

$$\begin{aligned} & v - \frac{\gamma^2\theta^2}{\nu + \gamma^2\theta^2} v - \frac{\gamma\nu}{\nu + \gamma^2\theta^2} v + D(v;\rho)\eta = \\ & = v\left(1 - \frac{\nu + \gamma\theta^2}{\nu + \gamma^2\theta^2}\gamma\right) + D(v;\rho)\eta \geq v\left(1 - \frac{\nu + \gamma}{\nu + \gamma^2}\gamma\right) + D(v;\rho)\eta \geq 0 \end{aligned}$$

where we have used that θ is a Bernoulli variable.

By hypothesis, $\exists c > 0$ such that $\eta \geq c\left(\frac{\nu+\gamma}{\nu+\gamma^2}\gamma - 1\right)$ and $D(v;\rho) \leq \frac{v}{c}$. This implies that

$$v\left(1 - \frac{\nu + \gamma}{\nu + \gamma^2}\gamma\right) + D(v;\rho)\eta \geq v\left(1 - \frac{\nu + \gamma}{\nu + \gamma^2}\gamma\right) + \frac{v}{c}c\left(\frac{\nu + \gamma}{\nu + \gamma^2}\gamma - 1\right) = 0 \ .$$

Analogously, let us prove that $v' \leq 1$. Due to the fact that $P(\rho)w$, $V_d(w;\rho) \leq 1$, the sufficient condition for $v' \leq 1$ is

$$\begin{aligned} & v + \frac{\gamma^2\theta^2}{\nu + \gamma^2\theta^2}(1 - v) + \frac{\gamma\nu}{\nu + \gamma^2\theta^2}(1 - v) + D(v;\rho)\eta = \\ & = v + \frac{\nu + \gamma\theta^2}{\nu + \gamma^2\theta^2}\gamma(1 - v) + D(v;\rho)\eta \leq v + \frac{\nu + \gamma}{\nu + \gamma^2}\gamma(1 - v) + D(v;\rho)\eta \leq 1 \ . \end{aligned}$$

By using the hypotheses $\exists c > 0$ such that $\eta \leq c\left(1 - \frac{\nu+\gamma}{\nu+\gamma^2}\gamma\right)$ and $D(v;\rho) \leq \frac{1-v}{c}$, we obtain

$$\begin{aligned} & v + \frac{\nu + \gamma}{\nu + \gamma^2}\gamma(1 - v) + D(v;\rho)\eta \leq \\ & \leq v + \frac{\nu + \gamma}{\nu + \gamma^2}\gamma(1 - v) + \frac{1 - v}{c}c\left(1 - \frac{\nu + \gamma}{\nu + \gamma^2}\gamma\right) = 1 \ . \end{aligned}$$

□

Remark 3.8.2. If the *infinite penalization limit* is considered i.e. $\nu \to +\infty$, conditions of proposition 3.8.1 become the ones of proposition 3.3.1. This is coherent with expectations since in this limit, the control u is so penalized that $u^* = 0$.

On the other hand, if the non penalized limit is considered i.e. $\nu \to 0^+$, $\eta \to 0$ and indeed, dynamics are purely deterministic. □

3.9 The controlled mean speed at equilibrium

The Boltzmann-type equation of the controlled system is [46]

$$\frac{d}{dt}\int_0^1 \phi(v) f^*(t,v)dv = \frac{1}{2}\mathbb{E}_\theta\left[\langle \int_0^1 \int_0^1 [\phi(v') - \phi(v)] f^*(t,v) f^*(t,w) dv dw \rangle_\eta\right], \tag{3.47}$$

where the expected value with respect to the Bernoulli random variable θ has been introduced and the superscript * refers to the fact the controlled case is considered.

In order to derive the evolution equation for the mean speed, we set $\phi(v) = v$ and by plugging the feedback interaction rules (3.46), we obtain [46]

$$\begin{aligned}\frac{dV^*}{dt} = \frac{\gamma}{2}\Bigg\{ &\frac{\nu + (1-p)\gamma^2}{\nu + \gamma^2}\Big\{P(\rho)\big[1 + (1 - P(\rho))V^*\big] - V^*\Big\} + \\ &+ \frac{p\gamma}{\nu + \gamma^2}\left(\int_0^1 V_d(w;\rho) f^*(t,w)dw - V^*\right)\Bigg\},\end{aligned} \tag{3.48}$$

where $V^* = V^*(t) := \int_0^1 v f^*(t,v)dv$ i.e. V^* is the mean speed in the controlled case [46].

Remark 3.9.1. Consistently, if $p = 0$ i.e. there are not autonomous vehicles, equation (3.7) is recovered from (3.48). This also occurs if $\nu \to +\infty$, which implies $u^* = 0$.

On the other hand, if $p \to 1$ i.e. all vehicles are autonomous and $\nu \to 0^+$, the control dominates the evolution of V^*. □

In order to solve (3.48), the *quasi-invariant interaction regime* is adopted [46]:

$$\gamma, \sigma^2, \nu \to 0^+ \text{ such that } \frac{\sigma^2}{\gamma} \to \lambda > 0 \text{ and } \frac{\nu}{\gamma} \to \kappa > 0\,. \tag{3.49}$$

In addition to the assumptions of the uncontrolled case (3.12), also the control contribution is considered negligible in the dynamics, but still of the same order of the interaction part.
The scaled speed distribution is defined as $\tilde{f}^*(\tau, v) := f^*(2\tau/\gamma, v)$ and the scaled mean speed as $\tilde{V}^*(\tau) := V(2\tau/\gamma)$ [46]. Therefore, in the *quasi-invariant interaction limit*, equation (3.48) becomes [46]

$$\frac{d\tilde{V}^*}{d\tau} = P(\rho)\Big[1 + (1 - P(\rho))V^*\Big] - (1 + p^*)\tilde{V}^* + p^*\left(\int_0^1 V_d(w;\rho)\tilde{f}^*(\tau, w)dw\right) \tag{3.50}$$

where p^* is the effective penetration rate [46] and is defined as $p^* := \frac{p}{\kappa}$.
If $\tau \to +\infty$, $\tilde{V}^* \to V^*_\infty$ and the mean speed at equilibrium V^*_∞ solves the following equation:

$$P(\rho)\Big[1 + (1 - P(\rho))V^*_\infty\Big] - (1 + p^*)V^*_\infty + p^*\left(\int_0^1 V_d(w;\rho)\tilde{f}^*(\tau, w)dw\right) = 0\ . \tag{3.51}$$

If the control strategy is the **binary variance control**, then $V_d(w;\rho) = w$ and we obtain

$$V^*_\infty(\rho) = \frac{P(\rho)}{P(\rho) + (1 - P(\rho))^2}\ , \tag{3.52}$$

which is equivalent to the uncontrolled case (3.10).

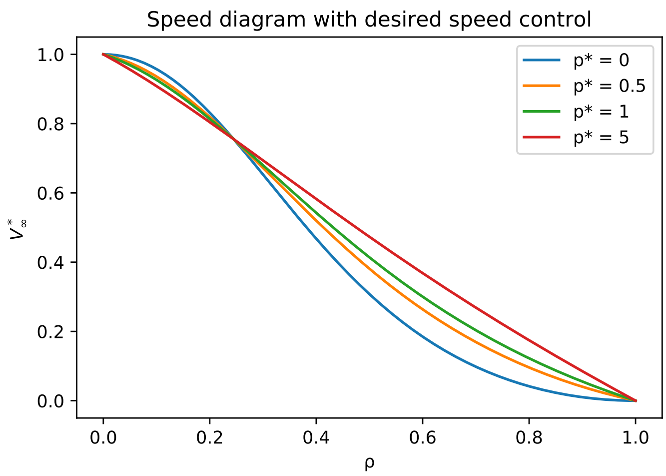

Figure 3.7: Mean speed at equilibrium (3.53) with the desired speed control for different values of the effective penetration rate p^*, $v_d(\rho) = 1 - \rho$

If the control strategy is the **desired speed control**, then $V_d(w;\rho) = v_d(\rho)$ and we obtain

$$V_\infty^*(\rho) = \frac{P(\rho) + p^* v_d(\rho)}{P(\rho) + (1 - P(\rho))^2 + p^*} \ , \tag{3.53}$$

which is plotted in figure 3.7 (p. 63).

Remark 3.9.2. If $p^* \to 0$, the uncontrolled case is recovered from (3.53): $V_\infty^*(\rho) \to V_\infty(\rho)$.
If $p^* \to +\infty$ i.e. $\nu \to 0^+$, the *speed diagram* corresponds to the one of the desired speed $v_d(\rho)$: $V_\infty^*(\rho) \to v_d(\rho)$. $\square$

3.10 The controlled asymptotic speed distribution

In the binary variance control case, if the analysis was just limited to *speed* and *fundamental diagrams*, no difference would be revealed compared to the uncontrolled case. Indeed, the mean speed at equilibrium is not affected by the introduction of the binary variance control. Instead, the study of the asymptotic speed distribution shows that the variance of the asymptotic speed distribution decreases thanks to the introduction of the control. Also in the case of the desired speed control, the analysis of the asymptotic speed at equilibrium allows to have a detailed insight on the impact of autonomous vehicles on risk mitigation.

Let us consider the *quasi-invariant interaction regime* (3.49) and the feedback controlled interaction rules (3.46). We observe that their form is equivalent to that of the uncontrolled case (3.1) with the new interaction function $\mathcal{I}(v, w; \rho)$. Therefore, an analogous equation of (3.21) holds for the controlled asymptotic speed distribution $\tilde{f}^*(\tau, v)$. In this case, the interaction function $I(v, w; \rho)$ is replaced by $\mathcal{I}(v, w; \rho)$.

In the *quasi-invariant interaction regime* (3.49), we have

$$\begin{aligned}&\mathbb{E}_\theta\Big\{\int_0^1 \mathcal{I}(v,w;\rho)\tilde{f}^*(\tau,w)dw\Big\} = \int_0^1 \Big\{\frac{p\gamma}{\nu+\gamma^2}\big[V_d(w;\rho)-v\big]+\\&+\frac{p\nu}{\nu+\gamma^2}I(v,w;\rho)+\frac{(1-p)\nu}{\nu+\gamma^2}I(v,w;\rho)\Big\}\tilde{f}^*(\tau,w)dw\\&\to\int_0^1\Big\{\frac{p}{\kappa}\big[V_d(w;\rho)-v\big]+pI(v,w;\rho)+(1-p)I(v,w;\rho)\Big\}\tilde{f}^*(\tau,w)dw=\\&=\int_0^1\Big\{p^*V_d(w;\rho)+I(v,w;\rho)\Big\}\tilde{f}^*(\tau,w)dw-p^*v\ .\end{aligned} \tag{3.54}$$

So, in the controlled case, the Fokker-Planck PDE is [46]

$$\begin{aligned}\partial_\tau\tilde{f}^* = &\frac{\lambda}{2}\partial_v^2\Big(D^2(v;\rho)\tilde{f}^*\Big)+\\&-\partial_v\Big\{\Big[\int_0^1\Big(I(v,w;\rho)+p^*V_d(w;\rho)\Big)\tilde{f}^*(\tau,w)dw-p^*v\Big]\tilde{f}^*\Big\}\ .\end{aligned} \tag{3.55}$$

If $\tau\to+\infty$ and by plugging the interaction function defined in (3.2), we obtain

$$\begin{aligned}&\frac{\lambda}{2}\partial_v^2\Big(D^2(v;\rho)\tilde{f}^*_\infty\Big)-\partial_v\Big\{\Big[P(\rho)\big(1+(1-P(\rho))\tilde{V}^*_\infty\big)-v+\\&+p^*\int_0^1 V_d(w;\rho)\tilde{f}^*_\infty(\tau,w)dw-p^*v\Big]\tilde{f}^*_\infty\Big\}=0\ .\end{aligned} \tag{3.56}$$

By referring to (3.51), the content of the square brackets in (3.56) can be rewritten as

$$\begin{aligned}&P(\rho)\big[1+(1-P(\rho))V^*_\infty\big]+p^*\int_0^1 V_d(w;\rho)\tilde{f}^*(\tau,w)dw-(1+p^*)v=\\&=(1+p^*)(V^*_\infty-v)\ .\end{aligned} \tag{3.57}$$

As in the uncontrolled case, the same form defined in (3.26) [46] is chosen for the diffusion coefficient. The asymptotic speed distribution is still a beta probability density function [46]

$$\tilde{f}^*_\infty(v)=\frac{v^{\alpha-1}(1-v)^{\beta-1}}{B(\alpha,\beta)}\ , \tag{3.58}$$

but now the parameters α and β are defined as [46]

$$\begin{aligned}\alpha &:= \frac{2(1+p^*)V_\infty^*(\rho)}{\lambda a^2(\rho)}\\ \beta &:= \frac{2(1+p^*)(1-V_\infty^*(\rho))}{\lambda a^2(\rho)}\ .\end{aligned} \tag{3.59}$$

Remark 3.10.1. If $p^*=0$ i.e. there are not autonomous vehicles, α and β in (3.59) are equivalent to the corresponding parameters in the uncontrolled case (3.29). $\square$

Let us note that (3.55) is accompanied with boundary conditions. These conditions are satisfied if $\tilde{f_\infty^*}$ and $\partial_v \tilde{f_\infty^*}$ are null in the extreme values of the speed domain i.e. $v=0,1$ [46]. This is equivalent to state that

$$a^2(\rho) \leq \frac{1+p^*}{\lambda}\min\{V_\infty^*(\rho), 1-V_\infty^*(\rho)\}\ . \tag{3.60}$$

If X^* is a random variable such that $X^* \sim \tilde{f_\infty^*}$,

$$\begin{aligned}\mathbb{E}[X^*] &= \frac{\alpha}{\alpha+\beta} = \tilde{V_\infty^*}\\ \mathrm{Var}(X^*) &= \frac{\alpha\beta}{(\alpha+\beta)^2(\alpha+\beta+1)} = \frac{\lambda a^2(\rho)}{2+\lambda a^2(\rho)+2p^*}V_\infty^*(\rho)(1-V_\infty^*(\rho))\ .\end{aligned} \tag{3.61}$$

Coherently, the expected value of a random variable distributed according to the asymptotic speed distribution (3.58) is the mean speed at equilibrium in the controlled case V_∞^*.

3.11 Risk mitigation

Let us consider the **binary variance control** with $p^*>0$. In this case, $V_\infty^* = V_\infty$ and

$$\underbrace{\frac{\lambda a^2(\rho)}{2+\lambda a^2(\rho)+2p^*}V_\infty^*(1-V_\infty^*)}_{\mathrm{Var}(X^*)} < \underbrace{\frac{\lambda a^2(\rho)}{2+\lambda a^2(\rho)}V_\infty(1-V_\infty)}_{\mathrm{Var}(X)}\ \forall\rho\in[0{,}1]\ . \tag{3.62}$$

This control strategy, which aims at reducing the binary speed variance, is effectively able to decrease speed variability and therefore, macroscopic road risk.

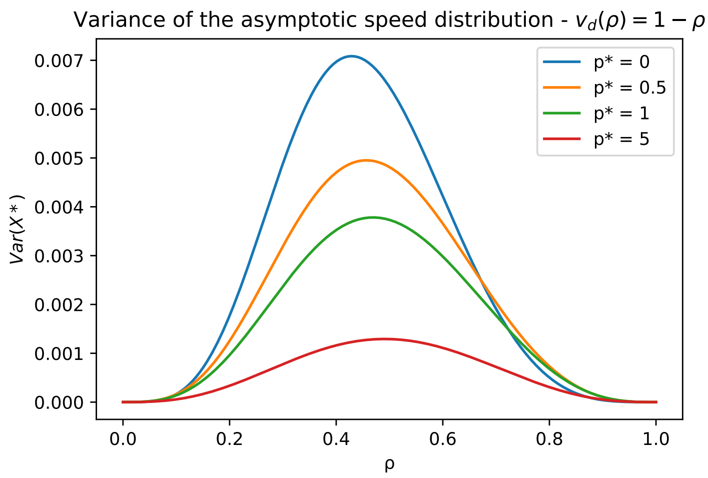

Figure 3.8: Variance of the asymptotic speed distribution (3.58) with the desired speed control $v_d(\rho) = 1 - \rho$ for different values of the effective penetration rate p^*

Instead, if the **desired speed control** is considered, the mean speed at equilibrium is affected by the introduction of the control, as it can be seen by setting (3.53) against (3.10). Therefore, it is more difficult to directly compare the variance of the asymptotic speed distribution in the uncontrolled case with that in the controlled case. In figure 3.8, the variance of the controlled asymptotic speed distribution (3.58) is plotted as a function of the density ρ, for different values of effective penetration rates p^* and for a desired speed control strategy. It is assumed that the desired speed is equal to $v_d(\rho) = 1 - \rho$ and the case $p^* = 0$ corresponds to the uncontrolled situation. It is evident that

$$\neg\Big(\mathrm{Var}(X^*) < \mathrm{Var}(X) \quad \forall \rho \in [0,1]\Big) \text{ with the desired speed control strategy.}$$

This means that there exist some values of densities for which the variance does not decrease compared to the uncontrolled case. However, a circumstance where the introduction of the desired speed control leads to a reduction in the variance of the asymptotic speed distribution can be identified. As pointed out in the remark 3.9.2, in the *infinite effective penetration rate limit*, $V^*_\infty \to v_d(\rho)$. Moreover, in this limit, $\mathrm{Var}(X^*) \to 0^+$. Thus, the introduction of the desired speed control leads to road risk mitigation when dynamics are fully controlled [46].

3.12 Numerical tests

In order to confirm theoretical findings, several numerical tests can be performed. As explained in section 2.2, the Nanbu-Babovsky's scheme [29; 30] is adopted. All simulations are carried out with MATLAB®.

3.12.1 Choice of parameters

In section 3.5, *speed* and *fundamental diagrams* are introduced and investigated. The exponent μ in the probability of accelerating $P(\rho) = (1-\rho)^{\mu}$, $\mu > 0$ is chosen equal to 2.

The Nanbu-Babovsky's scheme is used in order to solve the Boltzmann-type equation for the uncontrolled and controlled dynamics. Let us consider the controlled equation (3.47); the uncontrolled dynamics can be easily recovered from it by setting $p = 0$. We can rewrite equation (3.47) in such a way that the link with (2.43) becomes clearer [46]:

$$\partial_{\tau}\tilde{f}^*(\tau,v) = \frac{1}{\gamma}[Q_+(\tilde{f}^*,\tilde{f}^*)(\tau,v) - \tilde{f}^*(\tau,v)] \ , \tag{3.63}$$

where $\tau = \frac{\gamma}{2}t$ and $\tilde{f}^*$ is the controlled scaled speed distribution. Moreover, the *gain operator* $Q_+(\tilde{f}^*,\tilde{f}^*)$ is defined as [46]

$$Q_+(\tilde{f}^*,\tilde{f}^*)(\tau,v) = \mathbb{E}_{\theta}\Big[\langle\int_0^1 \frac{1}{'J}\tilde{f}^*(\tau,'v)\tilde{f}^*(\tau,'w)dw\rangle_{\eta}\Big], \tag{3.64}$$

where $('v,'w)$ and (v,w) are the speeds before and after the interaction respectively. $'J$ is the Jacobian of the change of variables $('v,'w) \to (v,w)$.

The requirement $\frac{\Delta t}{\epsilon} \leq 1$ must hold - see subsection 2.2.1. Moreover, the *quasi-invariant interaction regime* is considered: we would like to compare the numerical solution of the Boltzmann-type equation with the asymptotic Fokker-Planck distribution, obtained analytically in this regime. Therefore, we set

$$\epsilon = 0.01, \ \Delta t = \epsilon, \ \gamma = \epsilon, \ \sigma^2 = \gamma \ , \tag{3.65}$$

which imply $\lambda = 1$. Imposing $\Delta t = \epsilon$ means that all agents interact.

Remark 3.12.1. In section 3.6, the *quasi-invariant interaction regime* is introduced. The new time scale τ is such that interactions occur with frequency $1/\tau = O(1/\gamma) >> 1$ [46], coherently with $1/\gamma = 1/\epsilon$ and the definition of the Knudsen number, which represents the relaxation time of vehicles' interactions. □

In the controlled case, the following condition is also considered:

$$\nu = \gamma \ , \tag{3.66}$$

which implies $\kappa = 1$.

Remark 3.12.2. In this dissertation, vehicular traffic is studied in the *quasi-invariant interaction regime* and this leads to consider $\epsilon \ll 1$. As outlined in section 3.1, this regime identifies the so-called *continuum hypothesis*, which is the basis of the macroscopic approach contrary to the kinetic one that is employed if $\epsilon \sim 1$ [32]. Moreover, the DSMC schemes are not suited to describe the dynamics in this case [29; 33]. Indeed, in the hydrodynamic regime $\epsilon \to 0$, the mean free path of particles is much smaller than the characteristic scale of the system and dynamics are dominated by collision over transport. In order to capture all the dynamics, which occur in different time scales, a splitting approach is adopted in the inhomogeneous case. Due to the fact that we are studying the Boltzmann-type equation in the homogeneous case, the kinetic description and the Nanbu-Babovsky's scheme are preserved. In this situation, the convective term is not present in the Boltzmann-type equation: the only temporal scale is given by ϵ, which represents the relaxation time of the vehicles' interactions and therefore, its inverse is the interaction frequency. □

The agents considered in the simulations are 10^5 and their initial speeds are sampled from a uniform distribution in the interval of physical admissibility i.e. $\tilde{f}_0 \sim \mathcal{U}([0,1])$. The points considered in the speed interval [0,1] are $N_v = 101$ and so, the lattice step is equivalent to 0.01. They allow to reconstruct speed distributions.

We also have to set $a(\rho)$, which enters in the definition (3.26) of the diffusion coefficient $D(v, \rho)$ and of the parameters α and β of the asymptotic speed distribution. As previously explained, a suited choice, which satisfies boundary conditions of the Fokker-Planck PDE, is [46]

$$a(\rho) \coloneqq \rho(1 - \rho).$$

Finally, let us consider the proportionality parameter η of the diffusion coefficient $D(v; \rho)$. It is sampled from a uniform distribution with zero mean and variance σ^2 [46]. The zero mean condition is obtained by setting

$\eta \sim \mathcal{U}([-a, a])$ while the variance condition by letting

$$\frac{\big(a-(-a)\big)^2}{12} = \sigma^2 \iff a = \sqrt{3\sigma^2}\ .$$

To sum up, $\eta \sim \mathcal{U}[-a, a]$ with $a = \sqrt{3\sigma^2}$.

3.12.2 Uncontrolled case

Results of Monte Carlo simulations in the uncontrolled case are displayed. The theoretical asymptotic speed distribution defined in (3.28), or equivalently the one in (3.58) with $p^* = 0$, is compared to the stationary numerical solution of the Boltzmann-type equation. Distributions are plotted as functions of speed by using a suited histogram and simulations are run for a sufficiently long time such that convergence at equilibrium is achieved. This time will be specified for each simulation and justified by referring to the L^2-numerical relative error.

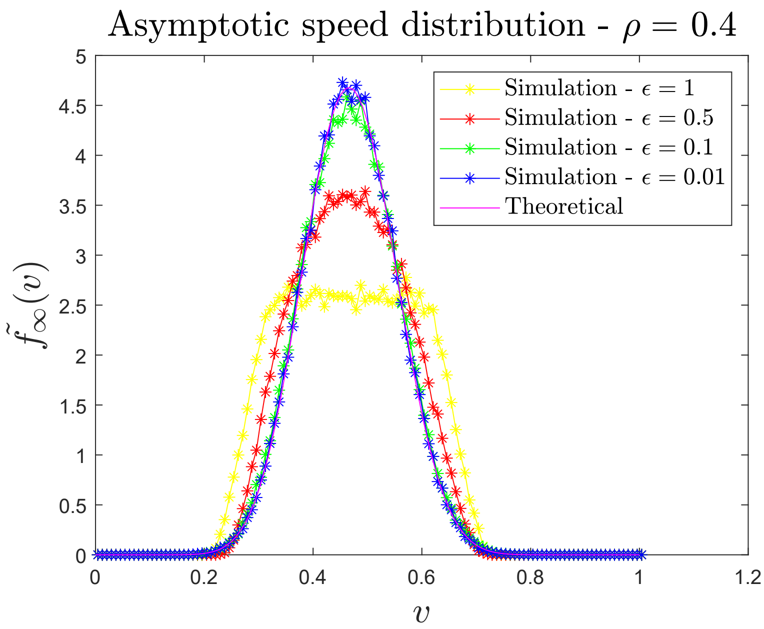

Figure 3.9: Comparison between the asymptotic Fokker-Planck distribution (3.28) (theoretical) and the numerical solution of the Boltzmann-type equation in the uncontrolled case (simulation). Several values of the parameter ϵ are considered, $\rho = 0.4$, $T = 20$

First, let us investigate the *quasi invariant interaction regime*. In figure 3.9, the asymptotic speed distribution (3.28) is plotted for $\rho = 0.4$ and for several values of the parameter ϵ. Final time T is set equal to 20 for all cases. Then, it is evident that the choice performed in (3.65) i.e. $\epsilon = \gamma = \sigma^2 = 0.01$ is justified: the more γ and σ^2 approach 0, the deeper we are in the *quasi-invariant interaction regime*.

In figures 3.10 - 3.11 (p. 72), numerical tests are performed for two more values of density by considering (3.65) i.e. $\epsilon = 0.01$. By qualitatively looking at these figures, it is evident that the agreement is strong: as theoretically expected, the numerical equilibrium solution of the Boltzmann-type equation converges toward the solution of the Fokker-Planck PDE, which is analytically obtained in the *quasi-invariant interaction regime*. A quantitative insight into this issue is gained by studying the L^2-numerical relative error. This is defined as

$$L^2\text{-numerical error} = \frac{\sqrt{\sum_{k=1}^{N_v}(\tilde{f}_\infty^{TH}(V_k) - \tilde{f}_\infty^{SIM}(V_k))^2}}{\sum_{k=1}^{N_v}\tilde{f}_\infty^{TH}(V_k)}\ , \tag{3.67}$$

where TH stands for theoretical, SIM stands for simulation and V_k with $k = 1, ...N_v$ are the points of the discretized speed domain. This error is plotted in figures 3.12 - 3.14 (pp. 73-74) for $\rho = 0.2,\ 0.4,\ 0.8$. If $\rho = 0.2,\ 0.4$, this numerical error drops to values which are of the order of 10^{-2} in a relatively small number of time steps. Instead, if $\rho = 0.8$, the numerical error stabilizes at values which are $O(10^{-1})$. These higher errors are due to the fact that $\rho = 0.8$ is a more extreme value of density. Figures 3.12 - 3.14 also justify the choice $T = 20$ indeed we observe that this time is sufficient for the system to reach equilibrium.

3.12.3 Controlled case

Similarly to the uncontrolled case, simulation results are displayed in the controlled case. Let us set $\rho = 0.4$ and $T = 20$. In figures 3.15 - 3.17 (pp. 74-75), numerical tests are performed with a binary variance control strategy and for different values of the penetration rate p. The same is done in figures 3.18 - 3.20 (pp. 76-77) for the desired speed control. As in the uncontrolled case, the numerical distribution perfectly fit the theoretical one. The L^2-numerical error's trend can also be obtained and it is analogous to that of figures 3.12 - 3.14; at equilibrium it is $O(10^{-2})$.

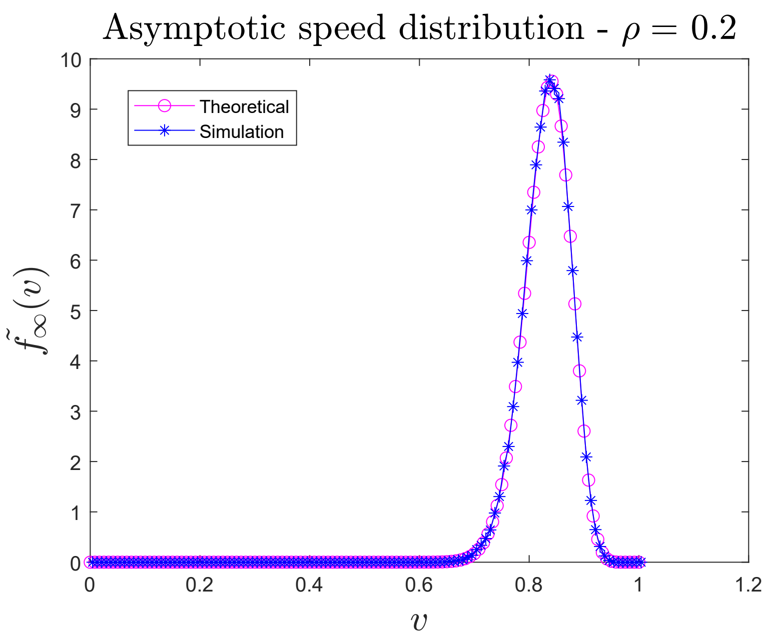

Figure 3.10: Comparison between the asymptotic Fokker-Planck distribution (3.28) (theoretical) and the numerical solution of the Boltzmann-type equation in the uncontrolled case (simulation) for $\rho = 0.2$, $T = 20$

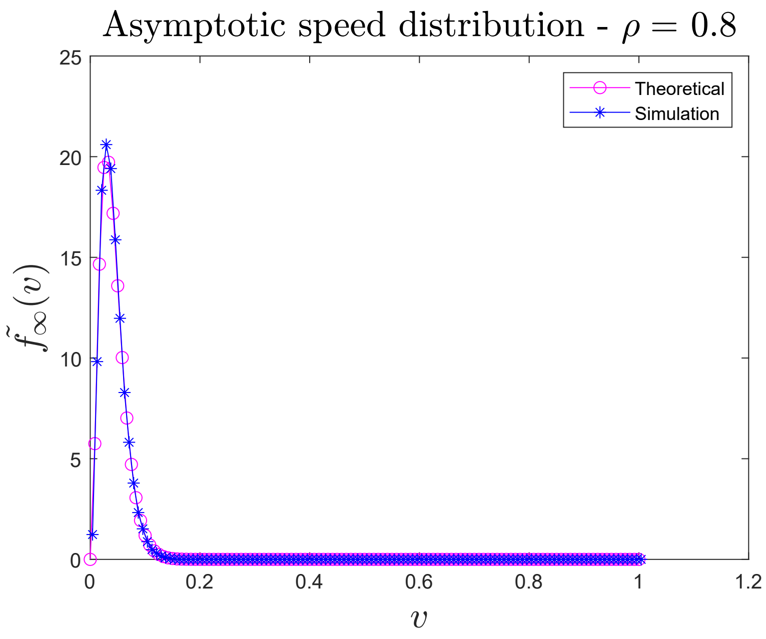

Figure 3.11: Comparison between the asymptotic Fokker-Planck distribution (3.28) (theoretical) and the numerical solution of the Boltzmann-type equation in the uncontrolled case (simulation) for $\rho = 0.8$, $T = 20$

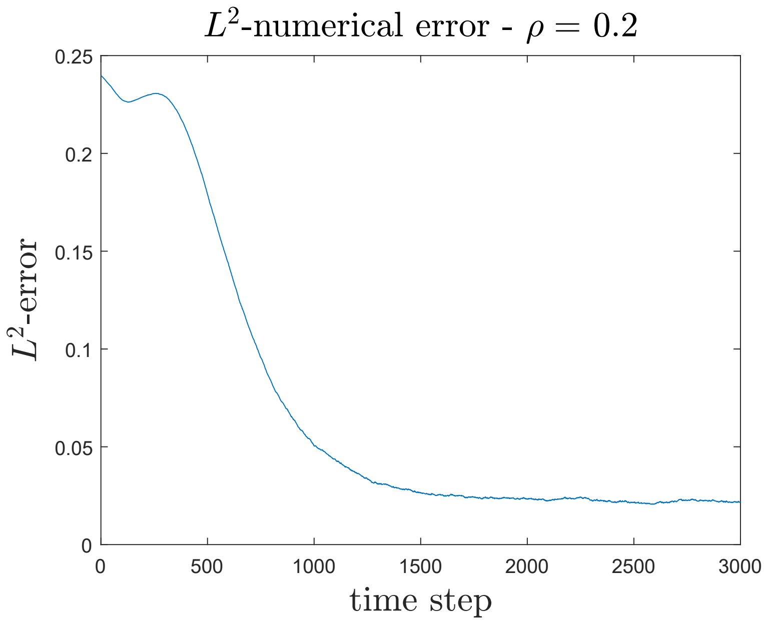

Figure 3.12: L^2-numerical error defined in (3.67) as a function of time for $\rho = 0.2$

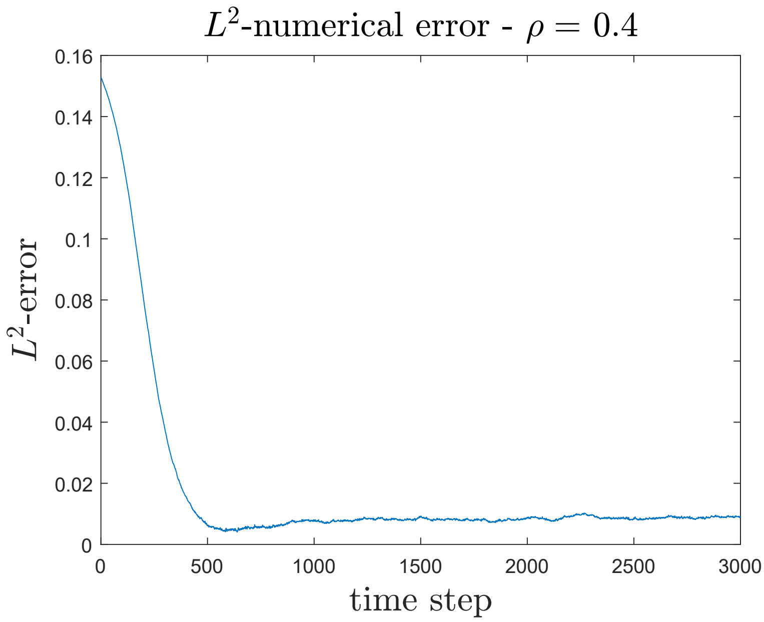

Figure 3.13: L^2-numerical error defined in (3.67) as a function of time for $\rho = 0.4$

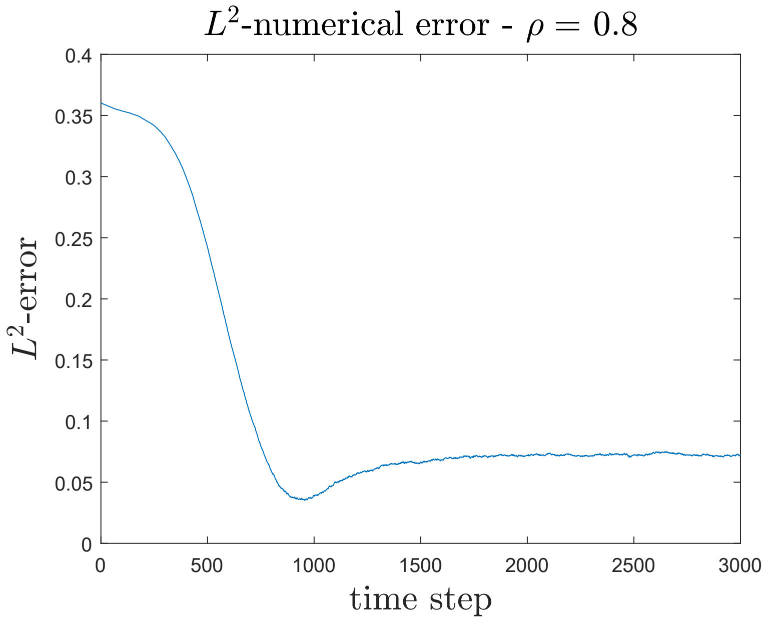

Figure 3.14: L^2-numerical error defined in (3.67) as a function of time for $\rho = 0.8$

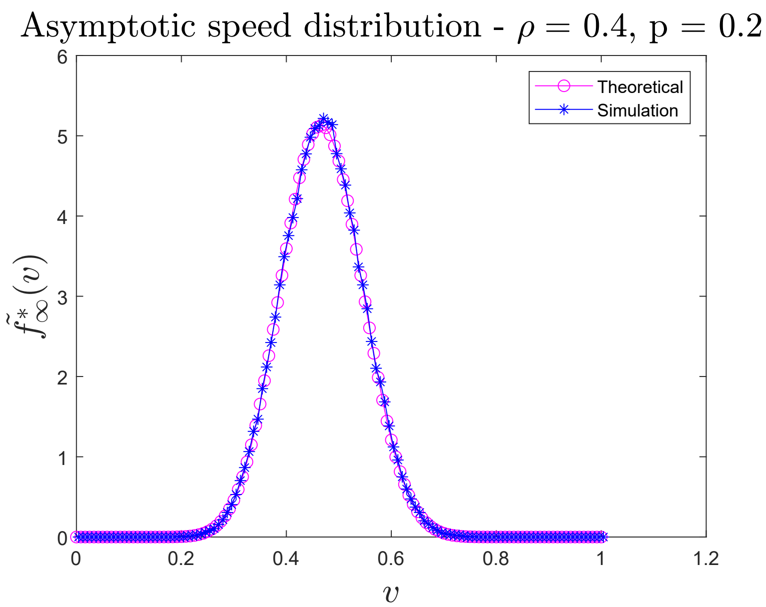

Figure 3.15: Comparison between the asymptotic Fokker-Planck distribution (3.58) (theoretical) and the numerical solution of the Boltzmann-type equation (simulation) with binary variance control for $\rho = 0.4$, $p = 0.2$, $T = 20$

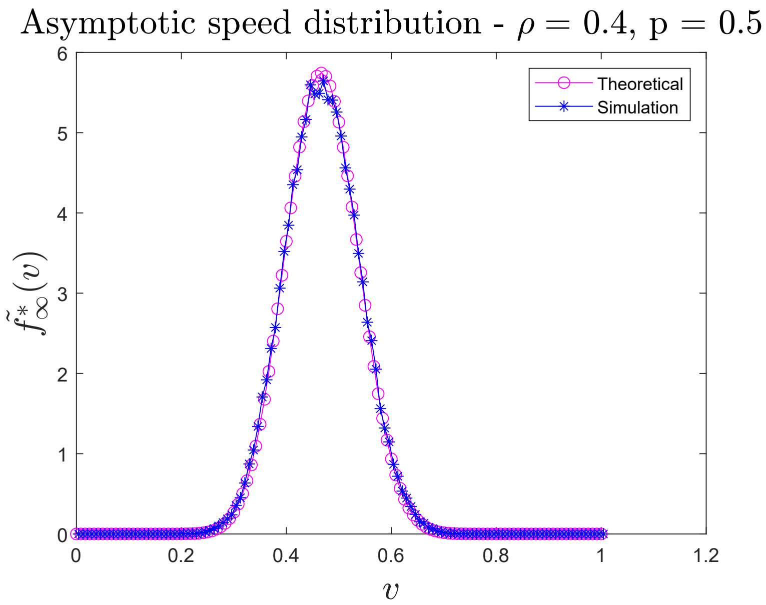

Figure 3.16: Comparison between the asymptotic Fokker-Planck distribution (3.58) (theoretical) and the numerical solution of the Boltzmann-type equation (simulation) with binary variance control for $\rho = 0.4$, $p = 0.5$, $T = 20$

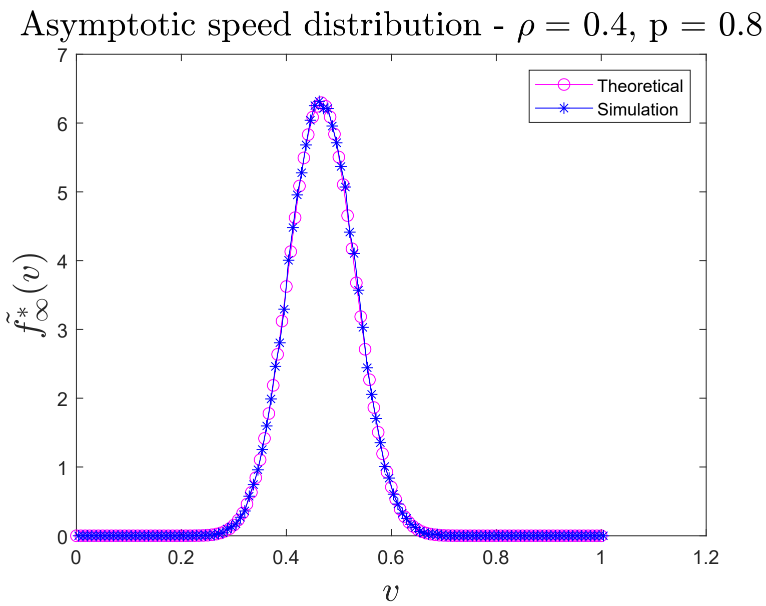

Figure 3.17: Comparison between the asymptotic Fokker-Planck distribution (3.58) (theoretical) and the numerical solution of the Boltzmann-type equation (simulation) with binary variance control for $\rho = 0.4$, $p = 0.8$, , $T = 20$

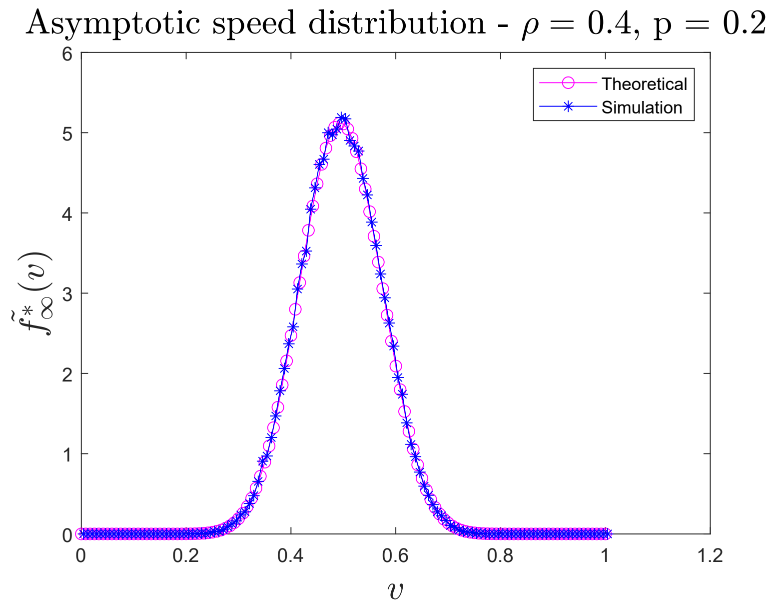

Figure 3.18: Comparison between the asymptotic Fokker-Planck distribution (3.58) (theoretical) and the numerical solution of the Boltzmann-type equation (simulation) with desired speed control for $\rho = 0.4$, $p = 0.2$, $T = 20$

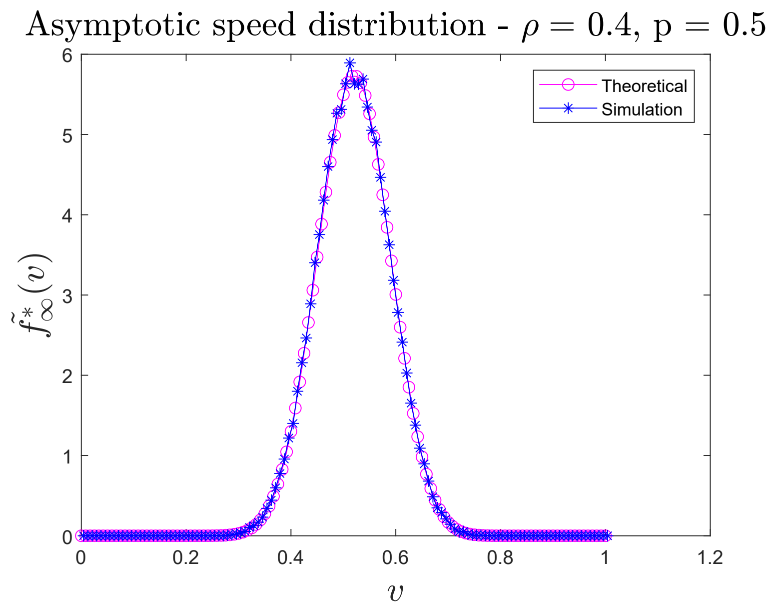

Figure 3.19: Comparison between the asymptotic Fokker-Planck distribution (3.58) (theoretical) and the numerical solution of the Boltzmann-type equation (simulation) with desired speed control for $\rho = 0.4$, $p = 0.5$, $T = 20$

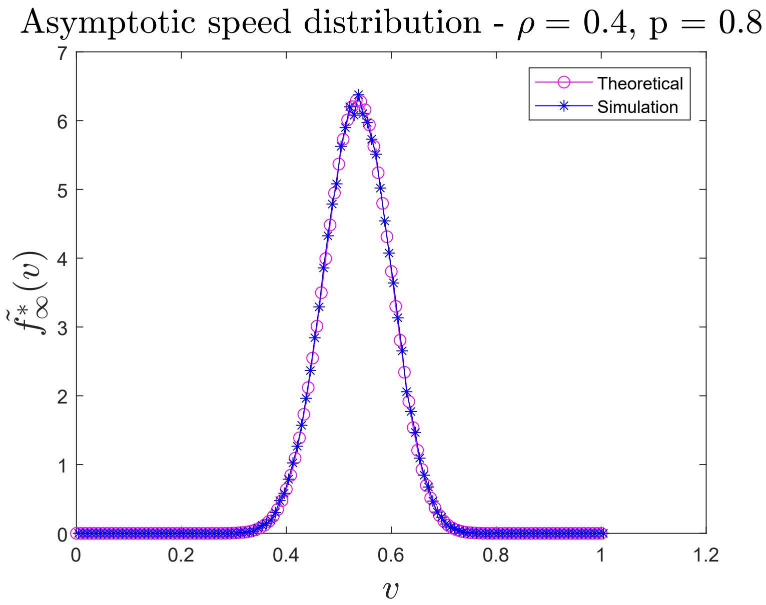

Figure 3.20: Comparison between the asymptotic Fokker-Planck distribution (3.58) (theoretical) and the numerical solution of the Boltzmann-type equation (simulation) with desired speed control for $\rho = 0.4$, $p = 0.8$, $T = 20$

3.13 Conclusion

In this chapter, the kinetic traffic model is deeply investigated by extensively referring to the literature, in particular to the article [46]. All the tools learned will be fundamental for subsequent studies, which represent the core of this thesis.

First, a system without autonomous vehicles is considered. The main features of mesoscopic modeling such as the *follow-the-leader approach*, *speed* and *fundamental diagrams*, the *quasi-invariant interaction regime* are explained. Next, autonomous vehicles are introduced in traffic and the *Model Predictive Control* strategy is investigated.
Both in the uncontrolled and in the controlled case, the mean speed at equilibrium and the asymptotic speed distribution are analytically derived. These findings are validated numerically by means of simulations based on the Nanbu-Babovsky's scheme.

It is important to notice that the two control strategies considered lead to different conclusions. The binary variance control turns out to be efficient at mitigating road risk for every value of traffic density. Instead, the desired speed control does not always guarantee this property.

Chapter 4

Phase transition in kinetic traffic modeling

The interaction rules represent the core of the kinetic model. They express in a microscopic fashion how agents change their velocities after binary interactions. Most importantly, they determine the time evolution of the speed distribution function f and therefore, macroscopic quantities such as the mean speed and the macroscopic flux. Changing the interaction rules would lead to substantial differences in final results and in the aggregate behavior, which naturally emerges from the Boltzmann-type kinetic approach.

In this chapter, the impact of the introduction of new interaction rules is investigated. In the first three sections, the uncontrolled case is studied: the *speed diagram* of the system reveals a phase transition, which determines the shape of the asymptotic speed distribution. Then, the control is introduced in the subsequent four sections. Two different control strategies are studied: binary variance and desired speed control. Finally, a section is dedicated to numerical tests and another to conclusions.

4.1 Nonlinear interaction rules

Let us consider two vehicles, one with speed v and another with speed w. Their post-interaction speeds, v' and w', follow the same interaction rules previously explained in chapter 3 and first introduced in [46], but with a different interaction function:

$$\begin{aligned} v' &= v + \gamma I(v, w; \rho) + D(v; \rho)\eta \\ w' &= w \ . \end{aligned} \tag{4.1}$$

As in [46], $\gamma > 0$ and it is a proportionality parameter, while η is a centered random variable, with zero mean and variance σ^2 and $D(v;\rho) \geq 0$ is a diffusion coefficient. Thanks to the term $D(v;\rho)\eta$, a stochastic component is included in the model, allowing to consider the intrinsic stochasticity in each agent's behavior.

The interaction function $I(v,w;\rho)$ is defined as

$$I(v,w;\rho) = P(\rho)(1-v) + (1-P(\rho))(vw - v), \tag{4.2}$$

where $P(\rho)$ is the probability of accelerating [46]

$$P(\rho) = (1-\rho)^{\mu}, \mu > 0. \tag{4.3}$$

As in [46], a microscopic *follow-the-leader approach* [18] is assumed. The difference compared to [46] consists in the term vw instead of $P(\rho)v$ in the interaction rule. As in [46], when the probability of accelerating is maximum and the density is small, the rear vehicle tends to the maximum allowed speed i.e. 1. The novelty occurs when the density increases and the probability of accelerating decreases: in this case, the rear vehicle tends to a fraction of the speed of the leading vehicle and this fraction is given by the speed of the rear vehicle itself. In other words, when the rear vehicle decelerates, it is sensitive to the leading vehicle's speed proportionally to its speed v: the bigger v is and the more it approaches 1, the higher the sensitivity to the speed w of the leading vehicle is. Vice versa, the smallest v is and the more it approaches 0, the less the sensitivity to w is; in particular, only a fraction of w, given by its own speed v, will be considered.

The physical admissibility of the nonlinear interaction rules (4.1) - (4.2) is guaranteed by proposition 3.3.1. It can be proved analogously to the situation with interaction rules (3.1) - (3.2): $P(\rho)w \in [0,1]$ is replaced by $vw \in$[0,1].

4.2 Mean speed at equilibrium: emergence of phase transition

Once the new interaction rules have been defined, a Boltzmann-type kinetic equation for binary interaction models can be written. We refer to [30] and to the derivation of this equation explained in detail in subsection 2.1.4.

As previously stated, this equation is fundamental since it rules the evolution of the speed distribution function $f = f(t,v)$. If $\phi = \phi(v)$ is a generic observable and $w' = w$ in (4.1), the equation in weak form is

$$\frac{d}{dt}\int_0^1 \phi(v)f(t,v)dv = \frac{1}{2}\langle\int_0^1\int_0^1 [\phi(v') - \phi(v)]f(t,v)f(t,w)dvdw\rangle, \qquad (4.4)$$

where $\langle\cdot\rangle$ is the expectation with respect to the distribution of the centered random variable η.

Let us proceed as in section 3.4. First, we observe that if $\phi(v) = 1$,

$$\frac{d}{dt}\int_0^1 \phi(v)f(t,v)dv = 0\ . \qquad (4.5)$$

This means that, given an initial condition $f_0(v) = f(0,v)$ properly normalized, $f(t,v)$ will be normalized and therefore, a distribution probability $\forall t > 0$ [46].

Instead, if $\phi(v) = v$, an equation which rules the evolution of the mean speed will be derived. Let us define the mean speed as [46]

$$V(t) := \int_0^1 vf(t,v)dv\ . \qquad (4.6)$$

Then, by plugging $\phi(v) = v$ in (4.4) together with (4.1) - (4.2), we obtain

$$\frac{d}{dt}\int_0^1 vf(t,v)dv = \frac{1}{2}\langle\int_0^1\int_0^1 \Big[\gamma I(v,w;\rho) + D(v;\rho)\eta\Big]f(t,v)f(t,w)dvdw\rangle, \qquad (4.7)$$

which is equivalent to

$$\begin{aligned}\frac{d}{dt}V(t) &= \frac{1}{2}\langle\int_0^1\int_0^1[\gamma I(v,w;\rho) + D(v;\rho)\eta]f(t,v)f(t,w)dvdw\rangle = \\ &= \frac{1}{2}\langle\int_0^1\int_0^1\{\gamma[P(\rho)(1-v) + (1-P(\rho))(vw-v)]+ \\ &+ D(v;\rho)\eta\}f(t,v)f(t,w)dvdw\rangle.\end{aligned} \qquad (4.8)$$

Due to the fact that

$$
\begin{aligned}
&\langle\int_0^1\int_0^1\{\gamma[P(\rho)(1-v)+(1-P(\rho))(vw-v)]\}f(t,v)f(t,w)dvdw\rangle = \\
&=\gamma P(\rho)\underbrace{\Big(\int_0^1 f(t,w)dw\Big)}_{=1}\underbrace{\Big(\int_0^1(1-v)f(t,v)dv\Big)}_{=1-V(t)}+ \\
&+\gamma(1-P(\rho))\Big\{\underbrace{\Big(\int_0^1 vf(t,v)dv\Big)}_{=V(t)}\underbrace{\Big(\int_0^1 wf(t,w)dw\Big)}_{=V(t)}+ \qquad (4.9)\\
&-\underbrace{\Big(\int_0^1 f(t,w)dw\Big)}_{=1}\underbrace{\Big(\int_0^1 vf(t,v)dv\Big)}_{=V(t)}\Big\}= \\
&=\gamma[P(\rho)(1-V(t))+(1-P(\rho))(V(t)^2-V(t))]\}
\end{aligned}
$$

and

$$\langle\int_0^1\int_0^1 D(v;\rho)\eta f(t,v)f(t,w)dvdw\rangle=\int_0^1 D(v;\rho)\langle\eta\rangle f(t,v)dv=0\ , \qquad (4.10)$$

the equation we end up with is the following:

$$\frac{d}{dt}V(t)=\frac{\gamma}{2}[P(\rho)+(1-P(\rho))V^2(t)-V(t)]\ . \qquad (4.11)$$

Contrary to equation (3.7) obtained with the interactions in [46], now the motion of the mean speed $V(t)$ is governed by a differential equation with a nonlinearity. This originates from the nonlinearity vw contained in the interaction rules (4.1) - (4.2).

The goal is to the determine the mean speed speed at equilibrium i.e. as $t\to+\infty$. Therefore, first, fixed points of the system are determined and then, linear stability analysis is performed [41].
Let us rewrite (4.11) as

$$\dot{V}=g(V;P), \qquad (4.12)$$

where $g(V;P)=\frac{\gamma}{2}[P+(1-P)V^2-V]$ and $V,P\in[0,1]$.
In order to determine the fixed points, which will be denoted by V^*, we need to solve

$$g(V;P)=0 \iff (1-P)V^2-V+P=0\ , \qquad (4.13)$$

which is equivalent to solve a quadratic equation. For the moment, the physical requirement $V\in[0,1]$ is dropped and only positive speeds are considered. We will be back to this requirement in a second moment. The solutions of (4.13) are

$$V^* = \frac{1 \pm \sqrt{1 - 4P(1-P)}}{2(1-P)} \tag{4.14}$$

and we observe that

$$1 - 4P(1-P) = 4\Big(P - \frac{1}{2}\Big)^2 \geq 0 \quad \forall P \;. \tag{4.15}$$

Therefore, the existence of the two fixed points is guaranteed $\forall P \neq 1$. If $P = 1$, from (4.13), we obtain $V = 1$.

Thanks to (4.15), the fixed points can be rewritten as

$$V^* = \frac{1 \pm \sqrt{4(P-\frac{1}{2})^2}}{2(1-P)} = \frac{1 \pm 2|P - \frac{1}{2}|}{2(1-P)} \;. \tag{4.16}$$

Three cases should be distinguished:

- if $P > \frac{1}{2}$,
$$V^* = \frac{1 \pm 2(P-\frac{1}{2})}{2(1-P)}$$
and the two solutions are
$$V_+^* = \frac{P}{1-P} \text{ and } V_-^* = 1; \tag{4.17}$$
- if $P = \frac{1}{2}$,
$$V^* = 1$$
and therefore, the fixed point is unique;
- if $P < \frac{1}{2}$,
$$V^* = \frac{1 \pm 2(\frac{1}{2}-P)}{2(1-P)}$$
and the two solutions are
$$V_+^* = 1 \text{ and } V_-^* = \frac{P}{1-P} \;. \tag{4.18}$$

In order to determine the stability of the fixed points, linear stability analysis is performed by referring to [41]. Let us introduce

$$\epsilon(t) := V(t) - V^*,$$

which is the perturbation with respect to the fixed point V^*. Given (4.12), $\epsilon(t)$ has the following evolution equation:

$$\dot{\epsilon}(t) = \frac{d}{dt}[V(t) - V^*] = g(V;P) = g(V^* + \epsilon; P) \ . \tag{4.19}$$

If a small perturbation with respect to the fixed point V^* is assumed i.e. we assume $\epsilon \to 0$, a Taylor expansion of $g(V^* + \epsilon; P)$ around V^* can be carried out. Therefore, at first order we obtain

$$\dot{\epsilon}(t) = g(V^*;P) + \epsilon g'(V^*;P) + O(\epsilon^2) = \epsilon g'(V^*;P) + O(\epsilon^2), \ \epsilon \to 0. \tag{4.20}$$

By neglecting second order terms, we get $\dot{\epsilon}(t) \simeq \epsilon g'(V^*;P)$ that is the linearization about V^* and therefore,

$$\epsilon(t) \simeq \epsilon(0) e^{g'(V^*;P)} \ . \tag{4.21}$$

This means that the sign of $g'(V^*;P)$ determines whether the perturbation grows or decay exponentially, $|g'(V^*;P)|$ represents the rate of growth or decay and its inverse is the characteristic time of growth or decay [41]. In any case, it is important to note that the convergence is exponential in time.

Let us compute the first derivative with respect to V of the function $g(V;P)$ in order to determine the stability of the fixed points [41]:

$$g'(V;P) = \gamma V(1-P) - \frac{\gamma}{2} \ . \tag{4.22}$$

Let us consider the expression of the fixed points defined in (4.16). If $V^* = V^*_+ = \frac{1+2|P-\frac{1}{2}|}{2(1-P)}$, then

$$g'(V^*;P) = \gamma \tfrac{1+2|P-\frac{1}{2}|}{2} - \tfrac{\gamma}{2} = \gamma |P - \tfrac{1}{2}| \ ,$$

and, due to the fact that $\gamma > 0$, $g'(V^*;P) > 0 \ \forall P \in [0,1)$. So, this fixed point is unstable $\forall P \in [0,1)$.

On the other hand, if $V^* = V^*_- = \frac{1-2|P-\frac{1}{2}|}{2(1-P)}$, then

$$g'(V^*;P) = \gamma \tfrac{1-2|P-\frac{1}{2}|}{2} - \tfrac{\gamma}{2} = -\gamma |P - \tfrac{1}{2}| < 0 \ \forall P \in [0,1) \ ,$$

and so, this other fixed point is stable $\forall P \in [0,1)$.

If $P = \frac{1}{2}$, $g'(V^*;P) = 0$. This means that we cannot rely on linear stability analysis anymore and nonlinear stability analysis has to be performed in order to determine the stability of the fixed point [41]. Terms of order ϵ^2 in (4.20) are not longer negligible and so, a Taylor expansion at second order is performed:

$$\dot{\epsilon}(t) = \epsilon g'(V^*; P) + \frac{\epsilon^2}{2} g''(V^*; P) + O(\epsilon^3), \ \epsilon \to 0 \ . \tag{4.23}$$

For $P = \frac{1}{2}$ and $V^* = 1$ and by neglecting terms of order ϵ^3, (4.23) becomes equivalent to

$$\dot{\epsilon}(t) \simeq \frac{\epsilon^2}{2} g''(V^*; P) = \frac{\gamma}{2}\epsilon^2 \ . \tag{4.24}$$

Therefore, by solving the evolution equation for the perturbation ϵ, the solution turns out to be

$$\epsilon(t) \simeq \left[\frac{1}{\epsilon(0)} - \frac{\gamma}{4} t\right]^{-1} \ . \tag{4.25}$$

Consequently, the fixed point $V^* = 1$, which is obtained for $P = \frac{1}{2}$, is stable but contrary to the fixed points previously found, the mean speed converges to it with a polynomial law. In particular, the mean speed converges to 1 as $t^{-\beta}$, where $\beta = 1$. Much longer time is needed to converge to the stationary solution at the critical point $P = 1/2$ than at other values of P.

If $P = 1$, we have previously computed the fixed point, which coincides with the solution of (4.11) with this value of P and it is $V = 1$. In this case,

$$g(V; P = 1) = \tfrac{\gamma}{2}(1 - V) \text{ and } g'(V; P = 1) = -\tfrac{\gamma}{2} < 0.$$

Therefore, $V^* = 1$ is a stable fixed point of the system if $P = 1$.

In figure 4.1 (p. 86), the bifurcation diagram of the system is displayed. On the top, the speed fixed point is plotted as a function of the probability of accelerating P. On the bottom, it is plotted as a function of the density ρ. In particular, it is assumed that the probability of accelerating P has the form defined in (4.3) and introduced in [46] with $\mu = 2$. This choice of the exponent μ is properly justified in section 4.8.

If the constraint of physical admissibility is reintroduced i.e. $V \in [0,1]$, we observe that for big values of P or equivalently for small ρ, the unstable fixed point assumes values outside of this domain. However, this is not a problem since this fixed point is unstable and at equilibrium the system will converge to the stable one.

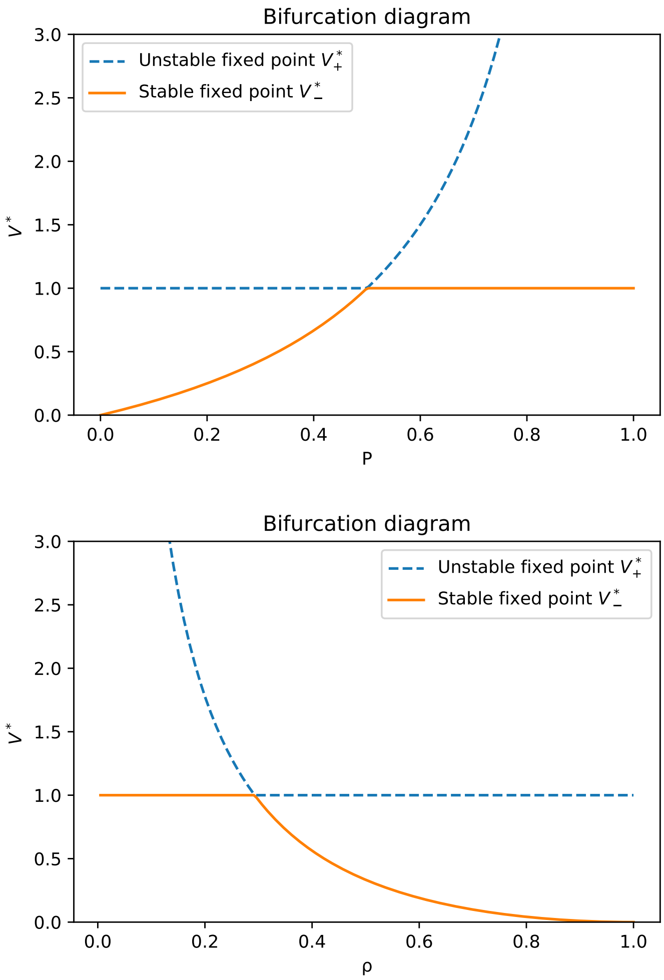

Figure 4.1: Bifurcation diagram of equation (4.11). On the top, the fixed point is plotted as a function of the probability of accelerating P. On the bottom, it is plotted as a function of the density ρ by referring to the definition (4.3) with $\mu = 2$

Most importantly, from this bifurcation diagram, the typical behavior of a bifurcation is evident: there are two fixed points, one stable and one unstable, for all values of density except for a critical value at which the two fixed points merge. This critical value of density is called critical density ρ_c of the system and it marks the passage from one phase to another. The stability of the two fixed points (FP) remains unchanged.

$$\begin{array}{ccccc} 2\text{ FP} & \rightarrow & 1\text{ FP} & \rightarrow & 2\text{ FP} \\ \rho \in [0, \rho_c) & & \rho_c & & \rho \in (\rho_c, 1] \end{array}$$

The merging of the two fixed points occurs for $P(\rho) = \frac{1}{2}$ and therefore, the critical density ρ_c can be determined as follows:

$$P(\rho_c) = \frac{1}{2} \iff (1-\rho_c)^\mu = \frac{1}{2} \iff \rho_c = 1 - 2^{-\frac{1}{\mu}} \ . \tag{4.26}$$

Therefore, the critical density turns to be only dependent on the exponent μ in the probability of accelerating $P(\rho)$.

For $\rho \in [0, \rho_c]$, the system is in the free flow phase: the density is low and the mean speed of agents coincides with the maximum allowed one. For $\rho \in (\rho_c, 1]$, the system in the congested phase: the density increases and consequently, the mean speed of agents decreases nonlinearly to 0.

We can summarize our results by saying:

- if $P \in [0, \frac{1}{2}) \iff \rho \in (\rho_c, 1]$, there are two fixed points: one stable (V_-^*) and one unstable (V_+^*). The mean speed at equilibrium is $V_-^* = \frac{P(\rho)}{1-P(\rho)}$ and the system is the congested flow phase;
- if $P = \frac{1}{2} \iff \rho = \rho_c$, there is just one fixed point which is stable and is $V^* = 1$. The system is at the critical point;
- if $P \in (\frac{1}{2}, 1] \iff \rho \in [0, \rho_c)$, there are two fixed points: one stable (V_-^*) e one unstable (V_+^*). The mean speed at equilibrium is $V_-^* = 1$ and the system is in the free flow phase.

$$V_\infty(\rho) = \begin{cases} \frac{P(\rho)}{1-P(\rho)} & \text{if } \rho \in (\rho_c, 1] \\ 1 & \text{if } \rho \in [0, \rho_c] \end{cases} \tag{4.27}$$

4.3 The asymptotic speed distribution with nonlinear interaction rules

The emergence of a phase transition is evident from the study of the mean speed at equilibrium. The next step in our analysis is to obtain the asymptotic speed distribution $f_\infty = f_\infty(v)$. It would be expected to obtain a sharp transition in the shape of the speed distribution function at equilibrium; in particular, this transition would occur for the critical density previously obtained.

As explained in detail in section 3.6, the *quasi-invariant interaction limit* is considered in order to analytically determine an expression for f_∞. Let us recall this limit:

$$\gamma, \sigma^2 \to 0^+ \text{ such that } \tfrac{\sigma^2}{\gamma} \to \lambda > 0 \ .$$

Calculations are identical to section 3.6 until the interaction function and the mean speed at equilibrium have to be plugged in. Therefore, let us consider equation (3.21) [46]:

$$\partial_\tau \tilde{f} = \frac{\lambda}{2}\partial_v^2\Big(D^2(v;\rho)\tilde{f}\Big) - \partial_v\Big(\big(\int_0^1 I(v,w;\rho)\tilde{f}(\tau,w)dw\big)\tilde{f}\Big) \tag{4.28}$$

with the boundary conditions

$$\begin{cases} \big(\int_0^1 I(v,w;\rho)\tilde{f}(\tau,w)dw\big)\tilde{f}(\tau,v) + \frac{\lambda}{2}\partial_v\Big(D^2(v;\rho)\tilde{f}(\tau,v)\Big) = 0 \\ D^2(v;\rho)\tilde{f}(\tau,v) = 0 \end{cases} \tag{4.29}$$

for $v = 0{,}1$ and $\forall \tau > 0$.

Let us compute the integral of the new interaction function (4.2) in the Fokker-Planck PDE (4.28):

$$\begin{aligned}\int_0^1 I(v,w;\rho)\tilde{f}(\tau,w)dw &= \int_0^1 \big[P(\rho)(1-v) + (1-P(\rho))(vw-v)\big]\tilde{f}(\tau,w)dw = \\ &= P(\rho)(1-v) + (1-P(\rho))v(\tilde{V}-1) \ ,\end{aligned} \tag{4.30}$$

where $\tilde{V}$ is the mean speed with respect to the distribution function $\tilde{f}$ i.e. $\tilde{V} = \int_0^1 w\tilde{f}(\tau,w)dw$.

At equilibrium i.e. for $\tau \to +\infty$, the Fokker-Planck type equation (4.28) becomes

$$\frac{\lambda}{2}\partial_v^2\Big(D^2(v;\rho)\tilde{f}_\infty\Big) - \partial_v\Big\{\big[P(\rho)(1-v) + (1-P(\rho))v(\tilde{V}_\infty - 1)\big]\tilde{f}_\infty\Big\} = 0 \ . \tag{4.31}$$

At this point, the analysis for the two different regimes have to be performed separately. Let us consider the **congested flow regime**. As derived in the previous section, it corresponds to $P \in [0, \frac{1}{2}) \iff \rho \in (\rho_c, 1]$. In this regime,

$$\tilde{V}_\infty(\rho) = \frac{P(\rho)}{1-P(\rho)} \iff \tilde{V}_\infty(\rho)(1-P(\rho)) = P(\rho) \ . \tag{4.32}$$

Therefore, we have

$$\begin{aligned}&\Big[P(\rho)(1-v)+(1-P(\rho))v(\tilde{V}_\infty-1)\Big]=\\&=P(\rho)-P(\rho)v+v\tilde{V}_\infty-v-P(\rho)v\tilde{V}_\infty+P(\rho)v=\\&=v\tilde{V}_\infty(1-P(\rho))+P(\rho)-v=vP(\rho)+P(\rho)-v=P(\rho)-v(1-P(\rho)),\end{aligned} \tag{4.33}$$

where in the penultimate equality, (4.32) has been plugged in.
This results is then used to rewrite (4.31):

$$\begin{aligned}&\frac{\lambda}{2}\partial_v^2\Big(D^2(v;\rho)\tilde{f}_\infty\Big)-\partial_v\Big\{\Big[P(\rho)-v(1-P(\rho))\Big]\tilde{f}_\infty\Big\}=0 \iff\\&\iff \partial_v\Big\{\lambda D(v;\rho)\tilde{f}_\infty\partial_v D(v;\rho)+\frac{\lambda}{2}D^2(v;\rho)\partial_v\tilde{f}_\infty+\\&\qquad\qquad -\Big[P(\rho)-v(1-P(\rho))\Big]\tilde{f}_\infty\Big\}=0\\&\implies \int\frac{d\tilde{f}_\infty}{\tilde{f}_\infty}=-2\int\frac{\partial_v D(v;\rho)}{D(v;\rho)}dv+\frac{2}{\lambda}\int\left[\frac{P(\rho)}{D^2(v;\rho)}-\frac{v(1-P(\rho))}{D^2(v;\rho)}\right]dv\ .\end{aligned} \tag{4.34}$$

In order to introduce the diffusion coefficient $D(v;\rho)$, we refer to section 3.6 and in particular, to definition (3.26) and remark 3.6.1:

$$D(v;\rho)=a(\rho)\sqrt{v(1-v)}\ ,a(\rho)\geq 0\ . \tag{4.35}$$

Then, the integrals in (4.34) can be solved:

$$\begin{aligned}&2\int\frac{\partial_v D(v;\rho)}{D(v;\rho)}dv=2\log D(v;\rho)\\&\int\frac{P(\rho)}{D^2(v;\rho)}dv=\frac{P(\rho)}{a^2(\rho)}\int\left[\frac{1}{v}+\frac{1}{1-v}\right]dv=\frac{P(\rho)}{a^2(\rho)}\log\left(\frac{v}{1-v}\right)\\&\int\frac{v(1-P(\rho))}{D^2(v;\rho)}dv=-\frac{1-P(\rho)}{a^2(\rho)}\log(1-v)\ .\end{aligned} \tag{4.36}$$

Eventually, the asymptotic speed distribution turns out to be a beta probability density function as in [46] - see (3.28) - (3.29):

$$\tilde{f}_\infty(v)=\frac{v^{\alpha-1}(1-v)^{\beta-1}}{B(\alpha,\beta)} \tag{4.37}$$

but with different parameters α and β. They are

$$\begin{aligned}\alpha &:= \frac{2P(\rho)}{\lambda a^2(\rho)}\\ \beta &:= \frac{2(1-P(\rho))}{\lambda a^2(\rho)} - \frac{2P(\rho)}{\lambda a^2(\rho)} = \frac{2(1-2P(\rho))}{\lambda a^2(\rho)} \ .\end{aligned} \tag{4.38}$$

$B(\alpha, \beta)$ is the beta function i.e. $B(\alpha, \beta) = \int_0^1 x^{\alpha-1}(1-x)^{\beta-1}dx$.

Remark 4.3.1.

- $\alpha = \frac{P(\rho)}{\lambda a^2(\rho)} \geq 0$ since $P(\rho) \in [0,1]$, $\lambda > 0$

  However, the case $\alpha = 0$ corresponds to maximum density i.e. $\rho = 1$ since $P(\rho) = (1-\rho)^\mu$, $\mu > 0$. We are confident enough it is highly improbable to have the system in such a situation. Therefore, we can consider $\alpha > 0$ and consequently, the beta distribution well-defined.

- $\beta = \frac{2(1-2P(\rho))}{\lambda a^2(\rho)} > 0 \iff 1 - 2P(\rho) > 0 \iff P(\rho) < \frac{1}{2}$
  $P(\rho) < \frac{1}{2}$ holds since we are in the congested flow regime. So, this implies $\beta > 0$.

□

Let us note that (4.28) is accompanied with boundary conditions. Analogously to [46], these conditions are satisfied if

$$a^2(\rho) \leq \frac{1}{\lambda} \min\{P(\rho), 2(1-2P(\rho))\} \ . \tag{4.39}$$

Indeed, if (4.39) holds, the asymptotic distribution function $\tilde{f}_\infty$ and its derivative $\partial_v \tilde{f}_\infty$ are null in the extreme values of the speed domain i.e. $v = 0, 1$.

If X is a random variable such that $X \sim \tilde{f}_\infty$,

$$\begin{aligned}\mathbb{E}[X] &= \frac{\alpha}{\alpha+\beta} = \frac{P(\rho)}{1-P(\rho)} = \tilde{V}_\infty(\rho)\\ \mathrm{Var}(X) &= \frac{\alpha\beta}{(\alpha+\beta)^2(\alpha+\beta+1)} = \frac{(1-\tilde{V}_\infty(\rho))\tilde{V}_\infty^2(\rho)}{2P(\rho)+\lambda a^2(\rho)\tilde{V}_\infty(\rho)}\lambda a^2(\rho) \ ,\end{aligned} \tag{4.40}$$

where the relation $\alpha + \beta = \frac{\alpha}{\tilde{V}_\infty}$ has been used.
Coherently, the expected value of a random variable distributed according

to the asymptotic speed distribution (4.37) is the mean speed at equilibrium $\tilde{V}_\infty(\rho)$.

Now, let us consider the **free flow regime**. As derived in the previous section, it corresponds to $P \in [\frac{1}{2},1] \iff \rho \in [0, \rho_c]$. In this regime,

$$\tilde{V}_\infty = 1.$$

In order to have insight on the change of shape of the asymptotic speed distribution which occurs at the critical point, we can approach the free flow regime. Therefore, let us introduce

$$\epsilon \coloneqq 1 - \tilde{V}_\infty \to 0^+.$$

The content of the square parenthesis in (4.31) can be rewritten as

$$P(\rho)(1-v) + (1-P(\rho))v(\tilde{V}_\infty - 1) = P(\rho)(1-v) - (1-P(\rho))v\epsilon \quad (4.41)$$

and by plugging it into (4.31), the following Fokker-Planck type equation at equilibrium is obtained:

$$\begin{aligned}
&\frac{\lambda}{2}\partial_v^2\Big(D^2(v;\rho)\tilde{f}_\infty\Big) - \partial_v\Big\{\Big[P(\rho)(1-v) - (1-P(\rho))v\epsilon\Big]\tilde{f}_\infty\Big\} = 0 \iff \\
&\iff \partial_v\Big\{\lambda D(v;\rho)\tilde{f}_\infty\partial_v D(v;\rho) + \frac{\lambda}{2}D^2(v;\rho)\partial_v\tilde{f}_\infty + \\
&\qquad\qquad - \Big[P(\rho)(1-v) - (1-P(\rho))v\epsilon\Big]\tilde{f}_\infty\Big\} = 0 \\
&\implies \int\frac{d\tilde{f}_\infty}{\tilde{f}_\infty} = -2\int\frac{\partial_v D(v;\rho)}{D(v;\rho)}dv + \frac{2}{\lambda}\int\left[\frac{P(\rho)(1-v)}{D^2(v;\rho)} - \frac{\epsilon v(1-P(\rho))}{D^2(v;\rho)}\right]dv\ .
\end{aligned} \quad (4.42)$$

By referring to (4.35), the integrals in (4.42) can be solved:

$$\begin{aligned}
2\int\frac{\partial_v D(v;\rho)}{D(v;\rho)}dv &= 2\log D(v;\rho) \\
\int\frac{P(\rho)(1-v)}{D^2(v;\rho)}dv &= \frac{P(\rho)}{a^2(\rho)}\log{(v)} \\
\int\frac{\epsilon v(1-P(\rho))}{D^2(v;\rho)}dv &= -\frac{1-P(\rho)}{a^2(\rho)}\epsilon\log{(1-v)}\ .
\end{aligned} \quad (4.43)$$

The asymptotic speed distribution is still a beta probability density function

$$\tilde{f}_\infty(v) = \frac{v^{\alpha-1}(1-v)^{\beta-1}}{B(\alpha,\beta)}\ , \quad (4.44)$$

but with different parameter β compared to the deep congested phase. Indeed, if we approach the free flow phase, the parameters of the asymptotic speed distribution are

$$\begin{aligned} \alpha &:= \frac{2P(\rho)}{\lambda a^2(\rho)} \\ \beta &:= \frac{2(1-P(\rho))}{\lambda a^2(\rho)}\epsilon \ . \end{aligned} \tag{4.45}$$

Remark 4.3.2.
- α is invariant compared to the congested flow phase and $\alpha > 0$.
- $\beta = \frac{2(1-P(\rho))}{\lambda a^2(\rho)}\epsilon \to 0^+$ since $\epsilon \to 0^+$.

□

As in the congested flow phase, fulfillment of the boundary conditions in (4.28) is required. Analogously to [46], these conditions are satisfied if

$$a^2(\rho) \leq \frac{1}{\lambda}\min\{2P(\rho),2(1-P(\rho))\epsilon\} \simeq \frac{1}{\lambda}\min\{2P(\rho),0\} \simeq 0 \ , \tag{4.46}$$

since $P(\rho) \in [0,1]$. Therefore, $a(\rho) \simeq 0$ in this regime. This is coherent indeed, if for example $a(\rho) = \rho(1-\rho)$, $a(\rho) \to 0^+$ in the free flow regime since $\rho \to 0^+$.

If X is a random variable such that $X \sim \tilde{f}_\infty$ and $\epsilon \to 0^+$,

$$\begin{aligned} \mathbb{E}[X] &= \frac{\alpha}{\alpha+\beta} \to 1 \\ \mathrm{Var}(X) &= \frac{\alpha\beta}{(\alpha+\beta)^2(\alpha+\beta+1)} \to 0^+ \ . \end{aligned} \tag{4.47}$$

By approaching the free flow regime, the expected value of a random variable distributed according to the asymptotic speed distribution tends to the maximum allowed speed. On the other hand, the variance shrinks to 0. This means that in the free flow phase, where $\epsilon = 0$, the asymptotic speed distribution is a Dirac delta distribution centered at 1:

$$\tilde{f}_\infty = \delta(v-1). \tag{4.48}$$

From the derivation of the asymptotic speed distribution in the two different regimes, the phase transition is evident. For densities greater than

the critical density ρ_c, the system is in the congested phase and the asymptotic speed distribution is a beta distribution function with parameters α, $\beta > 0$. When the density overcomes the threshold i.e. ρ_c, the asymptotic speed distribution suddenly shrinks to a Dirac delta centered at the maximum allowed speed i.e. 1.
This behavior reflects the piecewise-defined mean speed at equilibrium and this is in turn due to the nonlinearity in the new interaction rules introduced with (4.1) and (4.2).

The kinetic approach used in this dissertation expresses full potentiality in dealing with phase transition. Phase transition has been previously considered in macroscopic models and in this framework the approach is totally different. The existence of a phase transition is postulated a priori by assuming the existence of two different regions in the phase space, one for the free flow and another for the congested flow [32]. Different equations rule the dynamics in these two different regimes. In particular, in the free flow regime, the speed is uniquely determined by the density while, in the congested flow regime, it depends both on the density and on the flux.
Looking at the problem with the kinetic modeling's glasses means changing completely point of view. In this case, the phase transition naturally emerges from the derivation of macroscopic quantities, such as the mean speed and the asymptotic speed distribution, and it is due to the microscopic interaction rules, which determine the dynamics of the systems. No ansatz is needed. We only need to define the interaction rules by best modeling the real interactions between vehicles and let the system evolve.

Insight on the definition of phase transition

In the literature [16; 23; 32; 36; 37], phase transition is defined from a phenomenological point of view. Several definitions of this phenomenon exist and they are all based on the slope change in the *fundamental diagram*.

As explained in section 3.5, the *fundamental diagram* represents the flux $q(\rho) = \rho v(\rho)$ as a function of the density ρ. Therefore, the slope of this curve in the (ρ, q) plane is given by $q'(\rho) = v(\rho) + \rho v'(\rho)$.

If we consider the mean speed at equilibrium, which is defined in equation (4.27) then, we have that if $\rho \in [0, \rho_c]$, $v(\rho) = 1$ and $q'(\rho) = 1$ i.e. the slope of the flux in the *fundamental diagram* is positive for densities smaller than or equal to the critical. Instead, if $\rho \in (\rho_c,1]$, $v'(\rho) < 0$. Therefore, there exists a value of ρ such that $q'(\rho)$ is negative.
The value of density for which the slope of the flux becomes negative can be identified as follows. Let us impose that $q'(\rho) < 0$ if $\rho \in (\rho_c,1]$. This condition is equivalent to $v'/v < -1/\rho$ and it can be integrated in the density range $[\rho_c, \rho]$ where $\rho \in [\rho_c,1]$. So, we have

$$\int_{\rho_c}^{\rho} \frac{v'}{v} d\rho < -\int_{\rho_c}^{\rho} \frac{1}{\rho} d\rho \iff$$
$$\iff \log(v(\rho)) < -\log\left(\frac{\rho}{\rho_c}\right) \iff v(\rho) < \frac{\rho_c}{\rho} .$$

Due to the fact that if $\rho \to 1^-$, $v(\rho) \to 0$ and $\rho_c/\rho \to \rho_c$ and since $v(\rho)$ is continuous and monotonic if $\rho \in [\rho_c,1]$, we will have that $v(\rho) < \frac{\rho_c}{\rho}$ holds for $\rho \in [\rho_c,1]$. Consequently, the value of density for which the change of slope in the flux occurs, is the critical ρ_c and this is due to the bifurcation we obtain in the analysis of the mean speed at equilibrium.

An easier way to obtain the critical density and so, the phase transition could rely on determining the maximum flux. Indeed, this value of $q(\rho)$ marks the passage from the positive to negative slope. However, the definition which is based on the slope inversion is empirical and by referring to data, it is not possible to identify a density value for which the flux is maximum. From an experimental point of view, the so-called *capacity drop* is observed [23]: close to the critical density, the flux is discontinuous and once we are in the congested regime, flux sharply drops. Therefore, it is more significant to identify the phase transition by studying the bifurcation, which is a solid trait of the system dynamics, rather than identifying the maximum flux, which is not reproduced by experimental data.

4.4 Nonlinear interactions rules: controlled dynamics

As examined in depth in section 3.7 following the derivation in [46], it is possible to modify the interaction rules in order to take into account the presence of autonomous vehicles in traffic.

Let us consider the nonlinear interaction rules, defined in (4.1) - (4.2). The goal of this section is to introduce a control u [45; 46], in order to investigate the behavior of macroscopic quantities, such as mean speed at equilibrium and asymptotic speed distribution, in presence of a phase transition and for different control strategies.

Interaction rules are modified as follows by the introduction of the control [46]:

$$\begin{aligned} v' &= v + \gamma\Big[I(v, w; \rho) + \theta u\Big] + D(v; \rho)\eta \\ w' &= w \end{aligned} \tag{4.49}$$

where θ is a Bernoulli random variable of parameter p i.e. $\theta \sim$ Bernoulli(p) and p represents the penetration rate that means the percentage of autonomous vehicles in the traffic. The control u is actually [46]

$$u^* = \arg\min_{u \in \mathcal{U}} J(v'; u) \tag{4.50}$$

and $J(v'; u)$ is a least-square cost functional. As explained in section 3.7, the introduction of autonomous vehicles aims at the reduction of road risk, which is equivalent to the reduction of speed variability within the stream of vehicles [50]. Therefore,

$$J(v'; u) = \frac{1}{2}\langle \Big(V_d(w'; \rho) - v'\Big)^2 + \nu u^2 \rangle_\eta \ , \nu > 0 \tag{4.51}$$

where $V_d(w'; \rho) = w' = w$ if the control strategy is the **binary variance control**, and $V_d(w'; \rho) = v_d(\rho) \in [0,1]$ if the control strategy is the **desired speed control** [46]. We refer to section 3.7 for detailed explanations and for the derivation of the feedback controlled microscopic interaction rules, which is based on a *Model Predictive Control* approach [8] and the use of the Pontryagin's maximum principle [34]. Calculations are identical since the only difference between interaction rules is due to the interaction function $I(v, w; \rho)$.

Let us recall the expression of the feedback controlled microscopic interaction rules [46]:

$$\begin{aligned} v' &= v + \frac{\gamma^2\theta^2}{\nu+\gamma^2\theta^2}\Big[V_d(w;\rho)-v\Big] + \frac{\gamma\nu}{\nu+\gamma^2\theta^2} I(v,w;\rho) + D(v;\rho)\eta \\ w' &= w \end{aligned} \tag{4.52}$$

where $I(v,w;\rho)$ is defined in (4.2). The physical admissibility of these interaction rules is guaranteed by the criteria outlined in proposition 3.8.1.

4.5 Controlled dynamics: mean speed at equilibrium and asymptotic speed distribution

First, let us define the Boltzmann-type equation of the system [46]:

$$\frac{d}{dt}\int_0^1 \phi(v)f^*(t,v)dv = \frac{1}{2}\mathbb{E}_\theta\Big[\langle\int_0^1\int_0^1 [\phi(v')) - \phi(v)]f^*(t,v)f^*(t,w)dvdw\rangle_\eta\Big], \tag{4.53}$$

where, compared to (4.4), the expected value with respect to the Bernoulli random variable θ has been introduced and the superscript * refers to the fact that the controlled case is considered.

In order to derive the evolution equation for the mean speed, we set $\phi(v) = v$ and interaction rules (4.52) are plugged in (4.53):

$$\begin{aligned} \frac{dV^*}{dt} &= \frac{\gamma}{2}\Bigg\{\frac{p\gamma}{\nu+\gamma^2}\int_0^1 \Big[V_d(w;\rho)-v\Big]f^*(t,w)dw+ \\ &\quad + \frac{p\nu}{\nu+\gamma^2}\Big[P(\rho)(1-V^*) + (1-P(\rho))((V^*)^2-V^*)\Big]+ \\ &\quad + (1-p)\Big[P(\rho)(1-V^*) + (1-P(\rho))((V^*)^2-V^*)\Big]\Bigg\} \iff \\ \iff \frac{dV^*}{dt} &= \frac{\gamma}{2}\Bigg\{\frac{p\nu+(1-p)(\nu+\gamma^2)}{\nu+\gamma^2}\Big[P(\rho)(1-V^*)+ \\ &\quad + (1-P(\rho))((V^*)^2-V^*)\Big]+ \\ &\quad + \frac{p\gamma}{\nu+\gamma^2}\Big(\int_0^1 V_d(w;\rho)f^*(t,w)dw - V^*\Big)\Bigg\}, \end{aligned} \tag{4.54}$$

where $V^* = V^*(t) := \int_0^1 v f^*(t,v)dv$ i.e. V^* is the mean speed in the controlled case [46].

Remark 4.5.1. If $p = 0$ i.e. there are no autonomous vehicles in the traffic, (4.54) becomes equivalent to (4.11). This also occurs if $\nu \to +\infty$ indeed this case corresponds to the situation of maximum penalization of large controls and the cost functional is minimized by $u = 0$.

On the other hand, if $\nu \to 0^+$ i.e. large controls are not penalized at all and $p = 1$ i.e. the penetration rate is maximum, the evolution equation of the mean speed is dominated by the last term at the right-hand side of (4.54), which is absent in (4.11) and is completely due to the presence of the control. For $\nu \to 0^+$ and intermediate values of penetration rate p i.e. $p \in (0,1)$, both terms of the right-hand side of (4.54) play a role. $\square$

As in section 3.9, the *quasi-invariant interaction limit* is assumed in order to analytically determine an expression for V^*_∞ [46]. Let us recall this limit in the controlled case:

$$\gamma, \nu, \sigma^2 \to 0^+ \text{ such that } \frac{\sigma^2}{\gamma} \to \lambda > 0 \text{ and } \frac{\nu}{\gamma} \to \kappa > 0 \quad .$$

Moreover, the new time scale $\tau := \frac{\gamma}{2}t$, the scaled distribution function $\tilde{f}^*(\tau,v) := f^*(2\tau/\gamma, v)$ and the scaled mean speed $\tilde{V}^*(\tau) := V^*(2\tau/\gamma)$ are introduced. Therefore, we obtain

$$\begin{aligned} \frac{d\tilde{V}^*}{d\tau} &= \frac{\nu+\gamma^2}{\nu+\gamma^2}\Big[P(\rho)(1-\tilde{V}^*) + (1-P(\rho))\Big((\tilde{V}^*)^2 - \tilde{V}^*\Big)\Big] + \\ &\quad - \frac{p}{1+\frac{\nu}{\gamma^2}}\Big[P(\rho)(1-\tilde{V}^*) + (1-P(\rho))\Big((\tilde{V}^*)^2 - \tilde{V}^*\Big)\Big] + \\ &\quad + \frac{p}{\frac{\nu}{\gamma}+\gamma}\left(\int_0^1 V_d(w;\rho)\tilde{f}^*(\tau,w)dw - \tilde{V}^*\right) \end{aligned} \tag{4.55}$$

and in the *quasi-invariant interaction limit*, equation (4.55) becomes

$$\begin{aligned} \frac{d\tilde{V}^*}{d\tau} &= \Big[P(\rho)(1-\tilde{V}^*) + (1-P(\rho))\Big((\tilde{V}^*)^2 - \tilde{V}^*\Big)\Big] + \\ &\quad + \frac{p}{\kappa}\left(\int_0^1 V_d(w;\rho)\tilde{f}^*(\tau,w)dw - \tilde{V}^*\right) \iff \\ \iff \quad \frac{d\tilde{V}^*}{d\tau} &= P(\rho) + (\tilde{V}^*)^2(1-P(\rho)) - (1+p^*)\tilde{V}^* + \\ &\quad + p^*\left(\int_0^1 V_d(w;\rho)\tilde{f}^*(\tau,w)dw\right) , \end{aligned} \tag{4.56}$$

where p^* is the effective penetration rate and is defined as $p^* := \frac{p}{\kappa}$. In order to obtain the mean speed at equilibrium, the limit $\tau \to +\infty$ will be considered and so, the equation

$$P(\rho) + (\tilde{V}^*_\infty)^2(1 - P(\rho)) - (1 + p^*)\tilde{V}^*_\infty + p^*\bigg(\int_0^1 V_d(w;\rho)\tilde{f}^*(\tau, w)dw\bigg) = 0 \tag{4.57}$$

will be studied for the two different control strategies.

Analogously, an equation for the asymptotic speed distribution to be studied for the two different control strategies can be derived.
As explained in detail in section 3.10, the Fokker-Planck PDE for $\tilde{f}^*$, which is obtained in the *quasi-invariant interaction limit* is [46]

$$\begin{aligned} \partial_\tau \tilde{f}^* = \frac{\lambda}{2}\partial_v^2\Big(D^2(v;\rho)\tilde{f}^*\Big) + \\ - \partial_v\bigg\{\bigg[\int_0^1 \Big(I(v,w;\rho) + p^* V_d(w;\rho)\Big)\tilde{f}^*(\tau, w)dw - p^* v\bigg]\tilde{f}^*\bigg\} \ . \end{aligned} \tag{4.58}$$

If $\tau \to +\infty$ and by plugging the interaction function defined in (4.2), we obtain

$$\begin{aligned} \frac{\lambda}{2}\partial_v^2\Big(D^2(v;\rho)\tilde{f}^*\Big) - \partial_v\bigg\{\bigg[P(\rho)(1 - v) + (1 - P(\rho))v(\tilde{V}^*_\infty - 1) + \\ + p^*\int_0^1 V_d(w;\rho)\tilde{f}^*(\tau, w)dw - p^* v\bigg]\tilde{f}^*\bigg\} = 0 \ . \end{aligned} \tag{4.59}$$

The content of square brackets in (4.59) can be rewritten as follows:

$$\begin{aligned} & P(\rho)(1 - v) + (1 - P(\rho))v(\tilde{V}^*_\infty - 1) + p^*\int_0^1 V_d(w;\rho)\tilde{f}^*(\tau, w)dw - p^* v = \\ & = P(\rho) + v\tilde{V}^*_\infty(1 - P(\rho)) - (1 + p^*)v + p^*\int_0^1 V_d(w;\rho)\tilde{f}^*(\tau, w)dw = \\ & = P(\rho) + v\tilde{V}^*_\infty(1 - P(\rho)) - (1 + p^*)v + \\ & - \Big[P(\rho) + (\tilde{V}^*_\infty)^2(1 - P(\rho)) - (1 + p^*)\tilde{V}^*_\infty\Big] = \\ & = v\tilde{V}^*_\infty(1 - P(\rho)) + (1 + p^*)\big(\tilde{V}^*_\infty - v\big) - (\tilde{V}^*_\infty)^2(1 - P(\rho)) \ , \end{aligned} \tag{4.60}$$

where in the second equality, (4.57) is used in order to rewrite the last term.

Therefore, we obtain

$$
\begin{aligned}
\frac{\lambda}{2}\partial_v^2\Big(D^2(v;\rho)\tilde{f}^*\Big) &= \partial_v\Big\{\Big[v\tilde{V_\infty^*}(1-P(\rho)) + (1+p^*)\big(\tilde{V_\infty^*}-v\big)+ \\
&\quad -(\tilde{V_\infty^*})^2(1-P(\rho))\Big]\tilde{f}^*\Big\} \\
\Longrightarrow \int \frac{d\tilde{f}_\infty}{\tilde{f}_\infty} &= -2\int \frac{\partial_v D(v;\rho)}{D(v;\rho)}dv + \frac{2}{\lambda}\int\Big[\frac{v\tilde{V_\infty^*}(1-P(\rho))}{D^2(v;\rho)}+ \\
&\quad + \frac{(1+p^*)\big(\tilde{V_\infty^*}-v\big)}{D^2(v;\rho)} - \frac{(\tilde{V_\infty^*})^2(1-P(\rho))}{D^2(v;\rho)}\Big]dv\ .
\end{aligned}
\tag{4.61}
$$

As in the uncontrolled case, the diffusion coefficient is chosen by referring to section 3.6 and in particular, to definition (3.26) and remark 3.6.1. Then, the integrals in (4.61) can be solved:

$$
\begin{aligned}
&-2\int \frac{\partial_v D(v;\rho)}{D(v;\rho)}dv = -2\log D(v;\rho) \\
&\int \frac{v\tilde{V_\infty^*}(1-P(\rho))}{D^2(v;\rho)}dv = -\frac{\tilde{V_\infty^*}(1-P(\rho))}{a^2(\rho)}\log(1-v) \\
&\int \frac{(1+p^*)\big(\tilde{V_\infty^*}-v\big)}{D^2(v;\rho)}dv = \frac{(1+p^*)\tilde{V_\infty^*}}{a^2(\rho)}\log\left(\frac{v}{1-v}\right) + \frac{(1+p^*)}{a^2(\rho)}\log(1-v) \\
&-\int \frac{(\tilde{V_\infty^*})^2(1-P(\rho))}{D^2(v;\rho)}dv = -\frac{(\tilde{V_\infty^*})^2(1-P(\rho))}{a^2(\rho)}\log\left(\frac{v}{1-v}\right)\ .
\end{aligned}
\tag{4.62}
$$

The asymptotic speed distribution turns out to be a beta probability density function

$$
\tilde{f_\infty^*}(v) = \frac{v^{\alpha-1}(1-v)^{\beta-1}}{B(\alpha,\beta)}\ , \tag{4.63}
$$

with parameters α and β defined as follows:

$$\begin{aligned}
\alpha :=& \frac{2}{\lambda}\left\{\frac{(1+p^*)\tilde{V_\infty^*}}{a^2(\rho)} - \frac{(\tilde{V_\infty^*})^2(1-P(\rho))}{a^2(\rho)}\right\} = \frac{2\tilde{V_\infty^*}}{\lambda a^2(\rho)}\Big[(1+p^*) - \tilde{V_\infty^*}(1-P(\rho))\Big] \\
&\implies \alpha := \frac{2\tilde{V_\infty^*}}{\lambda a^2(\rho)}\Big[(1+p^*) - \tilde{V_\infty^*}(1-P(\rho))\Big] \\
\beta :=& \frac{2}{\lambda}\left\{-\frac{\tilde{V_\infty^*}(1-P(\rho))}{a^2(\rho)} + \frac{(1+p^*)(1-\tilde{V_\infty^*})}{a^2(\rho)} + \frac{(\tilde{V_\infty^*})^2(1-P(\rho))}{a^2(\rho)}\right\} = \\
=& \frac{2}{\lambda a^2(\rho)}\left\{\Big((\tilde{V_\infty^*})^2 - \tilde{V_\infty^*}\Big)(1-P(\rho)) + (1+p^*)(1-\tilde{V_\infty^*})\right\} \\
&\implies \beta := \frac{2}{\lambda a^2(\rho)}\left\{\Big((\tilde{V_\infty^*})^2 - \tilde{V_\infty^*}\Big)(1-P(\rho)) + (1+p^*)(1-\tilde{V_\infty^*})\right\}.
\end{aligned} \tag{4.64}$$

Remark 4.5.2.

- $\alpha = \underbrace{\frac{2\tilde{V_\infty^*}}{\lambda a^2(\rho)}}_{\geq 0}\Big[\underbrace{(1+p^*)}_{\geq 1} - \underbrace{\tilde{V_\infty^*}(1-P(\rho))}_{\in[0,1]}\Big] \geq 0$

  The case $\alpha = 0$ corresponds to minimum mean speed i.e. $\tilde{V_\infty^*} = 0$ and therefore, to maximum density i.e. $\rho = 1$. We are confident enough it is highly improbable to have the system in such a situation therefore, we can consider $\alpha > 0$ and consequently, the beta distribution well-defined.

- $\beta = \underbrace{\frac{2}{\lambda a^2(\rho)}}_{>0}\left\{\underbrace{\Big((\tilde{V_\infty^*})^2 - \tilde{V_\infty^*}\Big)(1-P(\rho))}_{\in[0,1]} + \underbrace{(1+p^*)}_{\geq 1}\underbrace{(1-\tilde{V_\infty^*})}_{\in[0,1]}\right\} \geq 0$

  The case $\beta = 0$ corresponds to maximum mean speed i.e. $\tilde{V_\infty^*} = 1$. We will see that this occurs in the free flow regime for the binary variance control. In this case, the beta distribution shrinks to a Dirac delta centered at 1. For all other cases $\beta > 0$ and consequently, the beta distribution can be considered well-defined.

$\square$

Remark 4.5.3. If $p^* = 0$ i.e. there are not autonomous vehicles, α and β in (4.64) turns out to be equivalent to the corresponding parameters in the uncontrolled case. Indeed, we obtain

$$\begin{aligned}
\alpha &:= \frac{2\tilde{V_\infty}}{\lambda a^2(\rho)}\Big[1-\tilde{V_\infty}(1-P(\rho))\Big] \\
\beta &:= \frac{2}{\lambda a^2(\rho)}\Big\{\Big((\tilde{V_\infty})^2-\tilde{V_\infty}\Big)(1-P(\rho))+(1-\tilde{V_\infty})\Big\}\,.
\end{aligned} \tag{4.65}$$

In the congested flow regime, where $\tilde{V_\infty}=\frac{P(\rho)}{1-P(\rho)}$, by reworking on (4.65) we have

$$\begin{aligned}
\alpha &:= \frac{2P(\rho)}{\lambda a^2(\rho)} \\
\beta &:= \frac{2(1-2P(\rho))}{\lambda a^2(\rho)}\,.
\end{aligned} \tag{4.66}$$

Instead, if we approach the free flow regime i.e. $\tilde{V_\infty}\to 1$, by reworking on (4.65) we obtain

$$\begin{aligned}
\alpha &:= \frac{2P(\rho)}{\lambda a^2(\rho)} \\
\beta &\to 0^+\,.
\end{aligned} \tag{4.67}$$

□

Let us note that (4.58) is accompanied with boundary conditions. These conditions are satisfied if the asymptotic distribution function $\tilde{f}^*_\infty$ and its derivative $\partial_v \tilde{f}^*_\infty$ are null in the extreme values of the speed domain i.e. $v=0,1$ [46]. This is equivalent to state that

$$\begin{cases} \alpha-2\geq 0 \\ \beta-2\geq 0 \end{cases} \tag{4.68}$$

and by reworking on it, a condition for $a^2(\rho)$, similar to the one obtained in the uncontrolled case, can be imposed.

If X^* is a random variable such that $X^*\sim \tilde{f}^*_\infty$,

$$\begin{aligned}
\mathbb{E}[X^*] &= \frac{\alpha}{\alpha+\beta}=\tilde{V^*_\infty} \\
\mathrm{Var}(X^*) &= \frac{\alpha\beta}{(\alpha+\beta)^2(\alpha+\beta+1)} = \frac{(1-\tilde{V^*_\infty})\tilde{V^*_\infty}^{\,2}}{\tilde{V^*_\infty}+\frac{2\tilde{V^*_\infty}}{\lambda a^2(\rho)}\Big[(1+p^*)-\tilde{V^*_\infty}(1-P(\rho))\Big]}\,,
\end{aligned} \tag{4.69}$$

where the relation $\alpha+\beta=\frac{\alpha}{\tilde{V}_\infty^*}$ has been used.
Coherently, the expected value of a random variable distributed according to the asymptotic speed distribution (4.63) is the mean speed at equilibrium in the controlled case $\tilde{V}_\infty^*$.

4.6 Binary variance control

The binary variance control is a strategy, which aims at reducing road risk. This is achieved by reducing the post-interaction speed variance of the two vehicles involved in a binary interaction.
In particular, this control strategy assumes: $V_d(w';\rho)=w'=w$. If this is plugged in equation (4.57), we obtain the mean speed at equilibrium in presence of a binary variance control. Indeed, (4.57) becomes

$$\begin{aligned} &P(\rho)+(\tilde{V}_\infty^*)^2(1-P(\rho))-(1+p^*)\tilde{V}_\infty^*+p^*\tilde{V}_\infty^*=0 \iff \\ \iff &P(\rho)+(\tilde{V}_\infty^*)^2(1-P(\rho))-\tilde{V}_\infty^*=0 \end{aligned} \tag{4.70}$$

and therefore, the analysis is equivalent to the one performed in the uncontrolled case - see equation (4.11) and subsequent calculations:

$$\tilde{V}_\infty^*(\rho)=\begin{cases} \frac{P(\rho)}{1-P(\rho)} & \text{if } \rho\in(\rho_c,1] \\ 1 & \text{if } \rho\in[0,\rho_c] \end{cases} . \tag{4.71}$$

The asymptotic speed distribution with this control strategy is the beta distribution defined in (4.63). The parameters α and β of this distribution are defined in (4.64) and they are functions of $\tilde{V}_\infty^*$, $P(\rho)$ and p^*. With the binary variance control, the mean speed at equilibrium $\tilde{V}_\infty^*$ has the form defined in (4.71). This means that, even if α and β have different expressions due to the presence of the control, the phase transition is still present and it occurs for the same critical density found in the uncontrolled case. For $\rho\in(\rho_c,1]$, the asymptotic speed distribution is a beta distribution with α, $\beta>0$. For densities smaller than or equal to ρ_c, the asymptotic speed distribution shrinks to a Dirac delta centered at 1. Indeed, if $\tilde{V}_\infty^*\to 1$ i.e. by approaching the free flow regime, we obtain

$$\begin{aligned} &\alpha\to\frac{2}{\lambda a^2(\rho)}\big(p^*+P(\rho)\big) \\ &\beta\to 0^+ . \end{aligned} \tag{4.72}$$

Therefore, in the free flow regime, $\tilde{f}_\infty^*(v)=\delta(v-1)$ as in the uncontrolled case.

If our analysis was just limited to the *speed* and the *fundamental diagrams*, no difference would be revealed compared to the uncontrolled case. Indeed, the mean speed at equilibrium is not affected by the introduction of the binary variance control. Instead, the study of the asymptotic speed distribution shows that, even though the phase transition from a beta distribution to a Dirac delta is preserved, the parameters which characterize the beta distribution are different. In the controlled case, the parameters α and β also depends on the effective penetration rate p^*.

Let us consider the free flow regime. In this regime, both in the uncontrolled and in the controlled case, the asymptotic speed distribution is a Dirac delta centered at 1. So, we have $\mathrm{Var}(X^*) = \mathrm{Var}(X) = 0$. On the other hand, in the congested flow regime, the variance of the beta distribution decreases once the binary variance control is introduced. We can directly compare variances in (4.40) and (4.69) since $\tilde{V_\infty} = \tilde{V_\infty^*}$. If we rework them by considering the expression of $\tilde{V_\infty}$ and $p^* > 0$, we obtain

$$\underbrace{\frac{(1-\tilde{V_\infty^*})\tilde{V_\infty^*}^2}{\tilde{V_\infty^*} + \frac{2\tilde{V_\infty^*}}{\lambda a^2(\rho)}\Big[(1+p^*) - \tilde{V_\infty^*}(1-P(\rho))\Big]}}_{\mathrm{Var}(X^*)} < \underbrace{\frac{(1-\tilde{V}_\infty)\tilde{V}_\infty^2}{\tilde{V}_\infty + \frac{2V_\infty(1-P(\rho))}{\lambda a^2(\rho)}}}_{\mathrm{Var}(X)} \quad \forall \rho \in (\rho_c,1] \tag{4.73}$$

$$\implies \mathrm{Var}(X^*) \leq \mathrm{Var}(X) \quad \forall \rho \in [0,1] \text{ with the binary control strategy.}$$

In figure 4.2 (p. 104), the variance of the asymptotic speed distribution is plotted as a function of the density ρ, in the congested flow regime and for different values of the effective penetration rate p^*. The case $p^* = 0$ corresponds to the uncontrolled case. It is evident that this variance is greater than others for every value of density. Coherently with the literature [46], the binary variance control strategy is able to effectively reduce the speed variability in the traffic and therefore, road risk. The novelty is that, due to the presence of the phase transition, a range of densities for which the variance is identically equal to 0 is identified and it corresponds to the free flow regime.

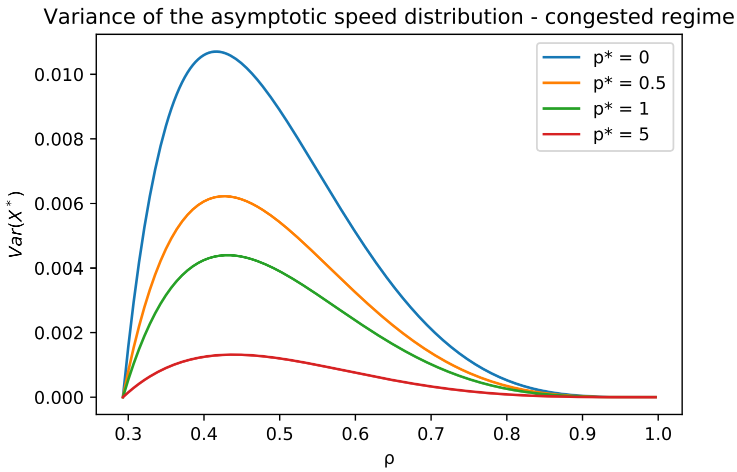

Figure 4.2: Variance in (4.69) related to the asymptotic speed distribution (4.63) in the congested flow regime. The control strategy is the binary variance control so, $\tilde{V}^*_\infty$ is given by (4.71)

4.7 Desired speed control

With the binary variance control strategy, the mean speed at equilibrium is equivalent to the one obtained in the uncontrolled case and the phase transition is preserved. This does not hold for all control strategies indeed, we will see that this is not the case of the desired speed control.

The desired speed control is a strategy, which aims at reducing the speed variance of one vehicle with the desired speed $v_d(\rho)$, which could be a suggested or a prescribed speed that just depends on the traffic density ρ. In particular, it is assumed that $V_d(w';\rho) = v_d(\rho)$. If this is plugged in equation (4.56), the evolution equation for the mean speed with desired speed control is obtained. Indeed, (4.56) becomes

$$\frac{d\tilde{V}^*}{d\tau} = P(\rho) + (\tilde{V}^*)^2(1 - P(\rho)) - (1 + p^*)\tilde{V}^* + p^* v_d(\rho) \ . \tag{4.74}$$

The goal is to the determine the mean speed speed at equilibrium i.e. as $t \to +\infty$. Therefore, first, fixed points of the system are determined and then, linear stability analysis [41] is performed.
Let us rewrite (4.74) as

$$\dot{\tilde{V}^*} = h(\tilde{V}^*; p^*, P, v_d), \tag{4.75}$$

where $h(\tilde{V}^*; p^*, P, v_d) = P + (\tilde{V}^*)^2(1 - P) - (1 + p^*)\tilde{V}^* + p^* v_d$ and $p^* > 0$, $\tilde{V}^*, P, v_d \in [0,1]$.

In order to determine fixed points, we need to solve

$$h(\tilde{V}^*; p^*, P, v_d) = 0 \iff (\tilde{V}^*)^2(1-P)-(1+p^*)\tilde{V}^*+(P+p^*v_d) = 0 \,, \quad (4.76)$$

which is equivalent to solve a quadratic equation. For the moment, the physical requirement $\tilde{V}^* \in [0,1]$ is dropped and only positive speeds are considered. We will be back to this requirement in a second moment. If $P(\rho) \in [0,1)$, the solutions of (4.76) are

$$\begin{aligned} \tilde{V}^*_{\pm} =& \frac{(1+p^*) \pm \sqrt{(1+p^*)^2 - 4(1-P)(P+p^*v_d)}}{2(1-P)} = \\ =& \frac{(1+p^*) \pm \sqrt{\Delta}}{2(1-P)} \,, \end{aligned} \quad (4.77)$$

where

$$\Delta := (1+p^*)^2 - 4(1-P)(P+p^*v_d) \,. \quad (4.78)$$

Δ can be considered as the discriminant of the quadratic equation (4.76). Let us assume for the moment that $\Delta \geq 0$ and therefore, both the fixed points exist. Indeed, if $\Delta < 0$, the quadratic equation has no solution and the system has not fixed points. We will come back to this issue later.

The stability of the fixed points (4.77) can be determined by performing linear stability analysis [41] as explained in detail in section 4.2.
Let us compute the first derivative with respect to $\tilde{V}^*$ of the function $h(\tilde{V}^*; p^*, P, v_d)$:

$$h'(\tilde{V}^*; p^*, P, v_d) = 2(1-P)\tilde{V}^* - (1+p^*) \,. \quad (4.79)$$

If the fixed points $\tilde{V}^*_{\pm}$ in (4.77) are plugged in (4.79), we obtain

$$h'(\tilde{V}^*_{\pm}; p^*, P, v_d) = \pm\sqrt{\Delta} \,.$$

Therefore, $\tilde{V}^*_{+} = \tilde{V}^*_{+}(\rho)$ is unstable $\forall \rho \in [0,1]$ while $\tilde{V}^*_{-} = \tilde{V}^*_{-}(\rho)$ is stable $\forall \rho \in [0,1]$.
Once the desired speed control is introduced, the mean speed at equilibrium is equal to the stable fixed point just found:

$$\tilde{V}^*_{\infty} = \frac{(1+p^*) - \sqrt{(1+p^*)^2 - 4(1-P)(P+p^*v_d)}}{2(1-P)} \,. \quad (4.80)$$

Contrary to the binary variance control, the mean speed at equilibrium is not invariant compared to the uncontrolled case.

Remark 4.7.1. If $p^* = 0$, from (4.77) the fixed points (4.14) obtained in the uncontrolled case are recovered. □

Remark 4.7.2. Let us study the *infinite effective penetration rate limit* i.e. $p^* \to +\infty$ [46]. In this limit, the control fully dominates the dynamics. Equation (4.80) can be rewritten as

$$\tilde{V^*_\infty} = \frac{(1+p^*)}{2(1-P)}\left\{1 - \sqrt{1 - \frac{4(1-P)(P+p^*v_d)}{(1+p^*)^2}}\right\} . \tag{4.81}$$

If $p^* \to +\infty$, the content of the square root can be rewritten as

$$1 - \frac{4(1-P)(P+p^*v_d)}{(1+p^*)^2} \simeq 1 - \frac{4(1-P)v_d}{p^*} := 1-y,$$
$$\text{where } y = \frac{4(1-P)v_d}{p^*} << 1 \text{ if } p^* \to +\infty \ .$$

A Taylor expansion can be performed: $\sqrt{1-y} = 1 + \frac{1}{2}y + O(y^2)$ if $y \to 0$. Therefore, we obtain

$$\tilde{V^*_\infty} \simeq \frac{(1+p^*)}{2(1-P)}\left\{\frac{1}{2}\left[\frac{4(1-P)(P+p^*v_d)}{(1+p^*)^2}\right]\right\} \tag{4.82}$$
$$\implies \lim_{p^* \to +\infty} \tilde{V^*_\infty} = v_d(\rho) \ .$$

In the limit $p^* \to +\infty$, the mean speed at equilibrium coincides with desired speed $v_d(\rho)$ and, because of (4.69), so does the expected value of the asymptotic speed distribution.
Moreover, let us consider the variance of the asymptotic speed distribution defined in (4.69). If $p^* \to +\infty$, $\mathrm{Var}(X^*) \to 0^+$. Therefore, when the desired speed control is introduced and the *infinite effective penetration rate limit* is considered, the asymptotic speed distribution tends to a Dirac delta centered at $v_d(\rho)$:

$$\tilde{f^*_\infty} \to \delta(v - v_d) \ .$$

□

The situation is specular to the one examined in depth in section 4.2 for the uncontrolled case. The fixed points of the system are two and their stability is invariant $\forall \rho \in [0,1]$. In that case, the bifurcation which leads to a phase transition, is due to the piecewise-defined mean speed at equilibrium. There exists a value of density, the critical density ρ_c, for which the two fixed points merge and collapse in just one fixed point. This critical density

marks the transition between two different regimes of traffic.
Therefore, analogously to this situation previously studied, it can be stated that a phase transition occurs in the controlled case with the desired speed control strategy, if there exists a value of density for which $\Delta = 0$ and the two fixed points merge.

In subsection 4.8.4, a detailed study of the discriminant Δ will be carried out. In particular, the desired speed will be set equal to $v_d(\rho) = 1 - \rho^a$ with $a \geq 1$ and the probability of accelerating to $P(\rho) = (1-\rho)^2$. It will be clear that $\Delta > 0 \ \forall \rho \in [0,1]$ and therefore, the existence of the fixed points will be ensured. However, due to the fact that

$$\nexists \rho \in [0,1] \text{ such that } \Delta = 0,$$

a phase transition does not occur with this control strategy.

The absence of the phase transition is evident if the asymptotic speed distribution is considered. It is the beta distribution (4.63) with parameters (4.64). These parameters depend on $\tilde{V}^*_\infty$, which is defined in (4.80).
The fact that the phase transition is not preserved with the desired speed control strategy can be a practical benefit. Indeed, the discontinuity in the traffic could be canceled by the introduction of autonomous vehicles equipped with this control.

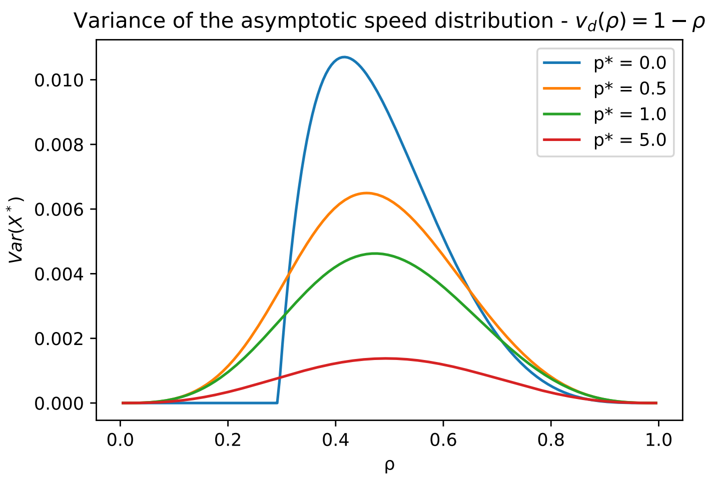

Figure 4.3: Variance in (4.69) related to the asymptotic speed distribution (4.63) with desired speed control $v_d(\rho) = 1 - \rho$. $\tilde{V}^*_\infty$ is given by (4.80) and $\mu = 2$

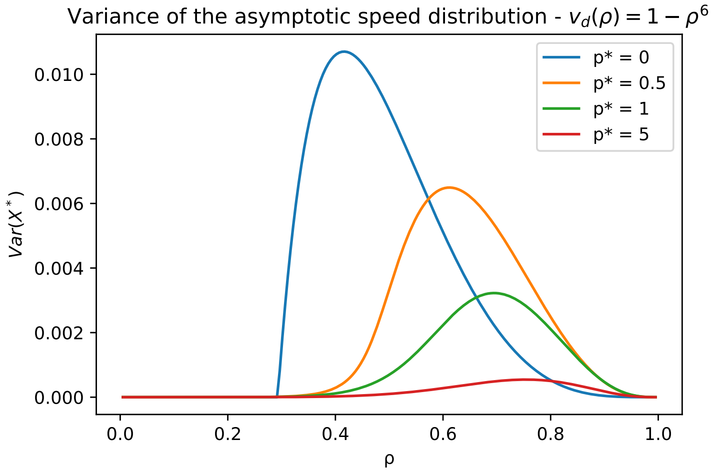

Figure 4.4: Variance in (4.69) related to the asymptotic speed distribution (4.63) with desired speed control $v_d(\rho) = 1 - \rho^6$. $\tilde{V}^*_\infty$ is given by (4.80) and $\mu = 2$

In figure 4.3, the variance of the asymptotic speed distribution with desired speed control is plotted as a function of the density ρ and for different values of effective penetration rate p^*. It is assumed that the desired speed is equal to $v_d(\rho) = 1-\rho$. The same plot is shown in figure 4.4 for $v_d(\rho) = 1-\rho^6$. In both figures, the case $p^* = 0$ corresponds to the uncontrolled case. It is evident that

$$\neg\Big(\mathrm{Var}(X^*) < \mathrm{Var}(X) \quad \forall\rho \in [0{,}1]\Big) \text{ with the desired speed control strategy.}$$

This means that there exist some values of densities for which the variance does not decrease compared to the uncontrolled case.

We can have a qualitative insight of this issue by considering that the phase transition is not preserved by the desired speed control. Let us focus on the uncontrolled case in the free flow regime i.e. $\rho \in [0, \rho_c]$: the variance is null since the asymptotic speed distribution is a Dirac delta centered at 1. If we consider the desired speed controlled case for the same range of densities i.e. $\rho \in [0, \rho_c]$ - remember that ρ_c just depends on the exponent μ in the probability of accelerating $P(\rho)$) - then the asymptotic speed distribution is a beta with parameters α, $\beta > 0$. Therefore, the variance of the asymptotic speed distribution with the desired speed control is greater than the one in the uncontrolled case. This is evident if $v_d(\rho) = 1 - \rho$ - see figure 4.3.

However, a case where the introduction of the desired speed control leads to a reduction in the variance of the asymptotic speed distribution can be identified. As pointed out in the remark 4.7.2, in the *infinite effective penetration rate limit*, the asymptotic speed distribution tends to a Dirac delta centered at $v_d(\rho)$. Therefore, in this limit, the introduction of the control leads to a decrease in the variance of the asymptotic speed distribution and consequently, of road risk.

4.8 Numerical tests

In order to confirm theoretical findings of this chapter, several numerical tests are performed. We proceed analogously to section 3.12.

4.8.1 Choice of μ and other parameters

The first issue to deal with is the choice of the exponent μ in the probability of accelerating $P(\rho) = (1-\rho)^{\mu}$, $\mu > 0$. In order to do this, the *speed* and the *fundamental diagram* have to be considered. The exponent μ has to chosen in a way such that the related diagrams reproduce experimental results. In section 3.5, the criteria which make it possible, are stated [32]. Let us consider figures 4.5 - 4.6: the diagrams (ρ, V_∞) and $(\rho, \rho V_\infty)$ are displayed for different values of μ in the uncontrolled case - see equation (4.27).

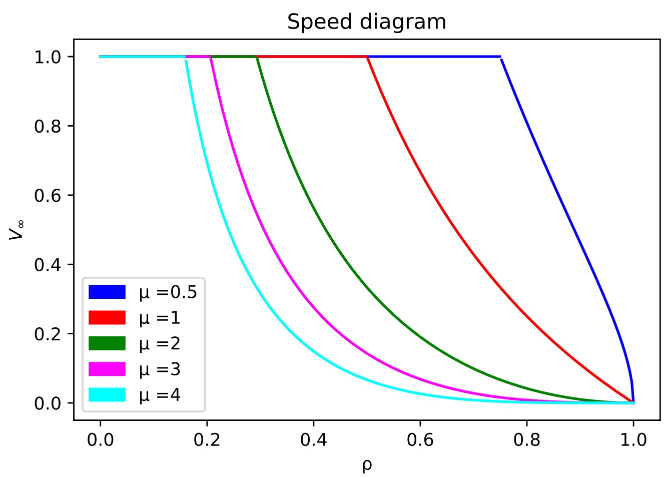

Figure 4.5: Speed diagram in the nonlinear uncontrolled case: the mean speed at equilibrium V_∞ is (4.27)

The choice $\mu = 2$ can be supported by the *speed* and the *fundamental diagrams*. In particular, in the latter the flux $\rho V_\infty(\rho)$ is linearly increasing from $\rho = 0$ to a value $\bar{\rho} \in [0,1]$, which is its unique maximum and it is non

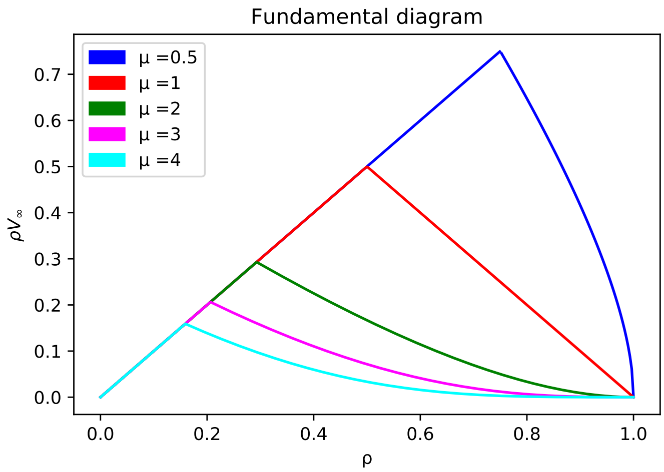

Figure 4.6: Fundamental diagram in the nonlinear uncontrolled case: the mean speed at equilibrium V_∞ is (4.27)

linearly decreasing from $[\bar{\rho},1]$. The flux is not concave but this requirement is not so strict [32]. Moreover, except for $\mu = 0.5$ and $\mu = 1$, other values of the exponent μ lead to convex flux in the decreasing branch. If $\mu = 0.5$, the mean speed at equilibrium is equal to 1 for almost 80% of the density interval, therefore this case is excluded. On the other hand, $\mu = 1$ roughly models the probability of accelerating. So, $\mu = 2$ is more suited to describe our dynamics compared to the other cases which lead to similar diagrams, since it captures all aspects without being too extreme.

As proved in section 4.2, the value of critical density ρ_c just depends on the exponent μ in the probability of accelerating $P(\rho)$. Let us compute ρ_c for $\mu = 2$ by referring to definition (4.26). It turns out to be equal to

$$\rho_c = 1 - 2^{-\frac{1}{2}} \simeq 0.2929.$$

Choices of other parameters are summarized in the following. They are analogous to those of section 3.12 and we recall to that section for more details.

- $\epsilon = 0.01,\ \Delta t = \epsilon,\ \gamma = \epsilon,\ \sigma^2 = \gamma,\ \nu = \gamma$
- number of agents $= 10^5$
- initial speed distribution $\tilde{f}_0 \sim \mathcal{U}([0,1])$

- speed domain [0,1] is discretized in $N_v = 121$ points
- $a(\rho) := \rho(1-\rho)$
- $\eta \sim \mathcal{U}[-a,a]$, $a = \sqrt{3\sigma^2}$

4.8.2 Uncontrolled case

In this subsection, results of simulations in the uncontrolled case are displayed. The Fokker-Planck asymptotic speed distribution defined in (4.37) for the congested flow regime and in (4.48) for the free flow regime, or equivalently the one in (4.63) with $p^* = 0$, is compared to the stationary numerical speed distribution, computed with the Nanbu-Babovsky's simulation scheme [29; 30]. In particular, distributions are plotted by using a suited histogram and simulations are run for a sufficiently long time such that convergence at equilibrium is achieved. This time will be specified for each simulation.

Simulations are performed for different values of density. The presence of the phase transition is evident: in the congested flow regime, the asymptotic speed distribution is a beta while for densities smaller than or equal to the critical point, it shrinks to a Dirac delta centered at 1.

From the analysis carried out in section 4.2, we expect a much longer time of convergence when the critical point is approached. Indeed, as stated by (4.25), the convergence at the critical point is polynomial in time, since it follows the law $(time)^{-1}$. This is in contrast with the exponential convergence we have for densities different than the critical, as stated by equation (4.21). The numerical evidence of this fact is gained by looking at the time of convergence related to each simulation. Even if this is not a proper proof, it is a first insight on this issue.

In figures 4.7 - 4.12 (pp. 112-115), the asymptotic speed distribution is studied as a function of the density. In all cases, the simulations are run for $T = 50$. Due to the fact that we set $\Delta t = 0.01$, this T corresponds to $5 \cdot 10^3$ time steps. By studying the L^2-numerical error, as done in section 3.12, it is evident that this time is generously sufficient for convergence if $\rho = 0.5,\ 0.8$ and the error is $O(10^{-2})/O(10^{-1})$. Instead, for $\rho = 0.3$ and $\rho = \rho_c = 1 - 2^{-\frac{1}{2}}$, this running time is not sufficient for the system to converge to equilibrium. In figures 4.13 - 4.14 (pp. 115-116), results related to $\rho = 0.3$ and $\rho = \rho_c = 1 - 2^{-\frac{1}{2}}$ are displayed for $T = 250$. As expected, in these two cases, the time needed to converge to the asymptotic speed distribution is much longer and the time steps are $2{,}5 \cdot 10^4$.

The agreement between the theoretical and the simulation results is strong: as theoretically expected, the numerical equilibrium solution of the Boltzmann-type equation converges toward the solution of the Fokker-Planck PDE, which is analytically obtained in the *quasi-invariant interaction regime*. It is important to observe that in the free flow regime, the value of the theoretical $\tilde{f_\infty}(v)$ corresponding to $v = 1$ is not visible in the plot. This is due to the fact that $\tilde{f_\infty}(v = 1) = +\infty$, since the asymptotic speed distribution is a Dirac delta in this case. This fact makes impossible to infer the convergence time by considering the L^2-numerical error; indeed, the value of the speed distribution corresponding to $v = 1$ drives the result, thus making the numerical error explode: it is impossible to numerically obtain the Dirac delta. Therefore, in the free flow regime, qualitative observations are employed to understand whether the system reaches equilibrium.

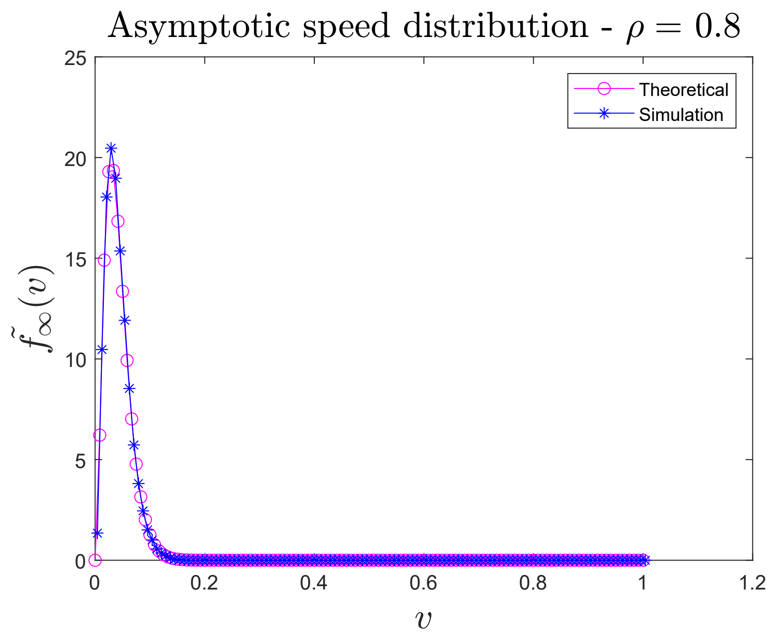

Figure 4.7: Congested flow regime: comparison between the asymptotic Fokker-Planck distribution (4.37) (theoretical) and the numerical solution of the Boltzmann-type equation (simulation) for $\rho = 0.8$, $T = 50$

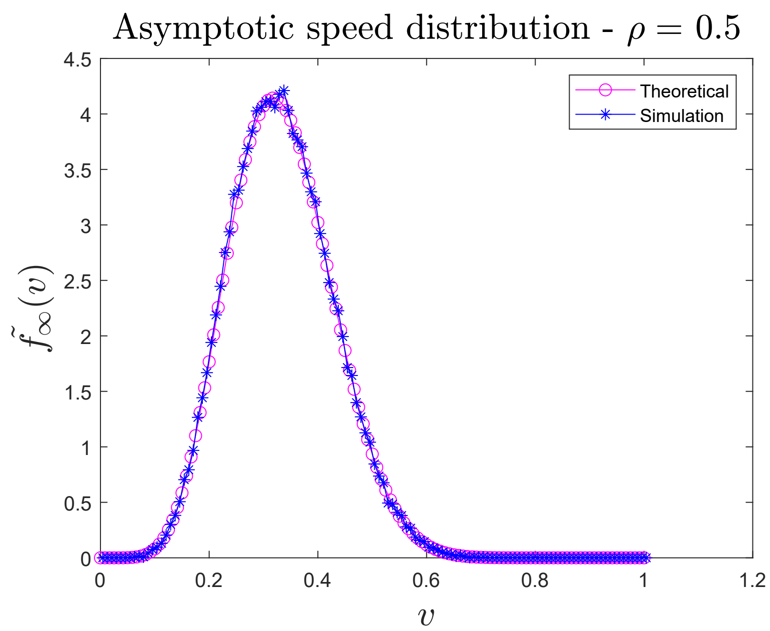

Figure 4.8: Congested flow regime: comparison between the asymptotic Fokker-Planck distribution (4.37) (theoretical) and the numerical solution of the Boltzmann-type equation (simulation) for $\rho = 0.5$, $T = 50$

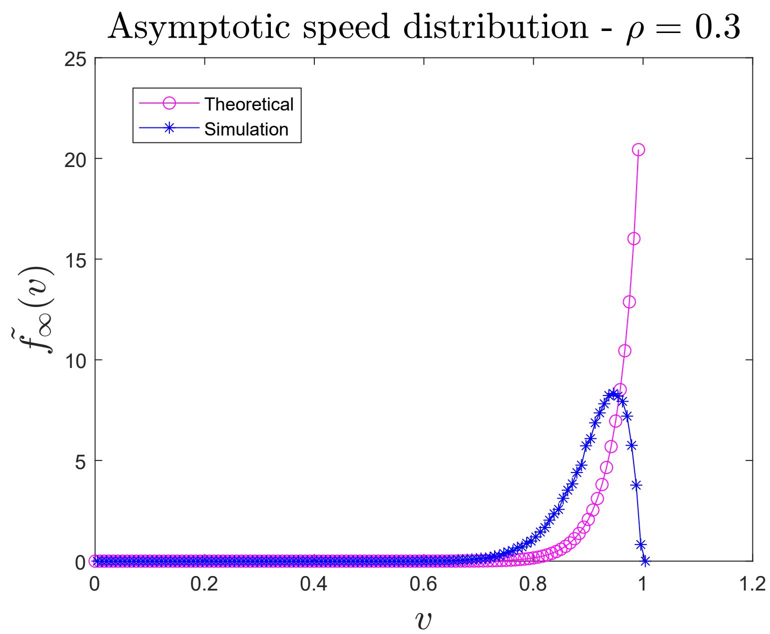

Figure 4.9: Congested flow regime: comparison between the asymptotic Fokker-Planck distribution (4.37) (theoretical) and the numerical solution of the Boltzmann-type equation (simulation) for $\rho = 0.3$, $T = 50$

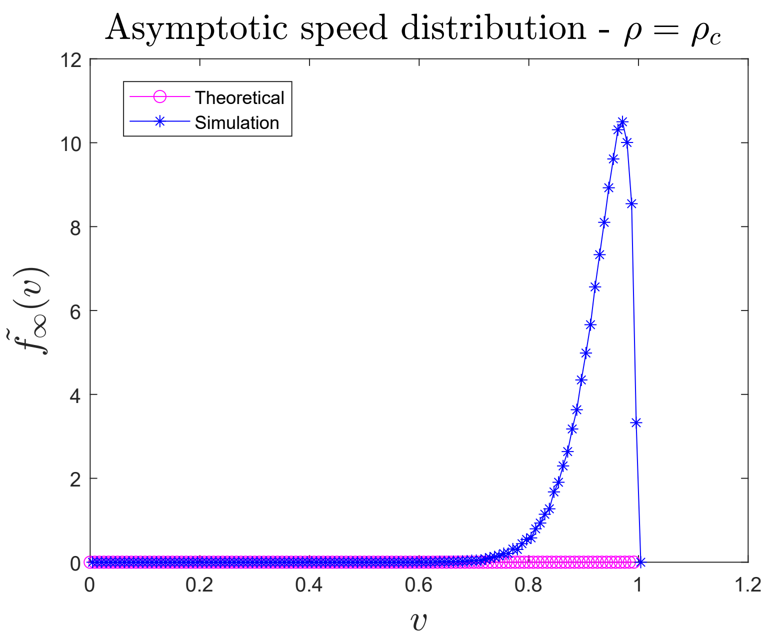

Figure 4.10: Critical point: comparison between the asymptotic Fokker-Planck distribution (4.48) (theoretical) and the numerical solution of the Boltzmann-type equation (simulation) for $\rho = 1 - 2^{-\frac{1}{2}}$, $T = 50$

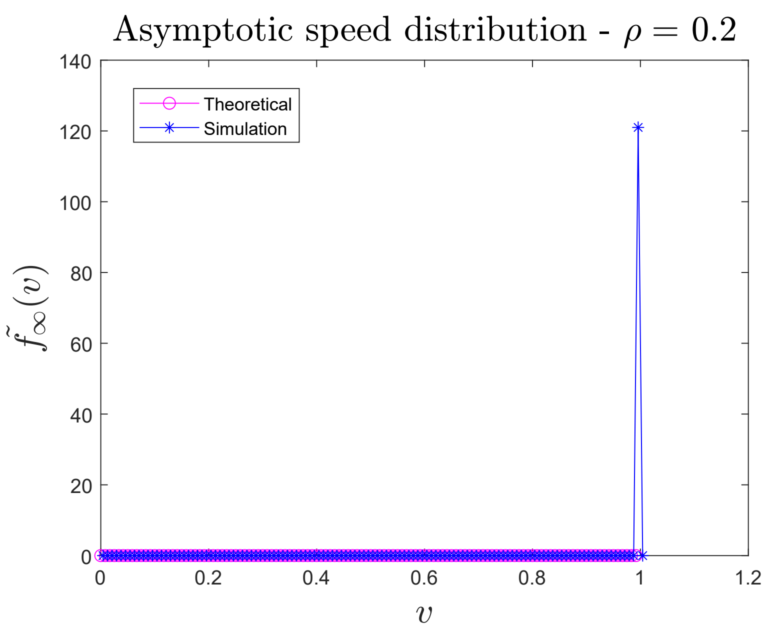

Figure 4.11: Free flow regime: comparison between the asymptotic Fokker-Planck distribution (4.48) (theoretical) and the numerical solution of the Boltzmann-type equation (simulation) for $\rho = 0.2$, $T = 50$

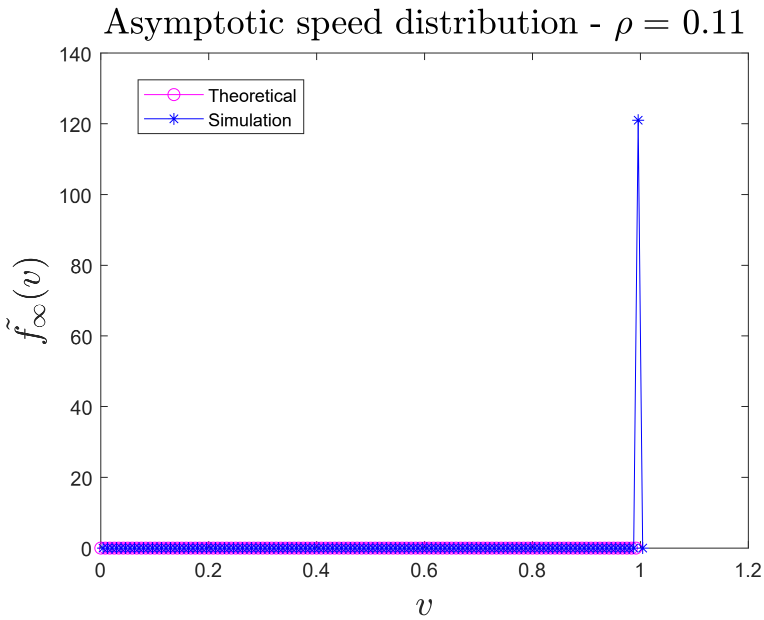

Figure 4.12: Free flow regime: comparison between the asymptotic Fokker-Planck distribution (4.48) (theoretical) and the numerical solution of the Boltzmann-type equation (simulation) for $\rho = 0.11$, $T = 50$

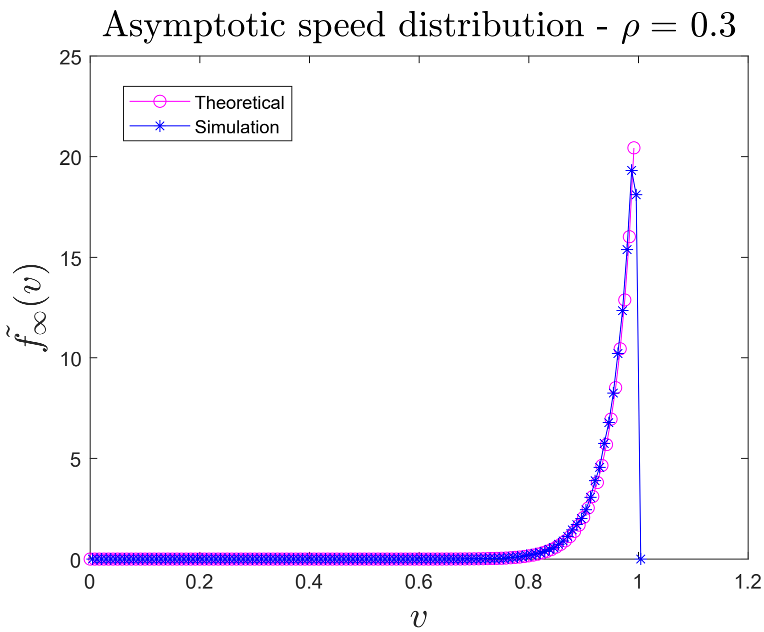

Figure 4.13: Congested flow regime: comparison between the asymptotic Fokker-Planck distribution (4.37) (theoretical) and the numerical solution of the Boltzmann-type equation (simulation) for $\rho = 0.3$, $T = 250$

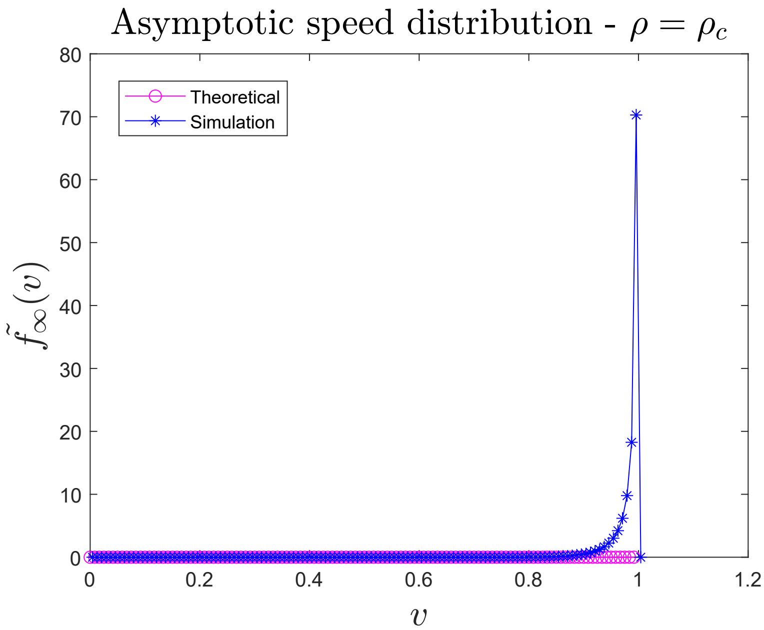

Figure 4.14: Critical point: comparison between the asymptotic Fokker-Planck distribution (4.48) (theoretical) and the numerical solution of the Boltzmann-type equation (simulation) for $\rho = 1 - 2^{-\frac{1}{2}}$, $T = 250$

4.8.3 Binary variance controlled case

In this subsection, results of simulations in the controlled case with binary variance control are displayed. The theoretical asymptotic speed distribution defined in (4.63), with the mean speed speed at equilibrium $\tilde{V}_\infty^*$ defined in (4.71), is compared to the stationary numerical speed distribution, computed with the Monte Carlo simulation scheme. As in the uncontrolled case, distributions are plotted by using a suited histogram and simulations are run for a sufficiently long time such that convergence at equilibrium is achieved. This time is specified for each simulation.

Simulations are performed for different values of density and we observe a similar behavior to the uncontrolled case. The presence of the phase transition is evident: in the congested flow regime, the asymptotic speed distribution is a beta while for densities smaller than or equal to the critical point, it shrinks to a Dirac delta centered at 1.

In figures 4.15 - 4.17 (pp. 117-118), the case corresponding to $\rho = 0.5$

is studied for different penetration rates: $p = 0.2,\ 0.5,\ 0.8$. As the penetration rate increases, the variance of the asymptotic distribution decreases coherently with what we explained in section 4.6.
In figures 4.18 - 4.20 (pp. 119-120), we set $p = 0.5$ and the asymptotic speed distribution is obtained for different values of densities. As in the uncontrolled case, if $\rho \to \rho_c$, the convergence time is decisively longer and we set $T = 250$ instead of $T = 50$.
In figures 4.21 - 4.23 (pp. 120-121), the same analysis is performed for $p = 0.2$.

As in the uncontrolled case, numerical results perfectly fit theoretical predictions.

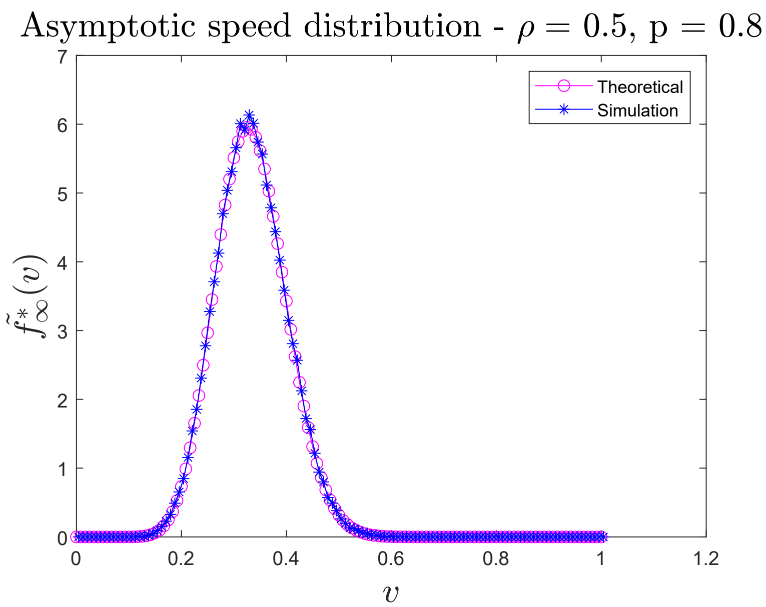

Figure 4.15: Congested flow regime: comparison between the asymptotic Fokker-Planck distribution (4.63) with $\tilde{V}^*_\infty$ defined in (4.71)(theoretical) and the numerical solution of the Boltzmann-type equation (simulation) for $\rho = 0.5$, $p = 0.8$, $T = 50$

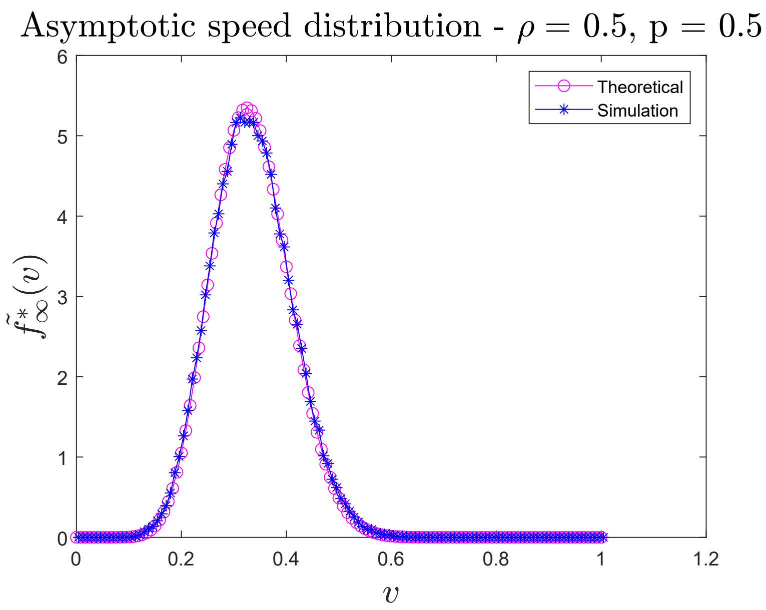

Figure 4.16: Congested flow regime: comparison between the asymptotic Fokker-Planck distribution (4.63) with $\tilde{V}^*_\infty$ defined in (4.71)(theoretical) and the numerical solution of the Boltzmann-type equation (simulation) for $\rho = 0.5$, $p = 0.5$, $T = 50$

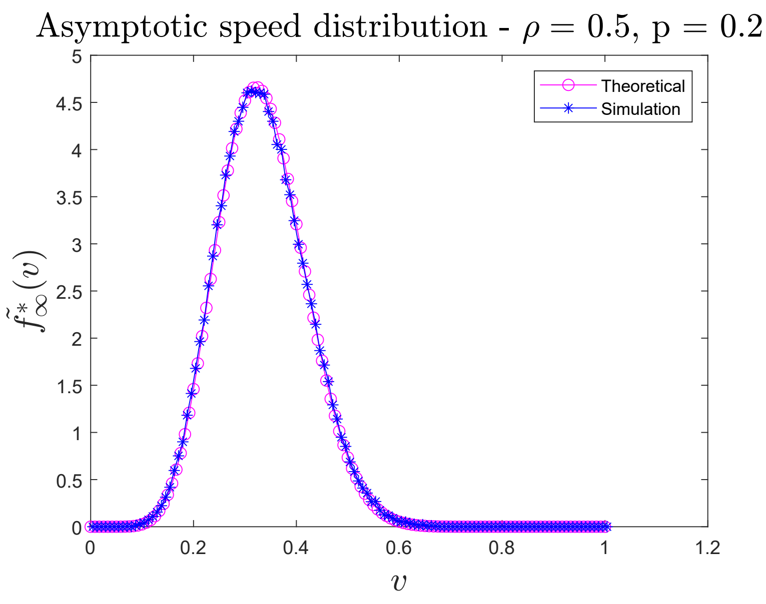

Figure 4.17: Congested flow regime: comparison between the asymptotic Fokker-Planck distribution (4.63) with $\tilde{V}^*_\infty$ defined in (4.71)(theoretical) and the numerical solution of the Boltzmann-type equation (simulation) for $\rho = 0.5$, $p = 0.2$, $T = 50$

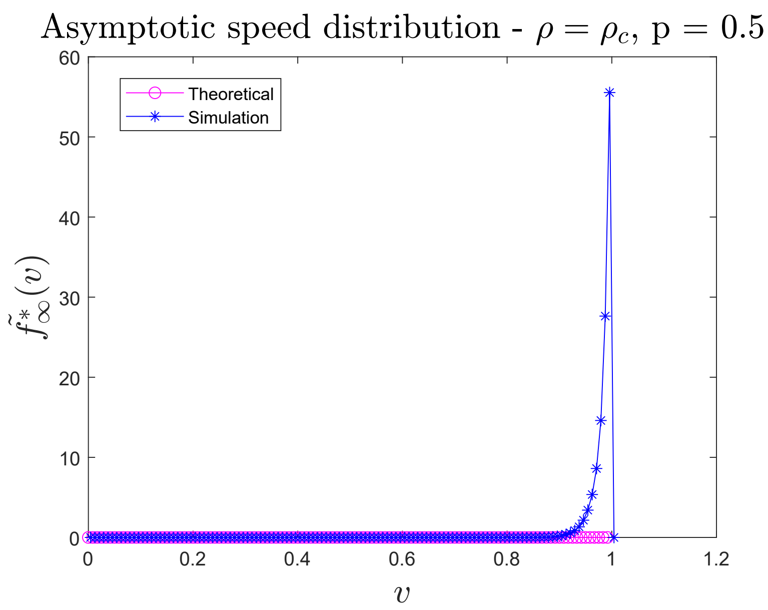

Figure 4.18: Critical point: comparison between the asymptotic Fokker-Planck distribution (4.63) with $\tilde{V}^*_\infty$ defined in (4.71)(theoretical) and the numerical solution of the Boltzmann-type equation (simulation) for $\rho = 1 - 2^{-\frac{1}{2}}$, $p = 0.5$, $T = 250$

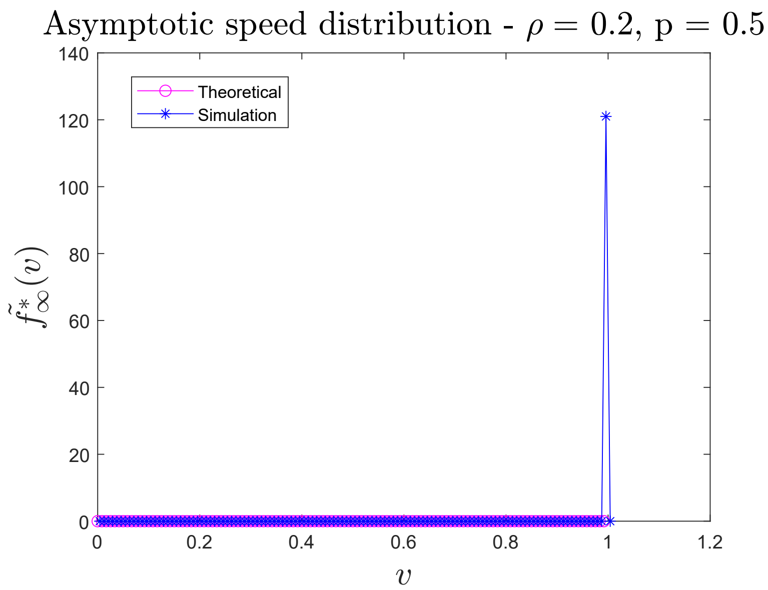

Figure 4.19: Free flow regime: comparison between the asymptotic Fokker-Planck distribution (4.63) with $\tilde{V}^*_\infty$ defined in (4.71)(theoretical) and the numerical solution of the Boltzmann-type equation (simulation) for $\rho = 0.2$, $p = 0.5$, $T = 50$

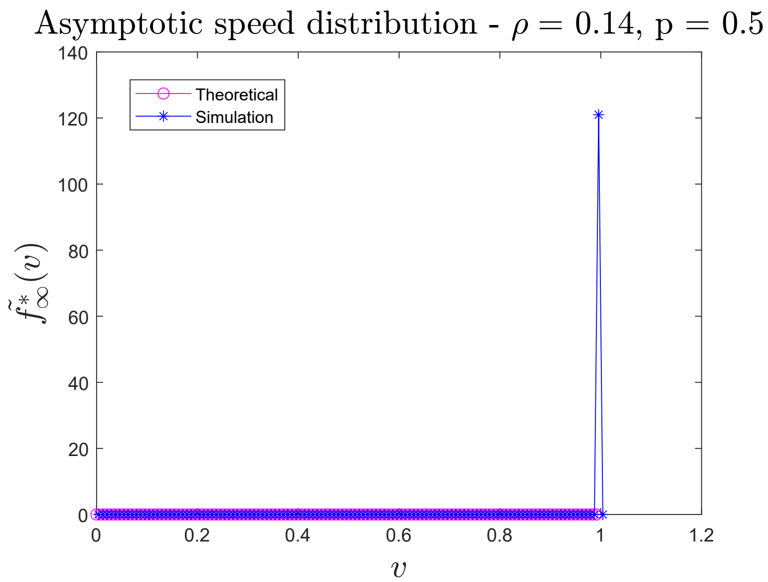

Figure 4.20: Free flow regime: comparison between the asymptotic Fokker-Planck distribution (4.63) with $\tilde{V}^*_\infty$ defined in (4.71)(theoretical) and the numerical solution of the Boltzmann-type equation (simulation) for $\rho = 0.14$, $p = 0.5$, $T = 50$

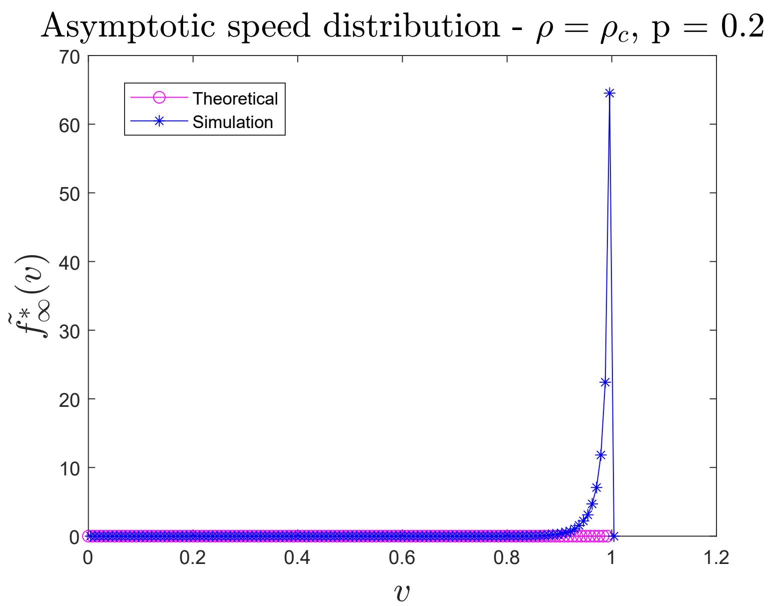

Figure 4.21: Critical point: comparison between the asymptotic Fokker-Planck distribution (4.63) with $\tilde{V}^*_\infty$ defined in (4.71)(theoretical) and the numerical solution of the Boltzmann-type equation (simulation) for $\rho = 1 - 2^{-\frac{1}{2}}$, $p = 0.2$, $T = 250$

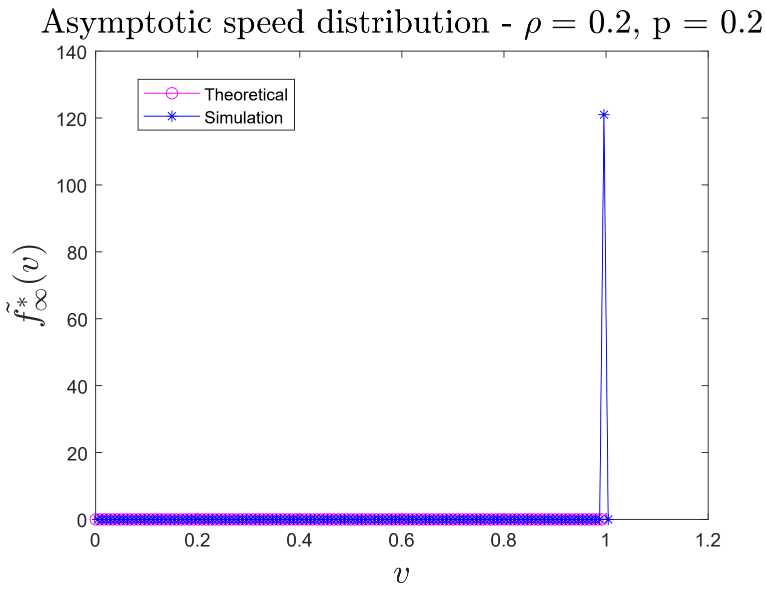

Figure 4.22: Free flow regime: comparison between the asymptotic Fokker-Planck distribution (4.63) with $\tilde{V}^*_\infty$ defined in (4.71)(theoretical) and the numerical solution of the Boltzmann-type equation (simulation) for $\rho = 0.2$, $p = 0.2$, $T = 50$

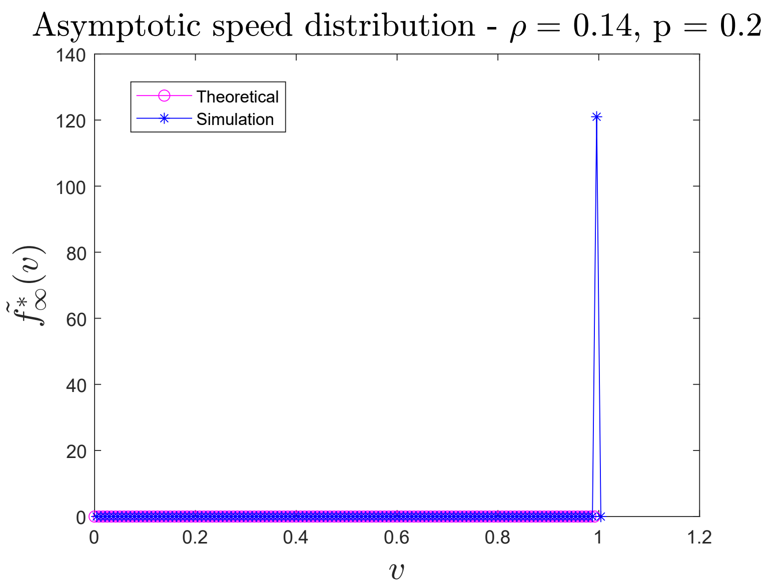

Figure 4.23: Free flow regime: comparison between the asymptotic Fokker-Planck distribution (4.63) with $\tilde{V}^*_\infty$ defined in (4.71)(theoretical) and the numerical solution of the Boltzmann-type equation (simulation) for $\rho = 0.14$, $p = 0.2$, $T = 50$

4.8.4 Desired speed controlled case

As it has been sketched in section 4.7, the desired speed control strategy does not preserve the phase transition. The discriminant Δ of the quadratic equation (4.76) has been defined as $\Delta := (1+p^*)^2 - 4(1-P)(P+p^* v_d)$. As previously stated, the phase transition occurs if and only if there exist a critical value of density for which $\Delta = 0$.
In the following, several plots of this discriminant are reported: in particular, it is studied with the choice of parameters of subsection 4.8.1 and several shapes of the desired speed are considered: $v_d(\rho) = 1-\rho^a$ with $a = 1,2,...,8$.

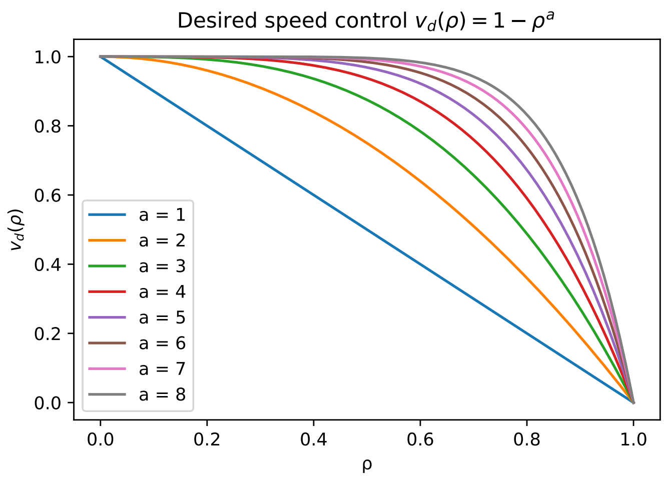

Figure 4.24: Desired speed $v_d(\rho) = 1 - \rho^a$, $a = 1,...,8$

First, let us study the shape of the desired speed $v_d(\rho) = 1 - \rho^a$ and its related physical meaning. The plots of this quantity for different values of a are shown in figure 4.24. The case $a = 1$ corresponds to the one adopted in [46]: agents tend to minimize the variance of their own speed after the interaction and the desired speed, which depends linearly on traffic density ρ. We observe that for bigger values of the exponent a, $v_d(\rho)$ turns out to be about the maximum value of allowed speeds for a wider and wider range of densities. In particular, if $a = 6$, the desired speed is about 1 for almost 50% of the density interval [0,1] and then, it steeply decreases to 0. From a physical point of view, this means that the choice $a = 6$, or more generally big a, is not suited to describe our process: agents would be required to tend to a desired speed which is maximum for a wide range of densities and then, to decrease their own speed very steeply. Therefore, cases with big a and in particular, $a = 6$ will be considered only for explanatory reasons and to outline some properties of the system.

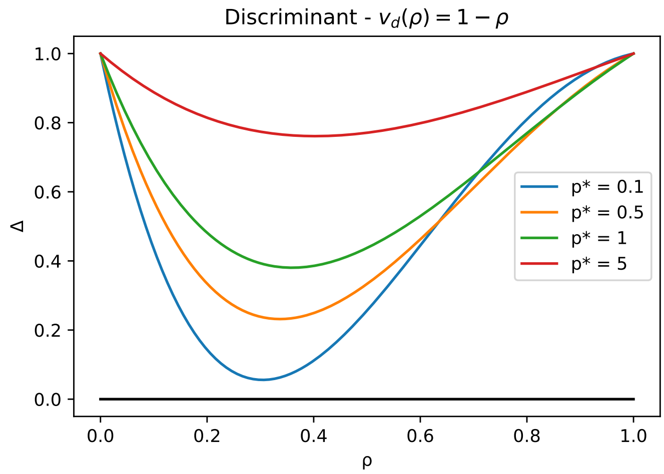

Figure 4.25: Discriminant (4.78) for different effective penetration rates p^*, $v_d(\rho) = 1 - \rho$, $\mu = 2$

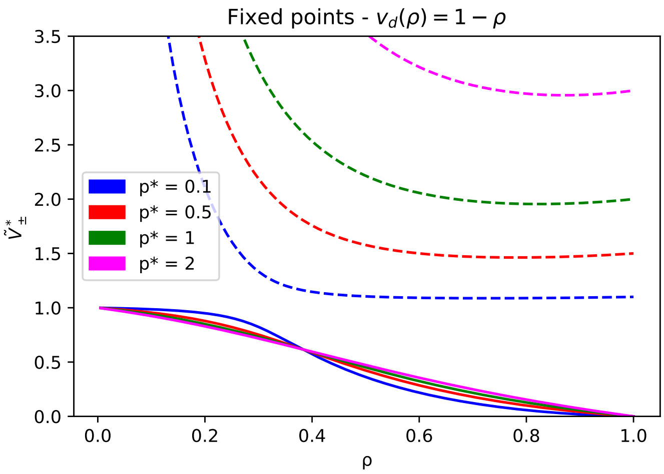

Figure 4.26: Fixed points (4.77) for different effective penetration rates p^*, $v_d(\rho) = 1 - \rho$, $\mu = 2$. Dashed lines are related to unstable fixed points i.e. $\tilde{V}^*_+$; solid lines are related to stable fixed points i.e. $\tilde{V}^*_-$

In the following, the case $a = 1$ i.e. the case in which the desired speed is equal to $v_d(\rho) = 1 - \rho$ is considered.
In figure 4.25, it is clear what we stated in section 4.7. There do not exist values of density for which the discriminant is equal to 0 and therefore, there is not phase transition. Evidence of this fact is also provided by figures 4.26

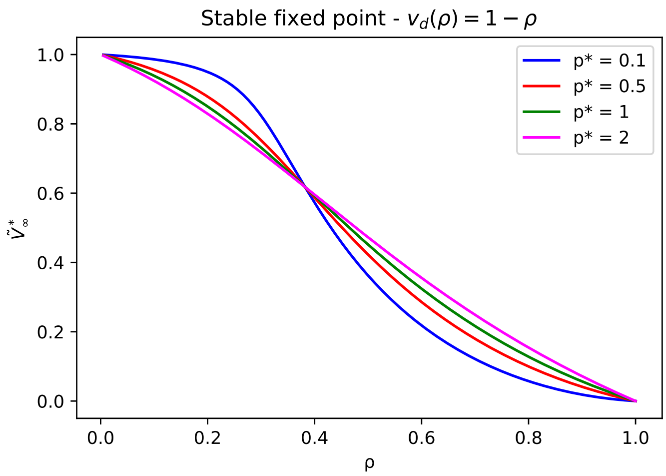

Figure 4.27: Stable fixed point (4.80) for different effective penetration rates p^*, $v_d(\rho) = 1 - \rho$, $\mu = 2$

and 4.27, where the fixed points (4.77) are plotted.

Therefore, by running simulations, it is numerically confirmed that the asymptotic speed distribution is a well-defined beta distribution for all values of density. Results for the effective penetration rate $p^* = 0.1$ (actually, we assumed $\kappa = 1$ and therefore, $p = p^*$) are displayed in figures 4.28 - 4.32 (pp. 126-128). This value of p^* is chosen since it is the one, among considered values, for which the discriminant is lower. In figures 4.31, 4.33 and 4.34 (pp. 128-129), results related to $\rho = 0.2$ and different penetration rates are displayed.

The plots of the discriminant and the fixed points are also considered for $a = 3, 6$ and are displayed in figures 4.35 - 4.40 (pp. 130-132). In appendix A, plots for $a = 2,\ 4,\ 5,\ 7,\ 8$ are also shown. We observe that as a increases, the discriminant turns out to be closer and closer to 0 for small values of the effective penetration rate ($p^* = 0.1$). Therefore, we expect a behavior closer and closer to the one obtained in the uncontrolled case and with the binary variance control. In other words, we expect that as a increases, the phase transition is approached.

In table 4.1 (p. 125), the minimum value ρ^* of the discriminant is reported for different values of the exponent a in the case $p^* = 0.1$. We also have the corresponding value of the determinant i.e. $\Delta(\rho^*)$. We observe that even with $a = 100$, the determinant approaches 0 but it is not exactly equal to it. In the case $a = 6$, the discriminant is of the order 10^{-4} in its minimum

a	ρ^*	$\Delta(\rho^*)$
1	0.304	$5.6 \cdot 10^{-2}$
2	0.316	$1.9 \cdot 10^{-2}$
3	0.323	$6.3 \cdot 10^{-3}$
4	0.327	$2.1 \cdot 10^{-3}$
5	0.328	$7.0 \cdot 10^{-4}$
6	0.329	$2.3 \cdot 10^{-4}$
7	0.329	$7.6 \cdot 10^{-5}$
8	0.329	$2.5 \cdot 10^{-5}$
100	0.329	$1.1 \cdot 10^{-19}$

Table 4.1: Minimum value $\rho*$ of Δ in (4.78) for different a ($v_d(\rho) = 1 - \rho^a$) and $p^* = 0.1$

and we consider this value sufficiently small to assume $\Delta \simeq 0$. The goal is to investigate this case and how the phase transition is approached. The value of density $\rho^* = 0.329$ is considered as a kind of critical density. A quite sharp change in the behavior of the asymptotic speed distribution is expected in correspondence of this value of density.
Evidence of this fact is also provided by the bifurcation diagram for $a = 6$ in figure 4.41 (p. 133). Indeed, by zooming around the point where the two fixed points are supposed to merge, a gap appears.

In figures 4.42 - 4.48 (pp. 133-136), results of simulations in the case $v_d(\rho) = 1 - \rho^6$ with $p = 0.1$ are displayed. As expected, the change in the behavior of the asymptotic speed distribution is not so sharp as in the cases previously considered but the phase transition is approached. For $\rho \in (0.329,1]$, the asymptotic speed distribution is a beta, while for $\rho \in [0,0.329)$, it shrinks to a Dirac delta centered at the maximum allowed speed i.e. 1. Due to the fact that we do not have a proper phase transition, in the neighborhood of $\rho = 0.329$, which is considered as a sort of critical density, the asymptotic speed distribution is still a beta distribution, which is approaching a Dirac delta.

Finally, let us consider the remark 4.7.2: we would like to test that in the *infinite effective penetration rate limit* i.e. $p^* \to +\infty$, the asymptotic speed distribution tends to a Dirac delta centered at $v_d(\rho)$. Let us set $v_d(\rho) = 1-\rho$ and

$$\nu = 0.1\epsilon = 0.1\gamma,$$

which implies $\kappa = 0.1$ and $p^* = 10p \in [0,10]$. This cannot be assimilated to

$p^* \to +\infty$ but it leads to $p^* >> 1$ and therefore, we expect the asymptotic speed distribution begins to tend to $\delta(v - v_d)$. Results of a simulation for $p = 0.4$ and $T = 100$ are displayed in figure 4.49 (p. 137). Even though p^* is just equal to 4, the asymptotic speed distribution shrinks compared to the uncontrolled case and it is centered at $v_d(\rho)$, which is equal to $v_d(0.5) = 0.5$ in this case. Theoretical findings are confirmed and the comparison with the uncontrolled case highlights how in this limit, the introduction of the desired speed control makes the variance decrease.

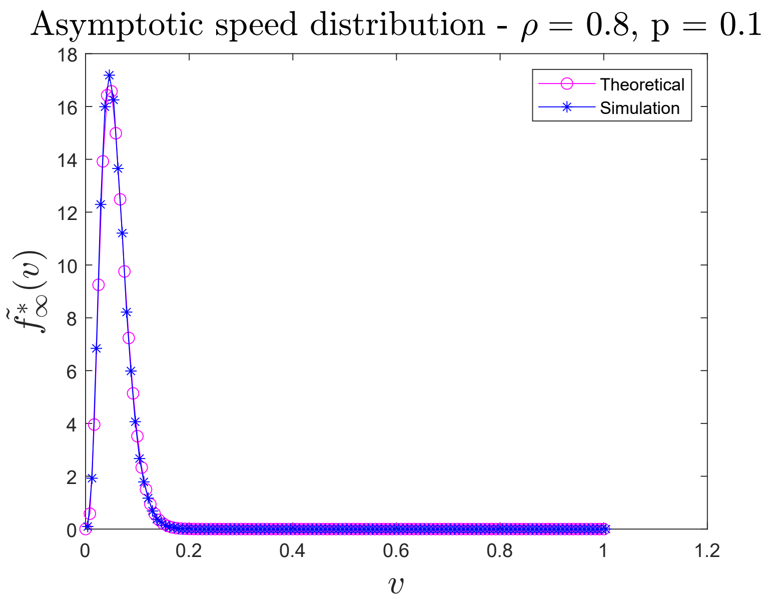

Figure 4.28: Desired speed control $v_d(\rho) = 1 - \rho$: comparison between the asymptotic Fokker-Planck distribution (4.63) with $\tilde{V}^*_\infty$ defined in (4.80)(theoretical) and the numerical solution of the Boltzmann-type equation (simulation) for $\rho = 0.8$, $p = 0.1$, $T = 50$

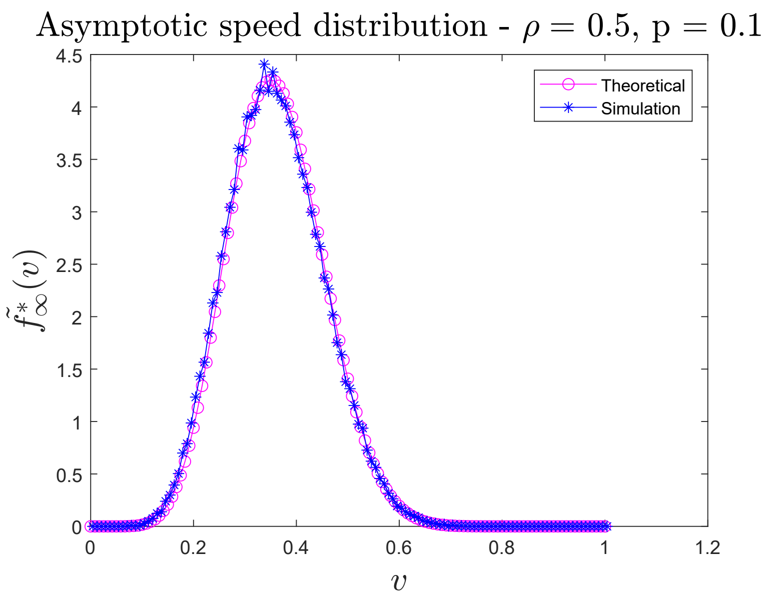

Figure 4.29: Desired speed control $v_d(\rho) = 1 - \rho$: comparison between the asymptotic Fokker-Planck distribution (4.63) with $\tilde{V}^*_\infty$ defined in (4.80)(theoretical) and the numerical solution of the Boltzmann-type equation (simulation) for $\rho = 0.5$, $p = 0.1$, $T = 50$

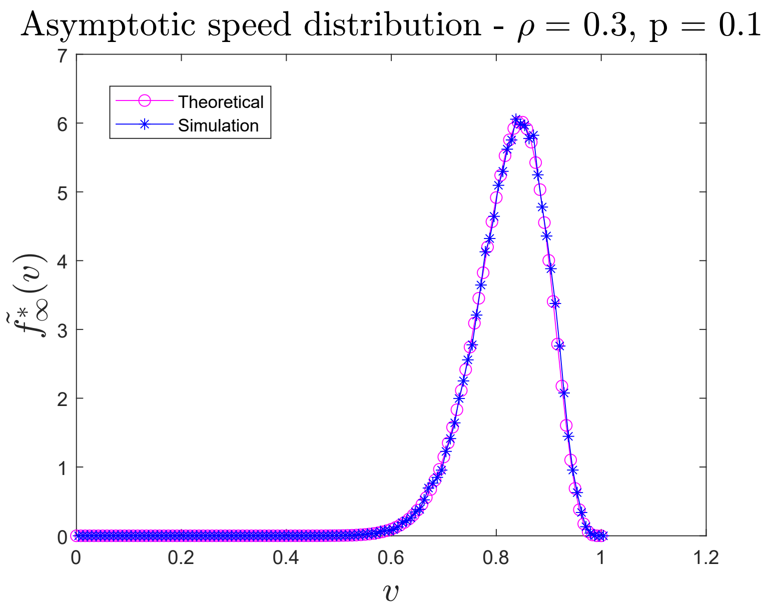

Figure 4.30: Desired speed control $v_d(\rho) = 1 - \rho$: comparison between the asymptotic Fokker-Planck distribution (4.63) with $\tilde{V}^*_\infty$ defined in (4.80)(theoretical) and the numerical solution of the Boltzmann-type equation (simulation) for $\rho = 0.3$, $p = 0.1$, $T = 50$

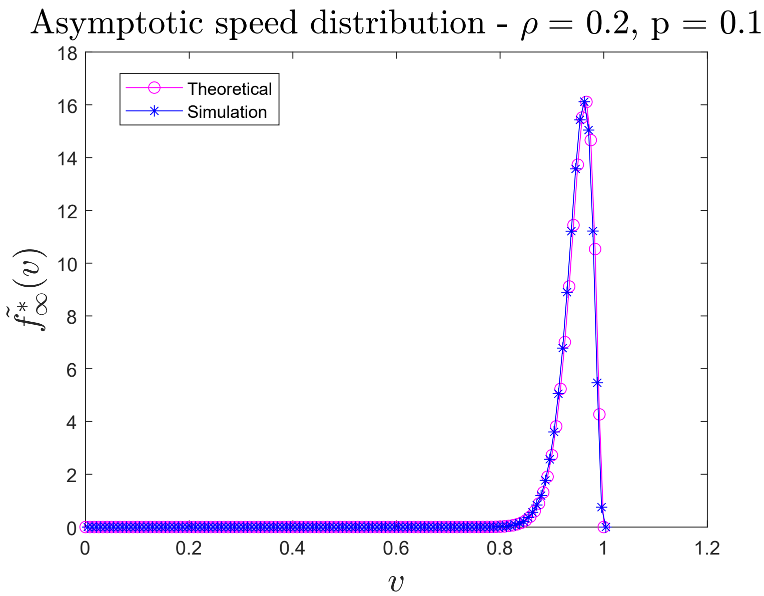

Figure 4.31: Desired speed control $v_d(\rho) = 1 - \rho$: comparison between the asymptotic Fokker-Planck distribution (4.63) with $\tilde{V}^*_\infty$ defined in (4.80)(theoretical) and the numerical solution of the Boltzmann-type equation (simulation) for $\rho = 0.2$, $p = 0.1$, $T = 50$

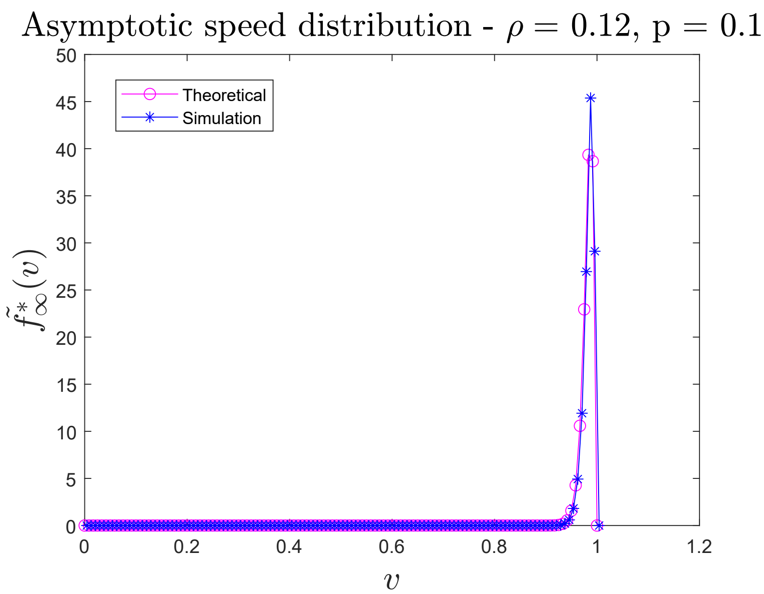

Figure 4.32: Desired speed control $v_d(\rho) = 1 - \rho$: comparison between the asymptotic Fokker-Planck distribution (4.63) with $\tilde{V}^*_\infty$ defined in (4.80)(theoretical) and the numerical solution of the Boltzmann-type equation (simulation) for $\rho = 0.12$, $p = 0.1$, $T = 50$

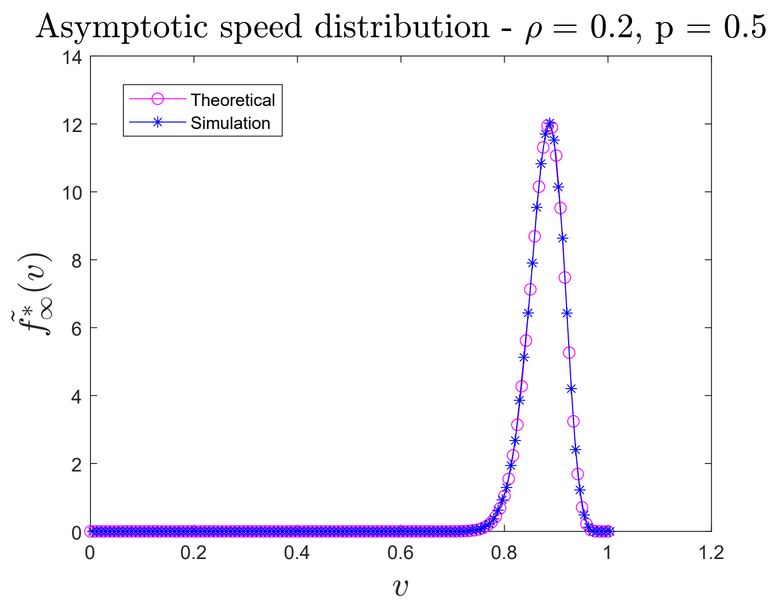

Figure 4.33: Desired speed control $v_d(\rho) = 1 - \rho$: comparison between the asymptotic Fokker-Planck distribution (4.63) with $\tilde{V}^*_\infty$ defined in (4.80)(theoretical) and the numerical solution of the Boltzmann-type equation (simulation) for $\rho = 0.2$, $p = 0.5$, $T = 50$

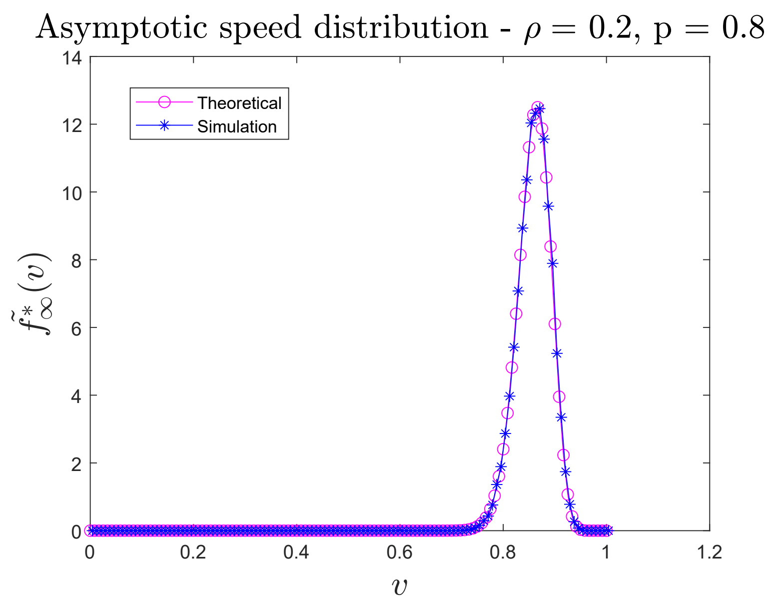

Figure 4.34: Desired speed control $v_d(\rho) = 1 - \rho$: comparison between the asymptotic Fokker-Planck distribution (4.63) with $\tilde{V}^*_\infty$ defined in (4.80)(theoretical) and the numerical solution of the Boltzmann-type equation (simulation) for $\rho = 0.2$, $p = 0.8$, $T = 50$

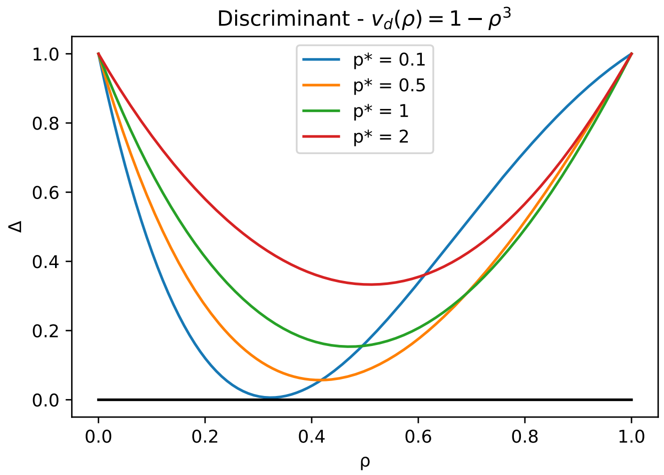

Figure 4.35: Discriminant (4.78) for different effective penetration rates p^*, $v_d(\rho) = 1 - \rho^3$, $\mu = 2$

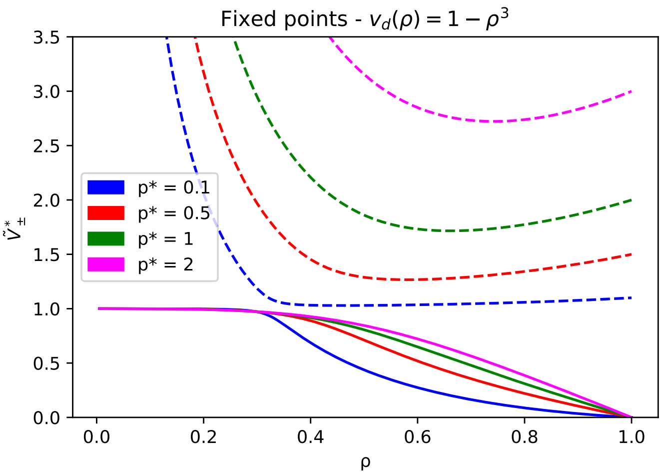

Figure 4.36: Fixed points (4.77) for different effective penetration rates p^*, $v_d(\rho) = 1 - \rho^3$, $\mu = 2$. Dashed lines are related to unstable fixed points i.e. $\tilde{V}^*_+$; solid lines are related to stable fixed points i.e. $\tilde{V}^*_-$

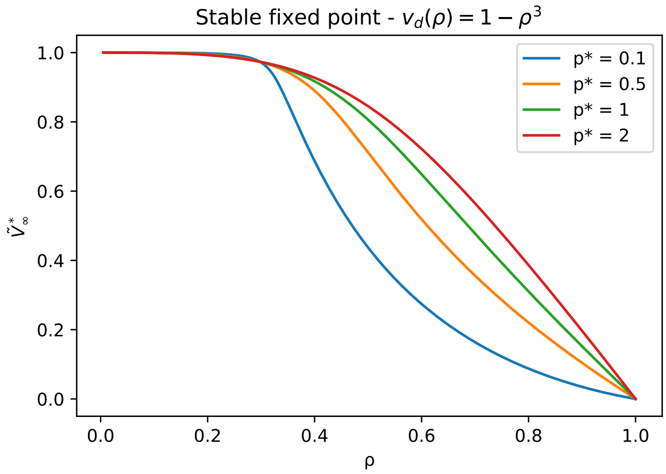

Figure 4.37: Stable fixed point (4.80) for different effective penetration rates p^*, $v_d(\rho) = 1 - \rho^3$, $\mu = 2$

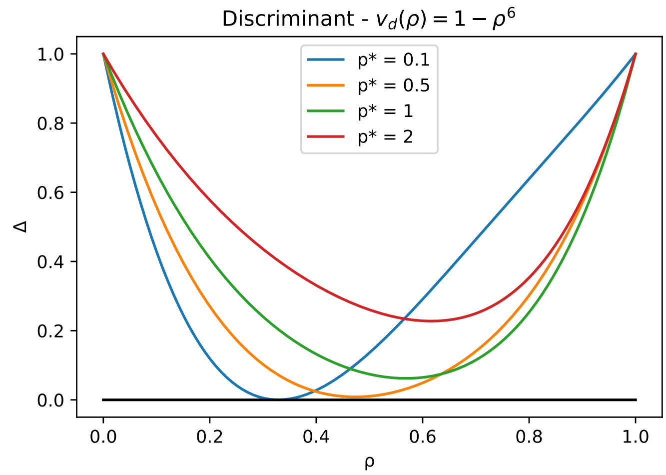

Figure 4.38: Discriminant (4.78) for different effective penetration rates p^*, $v_d(\rho) = 1 - \rho^6$, $\mu = 2$

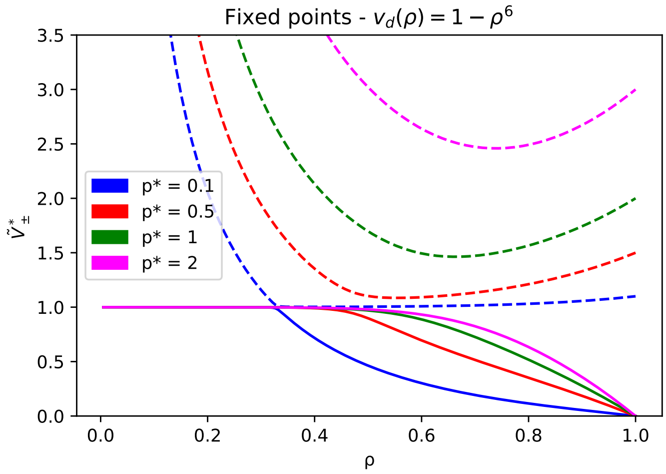

Figure 4.39: Fixed points (4.77) for different effective penetration rates p^*, $v_d(\rho) = 1 - \rho^6$, $\mu = 2$. Dashed lines are related to unstable fixed points i.e. $\tilde{V}^*_+$; solid lines are related to stable fixed points i.e. $\tilde{V}^*_-$

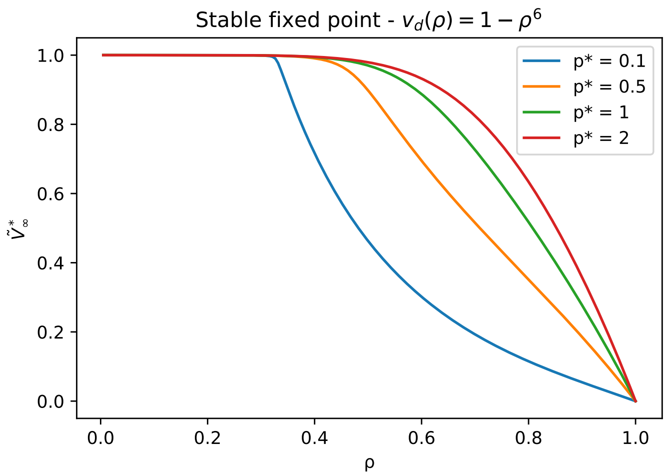

Figure 4.40: Stable fixed point (4.80) for different effective penetration rates p^*, $v_d(\rho) = 1 - \rho^6$, $\mu = 2$

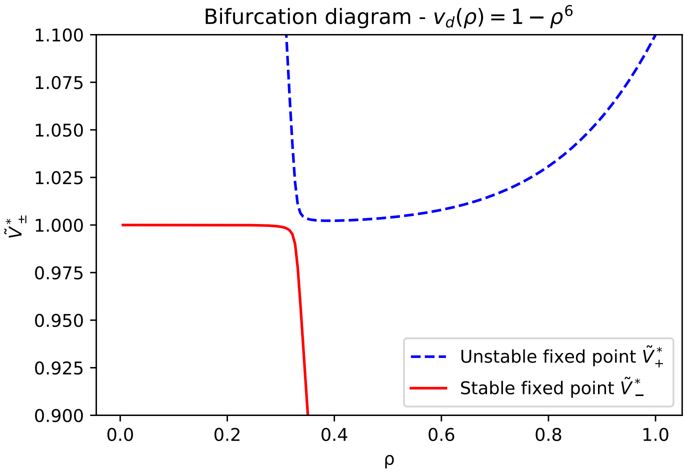

Figure 4.41: Bifurcation diagram of equation (4.74). Fixed points (4.77) are plotted for different effective penetration rates p^*, $v_d(\rho) = 1 - \rho^6$, $\mu = 2$.

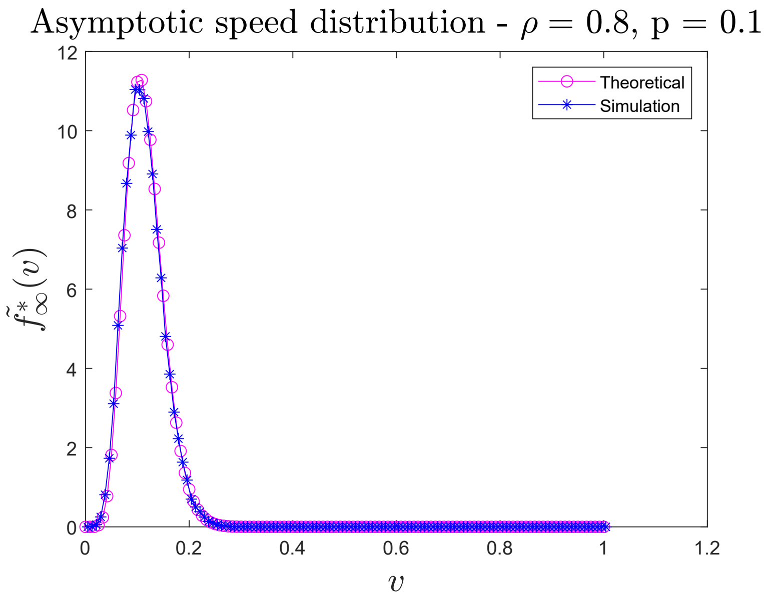

Figure 4.42: Desired speed control $v_d(\rho) = 1 - \rho^6$: comparison between the asymptotic Fokker-Planck distribution (4.63) with $\tilde{V}^*_\infty$ defined in (4.80)(theoretical) and the numerical solution of the Boltzmann-type equation (simulation) for $\rho = 0.8$, $p = 0.1$, $T = 50$

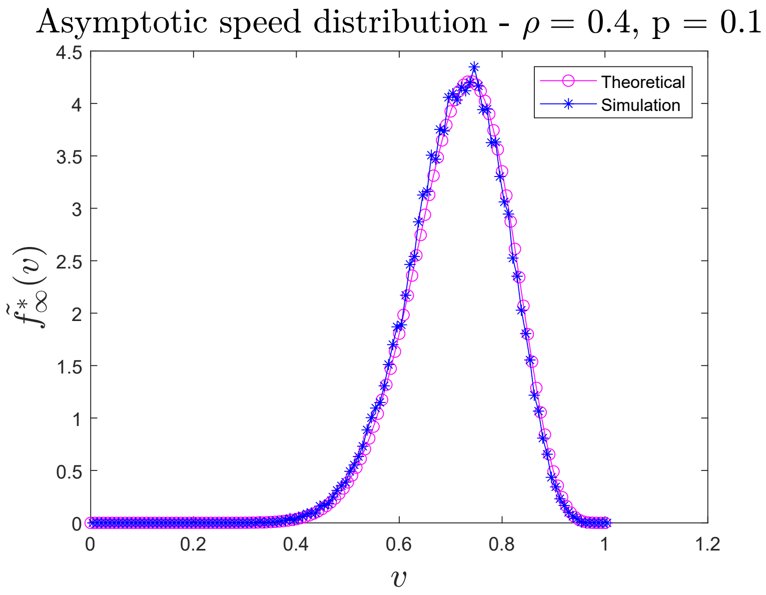

Figure 4.43: Desired speed control $v_d(\rho) = 1 - \rho^6$: comparison between the asymptotic Fokker-Planck distribution (4.63) with $\tilde{V}^*_\infty$ defined in (4.80)(theoretical) and the numerical solution of the Boltzmann-type equation (simulation) for $\rho = 0.4$, $p = 0.1$, $T = 50$

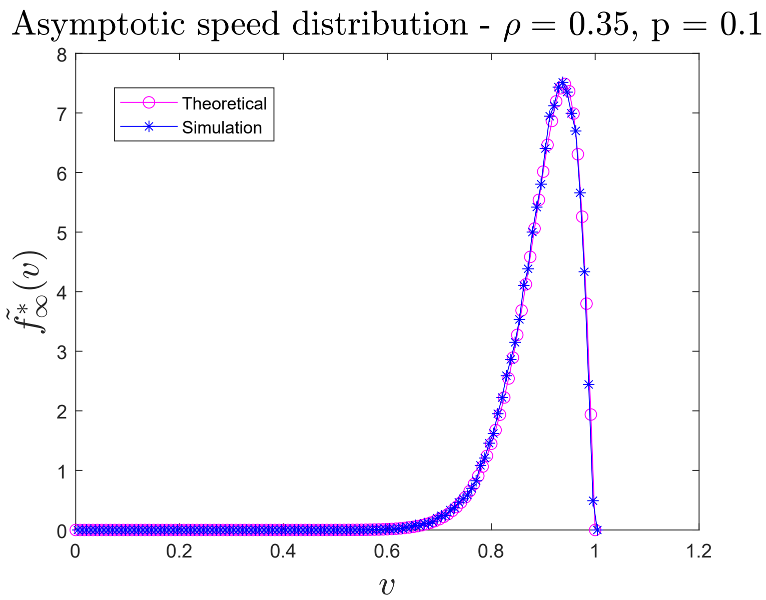

Figure 4.44: Desired speed control $v_d(\rho) = 1 - \rho^6$: comparison between the asymptotic Fokker-Planck distribution (4.63) with $\tilde{V}^*_\infty$ defined in (4.80)(theoretical) and the numerical solution of the Boltzmann-type equation (simulation) for $\rho = 0.35$, $p = 0.1$, $T = 200$

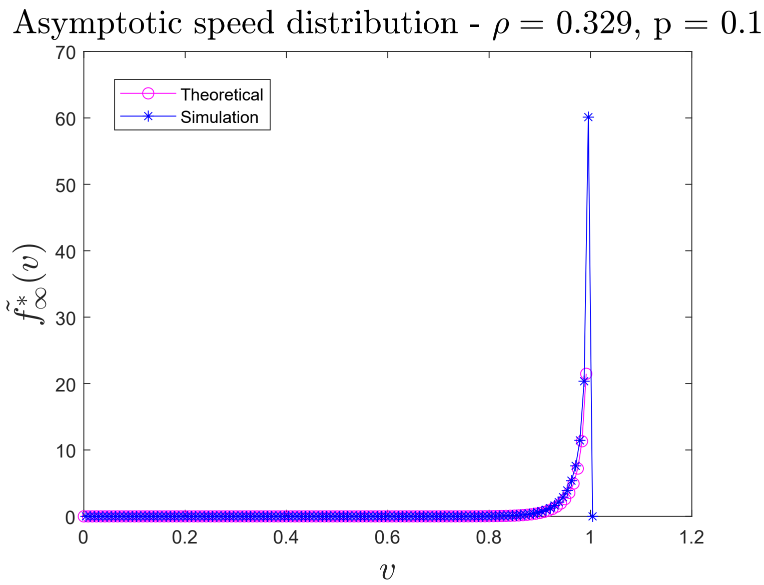

Figure 4.45: Desired speed control $v_d(\rho) = 1 - \rho^6$: comparison between the asymptotic Fokker-Planck distribution (4.63) with $\tilde{V}^*_\infty$ defined in (4.80)(theoretical) and the numerical solution of the Boltzmann-type equation (simulation) for $\rho = 0.329$, $p = 0.1$, $T = 200$

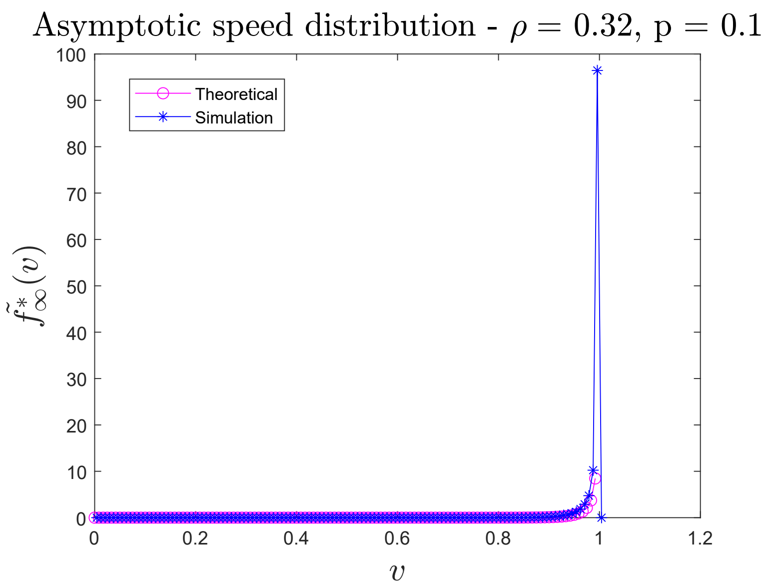

Figure 4.46: Desired speed control $v_d(\rho) = 1 - \rho^6$: comparison between the asymptotic Fokker-Planck distribution (4.63) with $\tilde{V}^*_\infty$ defined in (4.80)(theoretical) and the numerical solution of the Boltzmann-type equation (simulation) for $\rho = 0.32$, $p = 0.1$, $T = 200$

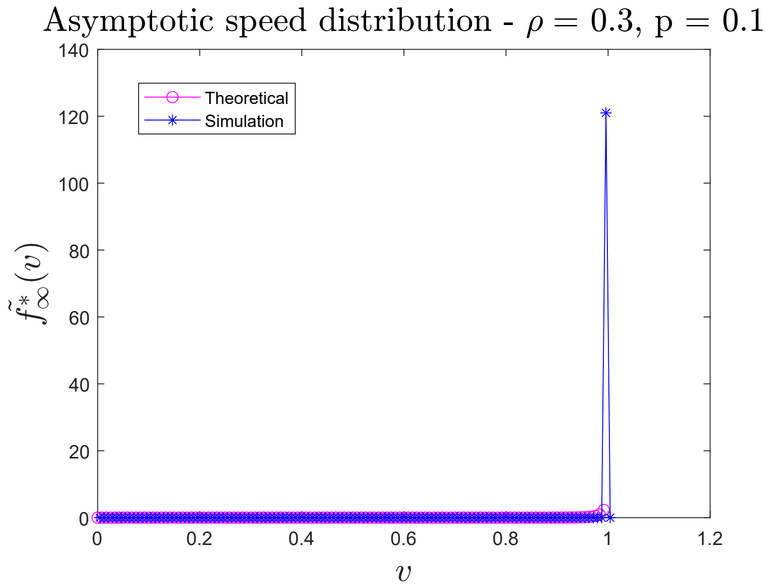

Figure 4.47: Desired speed control $v_d(\rho) = 1 - \rho^6$: comparison between the asymptotic Fokker-Planck distribution (4.63) with $\tilde{V}^*_\infty$ defined in (4.80)(theoretical) and the numerical solution of the Boltzmann-type equation (simulation) for $\rho = 0.3$, $p = 0.1$, $T = 200$

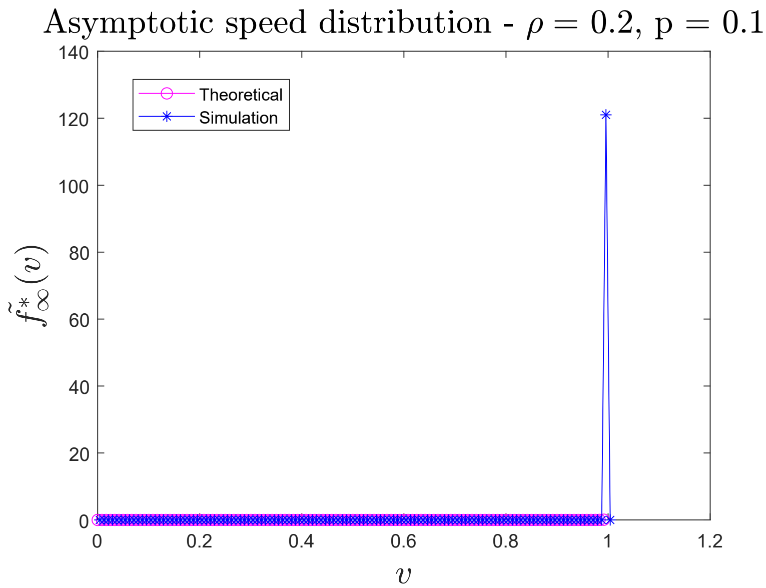

Figure 4.48: Desired speed control $v_d(\rho) = 1 - \rho^6$: comparison between the asymptotic Fokker-Planck distribution (4.63) with $\tilde{V}^*_\infty$ defined in (4.80)(theoretical) and the numerical solution of the Boltzmann-type equation (simulation) for $\rho = 0.2$, $p = 0.1$, $T = 200$

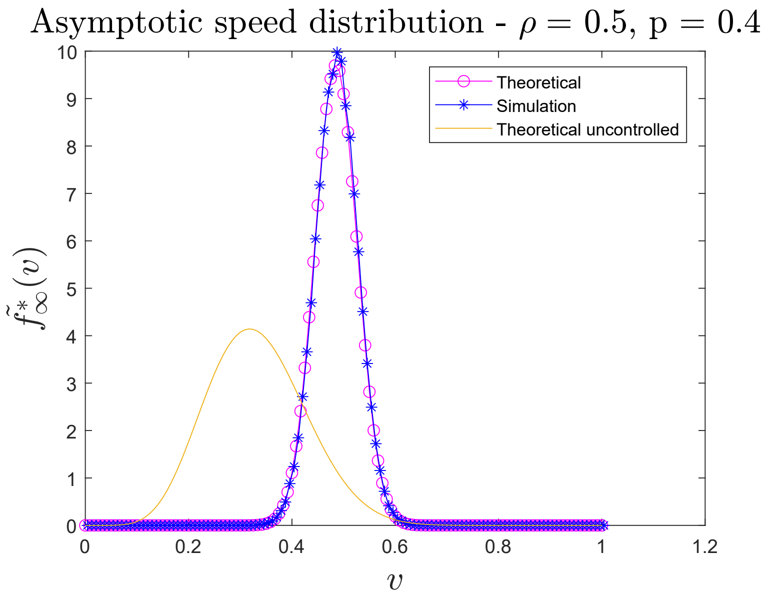

Figure 4.49: Infinite effective penetration rate limit ($\nu = 0.1\gamma$) with desired speed control $v_d(\rho) = 1-\rho$. Comparison between the asymptotic Fokker-Planck distribution (4.63) with $\tilde{V}^*_\infty$ defined in (4.80)(theoretical), the numerical solution of the Boltzmann-type equation (simulation) and the uncontrolled asymptotic Fokker-Planck distribution (4.37)(theoretical uncontrolled) for $\rho = 0.5$, $p = 0.4$, $T = 100$

4.9 Conclusion

In this chapter, new interaction rules have been introduced. Their nonlinear character leads to a piecewise-defined mean speed at equilibrium and therefore, to a phase transition between two different regimes, the free flow and the congested flow regime. The derivation of the asymptotic speed distribution in the *quasi-invariant interaction limit* provides further evidence of it: in the congested flow regime, the asymptotic speed distribution is a beta distribution while, in the free flow regime, it is a Dirac delta centered at 1. The phase transition naturally emerges from the derivation of macroscopic quantities and it is due to the microscopic binary interactions, which rule the dynamics of the systems.

In the second part of the chapter, a control is introduced in the interaction rules; in particular, two different control strategies are studied: binary variance control and desired speed control. With the former, the phase transition is preserved and coherently with the literature, this strategy can effectively reduce road risk. However, the novelty is that a range of densities for which the variance is identically equal to 0 is identified and it corresponds to the free flow regime.

With the desired speed control, the phase transition is not preserved. This can be a practical benefit: the discontinuity in the traffic could be canceled by introducing autonomous vehicles equipped with this control strategy. However, even though we cannot properly speak about phase transition, this can be approached in some specific conditions and a behavior similar to the one of the uncontrolled and the binary variance controlled cases can be achieved. Anyway, as in previous works, a specific regime for which the variance decreases by introducing the desired speed control, is identified: the so-called *infinite effective penetration rate limit*.

All theoretical findings are validated by Monte Carlo simulations based on the Nanbu-Babovsky's scheme. The agreement is strong: as theoretically expected, the numerical equilibrium solution of the Boltzmann-type equation converges toward the solution of the Fokker-Planck PDE, which is analytically obtained in the *quasi-invariant interaction regime*.

Chapter 5

Phase transition under uncertain vehicle interactions

So far, interaction rules with both a deterministic and a stochastic component have been considered. In this chapter, an uncertain parameter, which models the presence of different types of vehicles in traffic, is introduced in the nonlinear interaction rules previously studied. This uncertainty quantification analysis allows to explain two macroscopic features that are experimentally observed: the macroscopic scattering of the *fundamental diagram* and the multi-modal behavior of the asymptotic speed distribution.

In the first section, the theoretical model is derived referring to the literature [47]. The second section dwells upon the derivation of the mean speed at equilibrium and that of the critical point. Several discrete and continuous uncertain parameters are considered and general results which identify the stable fixed point of the system and the critical density of the phase transition, are stated and proved. The third section is devoted to the asymptotic speed distribution. In the penultimate section, theoretical findings are numerically validated by a Monte Carlo based scheme. Finally, conclusions are drawn.

5.1 Uncertainty meets nonlinearity

In [47], an uncertain parameter z is introduced in the interaction rules. The goal is to model the presence of different categories of vehicles in the traffic and to derive the macroscopic scattering of *fundamental diagrams*. In the following, we refer to [47] in order to obtain the mean speed at equilibrium and the asymptotic speed distribution with our new interaction rules, which contain both a nonlinearity vw and an uncertain parameter z. We would like to investigate whether the phase transition, which emerges in chapter 4, is preserved by the introduction of the uncertainty.

Let us introduce the probability of accelerating $P(\rho;z)$ [47], which depends both on the traffic density ρ and on the uncertain parameter z:

$$P(\rho;z) = (1-\rho)^z \ , \tag{5.1}$$

where z is a positive random variable such that $z \sim \psi(z)$, $\psi(z)$ is a probability distribution: $\psi : \mathbb{R}_+ \to \mathbb{R}_+$. If we refer to figure 3.1 (p. 44) with $\mu \to z$, it is clear that greater uncertain parameter z corresponds to vehicles which have a lower probability of accelerating such as lorries, while smaller z are related to vehicles which easily accelerate i.e. accelerate even with big values of density, such as cars.

The interaction rules, which represent the core of our model and determine the dynamics of the system, are defined as [47]

$$\begin{aligned} v' &= v + \gamma I(v,w;\rho,z) + D(v;\rho)\eta \\ w' &= w \ . \end{aligned} \tag{5.2}$$

As in previous chapters, $\gamma > 0$ and it is a proportionality parameter, while η is a centered random variable, with zero mean and variance σ^2 and $D(v;\rho) \geq 0$ is a diffusion coefficient. Thanks to the term $D(v;\rho)\eta$, a stochastic component is included in the model, allowing to consider the intrinsic stochasticity in each agent's behavior.
The interaction function $I(v,w;\rho,z)$ is defined as [47]

$$I(v,w;\rho,z) = P(\rho;z)(1-v) + (1-P(\rho;z))(vw-v) \ . \tag{5.3}$$

The physical admissibility of these interaction rules is guaranteed by proposition 3.3.1, in which the parameter μ is replaced by the random variable z.

5.2 Mean speed at equilibrium and the critical point

First, let us introduce the Boltzmann-type equation for the system. The speed distribution is also function of the uncertain parameter z: $f = f(t,v;z)$. It is such that $f(t,v;z)dv$ represents the fraction of vehicles which have speed in the interval $[v, v+dv]$ at time $t \geq 0$, given the uncertain parameter z.

If $\phi = \phi(v)$ is a generic observable, the Boltzmann-type equation in weak form is [47]

$$\frac{d}{dt}\int_0^1 \phi(v)f(t,v;z)dv = \frac{1}{2}\langle\int_0^1\int_0^1[\phi(v') - \phi(v)]f(t,v;z)f(t,w;z)dvdw\rangle, \tag{5.4}$$

where $\langle\cdot\rangle$ is the expectation with respect to the distribution of the centered random variable η.
Unlike the Boltzmann-type equations considered in chapters 3 - 4, equation (5.4) is stochastic since its solution $f(t,v;z)$ is a function of the random variable z. Therefore, first we will derive the evolution equations for z-dependent macroscopic quantities and then, we will average over z in order to rule this dependence out.

If $\phi(v) = 1$,

$$\frac{d}{dt}\int_0^1 \phi(v)f(t,v;z)dv = 0 \ . \tag{5.5}$$

This means that, given an initial condition $f_0(v;z) = f(0,v;z)$ properly normalized, $f(t,v;z)$ will be normalized and therefore, a distribution probability $\forall t > 0$ [47].

Instead, if $\phi(v) = v$, an equation which rules the evolution of the mean speed will be derived. Let us define the z-dependent mean speed as [47]

$$V(t;z) \coloneqq \int_0^1 vf(t,v;z)dv. \tag{5.6}$$

Then, by plugging $\phi(v) = v$ in (5.4), we obtain

$$\frac{d}{dt}V(t;z) = \frac{\gamma}{2}\Big[P(\rho;z) + (1 - P(\rho;z))V^2(t;z) - V(t;z)\Big] \ . \tag{5.7}$$

We have obtained an equation analogous to the case without uncertain parameter: equation (5.7) and (4.11) are equivalent if equation (5.7) is considered for a fixed value of the parameter z. Therefore, the analysis which leads to the solution at equilibrium of (5.7) is equivalent to the one performed in section 4.2 for equation (4.11). The only difference is that now the solution is a stochastic quantity. The z-dependent mean speed at equilibrium turns out to be

$$V_\infty(\rho;z) = \begin{cases} \frac{P(\rho;z)}{1-P(\rho;z)} & \text{if } \rho \in (\rho_c(z),1] \\ 1 & \text{if } \rho \in [0,\rho_c(z)] \end{cases} \tag{5.8}$$

where the z-dependent critical density $\rho_c(z)$ is defined as

$$\rho_c(z) := 1 - 2^{-\frac{1}{z}} \ .$$

Indeed, it corresponds to the value of the probability of accelerating $P(\rho; z)$ for which the two fixed points of the system merge i.e. $P(\rho; z) = \frac{1}{2}$. Equation (5.8) can be also written as

$$V_\infty(\rho; z) = \frac{P(\rho; z)}{1 - P(\rho; z)} \mathbb{I}\big[\rho \in (\rho_c(z), 1]\big] + \mathbb{I}\big[\rho \in [0, \rho_c(z)]\big] \ , \tag{5.9}$$

where $\mathbb{I}[x \in A] = 1$ if $x \in A$ and $\mathbb{I}[x \in A] = 0$ if $x \notin A$.

In order to rule the z dependence out, we should average $V_\infty(\rho; z)$ with respect to this parameter. This is equivalent to define the mean speed at equilibrium $\bar{V}_\infty(\rho)$ as [47]

$$\bar{V}_\infty(\rho) := \mathbb{E}_z[V_\infty(\rho; z)] = \int_{\mathbb{R}_+} V_\infty(\rho; z)\psi(z)dz \ . \tag{5.10}$$

At the same time, the variance of the z-dependent mean speed at equilibrium can be introduced [47]:

$$\zeta^2_\infty(\rho) := \mathrm{Var}_z\big(V_\infty(\rho; z)\big) = \int_{\mathbb{R}_+} V^2_\infty(\rho; z)\psi(z)dz - \big[\bar{V}_\infty(\rho)\big]^2 \ . \tag{5.11}$$

Then, it can be clarified what we mean by scattering of the *fundamental diagram* of the system. Let us define the flux at equilibrium as $q := \rho\bar{V}_\infty(\rho)$. As explained in section 3.5, the *fundamental diagram* is identified by the mapping $\rho \mapsto q = \rho\bar{V}_\infty(\rho)$. Due to the uncertainty that has been introduced in the interaction rules, the following set of points can be defined [47]:

$$S := \Big\{(\rho, q) \in [0,1] \times \mathbb{R}_+ : q \in \big[\rho\bar{V}_\infty(\rho) - \rho\zeta_\infty(\rho), \rho\bar{V}_\infty(\rho) + \rho\zeta_\infty(\rho)\big]\Big\} \ . \tag{5.12}$$

This set S represents a quantification of the uncertainty of the *fundamental diagram*. As in [47], the standard deviation $\zeta_\infty(\rho)$ is chosen as a measure of uncertainty. We speak about scattering of the *fundamental diagram*, since we can identify the entire region S in the density-flux plane together with the curve of the flux as a function of the density.

In the following, the mean speed at equilibrium $\bar{V}_\infty(\rho)$ will be computed for different probability distributions of the uncertain parameter z, by referring to [47].

5.2.1 Mean speed at equilibrium in the discrete case

Let us consider a discrete case. The uncertain parameter z assumes the following values:

$$z \in \{z_1, z_2, ..., z_n\}$$

and $z_i \in \mathbb{R}_+ \forall i = 1, ..., n$ .The probability distribution of z is defined as

$$\psi(z) = \sum_{k=1}^{n} \mathbb{P}(z = z_k)\delta(z - z_k) \ , \tag{5.13}$$

where

$$\mathbb{P}(z = z_k) \coloneqq \alpha_k \in [0,1] \text{ with } \textstyle\sum_{k=1}^{n} \alpha_k = 1.$$

Therefore, we obtain

$$\bar{V}_\infty(\rho) = \sum_{k=1}^{n} \alpha_k V_\infty(\rho; z_k) \tag{5.14}$$

and

$$\zeta_\infty^2(\rho) = \sum_{k=1}^{n} \alpha_k V_\infty^2(\rho; z_k) - \left(\sum_{k=1}^{n} \alpha_k V_\infty(\rho; z_k)\right)^2 . \tag{5.15}$$

For instance, n can be set equal to 2 and therefore, $z \in \{z_1, z_2\}$. Let us choose $z_1 = 1$ and $z_2 = 3$; they have associated probabilities α_1 and α_2. In this case, the mean speed at equilibrium turns out to be equivalent to

$$\bar{V}_\infty(\rho) = \alpha_1 V_\infty(\rho; z_1 = 1) + \alpha_2 V_\infty(\rho; z_2 = 3) \tag{5.16}$$

and its variance is

$$\begin{aligned} \zeta_\infty^2(\rho) = \alpha_1 V_\infty^2(\rho; z_1 = 1) + \alpha_2 V_\infty^2(\rho; z_2 = 3) + \\ - \Big[\alpha_1 V_\infty(\rho; z_1 = 1) + \alpha_2 V_\infty(\rho; z_2 = 3)\Big]^2 . \end{aligned} \tag{5.17}$$

Referring to (5.8), three cases should be distinguished:

$$\begin{aligned} &\text{if } \rho \in \Big(\rho_c(z_1),1\Big], \quad \bar{V}_\infty(\rho) = \alpha_1 \tfrac{P(\rho;z_1)}{1-P(\rho;z_1)} + \alpha_2 \tfrac{P(\rho;z_2)}{1-P(\rho;z_2)} \\ &\text{if } \rho \in \Big(\rho_c(z_2), \rho_c(z_1)\Big], \quad \bar{V}_\infty(\rho) = \alpha_1 + \alpha_2 \tfrac{P(\rho;z_2)}{1-P(\rho;z_2)} \\ &\text{if } \rho \in \Big[0, \rho_c(z_2)\Big], \quad \bar{V}_\infty(\rho) = 1 \end{aligned} \tag{5.18}$$

where $\rho_c(z_1) = 1 - 2^{-1} = 0.5$ and $\rho_c(z_2) = 1 - 2^{-\frac{1}{3}} \simeq 0.2063$.

In figures 5.1 - 5.4, *speed* and *fundamental diagrams* are displayed for two different choices of α_1 and α_2. In *fundamental diagrams* 5.3 - 5.4, the uncertainty region S can be identified since $\rho\bar{V}_\infty \pm \rho\zeta_\infty(\rho)$ is plotted together with the flux $\rho\bar{V}_\infty$.

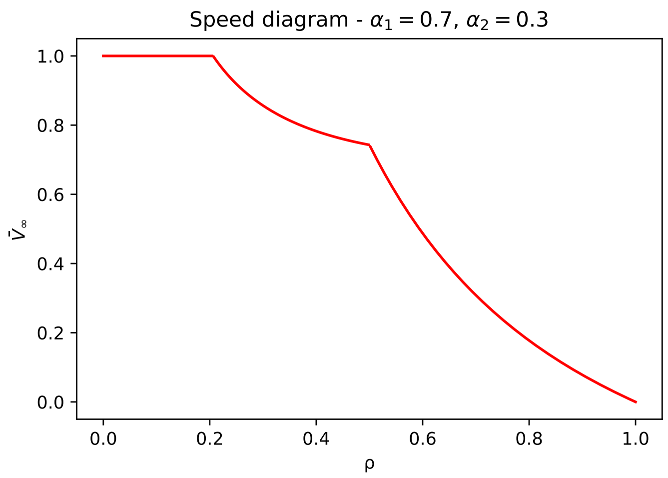

Figure 5.1: Speed diagram in the discrete case $z \in \{z_1 = 1, z_2 = 3\}$, $\alpha_1 = 0.7$, $\alpha_2 = 0.3$. $\bar{V}_\infty$ is defined in (5.18)

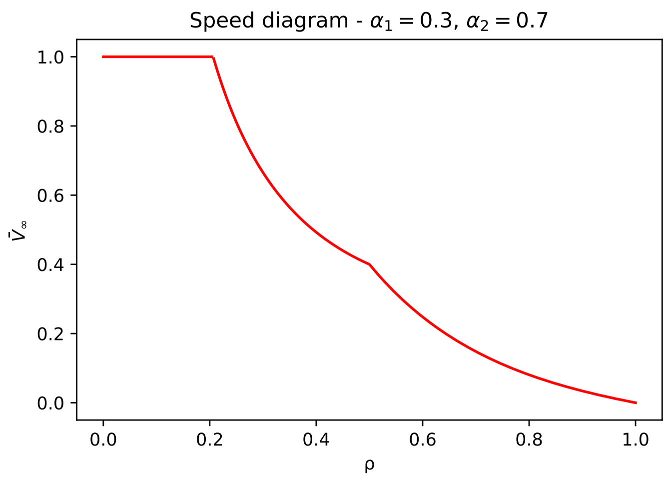

Figure 5.2: Speed diagram in the discrete case $z \in \{z_1 = 1, z_2 = 3\}$, $\alpha_1 = 0.3$, $\alpha_2 = 0.7$. $\bar{V}_\infty$ is defined in (5.18)

By studying these plots and by referring to the related analytical expressions, we observe that the mean speed at equilibrium is equal to the

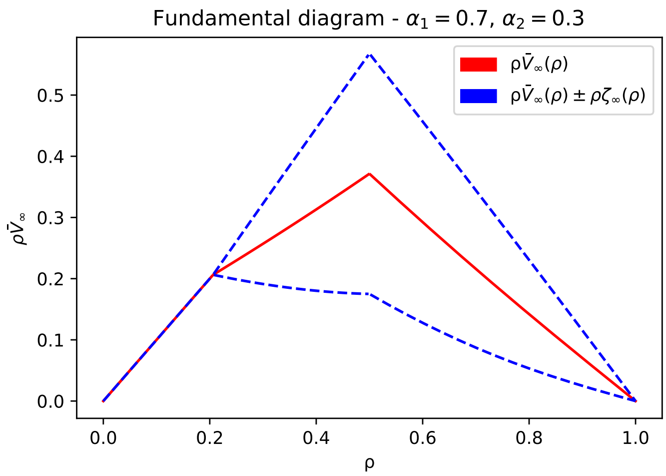

Figure 5.3: Fundamental diagram in the discrete case $z \in \{z_1 = 1, z_2 = 3\}$, $\alpha_1 = 0.7$, $\alpha_2 = 0.3$. $\bar{V}_\infty$ is defined in (5.18); $\zeta_\infty(\rho)$ is obtained with (5.17)

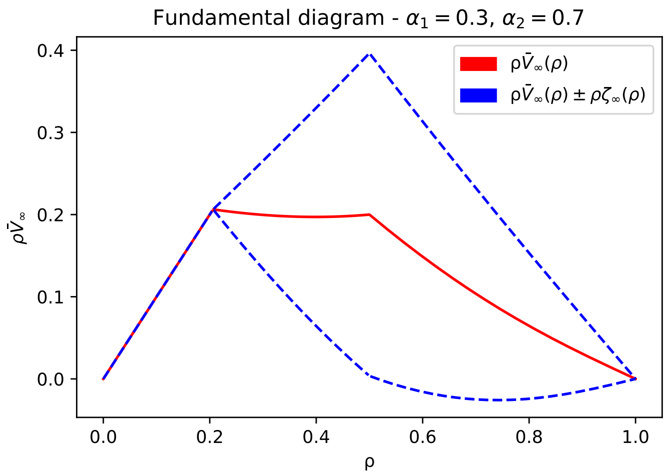

Figure 5.4: Fundamental diagram in the discrete case $z \in \{z_1 = 1, z_2 = 3\}$, $\alpha_1 = 0.3$, $\alpha_2 = 0.7$. $\bar{V}_\infty$ is defined in (5.18); $\zeta_\infty(\rho)$ is obtained with (5.17)

maximum allowed value i.e. 1 for densities smaller than the z_2-dependent critical density $\rho_c(z_2)$. We could start to think about $\rho_c(z_2)$ as the critical density which marks the phase transition between the free flow and the congested flow regime. This is just a first qualitative insight on the issue and a rigorous argument will be provided in the following.

5.2.2 Insight on the critical point

First, let us focus on the stability analysis of the fixed points related to the mean speed. In order to perform the linear stability analysis as done in chapter 4, we could think about averaging (5.7) with respect to z. In this way we obtain

$$\begin{aligned}\frac{d}{dt}\bar{V}(t;\rho) = \frac{\gamma}{2}\Big\{&\mathbb{E}_z\big[V^2(t;z)\big] - \mathbb{E}_z\big[P(\rho;z)V^2(t;z)\big] - \bar{V}(t;\rho)+ \\ &+\mathbb{E}_z\big[P(\rho;z)\big]\Big\}\,,\end{aligned} \tag{5.19}$$

where $\bar{V}(t;\rho) := \mathbb{E}_z[V(t;z)]$. We cannot determine the fixed points of this equation and study their stability since it is not possible to express $\mathbb{E}_z\big[V^2(t;z)\big]$ and $\mathbb{E}_z\big[P(\rho;z)V^2(t;z)\big]$ as functions of $\bar{V}(t;\rho)$. Therefore, we change our perspective to study the problem.

Proposition 5.2.1. *Let us consider a discrete uncertain parameter, in particular $z \in \{z_1, ..., z_n\}$ with $z_1, ..., z_n > 0$. Then, the system has a unique stable fixed point at equilibrium, which is denoted by $\bar{V}_\infty(\rho)$ and it is equal to*

$$\bar{V}_\infty(\rho) = \textstyle\sum_{k=1}^n \alpha_k V_\infty(\rho; z = z_k),$$

where $V_\infty(\rho; z = z_k)$ are the stable fixed points for fixed z.

Proof. Let us consider equation (5.7). Its equilibrium solution is derived: it is expressed in (5.8) and it is denoted by $V_\infty(\rho; z)$. This solution corresponds to the stable fixed point of the system, which is unique. Therefore, if the unstable fixed point is excluded as initial condition, we will have

$$\lim_{t\to+\infty} V(t;z) = V_\infty(\rho;z).$$

Due to the fact that we have $\bar{V}(t;\rho) = \sum_{k=1}^n \alpha_k V(t;z_k)$, then we obtain

$$\bar{V}_\infty(\rho) := \lim_{t\to\infty} \bar{V}(t;\rho) = \lim_{t\to\infty} \textstyle\sum_{k=1}^n \alpha_k V(t;z_k) = \sum_{k=1}^n \alpha_k V_\infty(\rho;z_k).$$

This means that the mean speed at equilibrium $\bar{V}_\infty(\rho)$ is equal to the average with respect to z of the z-dependent stable fixed points. □

Even though we are not able to derive an evolution equation for $\bar{V}(t;\rho)$, we have proved that the mean speed at equilibrium coincides with the unique stable fixed point of the system.

The same result can also be proved for a continuous uncertain parameter. Before doing it, let us recall the Lebesgue's dominated convergence theorem [38]. This theorem will be needed to prove the proposition analogous to 5.2.1 for the continuous case.

Theorem 5.2.2. *Let $(X, \mathcal{F}, \mu)$ be a measure space: X is a non empty set, $\mathcal{F} \subseteq \mathcal{P}(x)$ is a σ-algebra on X, $\mathcal{P}(x)$ is the collection of all subsets of X and μ is a measure on $\mathcal{F}$.*
Let us denote by $M = M(\mathcal{F})$ the space of measurable functions $f : X \to [-\infty, +\infty]$ and introduce $\{f_n\} \in M$ i.e. $\{f_n\}$ is a sequence of measurable functions on X such that $\lim_{n+\infty} f_n(x) = f(x)$ $\forall x \in X$.
Assume there exists a function $g \in L^1(\mu)$ i.e. integrable with respect to μ and such that $|f_n(x)| \leq g(x)$ $\forall n$ and $\forall x \in X$.
Then, $f \in L^1(\mu)$ and

$$\textstyle\int_X f d\mu = \lim_{n\to+\infty} \int_X f_n d\mu \quad .$$

The proof of this theorem is not reported in this dissertation, but we suggest [38] for it.

Proposition 5.2.3. *Let us consider a continuous uncertain parameter $z \sim \psi(z)$, $\psi(z)$ is a continuous probability distribution: $\psi : \mathbb{R}_+ \to \mathbb{R}_+$. Then, the system has a unique stable fixed point at equilibrium, which is denoted by $\bar{V}_\infty(\rho)$ and it is equal to*

$$\bar{V}_\infty(\rho) = \textstyle\int_{\mathbb{R}_+} V_\infty(\rho; z)\psi(z)dz,$$

where $V_\infty(\rho; z)$ is the stable fixed point for fixed z.

Proof. Let us consider equation (5.7). We derived its equilibrium solution, which is expressed in (5.8) and it is denoted by $V_\infty(\rho; z)$. This solution corresponds to the stable fixed point of the system, which is unique. Therefore, if the unstable fixed point is excluded as initial condition, we will have

$$\textstyle\lim_{t\to+\infty} V(t; z) = V_\infty(\rho; z).$$

We have that $\bar{V}(t; \rho) = \int_{\mathbb{R}_+} V(t; z)\psi(z)dz$. Then, by the Lebesgue's dominated convergence theorem 5.2.2, we obtain

$$\begin{aligned}\bar{V}_\infty(\rho) &:= \lim_{t\to+\infty} \bar{V}(t; \rho) = \lim_{t\to+\infty} \int_{\mathbb{R}_+} V(t; z)\psi(z)dz = \\ &= \int_{\mathbb{R}_+} \lim_{t\to+\infty} V(t; z)\psi(z)dz = \int_{\mathbb{R}_+} V_\infty(\rho; z)\psi(z)dz \ .\end{aligned}$$

In particular, the theorem is used in the third equality: it allows to take the limit for $t \to +\infty$ into the integral. The hypotheses of the theorem hold since $V(t;z)\psi(z) \leq \psi(z)$ because $V(t;z) \in [0,1]$ for all t, z and $\psi(z)$ is Lebesgue measurable by definition.
Therefore, the mean speed at equilibrium $\bar{V}_\infty(\rho)$ is equal to the average with respect to z of the z-dependent stable fixed points, as in the discrete case. $\square$

In order to identify the phase transition, we could refer to the in-depth box at the end of section 4.3. It explains that the bifurcation is a solid trait of the system's dynamics which identifies its critical point and that the phase transition is empirically linked to the slope change in the *fundamental diagram*. However, the situation is more complicated if uncertainty quantification is performed and this empirical definition has to be relaxed. In particular, the mathematical justification which is provided in the in-depth box does not hold because the derivative of the mean speed at equilibrium is not continuous in the congested flow regime. For instance, in the discrete case with $z \in \{z_1 = 1, z_2 = 3\}$, two angular points can be identified in the mean speed at equilibrium $\bar{V}_\infty(\rho)$, one which corresponds to $\rho_c(z_1) = 1 - 2^{-\frac{1}{z_1}} = 0.5$ and another to $\rho_c(z_2) = 1 - 2^{-\frac{1}{z_2}} \simeq 0.206$. This is pretty evident by studying equation (5.18) and figures 5.1 - 5.2 (p. 144). The smallest angular point i.e. $\rho_c(z_2)$ can be defined as the critical point of the system since it marks the passage from a density region where $\bar{V}_\infty(\rho) = 1$ to another where $\bar{V}_\infty(\rho) < 1$. On the other hand, $\rho_c(z_1)$ does not denote any phase transition but other changes which occur in the congested flow regime. In section 5.3, the mean (with respect to z) asymptotic speed distribution will be determined and it will be clear that for $\rho \in \big(\rho_c(z_2), \rho_c(z_1)\big]$, the mean asymptotic speed distribution is the linear combination of a beta and a Dirac delta distribution, while for $\rho \in \big(\rho_c(z_1), 1\big]$, it is a bimodal beta distribution. A qualitative insight of this issue can be gained by studying (5.18): for $\rho \in \big(\rho_c(z_2), \rho_c(z_1)\big]$, the mean asymptotic speed has just $V_\infty(\rho; z_2)$ different from 1, while for $\rho \in \big(\rho_c(z_1), 1\big]$, both $V_\infty(\rho; z_2)$ and $V_\infty(\rho; z_1)$ are different from 1.

The empirical definition of phase transition, which is based on the change of slope of the flux in the *fundamental diagram*, does not hold under uncertain vehicle interactions. The critical point of this phenomenon has to be identified as the density which marks the passage from a region where the mean speed at equilibrium is equal to 1 to another where it suddenly decreases to values smaller than 1. This physical-mathematical interpretation of the phase transition is more suited than the empirical since it holds for more complex cases such as the ones with uncertainty.

Therefore, by studying the simple discrete case $z \in \{z_1 = 1, z_2 = 3\}$, we have obtained that the critical point of the system coincides with the one corresponding to the type of vehicles with the biggest z. Let us generalize this result for $z \in \{z_1, ..., z_n\}$ with $z_1, ...z_n > 0$.

Proposition 5.2.4. *Let us consider a discrete uncertain parameter, in particular $z \in \{z_1, ..., z_n\}$ with $z_1, ..., z_n > 0$. Then, the system's critical point is*

$$\rho_c := \min_{k=1,...,n} \left\{\rho_c(z_k)\right\},$$

where $\rho_c(z_k) = 1 - 2^{-\frac{1}{z_k}}$.

Proof. Let us consider $\rho_c(z_k)$: it is defined as $\rho_c(z_k) = 1 - 2^{-\frac{1}{z_k}}$ and

$$\lim_{z_k \to +\infty} \rho_c(z_k) = 0 \ .$$

$\rho_c(z_k)$ is a decreasing function of z_k. If $\rho \leq \rho_c(z_k)$, $V_\infty(\rho; z_k) = 1$. Therefore, if we define

$$\rho_c := \min_{k=1,...,n} \left\{\rho_c(z_k)\right\} \implies \rho_c \leq \rho_c(z_k) \ \forall z_k,$$

we obtain

$$\bar{V}_\infty(\rho) = \sum_{k=1}^{n} \alpha_k V_\infty(\rho; z_k) = 1 \text{ for } \rho \leq \rho_c.$$

Consequently, ρ_c identifies the phase transition between the free flow and the congested flow regime. □

Let us have a graphical insight on this proposition by considering the discrete case with $z_1 = 1$, $z_2 = 2$,...,$z_{10} = 10$ and $\alpha_k = 0.1$ for $k = 1, ...10$. The related *speed diagram* is displayed in figure 5.5 (p. 150), where the vertical lines correspond to $\rho = \rho_c(z_k)$ with $k = 1, ..., 10$. By zooming on the region which identifies the critical point as it is done in figure 5.6 (p. 150), it is evident that the critical density is about 0.06697, coherently with $\rho_c(z_{10}) = 1 - 2^{-\frac{1}{10}}$. In this case, the discretisation of the density interval, which has been chosen to plot the mean speed at equilibrium is such that

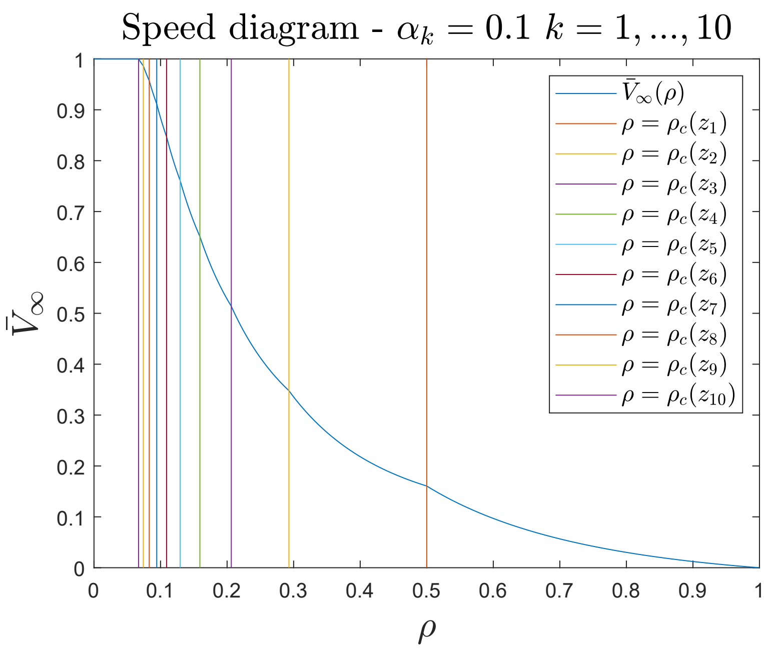

Figure 5.5: Speed diagram in the discrete case $z \in \{z_1 = 1, z_2 = 2, ..., z_{10} = 10\}$, $\alpha_k = 0.1$ $k = 1, ...,10$ together with $\rho = \rho_c(z_k)$ $k = 1, ...,10$

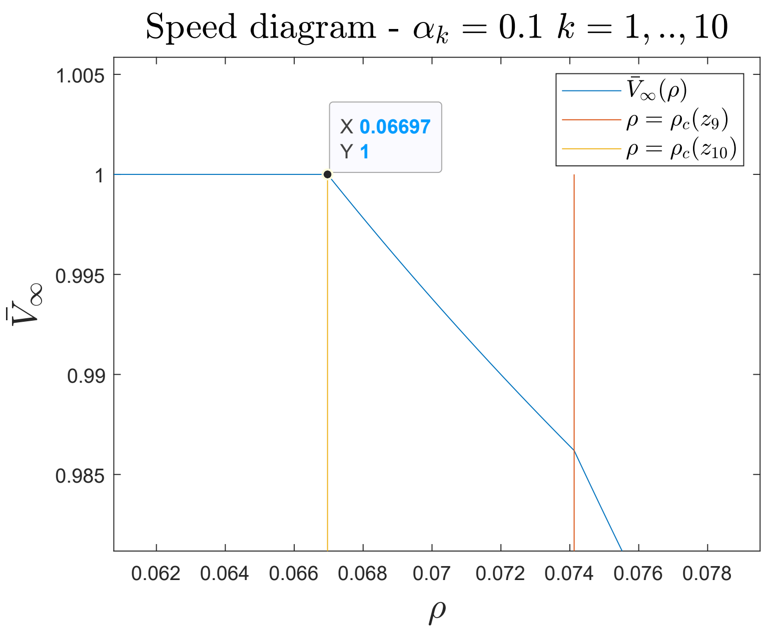

Figure 5.6: Zoom on the speed diagram in the discrete case $z \in \{z_1 = 1, z_2 = 2, ..., z_{10} = 10\}$, $\alpha_k = 0.1$ $k = 1, ...,10$ together with $\rho = \rho_c(z_k)$ $k = 1, ...,10$

the lattice step is equivalent to 0.00001. By refining it, convergence towards $\rho_c(z_{10})$ is achieved.

From proposition 5.2.4, the critical point in the continuous case can be deduced.

Corollary 5.2.5. *Let us consider* $z \sim \psi(z)$ *where* $\psi(z)$ *is a continuous probability distribution with bounded support i.e.* $\psi : [a, b] \to \mathbb{R}_+$, $0 < a < b < +\infty$. *Then, the system's critical point is*

$$\rho_c := 1 - 2^{-\frac{1}{b}} \ .$$

Proof. The proof is similar to the one of proposition 5.2.4. The only difference is that now, we have a continuum of points. $z = b$ corresponds to the biggest value of the uncertain parameter in the interval considered. Due to the fact that $\rho_c(z) := 1 - 2^{-\frac{1}{z}}$ and it is a decreasing function of z, we have

$$\rho_c = \min\nolimits_{z \in [a,b]} \left\{\rho_c(z)\right\} = 1 - 2^{-\frac{1}{b}} \quad .$$

□

From corollary 5.2.5, it can be deduced that if an uncertain parameter z with unbounded support is considered, there is not phase transition. For instance, let us consider $z \sim \psi(z)$ where $\psi(z)$ is a Gamma distribution:

$$\rho_c = \min_{z \in (0,\infty)} \left\{\rho_c(z)\right\} = \lim_{z \to \infty} \left\{\rho_c(z)\right\} = 0 \ . \tag{5.20}$$

As done in the discrete case, let us compute the mean speed at equilibrium $\bar{V}_\infty(\rho)$ in continuous cases. Then, we will able to plot the associated *speed* and *fundamental diagrams*.

5.2.3 Mean speed at equilibrium in the uniform case

If z is uniformly distributed in the interval $[a, b]$ with $a, b > 0$, we have

$$\begin{aligned} &z \sim \mathcal{U}([a, b]) \\ &\psi(z) = \frac{1}{b - a}\mathbb{I}[a \le z \le b] \ . \end{aligned} \tag{5.21}$$

In order to compute $\bar{V}_\infty(\rho)$, we refer to definition (5.10), where $V_\infty(\rho; z)$ has to be plugged in. We would like to use (5.9) and in order to do so, we have to express the conditions in the indicator functions in terms of z. Therefore, we obtain

$$\begin{aligned}\rho > \rho_c(z) = 1 - 2^{-\frac{1}{z}} &\iff P(\rho; z) = (1-\rho)^z < \frac{1}{2} \iff \\ &\iff z > -\frac{\log 2}{\log(1-\rho)} \equiv z_c\end{aligned} \tag{5.22}$$

and

$$V_\infty(\rho; z) = \frac{P(\rho; z)}{1 - P(\rho; z)} \mathbb{I}\big[z > z_c\big] + \mathbb{I}\big[z \leq z_c\big] \, . \tag{5.23}$$

Let us compute $\bar{V}_\infty(\rho)$ by using equation (5.23). We should distinguish several cases: $a \leq z_c < b$, $z_c < a$ and $z_c \geq b$. First, let us compute the following integrals:

$$\begin{aligned} I &= \int_{z_1}^{z_2} \frac{P(\rho; z)}{1 - P(\rho; z)} dz = \int_{z_1}^{z_2} \frac{(1-\rho)^z}{1 - (1-\rho)^z} dz = \int_{z_1}^{z_2} \frac{e^{z \log(1-\rho)}}{1 - e^{z \log(1-\rho)}} dz = \\ &= \left\{ - \frac{\log\left(1 - e^{z \log(1-\rho)}\right)}{\log(1-\rho)} \right\}\Bigg|_{z_1}^{z_2} = \frac{\log\left(1 - (1-\rho)^{z_1}\right) - \log\left(1 - (1-\rho)^{z_2}\right)}{\log(1-\rho)} \end{aligned} \tag{5.24}$$

and

$$\begin{aligned} J &= \int_{z_1}^{z_2} \frac{P^2(\rho; z)}{\big[1 - P(\rho; z)\big]^2} dz = \int_{z_1}^{z_2} \frac{(1-\rho)^{2z}}{\big[1 - (1-\rho)^z\big]^2} dz = \\ &= \int_{z_1}^{z_2} \left\{ \frac{(1-\rho)^z}{\big[1 - (1-\rho)^z\big]^2} - \frac{(1-\rho)^z}{1 - (1-\rho)^z} \right\} dz = \\ &= \frac{\big[1 - (1-\rho)^z\big]^{-1}}{\log(1-\rho)} - \left\{ - \frac{\log\left(1 - e^{z \log(1-\rho)}\right)}{\log(1-\rho)} \right\}\Bigg|_{z_1}^{z_2} . \end{aligned} \tag{5.25}$$

If $a \leq z_c < b$:

$$\begin{aligned} \bar{V}_\infty(\rho) &= \int_{\mathbb{R}_+} \left\{ \frac{P(\rho; z)}{1 - P(\rho; z)} \mathbb{I}\big[z > z_c\big] + \mathbb{I}\big[z \leq z_c\big] \right\} \psi(z) dz = \\ &= \frac{1}{b-a} \left\{ \int_{z_c}^{b} \frac{P(\rho; z)}{1 - P(\rho; z)} dz + \int_{a}^{z_c} dz \right\} = \\ &= \frac{1}{b-a} \left\{ \frac{\log\left(1 - (1-\rho)^{z_c}\right) - \log\left(1 - (1-\rho)^{b}\right)}{\log(1-\rho)} + (z_c - a) \right\} \end{aligned} \tag{5.26}$$

where in the last equality the integral I of equation (5.24) has been used.
If $z_c < a$:

$$\begin{aligned}\bar{V}_\infty(\rho) &= \int_{\mathbb{R}_+} \left\{ \frac{P(\rho;z)}{1-P(\rho;z)} \mathbb{I}\big[z > z_c\big] + \mathbb{I}\big[z \le z_c\big] \right\} \psi(z) dz = \\ &= \frac{1}{b-a} \left\{ \int_a^b \frac{P(\rho;z)}{1-P(\rho;z)} dz \right\} = \\ &= \frac{1}{b-a} \left\{ \frac{\log\big(1-(1-\rho)^a\big) - \log\big(1-(1-\rho)^b\big)}{\log(1-\rho)} \right\}\end{aligned} \tag{5.27}$$

where in the last equality the integral I of equation (5.24) has been used.
If $z_c \ge b$:

$$\begin{aligned}\bar{V}_\infty(\rho) &= \int_{\mathbb{R}_+} \left\{ \frac{P(\rho;z)}{1-P(\rho;z)} \mathbb{I}\big[z > z_c\big] + \mathbb{I}\big[z \le z_c\big] \right\} \psi(z) dz = \\ &= \frac{1}{b-a} \left\{ \int_a^b dz \right\} = 1 \ .\end{aligned} \tag{5.28}$$

Analogously, the variance of the mean speed at equilibrium i.e. $\zeta_\infty^2(\rho) := \mathrm{Var}_z\big(V_\infty(\rho;z)\big)$ can be obtained by referring to equation (5.11).
If $a \le z_c < b$:

$$\begin{aligned}\zeta_\infty^2(\rho) &= \frac{1}{b-a} \left\{ \int_b^{z_c} \frac{(1-\rho)^{2z}}{\big[1-(1-\rho)^z\big]^2} dz + \int_a^{z_c} dz \right\} - \big[V_\infty(\rho;z)\big]^2 = \\ &= \frac{1}{(b-a)\log(1-\rho)} \left\{ \frac{1}{1-(1-\rho)^b} + \log\big(1-(1-\rho)^b\big) + \right. \\ &\quad \left. - \frac{1}{1-(1-\rho)^{z_c}} - \log\big(1-(1-\rho)^{z_c}\big) \right\} + \frac{z_c - a}{b-a} + \\ &\quad - \frac{1}{(b-a)^2} \left\{ \frac{\log\big(1-(1-\rho)^{z_c}\big) - \log\big(1-(1-\rho)^b\big)}{\log(1-\rho)} + (z_c - a) \right\}^2\end{aligned} \tag{5.29}$$

where the integral J of (5.25) has been used.

If $z_c < a$:

$$\begin{aligned}\zeta^2_\infty(\rho) = & \frac{1}{(b-a)\log(1-\rho)}\left\{\frac{1}{1-(1-\rho)^b} + \log\left(1-(1-\rho)^b\right) + \right. \\ & \left. - \frac{1}{1-(1-\rho)^a} - \log\left(1-(1-\rho)^a\right)\right\} + \\ & - \frac{1}{\left[(b-a)\log(1-\rho)\right]^2}\left\{\log\left(1-(1-\rho)^a\right) - \log\left(1-(1-\rho)^b\right)\right\}^2\end{aligned} \tag{5.30}$$

where again the integral J of (5.25) has been used.
Finally, if $z_c \geq b$:

$$\zeta^2_\infty(\rho) = 0 \ . \tag{5.31}$$

The critical density of the phase transition can be obtained by referring to (5.28): it corresponds to $z_c = b \iff \rho_c = 1 - 2^{-\frac{1}{b}}$, coherently with the corollary 5.2.5. Moreover, the density $1-2^{-\frac{1}{a}}$, which corresponds to $z_c = a$, divides the congested flow regime into two density regions, where the mean speed at equilibrium has different expressions. We expect this behavior will be reflected in the change of shape of the asymptotic speed distribution, as we will see in subsection 5.3.2.

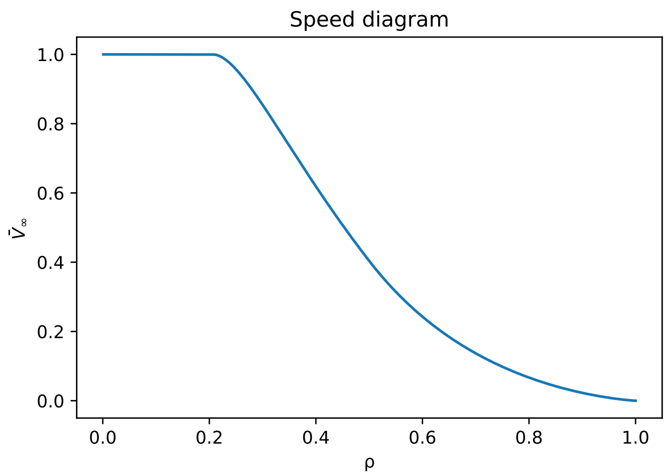

Figure 5.7: Speed diagram in the continuous case $z \sim \mathcal{U}([a,b])$ with $a = 1$ and $b = 3$. $\bar{V}_\infty$ is defined in (5.26) - (5.28)

In figures 5.7 - 5.8, the *speed* and the *fundamental diagram* with $a = 1$ and $b = 3$ are respectively displayed. In this case, the critical density is

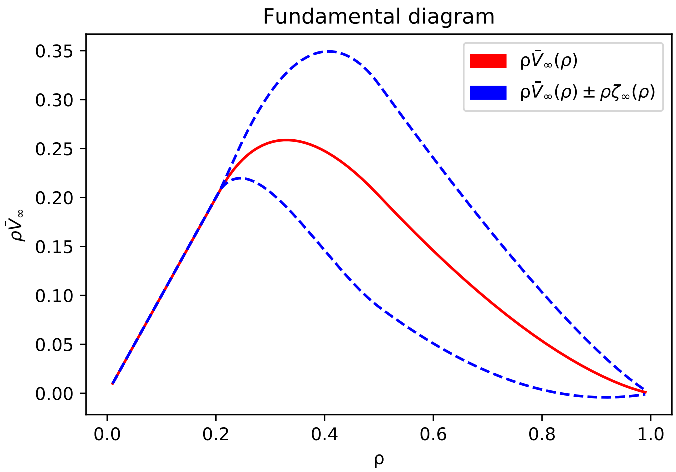

Figure 5.8: Fundamental diagram in the continuous case $z \sim \mathcal{U}([a, b])$ with $a = 1$ and $b = 3$. $\bar{V}_\infty$ is defined in (5.26) - (5.28); $\zeta_\infty(\rho)$ is defined in (5.29) - (5.31)

$\rho_c = 1 - 2^{-\frac{1}{3}} \simeq 0.206$ and the density which divides the congested flow regime into two regions is $1 - 2^{-1} = 0.5$.

5.2.4 Mean speed at equilibrium in the gamma case

These diagrams can also be obtained for other continuous distributions of the uncertainty parameter z. Let us consider:

$$z - p \sim \text{Gamma}(\alpha, \beta)$$
$$\psi(z) = \frac{\beta^\alpha}{\Gamma(\alpha)} e^{-\beta(z-p)}(z-p)^{\alpha-1} \ , \ z > p \ . \tag{5.32}$$

If $z_c < p$:

$$\bar{V}_\infty(\rho) = \int_p^\infty \frac{P(\rho, z)}{1 - P(\rho, z)} \psi(z) dz \ , \tag{5.33}$$

while if $z_c \geq p$:

$$\bar{V}_\infty(\rho) = \int_{z_c}^\infty \frac{P(\rho, z)}{1 - P(\rho, z)} \psi(z) dz + \int_p^{z_c} \psi(z) dz \ . \tag{5.34}$$

Referring to (5.11), the variance $\zeta^2_\infty(\rho)$ of the asymptotic speed distribution can be computed analogously.

The computation of $\bar{V}_\infty(\rho)$ and $\zeta^2_\infty(\rho)$ cannot be carried out analytically and suited quadrature methods [3; 39; 48] have to be employed. By calculating $\bar{V}_\infty(\rho)$, it is evident that $\bar{V}_\infty(\rho) < 1 \ \forall \rho \in [0,1]$ and so, there is not phase transition, coherently with (5.20).

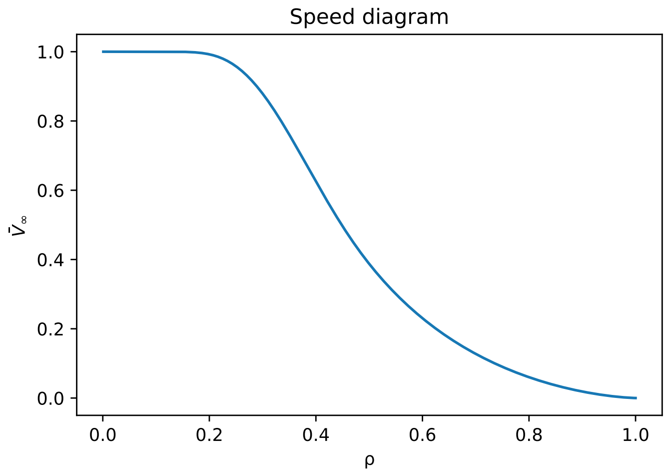

Figure 5.9: Speed diagram in the continuous case $z - 1 \sim \text{Gamma}(\alpha, \beta])$ with $\alpha = 3$ and $\beta = 3$. $\bar{V}_\infty$ is defined in (5.33) - (5.34)

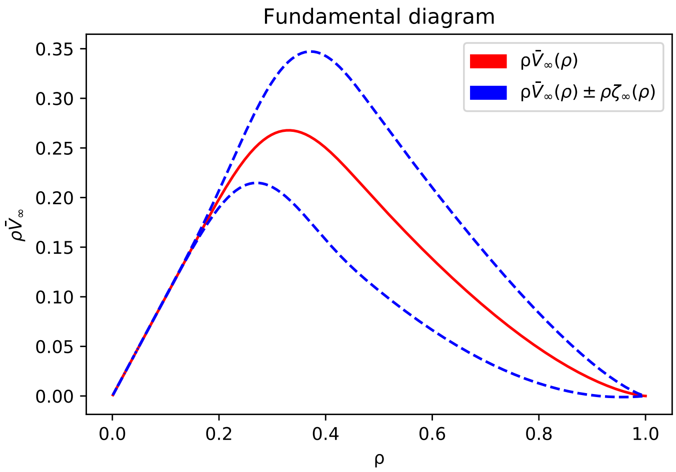

Figure 5.10: Fundamental diagram in the continuous case $z - 1 \sim \text{Gamma}(\alpha, \beta])$ with $\alpha = 3$ and $\beta = 3$. $\bar{V}_\infty$ is defined in (5.33) - (5.34); $\zeta_\infty(\rho)$ is defined in (5.11)

The parameter p is chosen such that the expected valued of z is equivalent to 2, as in the uniform case previously considered. Therefore, we can set $\alpha = \beta = 3$ and $p = 1$ since $\mathbb{E}(z) = \alpha/\beta + p$.

In figures 5.9 - 5.10, the *speed* and the *fundamental diagram* are displayed. They have been obtained by means of Gaussian quadrature formulae [3; 39; 48]; in particular, the Python™ sub-package *scipy.integrate* has been used. This sub-package has functions, such as *quadrature*, which perform Gaussian quadrature of multiple orders. The integration result is returned when the difference in the estimate becomes smaller than a given tolerance, which is set equal to 1.49e-08 by default.

Similarly, *speed* and *fundamental diagrams* can be obtained for other probability distributions of the uncertain parameter z, both discrete and continuous.

5.3 The asymptotic speed distribution with nonlinear and uncertain interaction rules

The next step in our analysis is to obtain the mean equilibrium speed distribution, where mean denotes the average with respect to the probability distribution of the uncertain parameter z [47]. First, the z-dependent asymptotic speed distribution will be obtained by solving the stochastic Boltzmann-type equation (5.4). This will be done by considering the *quasi-invariant interaction regime*: from the integro-differential equation (5.4), a z-dependent Fokker-Planck PDE will be obtained. Then, its result will be averaged with respect to the probability distribution of z. Few different distributions will be considered.

As in chapters 3 - 4, the *quasi-invariant interaction limit* is considered in order to determine the asymptotic speed distribution analytically. Let us recall this limit:

$$\gamma, \sigma^2 \to 0^+ \text{ such that } \tfrac{\sigma^2}{\gamma} \to \lambda > 0 \; .$$

A new time scale $\tau := \frac{\gamma}{2}t$ and the scaled z-dependent distribution function $g(\tau, v; z) := f\left(\frac{2\tau}{\gamma}, v; z\right)$ are introduced [47]. Calculations are analogous to the case without uncertainty; the only difference relies on the z dependence indeed the solution of (5.4) is a stochastic quantity. Therefore, as in the uncontrolled case, we obtain the following equation:

$$\partial_\tau g = \frac{\lambda}{2}\partial_v^2\Big(D^2(v;\rho)g\Big) - \partial_v\Big(\big(\int_0^1 I(v,w;z)g(\tau,w;z)dw\big)g\Big) \; . \qquad (5.35)$$

Let us compute the integral of the interaction function (5.3) in (5.35):

$$\begin{aligned}&\int_0^1 I(v,w;z)g(\tau,w;z)dw = \\&= \int_0^1 \Big[P(\rho;z)(1-v)+(1-P(\rho;z))(vw-v)\Big]g(\tau,w;z)dw = \\&= P(\rho;z)(1-v)+(1-P(\rho;z))v(U-1)\ ,\end{aligned} \tag{5.36}$$

where $U = U(\tau;z)$ is the mean speed with respect to the distribution function g i.e. $U = \int_0^1 wg(\tau,w;z)dw$ [47].

At equilibrium i.e. for $\tau \to +\infty$, the Fokker-Planck type equation (5.35) becomes

$$\frac{\lambda}{2}\partial_v^2\Big(D^2(v;\rho)g_\infty\Big) - \partial_v\Big\{\Big[P(\rho;z)(1-v)+(1-P(\rho;z))v(U_\infty-1)\Big]g_\infty\Big\} = 0\ . \tag{5.37}$$

The analysis for the two different regimes have to be performed separately, analogously to the uncontrolled case. Let us consider the **congested flow regime**. As previously derived, it corresponds to $P \in [0,\frac{1}{2}) \iff \rho \in (\rho_c(z),1]$. In this regime,

$$U_\infty(\rho;z) = \frac{P(\rho;z)}{1-P(\rho;z)}\ . \tag{5.38}$$

As in chapters 3 - 4, the following diffusion coefficient is considered:

$$D(v;\rho) := a(\rho)\sqrt{v(1-v)}\ ,\ a(\rho) \geq 0\ . \tag{5.39}$$

Therefore, by referring to section 4.3 and to the calculations carried out in the case without uncertainty, the z-dependent asymptotic speed distribution turns out to be a beta probability density function

$$g_\infty(v;z) = \frac{v^{\alpha-1}(1-v)^{\beta-1}}{B(\alpha,\beta)}\ , \tag{5.40}$$

where the parameters α and β depend on z. They are

$$\begin{aligned}\alpha &:= \frac{2P(\rho;z)}{\lambda a^2(\rho)}\\ \beta &:= \frac{2(1-2P(\rho;z))}{\lambda a^2(\rho)}\ .\end{aligned} \tag{5.41}$$

If X is a random variable such that $X \sim g_\infty$,

$$
\begin{aligned}
\mathbb{E}[X] &= \frac{\alpha}{\alpha+\beta} = \frac{P(\rho;z)}{1-P(\rho;z)} = U_\infty(\rho;z) \\
\mathrm{Var}(X) &= \frac{\alpha\beta}{(\alpha+\beta)^2(\alpha+\beta+1)} = \frac{(1-U_\infty(\rho;z))U_\infty^2(\rho;z)}{2P(\rho;z)+\lambda a^2(\rho)U_\infty(\rho,z)}\lambda a^2(\rho) \ ,
\end{aligned}
\tag{5.42}
$$

where the relation $\alpha+\beta = \frac{\alpha}{U_\infty}$ has been used.

Now, let us consider the **free flow regime**. As previously derived, it corresponds to $P \in \left[\frac{1}{2},1\right] \iff \rho \in [0,\rho_c(z)]$. In this regime,

$$
U_\infty = 1.
$$

Let us introduce

$$
\epsilon := 1 - U_\infty \to 0^+
$$

and let us perform an analysis analogous to the one of the case without uncertainty - see section 4.3. Therefore, by approaching the free flow regime, the z-dependent asymptotic speed distribution turns out to be a beta distribution

$$
g_\infty(v;z) = \frac{v^{\alpha-1}(1-v)^{\beta-1}}{B(\alpha,\beta)} \ , \tag{5.43}
$$

but with different parameter β than the deep congested phase. Indeed, the parameters of the asymptotic speed distribution are

$$
\begin{aligned}
\alpha &:= \frac{2P(\rho;z)}{\lambda a^2(\rho)} \\
\beta &:= \frac{2(1-P(\rho;z))}{\lambda a^2(\rho)}\epsilon \ .
\end{aligned}
\tag{5.44}
$$

Remark 5.3.1. Parameters of the z-dependent asymptotic speed distribution, in (5.41) and (5.44), have the same form of the case without uncertain parameter. The only difference is the dependence on z and the fact that in the case with uncertain parameter, both the mean speed at equilibrium and the asymptotic speed distribution are stochastic quantities. □

If X is a random variable such that $X \sim g_\infty$ and $\epsilon \to 0^+$,

$$\begin{aligned}\mathbb{E}[X] &= \frac{\alpha}{\alpha+\beta} \to 1 \\ \mathrm{Var}(X) &= \frac{\alpha\beta}{(\alpha+\beta)^2(\alpha+\beta+1)} \to 0^+ \ .\end{aligned} \tag{5.45}$$

If the free flow phase is approached, the expected value of a random variable distributed according to the z-dependent asymptotic speed distribution (5.43) tends to the maximum allowed speed. On the other hand, the variance shrinks to 0. This means that in the free flow phase, the z-dependent asymptotic speed distribution is a Dirac delta distribution centered at 1:

$$g_\infty = \delta(v-1).$$

To sum up, the z-dependent asymptotic speed distribution can be rewritten as

$$g_\infty(v;z) = \mathrm{B}_1(v;z)\mathbb{I}[z > z_c] + \delta(v-1)\mathbb{I}[z \leq z_c] \tag{5.46}$$

where z_c is defined in (5.22) and $\mathrm{B}_1(v;z)$ is the z-dependent asymptotic speed distribution in the congested flow regime (5.40).

Now, it is possible to average the z-dependent asymptotic speed distribution with the expectation using the probability distribution of z. If $z \sim \psi(z)$, the mean asymptotic speed distribution is

$$\bar{g}_\infty(v) := \mathbb{E}_z[g_\infty(v;z)] = \int_{\mathbb{R}_+} g_\infty(v;z)\psi(z)dz \tag{5.47}$$

and its variance

$$\mathrm{Var}_z\Big(g_\infty(v;z)\Big) := \int_{\mathbb{R}_+} g^2_\infty(v;z)\psi(z)dz - \Big[\bar{g}_\infty(v)\Big]^2 \ . \tag{5.48}$$

As for the mean speed at equilibrium, $\bar{g}_\infty(v)$ and $\mathrm{Var}_z\Big(g_\infty(v;z)\Big)$ are obtained for different probability distributions of the uncertain parameter z.

Remark 5.3.2. The derivation of macroscopic quantities averaged with respect to z is innovative and simpler than the traditional approach, which would require an evolution equation for each class of vehicles. □

5.3.1 The mean equilibrium speed distribution in the discrete case

Let us consider the following discrete case:

$$z \in \{z_1, z_2, ..., z_n\} \text{ and } z_i \in \mathbb{R}_+ \forall i = 1, ..., n$$

where the probability distribution of z is $\psi(z) = \sum_{k=1}^{n} \alpha_k \delta(z - z_k)$. Therefore, we obtain

$$\bar{g}_\infty(v) = \sum_{k=1}^{n} \alpha_k g_\infty(v; z_k) \tag{5.49}$$

and

$$\mathrm{Var}_z\big(g_\infty(v; z)\big) = \sum_{k=1}^{n} \alpha_k g_\infty^2(v; z_k) - \left(\sum_{k=1}^{n} \alpha_k g_\infty(v; z_k)\right)^2 . \tag{5.50}$$

If $n = 2$, the mean equilibrium speed distribution turns out to be

$$\bar{g}_\infty(v) = \alpha_1 g_\infty(v; z_1) + \alpha_2 g_\infty(v; z_2) . \tag{5.51}$$

Referring to (5.46), several cases should be distinguished.
If $z_c < z_1$:

$$\bar{g}_\infty(v) = \alpha_1 \mathrm{B}_1(v; z_1) + \alpha_2 \mathrm{B}_1(v; z_2) , \tag{5.52}$$

if $z_1 \leq z_c < z_2$:

$$\bar{g}_\infty(v) = \alpha_1 \delta(v - 1) + \alpha_2 \mathrm{B}_1(v; z_2) \tag{5.53}$$

and if $z_c \geq z_2$:

$$\bar{g}_\infty(v) = \delta(v - 1) . \tag{5.54}$$

Similarly, if $n = 2$, its variance is equivalent to

$$\mathrm{Var}_z\big(g_\infty(v; z)\big) = \Big[\alpha_1 g_\infty^2(v; z_1) + \alpha_2 g_\infty^2(v; z_2)\Big] - \Big[\alpha_1 g_\infty(v; z_1) + \alpha_2 g_\infty(v; z_2)\Big]^2 \tag{5.55}$$

and it assumes different values depending on z_c.

In figures 5.11 - 5.15 (pp. 162-164), results related to the discrete case with $n = 2$, $z_1 = 1$, $z_2 = 3$, $\alpha_1 = 0.7$ and $\alpha_2 = 0.3$ are reported; the parameter λ is set equal to 1 and $a(\rho) = \rho(1 - \rho)$. In particular, in figure 5.11, the mean equilibrium speed distribution is displayed in the congested flow regime. The critical density ρ_c which marks the passage from the free flow to the congested flow regime is $\rho_c = \rho_c(z_1) = 1 - 2^{-\frac{1}{3}} \simeq 0.206$. As explained in section 5.2, another angular point of the mean speed at equilibrium $\bar{V}_\infty(\rho)$ is identified i.e. $\rho_c(z_1) = 0.5$ and it divides the congested flow region into two different sub-regimes. If $z_c < z_1$ holds, this is equivalent to consider $\rho > \rho_c(z_1) = 1 - 2^{-\frac{1}{z_1}} = 0.5$ and the mean equilibrium speed distribution $\bar{g}_\infty(v)$ is plotted in figure 5.12. By referring to (5.52) - (5.54), it is evident that if $\rho_c(z_1) < \rho \leq 1$, $\bar{g}_\infty(v)$ is the linear combination of two beta distributions while if $\rho_c(z_2) < \rho \leq \rho_c(z_1)$, $\bar{g}_\infty(v)$ is the linear combination of a Dirac delta centered at 1 and a beta distribution. In the free flow regime i.e. if $0 < \rho \leq \rho_c(z_1)$, $\bar{g}_\infty(v)$ is a Dirac delta.

It is important to observe that in the figures, Dirac deltas are not plotted since the value returned is infinity. For instance, this is the case of the asymptotic speed distribution related to $\rho = 0.4$, which is plotted in figure 5.11 and that is the linear combination of a beta and a Dirac delta distribution.

In figures 5.13 - 5.15, the mean equilibrium speed distribution is displayed together with its uncertainty region. As in [47], the standard deviation $\sqrt{\mathrm{Var}_z\big(g_\infty(v;z)\big)}$ is chosen as a measure of uncertainty.

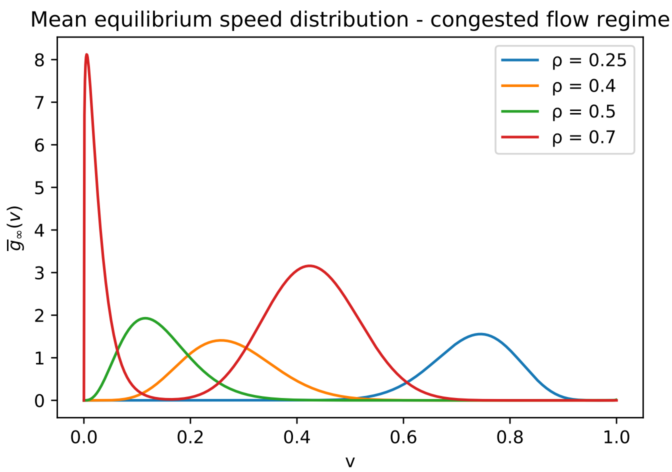

Figure 5.11: Congested flow regime: the mean equilibrium speed distribution with $z \in \{z_1 = 1, z_2 = 3\}$, $\alpha_1 = 0.7$, $\alpha_2 = 0.3$, $\lambda = 1$, $a(\rho) = \rho(1-\rho)$

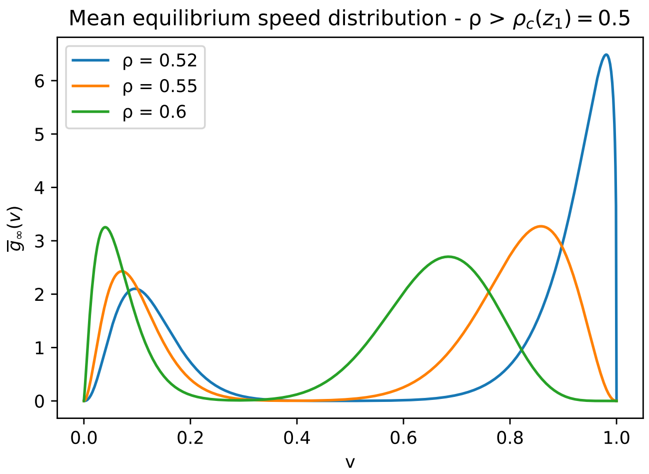

Figure 5.12: The mean equilibrium speed distribution with $\rho > \rho_c(z_1)$, $z \in \{z_1 = 1, z_2 = 3\}$, $\alpha_1 = 0.7$, $\alpha_2 = 0.3$, $\lambda = 1$, $a(\rho) = \rho(1 - \rho)$

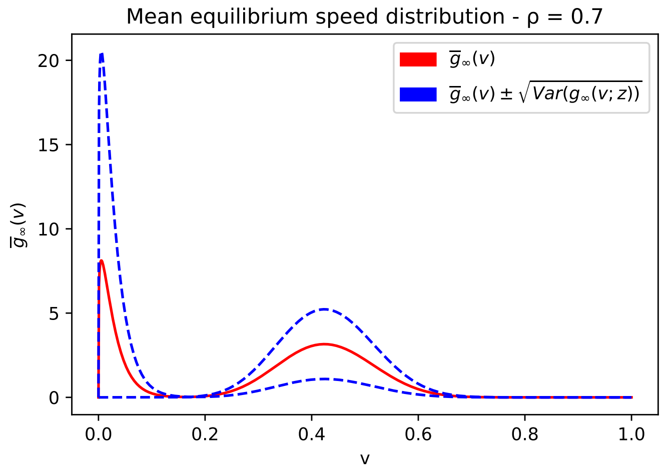

Figure 5.13: The mean equilibrium speed distribution and its uncertainty region with $\rho = 0.7$, $z \in \{z_1 = 1, z_2 = 3\}$, $\alpha_1 = 0.7$, $\alpha_2 = 0.3$, $\lambda = 1$, $a(\rho) = \rho(1 - \rho)$

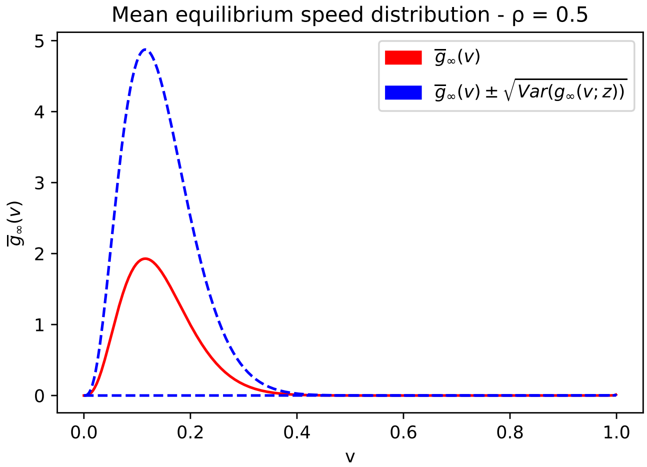

Figure 5.14: The mean equilibrium speed distribution and its uncertainty region for $\rho = 0.5$, $z \in \{z_1 = 1, z_2 = 3\}$, $\alpha_1 = 0.7$, $\alpha_2 = 0.3$, $\lambda = 1$, $a(\rho) = \rho(1 - \rho)$

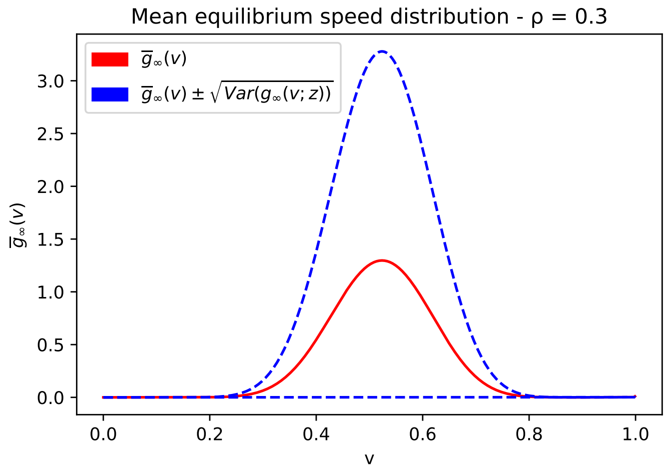

Figure 5.15: The mean equilibrium speed distribution and its uncertainty region for $\rho = 0.3$, $z \in \{z_1 = 1, z_2 = 3\}$, $\alpha_1 = 0.7$, $\alpha_2 = 0.3$, $\lambda = 1$, $a(\rho) = \rho(1 - \rho)$

5.3.2 The mean equilibrium speed distribution in the uniform case

Let us consider a uniformly distributed uncertain parameter z. In particular, we set

$$z \sim \mathcal{U}([a,b])$$
$$\psi(z) = \frac{1}{b-a}\mathbb{I}[a \leq z \leq b] \ .$$

Then, if $z_c \geq b$:

$$\bar{g}_\infty(v) = \delta(v-1) \ ,$$

if $a \leq z_c < b$:

$$\bar{g}_\infty(v) = \frac{1}{b-a}\left\{ \int_{z_c}^{b} \mathrm{B}_1(v;z)dz + (z_c - a)\delta(v-1)\right\}$$

and if $z_c < a$:

$$\bar{g}_\infty(v) = \frac{1}{b-a}\int_a^b \mathrm{B}_1(v;z)dz \ .$$

Similarly, its variance can be obtained.

As explained in subsection 5.2.3 and by referring to corollary 5.2.5, the critical density is $\rho_c = 1 - 2^{-\frac{1}{b}}$. If we consider $a = 1$ and $b = 3$, $\rho_c = 1 - 2^{-\frac{1}{3}} \simeq 0.206$. Moreover, the density 0.5 divides the congested flow regime into two regions, where the behavior of the mean equilibrium speed distribution $\bar{g}_\infty(v)$ is different: for $\rho \in (\rho_c,0.5]$, $\bar{g}_\infty(v)$ is the linear combination of a Dirac delta and the integral over the interval $[z_c,3]$ of the beta probability density function $\mathrm{B}_1(v;z)$ while for $\rho \in (0.5,1]$, it the mean of the beta probability density function $\mathrm{B}_1(v;z)$ with respect to the uniformly distributed z in the interval $[1,3]$.

In figure 5.16 - 5.19 (pp. 166-167), plots related to $a = 1$ and $b = 3$ are displayed; $a(\rho) = \rho(1-\rho)$ and the parameter λ is set equal to 1. They have been obtained by means of Gaussian quadrature functions of the Python™ sub-package *scipy.integrate*. As in previous figures related to the discrete case, infinite values which occur for $\rho = 0.25$ or $\rho = 0.4$ in $v = 1$, cannot be plotted.

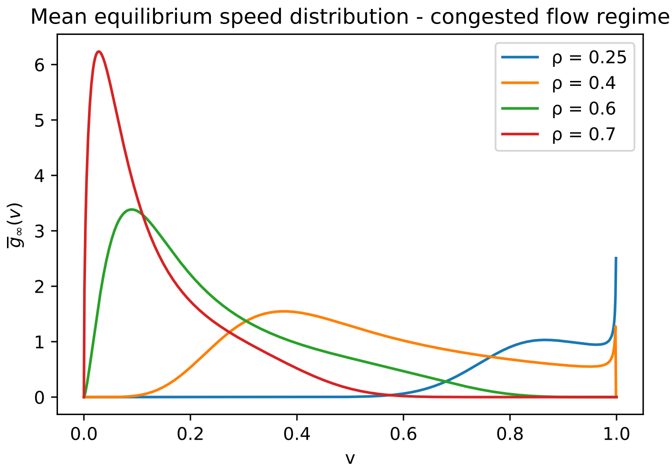

Figure 5.16: Congested flow regime: the mean equilibrium speed distribution with $z \sim \mathcal{U}([a,b])$, $a = 1$, $b = 3$, $\lambda = 1$, $a(\rho) = \rho(1-\rho)$

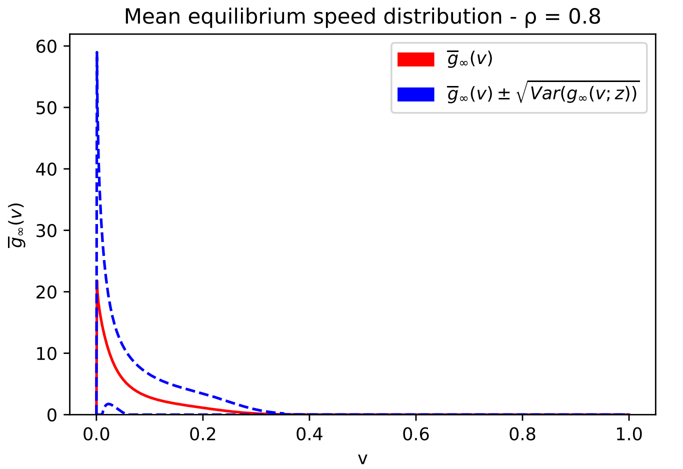

Figure 5.17: The mean equilibrium speed distribution and its uncertainty region for $\rho = 0.8$, $z \sim \mathcal{U}([a,b])$, $a = 1$, $b = 3$, $\lambda = 1$, $a(\rho) = \rho(1-\rho)$

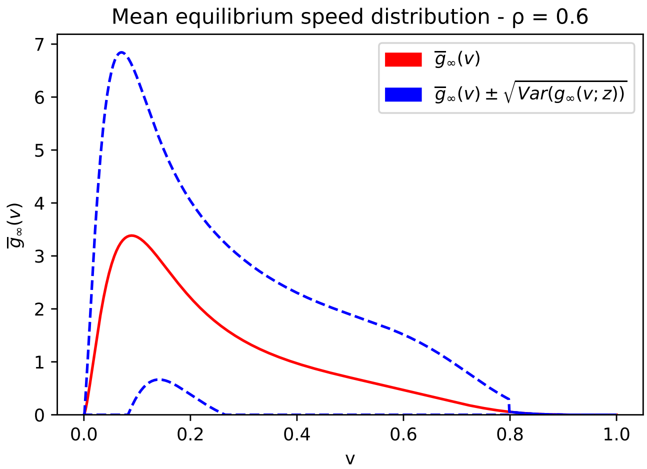

Figure 5.18: The mean equilibrium speed distribution and its uncertainty region for $\rho = 0.6$, $z \sim \mathcal{U}([a,b])$, $a = 1$, $b = 3$, $\lambda = 1$, $a(\rho) = \rho(1-\rho)$

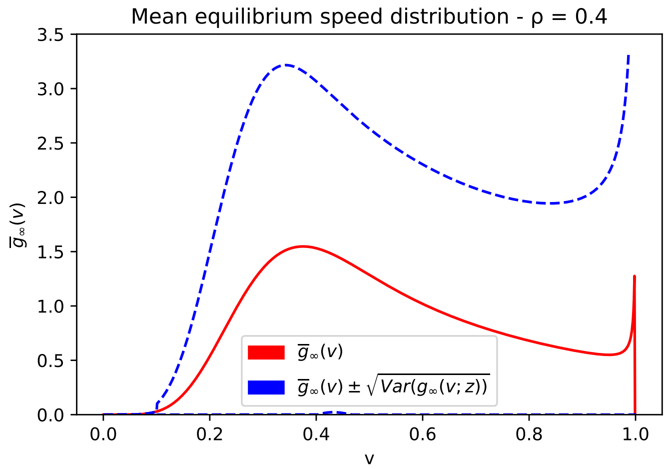

Figure 5.19: The mean equilibrium speed distribution and its uncertainty region for $\rho = 0.4$, $z \sim \mathcal{U}([a,b])$, $a = 1$, $b = 3$, $\lambda = 1$, $a(\rho) = \rho(1-\rho)$

5.3.3 The mean equilibrium speed distribution in the gamma case

Let us consider an uncertain parameter z, which is distributed according to a Gamma distribution of parameter α and β. In particular, we set

$$z - p \sim \mathrm{Gamma}(\alpha, \beta)$$
$$\psi(z) = \frac{\beta^\alpha}{\Gamma(\alpha)} e^{-\beta(z-p)}(z-p)^{\alpha-1} \ , \ z > p \ .$$

Then, if $z_c < p$:

$$\bar{g}_\infty(v) = \int_p^\infty \mathrm{B}_1(v; z)\psi(z)dz \ ,$$

and if $z_c \geq p$:

$$\bar{g}_\infty(v) = \int_p^\infty \mathrm{B}_1(v; z)\psi(z)dz + \delta(v-1)\int_p^{z_c} \psi(z)dz \ .$$

Its variance can be analogously obtained.

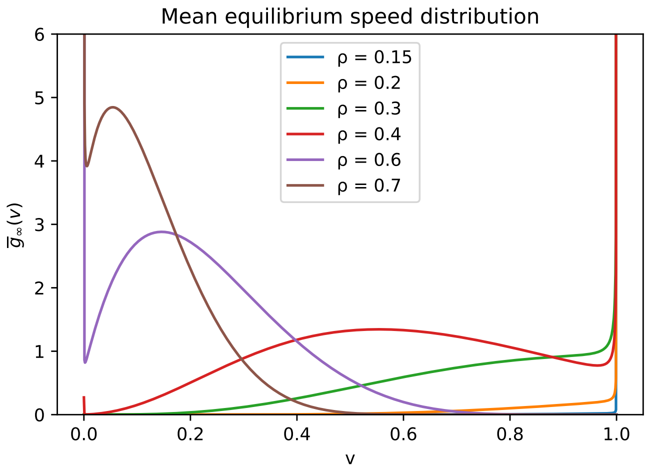

Figure 5.20: The mean equilibrium speed distribution with $z - 1 \sim \mathrm{Gamma}(\alpha, \beta)$, $\alpha = \beta = 3$, $\lambda = 1$, $a(\rho) = \rho(1-\rho)$

In figure 5.20, the mean equilibrium speed distribution $\bar{g}_\infty(v)$ is displayed for $p = 1$; the parameter λ is set equal to 1 and $a(\rho) = \rho(1-\rho)$. Also in this case, Gaussian quadrature functions of the Python™ sub-package *scipy.integrate* have been used. As proved in subsection 5.2.2, there is not phase transition when z is Gamma distributed and indeed, the transition from a beta distribution to a Dirac delta is smooth.

Coherently with literature [47] and with experimental data [27], multi-modal mean equilibrium speed distributions are obtained, due to the introduction of the uncertain parameter. However, because of the nonlinearity in the interaction rules, density intervals in which the behavior of the mean equilibrium speed is different are distinguished

5.4 Numerical tests

In this section, several numerical tests are performed in order to confirm theoretical findings.

5.4.1 Monte Carlo methods for uncertainty quantification

Uncertainty quantification (UQ) is a research topic, which is having a great boost in recent times and is increasingly showing its potentiality in complex system studies [13]. A first numerical approach to UQ is based on a Monte Carlo (MC) based scheme [13; 28].

Let us assume that $f(t, v, z),\ v \in V \subseteq \mathbb{R}^{d_v},\ z \in \Omega \subseteq \mathbb{R}^{d_z}$ is the solution of a PDE with uncertainties only in the initial distribution $f_0(v, z)$. Then, the standard MC method for UQ of kinetic models is presented in the following algorithm [13; 28].

Algorithm 3: MC-MC algorithm

1. **Sampling:** Sample M independent identically distributed (i.i.d.) initial distribution $f_0^k,\ k = 1, ..., M$ from the random initial data f_0.

2. **Solving:** For each f_0^k, the kinetic equation is solved numerically by a MC solver. The numerical solution at time t^j is denoted by $f_{N_v}^{k,j},\ k = 1, ..., M$ where N_v is the sample size of the MC solver for the kinetic equation.

3. **Estimation:** Estimate statistical moments of any quantity of interest $g[f]$ of the random solution field, e.g. for the first moment

$$\mathbb{E}[g[f^j]] \approx E_M[g[f_{N_v}^{k,j}]] := \frac{1}{M}\sum_{k=1}^{M} g[f_{N_v}^{k,j}].$$

Algorithm 3 refers to the general context of kinetic equations. If we consider our problem, that means the solution of the Boltzmann-type equation under uncertain vehicle interactions, these steps translate in the following way. A Monte Carlo sampling of the uncertain parameter z is performed according to its probability distribution. For each value of the uncertain parameter in the sample, the problem is deterministic and it is solved by means of the Nanbu-Babovsky's scheme, explained in section 2.2 and used in chapters 3 and 4. Then, statistical information about the quantities of interest, such as the mean equilibrium speed distribution, can be obtained by means of statistical estimators such as the mean.
Algorithm 4 [13] is the scheme, which will be used to perform simulations.

Algorithm 4: MC-MC algorithm for the Boltzmann-type equation

Set parameters N, ρ, ϵ, Δt, γ, σ^2, N_v

Sampling

Sample M independent identically distributed values of the uncertain parameter z: $\{z_1, z_2, ..., z_M\}$

Solving

For j=1,...,M

Set $z = z_j$

Solve the Boltzmann-type equation for $z = z_j$ by means of the Nanbu-Babovsky's scheme

Save the resulting asymptotic speed distribution $g^j_\infty(v)$ or other quantities of interest

Estimating

Estimate the mean asymptotic speed distribution $\bar{g}^{SIM}_\infty(v)$ by means of the statistical mean: $\bar{g}^{SIM}_\infty(v) \leftarrow \sum_{j=1}^{M} g^j_\infty(v)/M$ or other quantities of interest

Compute the L^2-numerical error with respect to the exact solution $\bar{g}^{TH}_\infty(v)$, which can be obtained by means of quadrature formulae:

L^2-numerical error $= \sqrt{\sum_{k=1}^{N_v}(\bar{g}^{TH}_\infty(v_k) - \bar{g}^{SIM}_\infty(v_k))^2 / \sum_{k=1}^{N_v} \bar{g}^{TH}_\infty(v_k)}$

Return $\bar{g}^{SIM}_\infty(v)$ and L^2-numerical error

Monte Carlo methods for UQ are easily implementable as it is shown by algorithms 3 and 4 since they manly rely on MC solvers of kinetic equations such as the Nanbu-Babovsky's scheme for Boltzmann-type kinetic equations. Therefore, the MC-MC algorithm is non-intrusive and parallelizable since estimation is a post-processing step. It also inherits from the MC solver its efficiency: as explained in section 2.2, Nanbu-Babovsky's scheme has a computational cost, which is linearly proportional to the number of agents and it preserves the main physical properties of the solution [29; 30]. Moreover, the impact of this method on the curse of dimensionality is lower [28]. This means that it weakly has impact on the increase of computational cost due to the size of the uncertain parameter's sample. However, its drawbacks are related to its Monte Carlo trait: as explained in subsection 2.2.2, MC methods are slow, their convergence is $O(N^{-\frac{1}{2}})$, where N is the sample size and fluctuations are present in the solution statistics [7].

Algorithm 4 can be classified as a Monte Carlo-Monte Carlo scheme since both the solution for fixed z of the Boltzmann-type equation and uncertainty quantification are performed with Monte Carlo procedures. Therefore, the overall error has three different contributions [13]. The first is related to UQ and it is $O(M^{-\frac{1}{2}})$, where M is the size of the uncertain parameter's sample; the second is due to the Nanbu-Babovsky's scheme and it is $O(N_v^{-\frac{1}{2}})$ [7], where N_v is the number of lattice points in the speed interval; finally, the last contribution to the error is due to the choice of the parameters such as γ and σ^2, which should be performed such that the *quasi-invariant interaction regime* holds.

In the more general context of algorithm 3, this MC-MC method satisfies the error bound

$$||\mathbb{E}[g[f]] - E_M[g[f_{N_v}]]||_{L^2(V,\Omega)} \leq C(\sigma_z, \sigma_{f_0}, T, f_0, \Delta t)\ (M^{-\frac{1}{2}} + N_v^{-\frac{1}{2}}), \tag{5.56}$$

where C is a function of σ_z i.e. the variance of the random variable z, σ_{f_0} i.e. the variance of the random initial data f_0, T i.e. the final time, f_0 and Δt i.e. the time step.

5.4.2 Choice of parameters

In order to perform simulations, the uniform case has been considered: this means that the uncertain parameter z is uniformly distributed in the interval $[a, b]$. In subsections 5.2.3 and 5.3.2, the mean speed at equilibrium and the mean equilibrium speed distribution have been computed respectively. If $a = 1$ and $b = 3$, the critical density turns out to be $\rho_c = 1 - 2^{-\frac{1}{3}} \simeq 0.206$.

Due to the fact that algorithm 4 is based on the Nanbu-Babovsky's scheme and the requirement $\frac{\Delta t}{\epsilon} \leq 1$ must hold - see subsection 2.2.1, we set

$$\Delta t = \epsilon,\ \gamma = \epsilon,\ \sigma^2 = \gamma\ , \tag{5.57}$$

which imply $\lambda = 1$. The choice $\Delta t = \epsilon$ implies that all agents interact. Several values of ϵ will be considered and it will be evident that as ϵ gets smaller, the solution of the Boltzmann-type kinetic equation better approaches the Fokker-Planck mean equilibrium speed distribution since we are closer to the *quasi-invariant interaction regime*.
As in sections 3.12 and 4.8, we set:

- number of agents $= 10^5$;
- initial speed distribution $f_0 \sim \mathcal{U}([0,1])$;
- speed domain [0,1] is discretized in $N_v = 101$ points;
- $a(\rho) := \rho(1-\rho)$;
- $\eta \sim \mathcal{U}[-a, a]$, $a = \sqrt{3\sigma^2}$.

5.4.3 Results

Let us consider the congested flow regime therefore, we set $\rho = 0.6$. By referring to the deterministic case extensively studied in chapter 4, we set $T = 20$ since this time is sufficient to reach equilibrium with this density. For the parameter ϵ, the following values are considered: 0.5, 0.1, 0.01.

In figures 5.21 - 5.23 (pp. 173-174), results related to the case $\epsilon = 0.5$ are displayed, respectively for $M = 10$, $M = 50$ and $M = 100$. In particular, a comparison between the theoretical and the simulation mean equilibrium speed distribution $\bar{g}_\infty(v)$ can be appreciated. The theoretical $\bar{g}_\infty(v)$ is the mean solution of the Fokker-Planck PDE, which is obtained in the *quasi-invariant interaction regime*. It is calculated numerically by means of the Legendre-Gauss Quadrature formula with 20 nodes [3; 39; 48]. Instead, the simulation $\bar{g}_\infty(v)$ is the solution of the Boltzmann-type equation obtained by means of algorithm 4. Due to the fact that $\gamma = \sigma^2 = \epsilon = 0.5$, we are far from the *quasi-invariant interaction regime*, which requires $\gamma, \sigma^2 \to 0^+$ and $\frac{\sigma^2}{\gamma} \to \lambda > 0$, and consequently, the simulation $\bar{g}_\infty(v)$ does not fit the theoretical one.

Analogous plots are reported in figures 5.24 - 5.26 (pp. 175-176) for $\epsilon = 0.1$ and in figures 5.27 - 5.29 (pp. 176-177) for $\epsilon = 0.01$. As ϵ decreases, the matching between the simulation and the theoretical mean equilibrium speed distribution improves.

Due to the Monte Carlo trait of this approach, considering big values of M is a necessary condition in order to obtain better matching between simulation and theoretical results. In figure 5.30 (p. 178), $M = 500$ is considered together with $\epsilon = 0.01$; the improvement is evident.

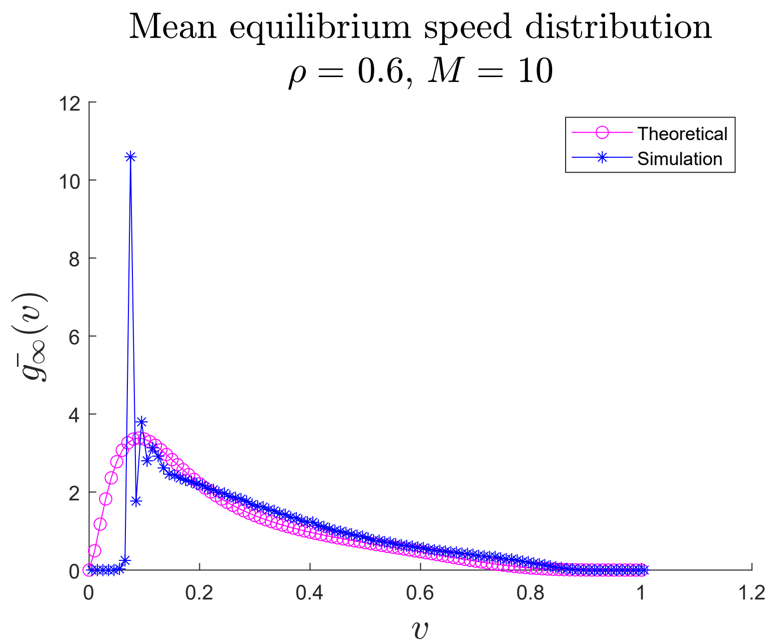

Figure 5.21: Comparison between the mean Fokker-Planck equilibrium speed distribution - see subsection 5.3.2 (theoretical) and the numerical distribution obtained with algorithm 4 (simulation) with $z \sim \mathcal{U}([1,3])$, $\rho = 0.6$, $M = 10$, $\epsilon = 0.5$, $T = 20$

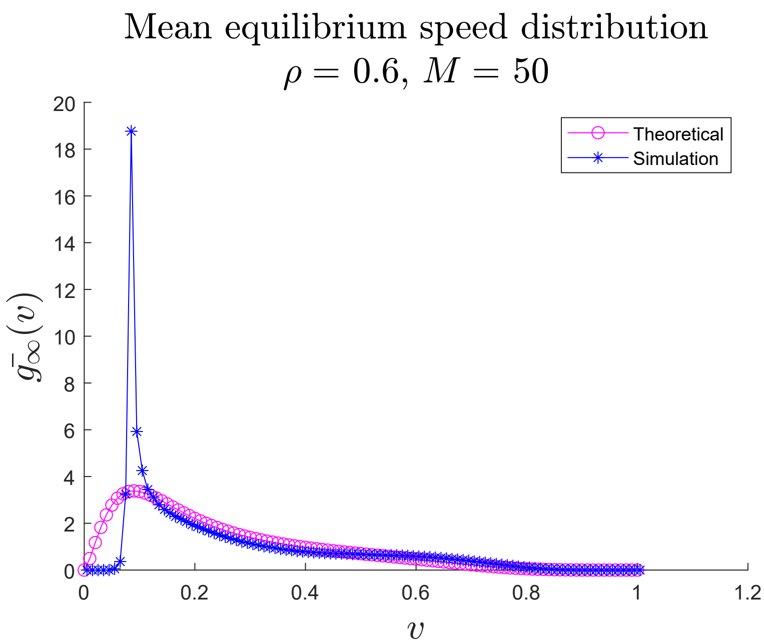

Figure 5.22: Comparison between the mean Fokker-Planck equilibrium speed distribution - see subsection 5.3.2 (theoretical) and the numerical distribution obtained with algorithm 4 (simulation) with $z \sim \mathcal{U}([1,3])$, $\rho = 0.6$, $M = 50$, $\epsilon = 0.5$, $T = 20$

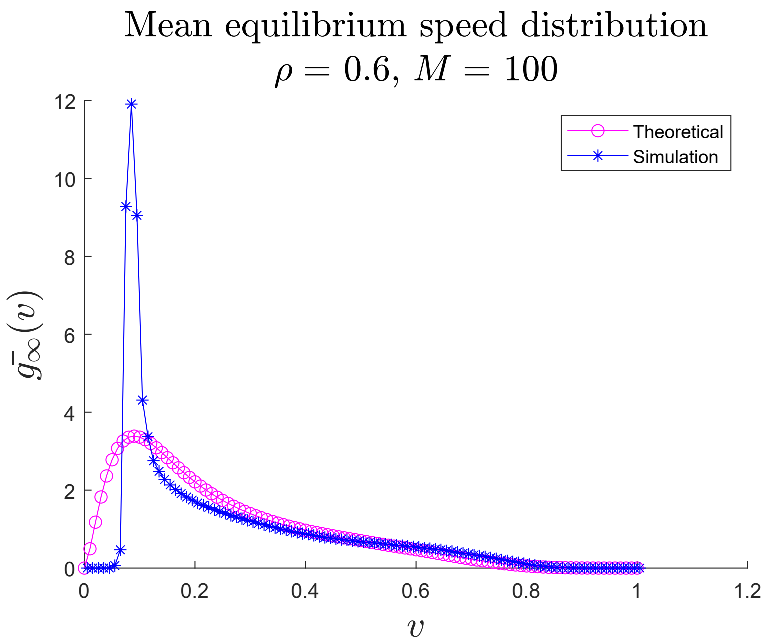

Figure 5.23: Comparison between the mean Fokker-Planck equilibrium speed distribution - see subsection 5.3.2 (theoretical) and the numerical distribution obtained with algorithm 4 (simulation) with $z \sim \mathcal{U}([1,3])$, $\rho = 0.6$, $M = 100$, $\epsilon = 0.5$, $T = 20$

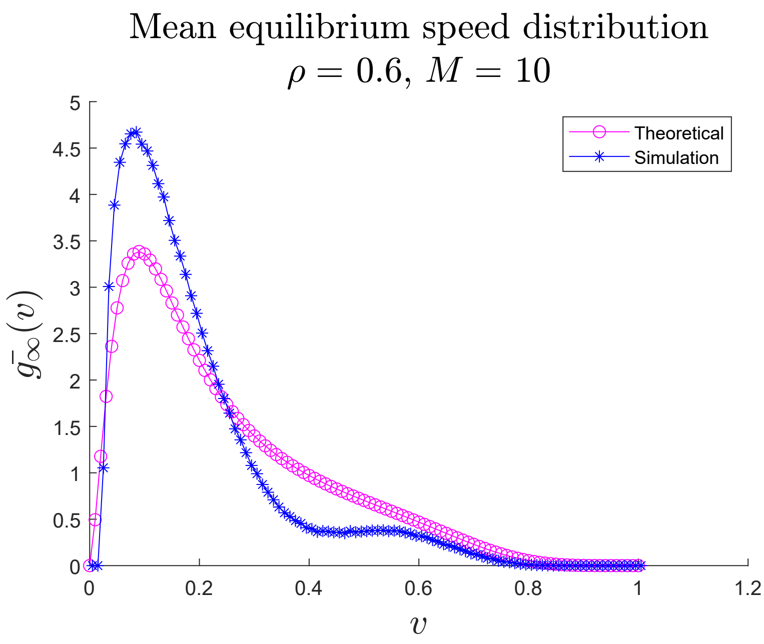

Figure 5.24: Comparison between the mean Fokker-Planck equilibrium speed distribution - see subsection 5.3.2 (theoretical) and the numerical distribution obtained with algorithm 4 (simulation) with $z \sim \mathcal{U}([1,3])$, $\rho = 0.6$, $M = 10$, $\epsilon = 0.1$, $T = 20$

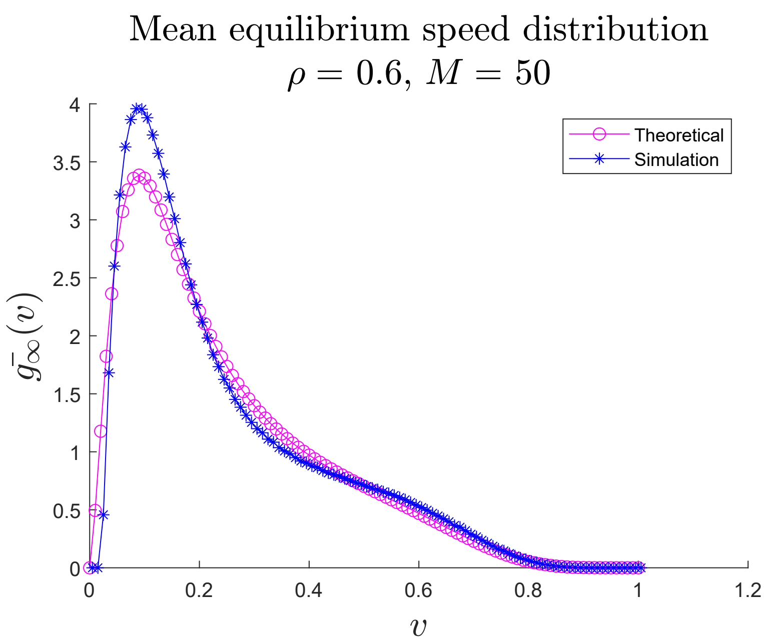

Figure 5.25: Comparison between the mean Fokker-Planck equilibrium speed distribution - see subsection 5.3.2 (theoretical) and the numerical distribution obtained with algorithm 4 (simulation) with $z \sim \mathcal{U}([1,3])$, $\rho = 0.6$, $M = 50$, $\epsilon = 0.1$, $T = 20$

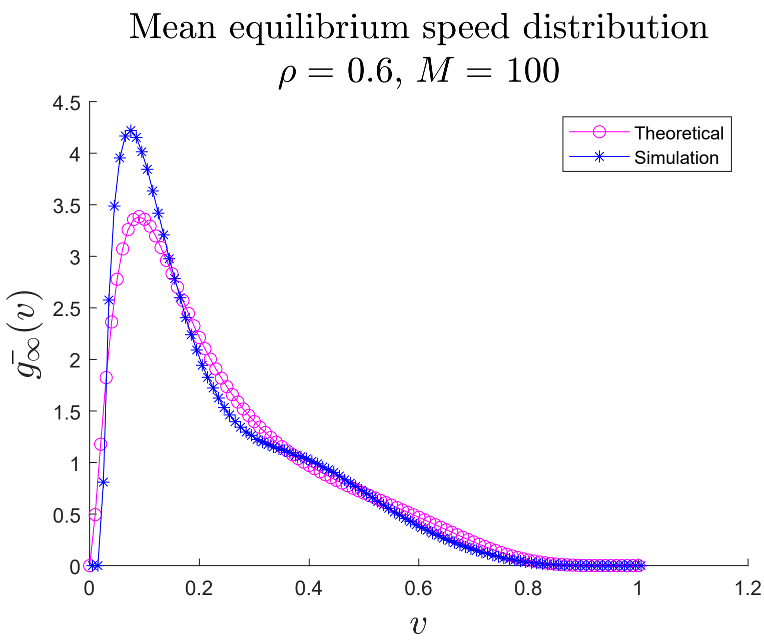

Figure 5.26: Comparison between the mean Fokker-Planck equilibrium speed distribution - see subsection 5.3.2 (theoretical) and the numerical distribution obtained with algorithm 4 (simulation) with $z \sim \mathcal{U}([1,3])$, $\rho = 0.6$, $M = 100$, $\epsilon = 0.1$, $T = 20$

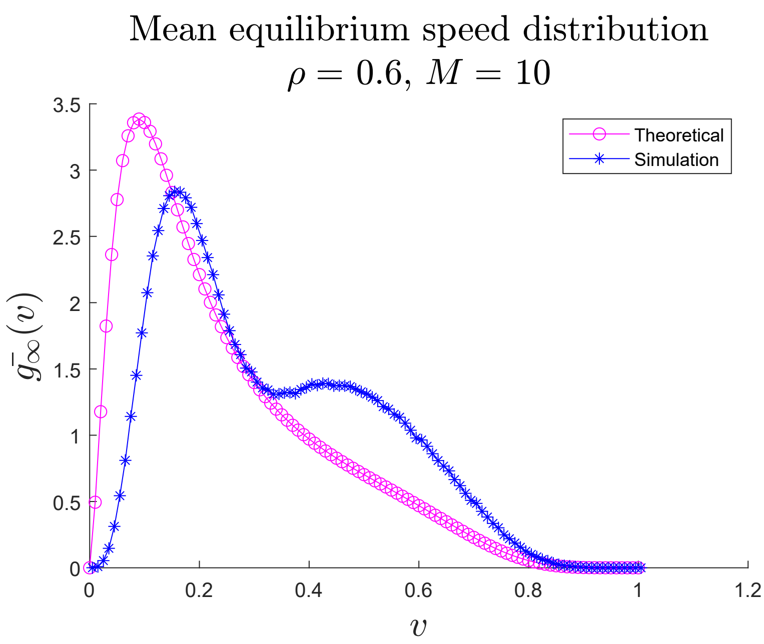

Figure 5.27: Comparison between the mean Fokker-Planck equilibrium speed distribution - see subsection 5.3.2 (theoretical) and the numerical distribution obtained with algorithm 4 (simulation) with $z \sim \mathcal{U}([1,3])$, $\rho = 0.6$, $M = 10$, $\epsilon = 0.01$, $T = 20$

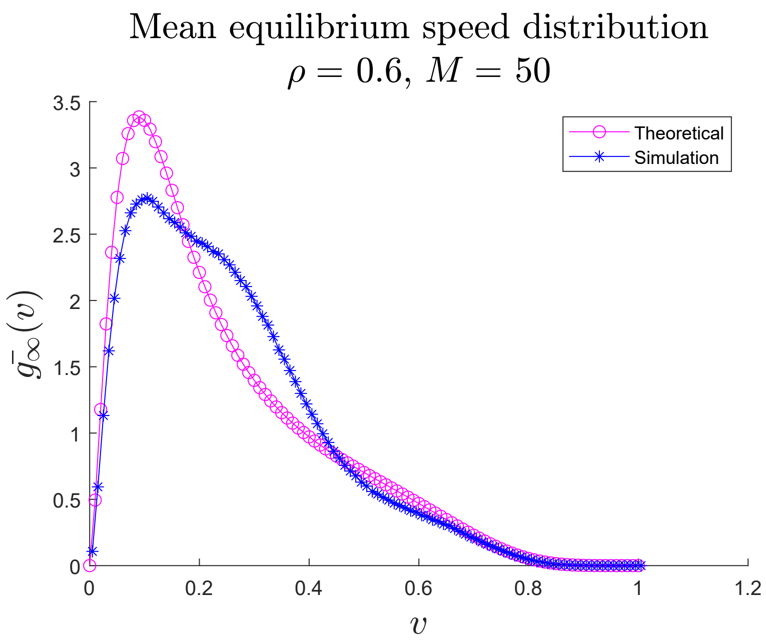

Figure 5.28: Comparison between the mean Fokker-Planck equilibrium speed distribution - see subsection 5.3.2 (theoretical) and the numerical distribution obtained with algorithm 4 (simulation) with $z \sim \mathcal{U}([1,3])$, $\rho = 0.6$, $M = 50$, $\epsilon = 0.01$, $T = 20$

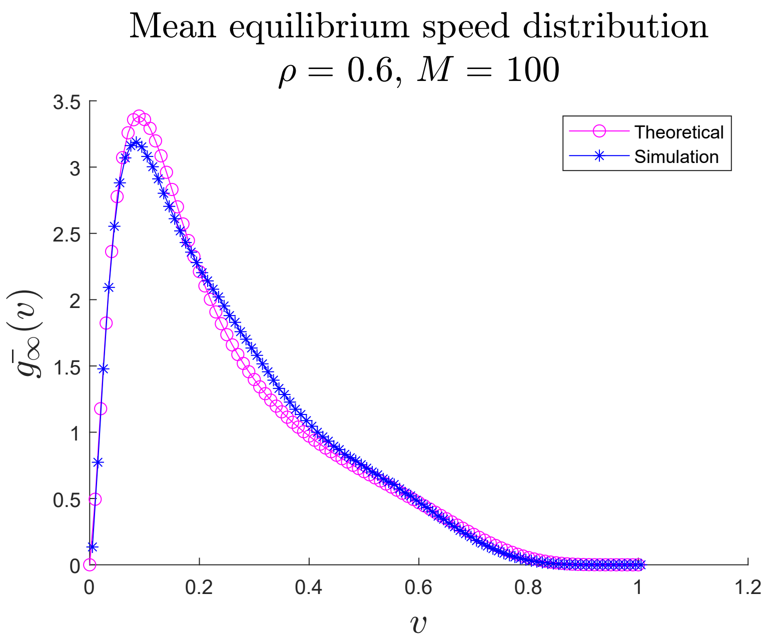

Figure 5.29: Comparison between the mean Fokker-Planck equilibrium speed distribution - see subsection 5.3.2 (theoretical) and the numerical distribution obtained with algorithm 4 (simulation) with $z \sim \mathcal{U}([1,3])$, $\rho = 0.6$, $M = 100$, $\epsilon = 0.01$, $T = 20$

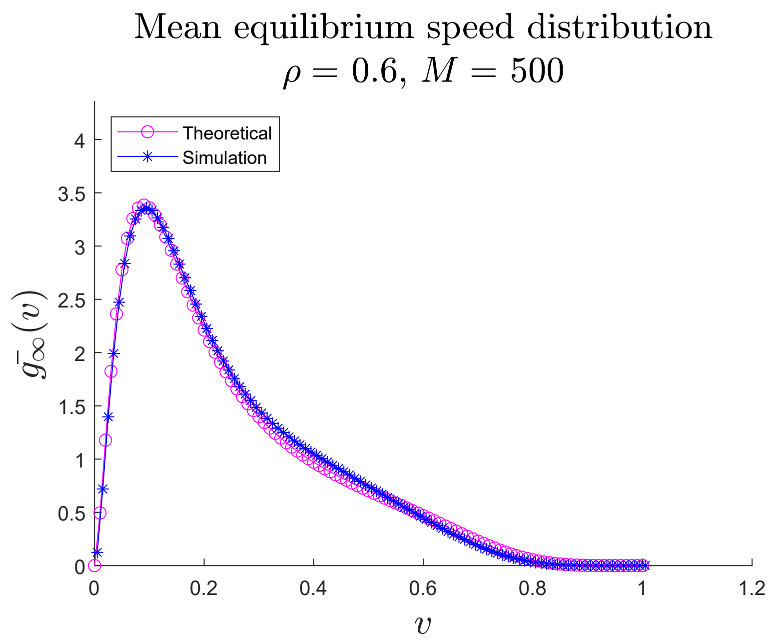

Figure 5.30: Comparison between the mean Fokker-Planck equilibrium speed distribution - see subsection 5.3.2 (theoretical) and the numerical distribution obtained with algorithm 4 (simulation) with $z \sim \mathcal{U}([1,3])$, $\rho = 0.6$, $M = 500$, $\epsilon = 0.01$, $T = 20$

A more quantitative insight on the matching between the simulation and the theoretical mean equilibrium speed distribution can be had by studying the L^2-numerical relative error, as it is defined in algorithm 4:

$$L^2\text{-numerical error} = \frac{\sqrt{\sum_{k=1}^{N_v} (\bar{g}_\infty^{TH}(v_k) - \bar{g}_\infty^{SIM}(v_k))^2}}{\sum_{k=1}^{N_v} \bar{g}_\infty^{TH}(v_k)} \tag{5.58}$$

where $\bar{g}_\infty^{TH}$ and $\bar{g}_\infty^{SIM}$ are the theoretical and the simulation mean asymptotic speed distribution respectively.
The typical behavior of Monte Carlo methods is expected i.e. L^2-numerical error $\sim O(M^{-\frac{1}{2}})$. In figure 5.31 (p. 179), the L^2-numerical error related to the mean equilibrium speed distribution is compared to the theoretical expected. The log-log plot displays results for $\epsilon = 0.5,\ 0.1,\ 0.01$ and for $M \in [0{,}100]$.

Since we have observed that the numerical $\bar{g}_\infty(v)$ better fit the theoretical distribution if M increases, a smoother behavior of the L^2-numerical error would be expected if M increases. In figure 5.32 (p. 180), the L^2-numerical error is compared to the theoretical one for $\epsilon = 0.01$ and for $M \in [100{,}1000]$. The numerical curve is smoother than figure 5.31, where $M \in [0{,}100]$ and the theoretical curve is better reproduced.

The same numerical relative error can be computed referring to the first moment i.e. $\bar{V}_\infty$ and it is defined as

$$L^2\text{-numerical error}_V = \sqrt{(\bar{V}_\infty^{TH} - \bar{V}_\infty^{SIM})^2 / \bar{V}_\infty^{TH}}\ , \tag{5.59}$$

where $\bar{V}_\infty^{TH}$ and $\bar{V}_\infty^{SIM}$ are the theoretical and the simulation mean speed at equilibrium respectively.
In order to observe a smoother behavior of the L^2-numerical error, a wider interval of M is considered. In figure 5.34 (p. 181), the L^2-numerical error related to $\bar{V}_\infty$ is compared to the MC error with $\epsilon = 0.01$ and $M \in$ [100,1000].

Now, let us focus on another source of error. The Nanbu-Babovsky's scheme is used to solve the Boltzmann-type equation at fixed z. It is a Monte Carlo approach and as mentioned in subsection 5.4.2, the speed domain is discretized in $N_v = 101$ points. In figures 5.35 - 5.37 (pp. 181-182), the L^2-numerical error is plotted for various N_v values. As expected, a finer choice of the speed discretization domain leads to results which are more consistent with theoretical predictions.

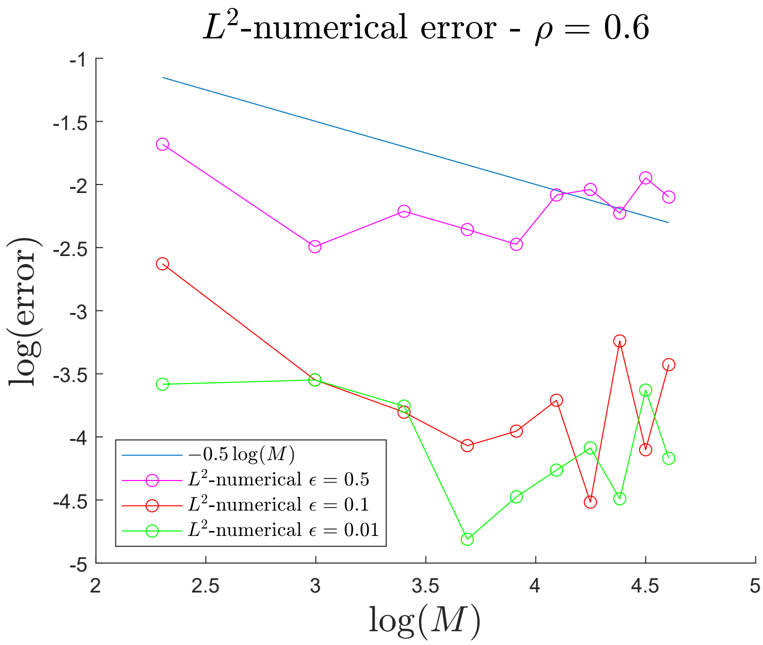

Figure 5.31: Comparison between the L^2-numerical error defined in (5.58) and the theoretical expected error i.e. $O(M^{-\frac{1}{2}})$ for $\rho = 0.6$, $T = 20$, various ϵ and $M \in [0,100]$

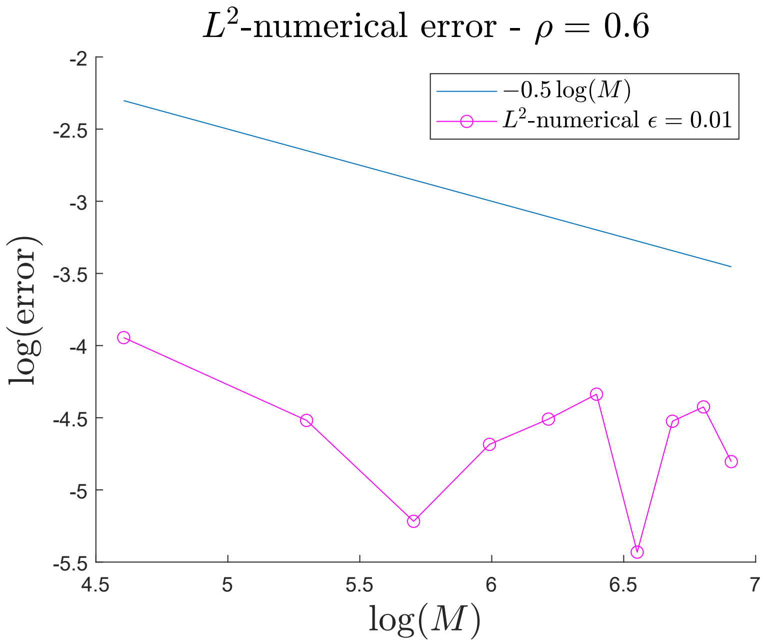

Figure 5.32: Comparison between the L^2-numerical error defined in (5.58) and the theoretical expected error i.e. $O(M^{-\frac{1}{2}})$ for $\rho = 0.6$, $\epsilon = 0.01$, $T = 20$ and $M \in [100,1000]$

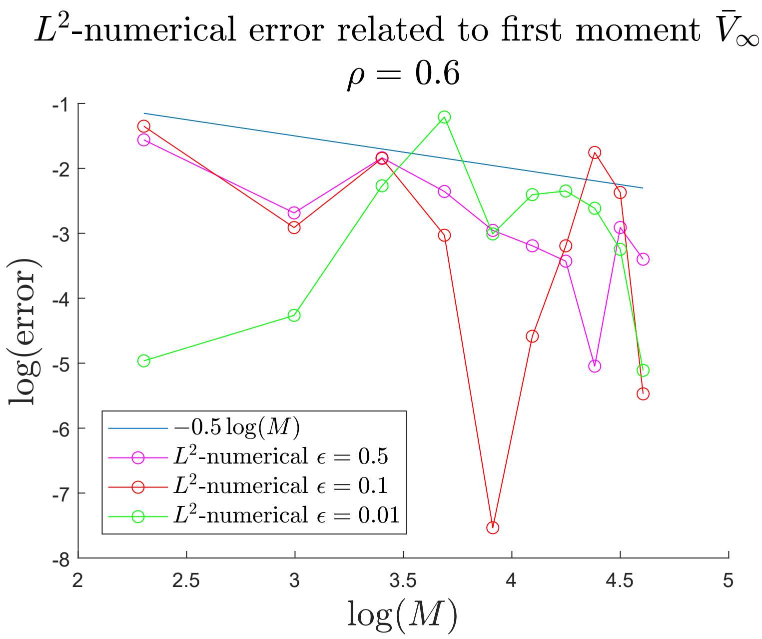

Figure 5.33: Comparison between the L^2-numerical error defined in (5.59) and the theoretical expected error i.e. $O(M^{-\frac{1}{2}})$ for $\rho = 0.6$, $T = 20$, various ϵ and $M \in [0,100]$

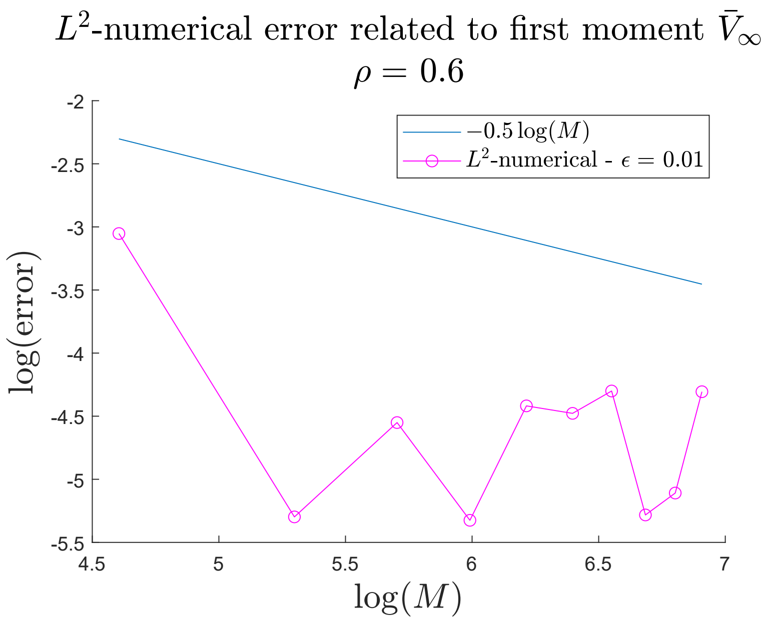

Figure 5.34: Comparison between the L^2-numerical error defined in (5.59) and the theoretical expected error i.e. $\mathrm{O}(M^{-\frac{1}{2}})$ for $\rho = 0.6$, $T = 20$, various ϵ and $M \in [100,1000]$

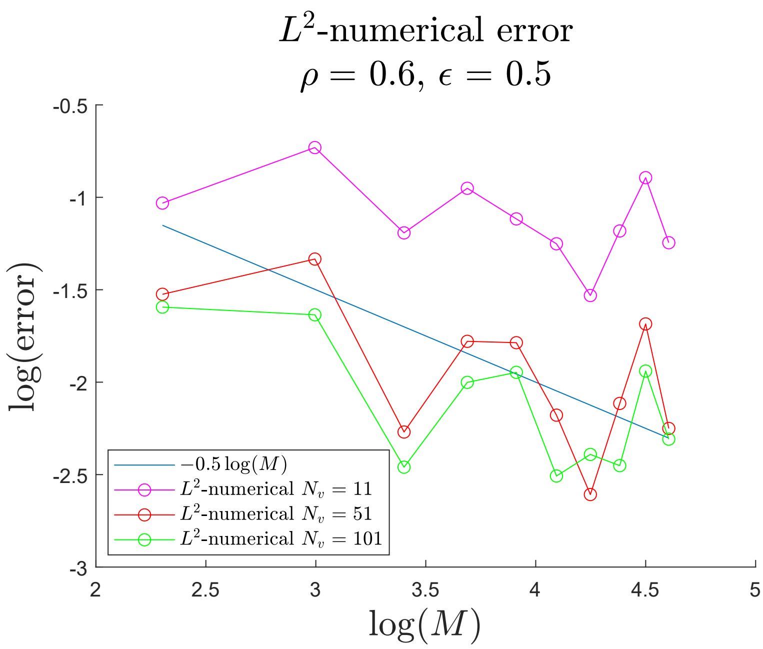

Figure 5.35: Comparison between the L^2-numerical error defined in (5.58) and the theoretical expected error i.e. $\mathrm{O}(M^{-\frac{1}{2}})$ for $\rho = 0.6$, $\epsilon = 0.5$, $T = 20$ and various N_v

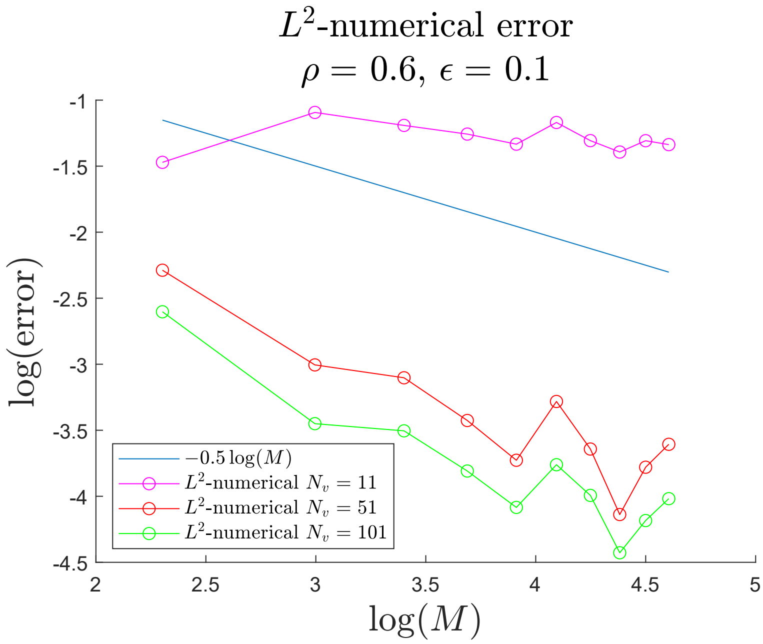

Figure 5.36: Comparison between the L^2-numerical error defined in (5.58) and the theoretical expected error i.e. $\mathrm{O}(M^{-\frac{1}{2}})$ for $\rho = 0.6$, $\epsilon = 0.1$, $T = 20$ and various N_v

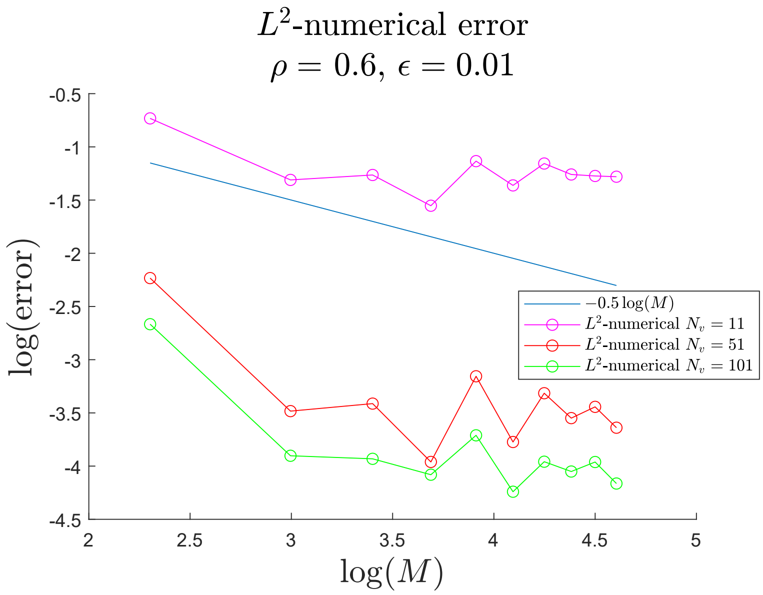

Figure 5.37: Comparison between the L^2-numerical error defined in (5.58) and the theoretical expected error i.e. $\mathrm{O}(M^{-\frac{1}{2}})$ for $\rho = 0.6$, $\epsilon = 0.01$, $T = 20$ and various N_v

In previous plots, the density $\rho = 0.6$ has been considered. Since z is uniformly distributed in the interval [1,3], the critical density is about 0.206. Consequently, if $\rho = 0.6$, we are in the deep congested regime. Let us set $\rho = 0.4$. The associated mean equilibrium speed distribution is plotted in figure 5.19 (p. 167) together with its uncertainty region. In $v = 1$, $\bar{g}_\infty(v = 1) = +\infty$ and this value is not visible in the plot. Therefore, we expect we will face some difficulties in deriving $\bar{g}_\infty$ in the neighborhood of $v = 1$ numerically.
Moreover, by running simulations at fixed z, it is evident that the time for convergence at equilibrium is longer than the case $\rho = 0.6$ and we set $T = 150$.

In figures 5.38 - 5.40 (pp. 183-184), the mean equilibrium speed distribution computed with simulations is compared to the theoretical one, which is obtained by mean of the Legendre-Gauss Quadrature formula with 20 nodes, in the case $\epsilon = 0.01$. The discrepancy in the neighborhood of $v = 1$ is high and this is due to the fact that it is impossible to obtain a Dirac delta numerically. Indeed, the points of $\bar{g}_\infty$ in the neighborhood of $v = 1$ are not even plotted since they assume extremely high values e.g. $\sim 10^8$ and $\bar{g}_\infty(v = 1) = +\infty$. Consequently, computing the numerical error is not significant.

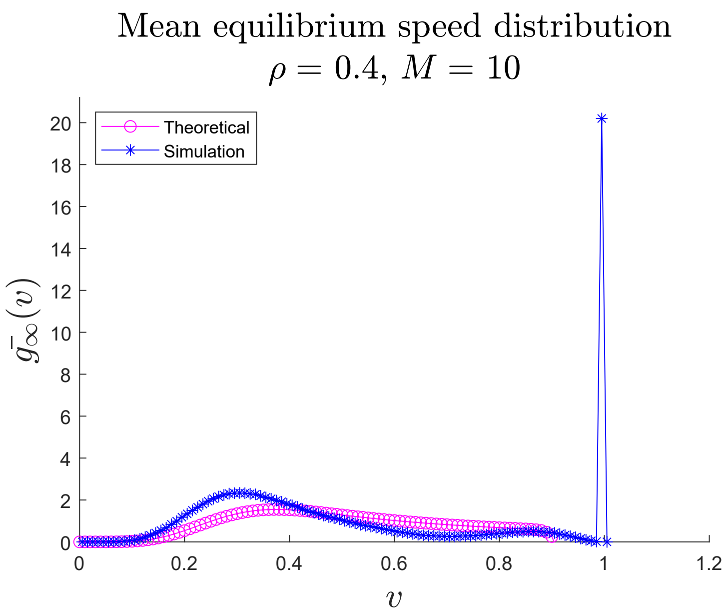

Figure 5.38: Comparison between the mean Fokker-Planck equilibrium speed distribution - see subsection 5.3.2 (theoretical) and the numerical distribution obtained with algorithm 4 (simulation) with $z \sim \mathcal{U}([1,3])$, $\rho = 0.4$, $M = 10$, $\epsilon = 0.01$, $T = 150$

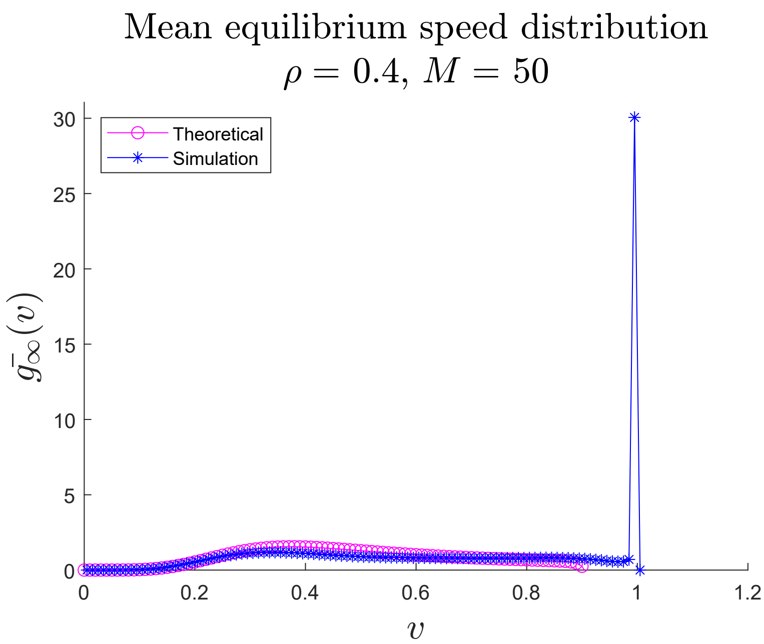

Figure 5.39: Comparison between the mean Fokker-Planck equilibrium speed distribution - see subsection 5.3.2 (theoretical) and the numerical distribution obtained with algorithm 4 (simulation) with $z \sim \mathcal{U}([1,3])$, $\rho = 0.4$, $M = 50$, $\epsilon = 0.01$, $T = 150$

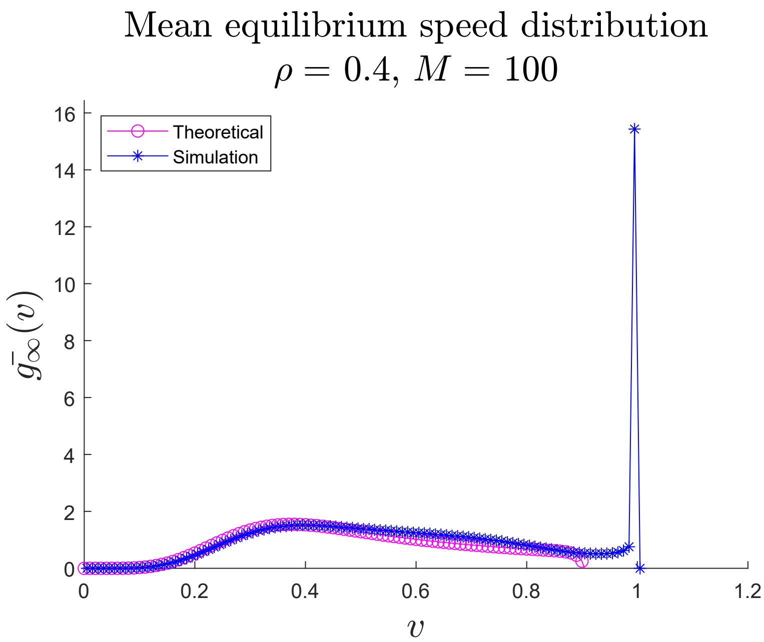

Figure 5.40: Comparison between the mean Fokker-Planck equilibrium speed distribution - see subsection 5.3.2 (theoretical) and the numerical distribution obtained with algorithm 4 (simulation) with $z \sim \mathcal{U}([1,3])$, $\rho = 0.4$, $M = 100$, $\epsilon = 0.01$, $T = 150$

5.5 Conclusion

In this chapter, an uncertainty parameter z is introduced in the nonlinear interaction rules by referring to previous works. Different probability distributions for z are considered and mean macroscopic quantities are obtained. For some probability distributions of the uncertain parameter, calculations can be carried out analytically while for others numerical methods such as Gaussian quadrature formulae are employed.

Several innovative results are obtained. In particular, two general results, one for discrete and another for continuous uncertain parameters, identify the stable fixed point of the system and the critical density of the phase transition. The mean speed at equilibrium turns out to be equivalent to the average, with respect to z, of the stable fixed points, which are derived in the deterministic case i.e. for fixed z. Instead, if we focus on the phase transition, it is preserved by the introduction of the uncertainty if the uncertain parameter is discrete. In this case, the critical point of the system coincides with the one corresponding to the type of vehicles with the biggest z. An analogous result is derived for an uncertain parameter which is uniformly distributed in a bounded interval. On the other hand, the phase transition is not preserved if the uncertain parameter follows a Gamma distribution.

As in deterministic cases, the *quasi-invariant interaction regime* is considered in order to derive mean equilibrium speed distributions. The piecewise trait of the mean speed at equilibrium is reflected in the shape of the mean equilibrium speed distribution. Coherently with literature [47] and with experimental data [27], multi-modal mean equilibrium speed distributions are obtained, due to the introduction of the uncertain parameter. However, because of the nonlinearity in the interaction rules, density intervals in which the behavior of the mean equilibrium speed distribution is different are distinguished.

Finally, numerical tests are performed thanks to a Monte Carlo method for UQ. The numerical solution of the Boltzmann-type equation averaged with respect to z is compared to the mean Fokker-Planck solution obtained in the *quasi-invariant interaction regime*. Due to the Monte Carlo trait of the algorithm employed, the numerical error made with respect to the mean Fokker-Planck theoretical solution is $O(M^{-\frac{1}{2}})$ where M is the uncertain parameter's sample size. The other two contributions to the numerical error, one related to the Nanbu-Babovsky's scheme and the other to the *quasi-invariant interaction regime*, are also analyzed. More accurate numerical results could be obtained by using more sophisticated numerical methods for UQ such as Stochastic Collocation and Stochastic Galerkin-generalized Polynomial Chaos [13; 51].

Conclusion

This dissertation highlights the potentiality of the mesoscopic approach to study phase transition and provides several original contributions to the research topic of kinetic traffic modeling.

Contrary to macroscopic models which were already used to investigate this feature [32], the Boltzmann-type kinetic approach does not require any assumptions a priori. The phase transition naturally emerges from the derivation of macroscopic quantities and it is a consequence of nonlinear microscopic interaction rules. In particular, a bifurcation emerges in the stability analysis of the mean speed at equilibrium and it identifies the critical point of the phase transition. This critical density marks the passage from the free flow regime, in which the mean speed at equilibrium is equal to its maximum value and the asymptotic speed distribution is a Dirac delta, to the congested flow regime, in which the mean speed at equilibrium decreases nonlinearly to 0 as a function of the density and the asymptotic speed distribution is a beta probability density function.

Nonlinear interaction rules are also considered when dynamics are controlled i.e. a percentage of autonomous vehicles is introduced in the system. The phase transition is preserved by the binary variance control while it is not by the desired speed control. Risk mitigation is also investigated. Coherently with literature [46], the binary variance control can reduce the variance of the asymptotic speed distribution and therefore, road risk. However, the novelty is that a range of densities for which the variance is identically equal to 0 is identified and it corresponds to the free flow regime. Instead, the desired speed control manages to reduce road risk only in the *infinite effective penetration rate limit* as in previous works [46].

Finally, phase transition is also investigated under uncertain vehicle interactions. Two general results, one for discrete and another for continuous uncertain parameters, identify the stable fixed point of the system and the critical density of the phase transition. The mean speed at equilibrium turns out to be equivalent to the average of the stable fixed points which are derived in deterministic cases. The phase transition is preserved by the introduction of the uncertainty if the uncertain parameter is discrete. In this case, the critical point of the system coincides with the one corresponding to the type of vehicles with the biggest uncertain parameter. An analogous result is derived for an uncertain parameter which is uniformly distributed in a bounded interval. On the other hand, the phase transition is not preserved if the uncertain parameter follows a Gamma distribution. Coherently with literature [47] and with experimental data [27], multi-modal mean equilibrium speed distributions are obtained, due to the introduction of the uncertain parameter. However, because of the nonlinearity in the interaction rules, density intervals in which the behavior of the mean equilibrium speed is different are distinguished.

The reach of these studies is both theoretical and practical. Kinetic modeling is a powerful tool which allows to characterize in detail the unsteady dynamics of traffic, thus marking new research directions which inspire the development and the evolution of broader theoretical and computational topics. Furthermore, understanding vehicular traffic has social and economic consequences: it can lead to replan urban mobility in order to consider environmental and management issues.

The findings of this dissertation provide an overview of phase transition in vehicular traffic with a Boltzmann-type kinetic approach. However, this research topic could still be deepened by referring to this thesis as a benchmark. In the following, possible research ideas are presented.

- As in [46], the Boltzmann-type equation of the kinetic traffic model could be reformulated in space inhomogeneous setting. In this way, hydrodynamic models with nonlinear interaction rules could be derived. The idea is to understand which is the impact of the nonlinearity and how these kinetic based models relate to the macroscopic ones. This analysis would also allow to focus on the derivation of hydrodynamic models, which is an under-explored topic in the context of multi-agent kinetic systems.

- The Uncertainty Quantification (UQ) study can be extended to the controlled dynamics. As in [47], the stochastic and the deterministic control strategy would be considered. The former leads to a model for Maxwellian molecules, which can be tackled with techniques similar to the ones employed in the uncontrolled case. The latter leads to a more easily implementable model for non-Maxwellian molecules with a non constant kernel that ensures the physical admissibility of the interactions. This model is more difficult to tackle and it can be solved by referring to a work related to a market economy [12]. In [47], the macroscopic features, which result from the two different control strategies, are equivalent. It would be interesting to understand whether this also occurs in the case of a phase transition and if this phenomenon is preserved by the introduction of the control. Moreover, also non-Maxwellian models are under-explored in the context of multi-agent kinetic systems and therefore, in this way they could be deepened.

- UQ results could be tested with more sophisticated and efficient procedures then the Monte Carlo-Monte Carlo scheme used in chapter 5. The goal would be to compare several existing methods [13; 51], in particular Stochastic Collocation (SC) and Stochastic Galerkin-generalized Polynomial Chaos (SG-gPC) methods. It could be interesting and useful to devise hybrid methods, which combine the bright sides of different approaches. This is a current research direction as shown in [31], where the efficiency of DSMC methods is combined with the accuracy of SG-gPC.

- In [45; 46] and in this thesis, autonomous vehicles are introduced as hidden leaders: their are standard agents and others do not interact with them differently. The problem could be studied by treating autonomous vehicles as labeled leaders: they are distinguished as leaders by other agents and the interaction with them is different from the one with standard vehicles. This issue has been traditionally tackled with fluid-dynamic models [21] and in order to do it in a kinetic fashion, we could be inspired by the paper [2], where leaders allow to control opinion consensus. It would be fascinating to compare implementation costs and benefits of different modeling approaches. Investigating autonomous vehicles with a Boltzmann-type kinetic approach could also be the basis to devise automatic decision algorithms in the context of Artificial Intelligence and study their multiscale collective impact.

- The modeling of traffic interactions could be enriched by considering that an agent is pushed to change its speed not only because of the leading vehicle's speed and the level of congestion. Behavioral and psychological aspects should be considered. In analogy with an economic

model that studies wealth distribution [6], the traffic model could consider agents' utility in the interaction rules. This utility would be based on psychological studies such as [19; 35], which dwell upon gender differences in traffic behavior due to the endorsement of stereotypes. Alternatively, research could be based on a model for a speculative financial market with a single stock that couples the financial with the opinion dynamics [26]. In this work, two different populations of traders are considered and their interplay determines the stock's price dynamics. In a similar way, women and men could be considered and the contribution of each population to road risk could be understood.
These studies could pave the way for further research, which would take into account psychological aspects in traffic modeling with a multi-agent kinetic approach.

Appendix A

Desired speed control and phase transition

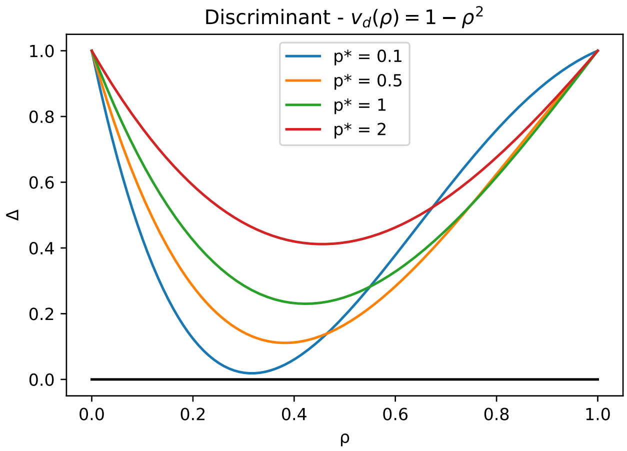

Figure A.1: Discriminant (4.78) for different effective penetration rates p^*, $v_d(\rho) = 1 - \rho^2$, $\mu = 2$

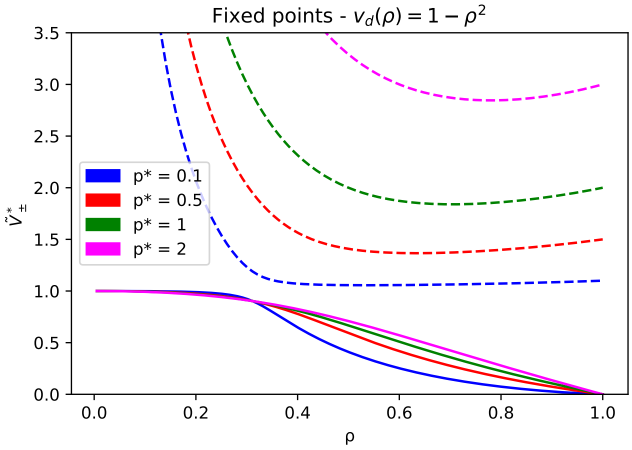

Figure A.2: Fixed points (4.77) for different effective penetration rates p^*, $v_d(\rho) = 1 - \rho^2$, $\mu = 2$. Dashed lines are related to unstable fixed points i.e. $\tilde{V}^*_+$; solid lines are related to stable fixed points i.e. $\tilde{V}^*_-$

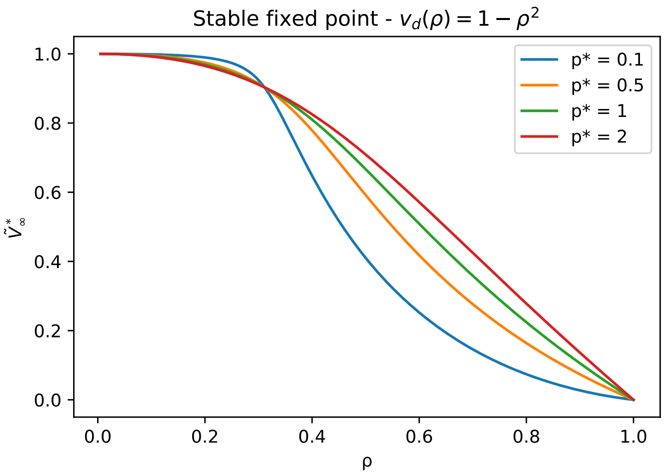

Figure A.3: Stable fixed point (4.80) for different effective penetration rates p^*, $v_d(\rho) = 1 - \rho^2$, $\mu = 2$

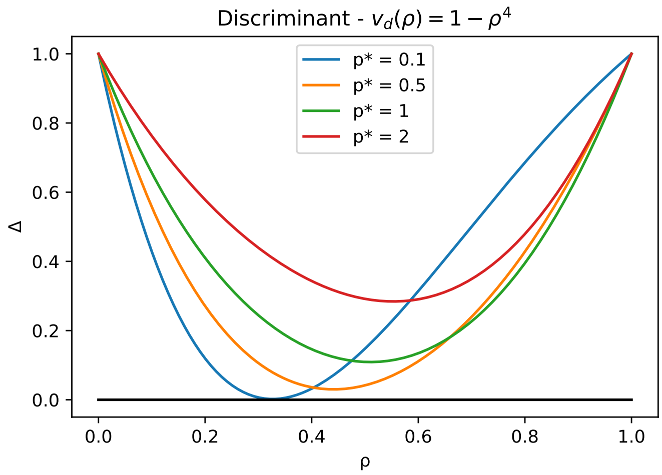

Figure A.4: Discriminant (4.78) for different effective penetration rates p^*, $v_d(\rho) = 1 - \rho^4$, $\mu = 2$

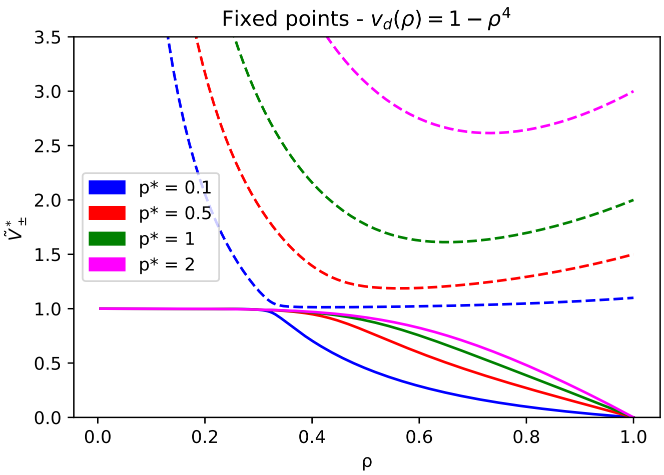

Figure A.5: Fixed points (4.77) for different effective penetration rates p^*, $v_d(\rho) = 1 - \rho^4$, $\mu = 2$. Dashed lines are related to unstable fixed points i.e. $\tilde{V}^*_+$; solid lines are related to stable fixed points i.e. $\tilde{V}^*_-$

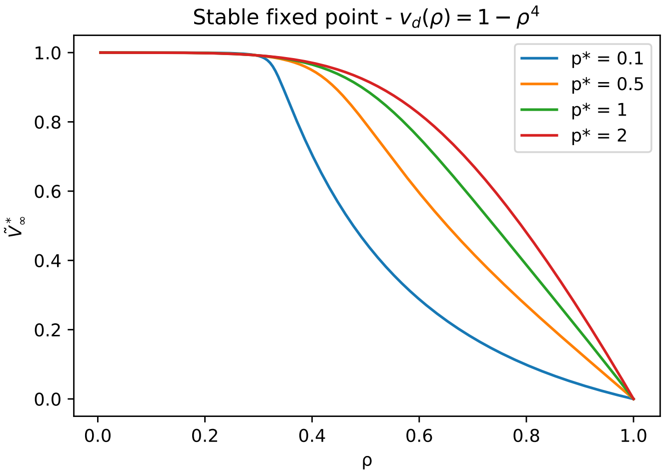

Figure A.6: Stable fixed point (4.80) for different effective penetration rates p^*, $v_d(\rho) = 1 - \rho^4$, $\mu = 2$

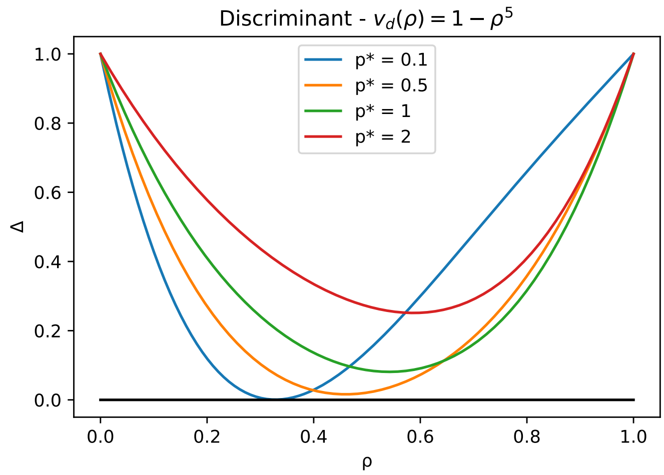

Figure A.7: Discriminant (4.78) for different effective penetration rates p^*, $v_d(\rho) = 1 - \rho^5$, $\mu = 2$

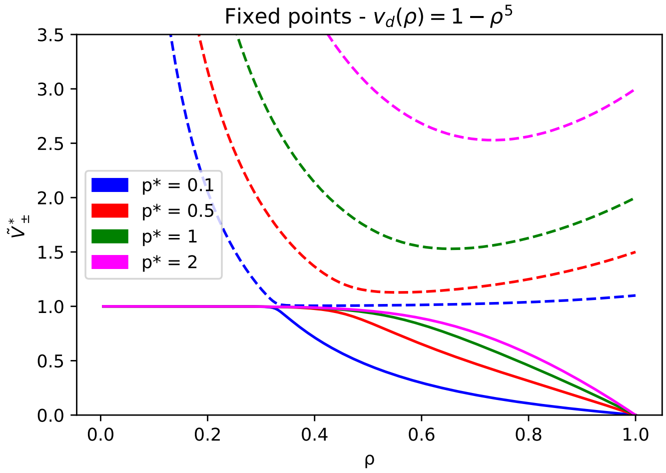

Figure A.8: Fixed points (4.77) for different effective penetration rates p^*, $v_d(\rho) = 1 - \rho^5$, $\mu = 2$. Dashed lines are related to unstable fixed points i.e. $\tilde{V}^*_+$; solid lines are related to stable fixed points i.e. $\tilde{V}^*_-$

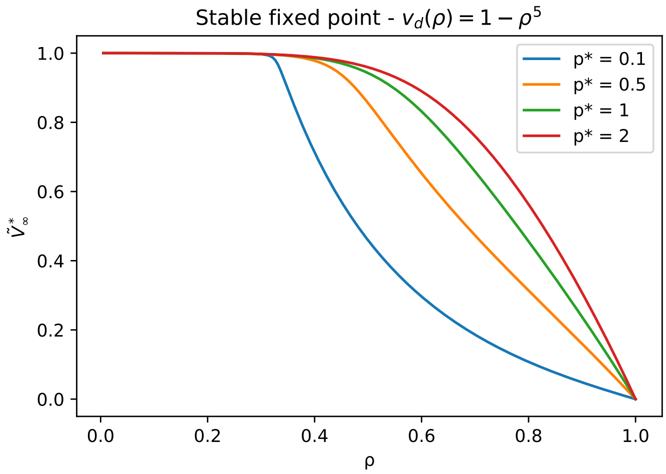

Figure A.9: Stable fixed point (4.80) for different effective penetration rates p^*, $v_d(\rho) = 1 - \rho^5$, $\mu = 2$

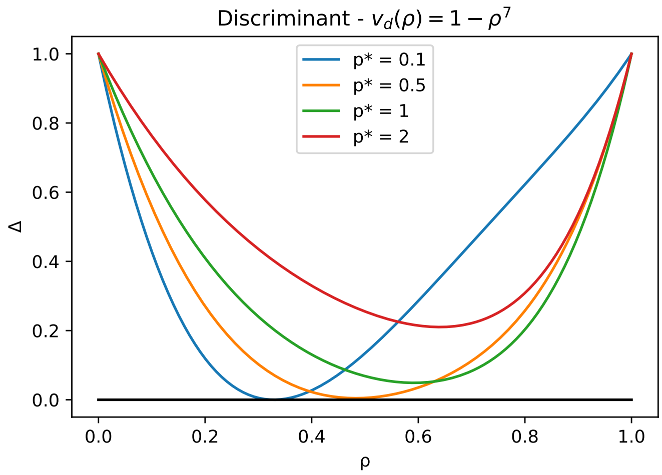

Figure A.10: Discriminant (4.78) for different effective penetration rates p^*, $v_d(\rho) = 1 - \rho^7$, $\mu = 2$

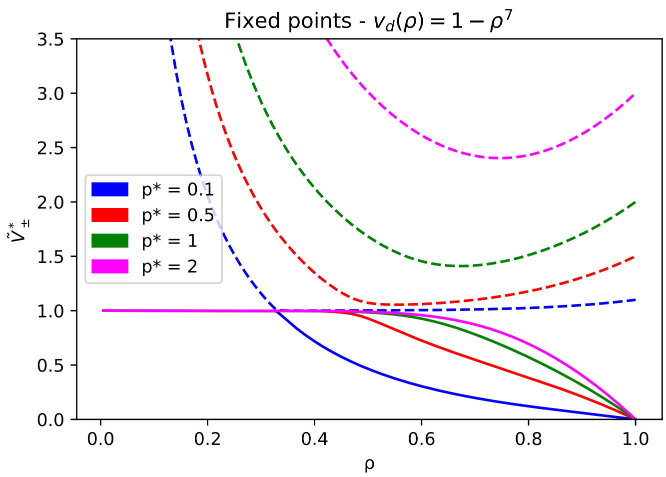

Figure A.11: Fixed points (4.77) for different effective penetration rates p^*, $v_d(\rho) = 1 - \rho^7$, $\mu = 2$. Dashed lines are related to unstable fixed points i.e. $\tilde{V}^*_+$; solid lines are related to stable fixed points i.e. $\tilde{V}^*_-$

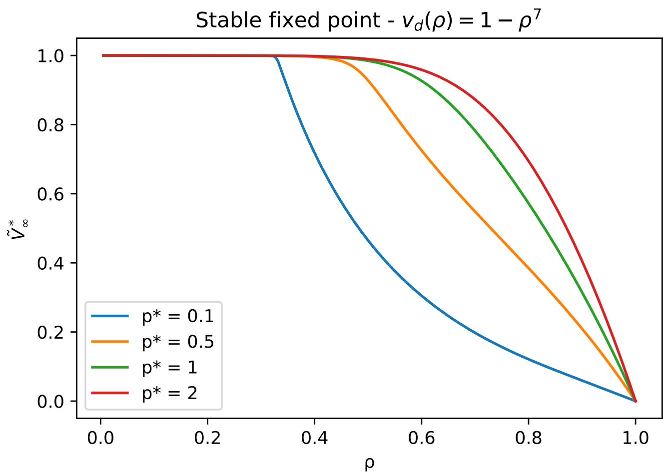

Figure A.12: Stable fixed point (4.80) for different effective penetration rates p^*, $v_d(\rho) = 1 - \rho^7$, $\mu = 2$

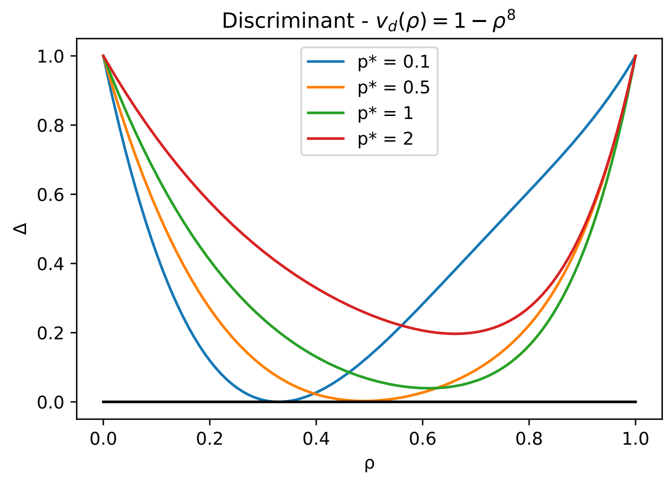

Figure A.13: Discriminant (4.78) for different effective penetration rates p^*, $v_d(\rho) = 1 - \rho^8$, $\mu = 2$

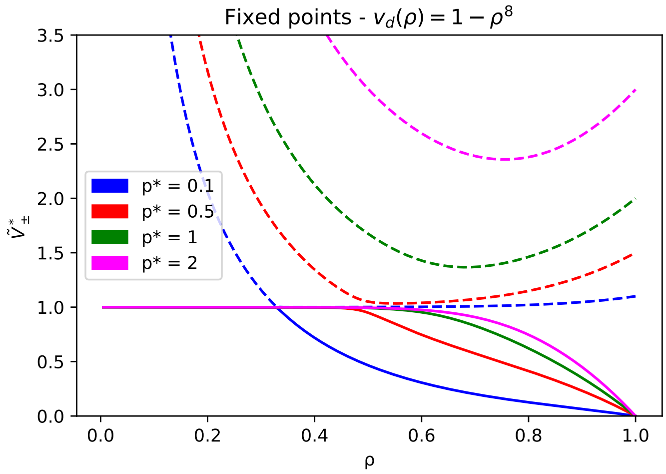

Figure A.14: Fixed points (4.77) for different effective penetration rates p^*, $v_d(\rho) = 1 - \rho^8$, $\mu = 2$. Dashed lines are related to unstable fixed points i.e. $\tilde{V}^*_+$; solid lines are related to stable fixed points i.e. $\tilde{V}^*_-$

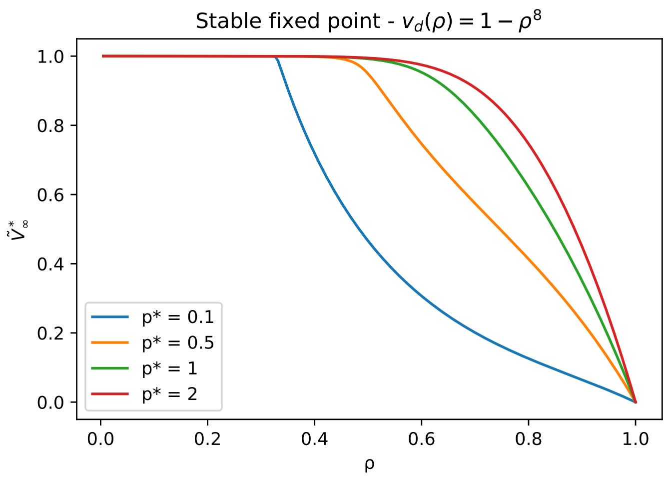

Figure A.15: Stable fixed point (4.80) for different effective penetration rates p^*, $v_d(\rho) = 1 - \rho^8$, $\mu = 2$

Bibliography

[1] G. Albi, M. Herty and L. Pareschi, *Kinetic description of optimal control problems and application to opinion consensus*, Commun. Math. Sci., 13(6):1407-1429, 2015

[2] G. Albi, L. Pareschi and M. Zanella, *Boltzmann-type control of opinion consensus through leaders*, Phil. Trans. R. Soc. A, 372(2028):20140138/1-18, 2014

[3] K. Atkinson, *Introduction to Numerical Analysis*, Wiley, 1989

[4] H. Babovsky and R. Illner, *A convergence proof for Nanbu's simulation method for the full Boltzmann equation*, SIAM J. Numer. Anal. 26(1):45–65, 1989

[5] A. Bressan, *Notes on the Boltzmann equation*, Lecture notes for a summer course given at SISSA, Trieste (Italy), 2005

[6] C. Brugna, S. Demichelis and G. Toscani, *Kinetic models for the trading of goods*, J. Stat. Phys., 151: 549-566, 2013

[7] R.E. Caflisch, *Monte Carlo and quasi-Monte Carlo methods*, Acta Numerica, 7: 1-49, 1998

[8] E. F. Camacho and C. Bordons Alba, *Model Predictive Control*, Springer-Verlag, 2007

[9] C. Cercignani, *The Boltzmann Equation and Its Applications*, Springer-Verlag, 1988

[10] C. Cercignani, *Ludwig Boltzmann: The Man Who Trusted Atoms*, Oxford University Press, 2000

[11] C. Cercignani, R. Illner and M. Pulvirenti, *The Mathematical Theory of Dilute Gases*, Springer-Verlag, 1994

[12] S. Cordier, L. Pareschi and G. Toscani, *On a kinetic model for a simple market economy*, J. Stat. Phys., 120(1):253-277, 2005

[13] G. Dimarco, L. Pareschi and M. Zanella, *Uncertainty quantification for kinetic models in socio-economic and life sciences* in S. Jin and L. Pareschi (Eds.), Uncertainty quantification for Hyperbolic and Kinetic Equations, vol. 14 of SEMA-SIMAI Springer Series, Springer, 2017

[14] B. Düring, L. Pareschi and G. Toscani, *Kinetic models for optimal control of wealth inequalities*, Eur. Phys. J. B 91, 265, 2018

[15] W. Feller, *An Introduction to Probability Theory and its Applications: Vol. I*, Wiley, 1971

[16] L. Fermo and A. Tosin, *Fundamental diagrams for kinetic equations of traffic flow*, Discrete Contin. Dyn. Syst. Ser. S, 7(3):449-462, 2014

[17] M. Fraia and A. Tosin, *The Boltzmann legacy revisited: kinetic models of social interactions*, preprint arXiv:2003.14225, 2020

[18] D. C. Gazis, R. Herman and R. W. Rothery, *Nonlinear follow-the-leader models of traffic flow*, Operations Res., 9:545-567, 1961

[19] M.A. Granié and E. Papafava, *Gender stereotypes associated with vehicle driving among French preadolescents and adolescents*, Transportation Research Part F: Traffic Psychology and Behaviour, 14, 341–353, 2011

[20] L. Grüne, *Analysis and design of unconstrained nonlinear MPC schemes for finite and infinite dimensional systems*, SIAM J. Control. Optim., 48(2):1206-1228, 2009

[21] D. Helbing, S. Lämmer and J.-P. Lebacque, *Self-organized control of irregular or perturbed network traffic* in C. Deissenberg and R. Hartl (Eds.), Optimal Control and Dynamic Games. Advances in Computational Management Science, vol. 7, Springer, 2005

[22] M. Herty and M. Zanella, *Performance bounds for the mean-field limit of constrained dynamics*, Discrete Contin. Dyn. Syst., 37(4):2023-2043, 2017

[23] B.S. Kerner, *Phase Transitions in Traffic Flow* in D. Helbing, H.J. Herrmann, M. Schreckenberg, D.E. Wolf (Eds.), Traffic and Granular Flow, Springer, 2000

[24] A. Klar and R. Wegener, *Enskog-like kinetic models for vehicular traffic*, J. Stat. Phys., 87(1-12):91-114, 1997

[25] M. Kac, *Probability and Related Topics in the Physical Sciences*, London, New York: Interscience, 1959

[26] D. Maldarella and L. Pareschi, *Kinetic models for socio-economic dynamics of speculative markets*, Physica A, 391: 715-730, 2012

[27] D. Ni, H. K. Hsieh, and T. Jiang, *Modeling phase diagrams as stochastic processes with application in vehicular traffic flow*, Appl. Math. Model., 53:106-117, 2018.

[28] L. Pareschi, *Lectures on Uncertainty quantification for kinetic equations*, Lectures for the summer school "Trails in kinetic theory" given in Hausdorff Institute for Mathematics Bonn, 2019

[29] L. Pareschi and G. Russo, *An introduction to Monte Carlo methods for the Boltzmann equation*, ESAIM: Proc., 10:35-75, 2001

[30] L. Pareschi and G. Toscani, *Interacting Multiagent Systems: Kinetic equations and Monte Carlo methods*, Oxford University Press, 2013

[31] L. Pareschi and M. Zanella, *Monte Carlo stochastic Galerkin methods for the Boltzmann equation with uncertainties: space-homogeneous case*, preprint arXiv:2003.06716, 2020

[32] B. Piccoli and A. Tosin, *Vehicular traffic: A review of continuum mathematical models* in R. A. Meyers (Ed.), Encyclopedia of Complexity and Systems Science vol. 22, pp. 9727-9749, Springer, 2009

[33] H. Ploss, *On simulation methods for solving the Boltzmann equation*, Computing 38, 101–115, 1987

[34] L. S. Pontryagin, V. G. Boltyanskii, R. V. Gamkrelidze and E. F. Mishchenko, *The Mathematical Theory of Optimal Processes*, Wiley & Sons, 1962

[35] K. Pravossoudovitch, C. Martha, F. Cury and M.A. Granié, *Sex and age differences in the endorsement of sex stereotypes associated with driving*, Spanish Journal of Psychology, 18, E100, 2015

[36] G. Puppo, M. Semplice, A. Tosin and G. Visconti *Fundamental diagrams in traffic flow: the case of heterogeneous kinetic models*, Commun. Math. Sci., 14(3):643-669, 2016

[37] G. Puppo, M. Semplice, A. Tosin and G. Visconti, *Analysis of a multi-population kinetic model for traffic flow*, Commun. Math. Sci., 15(2):379-412, 2017

[38] W. Rudin, *Real and Complex Analysis*, McGraw-Hill Book Company, International Edition 1987

[39] A. Sommariva, *Dispense Quadratura numerica*, Lecture notes for the Numerical Analysis course given at University of Padua, 2020

[40] E. D. Sontag, *Mathematical Control Theory: Deterministic Finite Dimensional Systems*, Springer, 1998

[41] S. H. Strogatz, *Nonlinear Dynamics and Chaos: With Applications to Physics, Biology, Chemistry, and Engineering*, Perseus Books Publishing L.L.C., 1994

[42] G. Toscani, *Kinetic models of opinion formation* Commun. Math. Sci., 4(3):481-496, 2006

[43] G. Toscani, A. Tosin and M. Zanella, *Multiple-interaction kinetic modeling of a virtual-item gambling economy*, Phys. Rev. E, 100(1):012308/1-16, 2019

[44] A. Tosin and M. Zanella, *Boltzmann-type models with uncertain binary interactions*, Commun. Math. Sci., 16(4):963-985, 2018

[45] A. Tosin and M. Zanella, *Control strategies for road risk mitigation in kinetic traffic modelling*, IFAC-PapersOnLine, 51(9):67-72, 2018

[46] A. Tosin and M. Zanella, *Kinetic-controlled hydrodynamics for traffic models with driver-assist vehicles*, Multiscale Model. Simul., 2019

[47] A. Tosin and M. Zanella, *Uncertainty damping in kinetic traffic models by driver-assist controls*, Math. Control Relat. Fields, 2020

[48] E. Venturino, *Appunti ragionati di calcolo numerico*, Aracne, 2015

[49] C. Villani, *On a new class of weak solutions to the spatially homogeneous Boltzmann and Landau equations*, Arch. Ration. Mech. Anal., 143(3):273-307, 1998

[50] World Health Organization, *Global status report on road safety*, Technical report, World Health Organization, 2015

[51] D. Xiu, *Numerical methods for stochastic computations: a spectral method approach*, Princeton University Press, 2010